UNIVERSITEIT VAN PRETORIA
UNIVERSITY OF PRETORIA
YUNIBESITHI YA PRETORIA

FUNDAMENTAL ELECTROCHEMICAL BEHAVIOUR OF PENTLANDITE

by

Getrude Marape

Submitted in partial fulfillment of the requirements for the degree

Masters in Engineering (Metallurgical Engineering)

in the Faculty of Engineering, Built Environment and Information Technology

Supervisor: Dr M.K.G. Vermaak

August 2010

Acknowledgements

I would like to thank God for His support and the strength He has given me throughout this research project.

I would like to express my sincere gratitude to the following people:

- My supervisor, Dr Thys Vermaak for his continuous support, guidance and patience
- Prof Chris Pistorius, for his support and the use of his samples
- My siblings, Joshua, Jacoline and Aubrey, for their continuous support and patience
- Sarah Havenga and the Department of Materials Science and Metallurgical Engineering, for their support to complete this research
- All my friends, for their support, advice and friendship
- Maggy Loubser and Sabine Verryn, for the XRD and XRF analyses
- Prof R.W. Merkle, for his sample and support
- Peter Graser, for the microprobe analyses
- Luukkanen Saaija of Geological Survey of Finland (GTK) for pentlandite samples
- Mintek, for the financial assistance that allowed me to conduct the research

UNIVERSITEIT VAN PRETORIA
UNIVERSITY OF PRETORIA
YUNIBESITHI YA PRETORIA

FUNDAMENTAL ELECTROCHEMICAL BEHAVIOUR OF PENTLANDITE

by

Getrude Marape

Supervisor: Dr M.K.G. Vermaak

Department of Materials Science and Metallurgical Engineering

Masters Degree in Engineering

ABSTRACT

Previous research indicates compositional variation of pentlandite [$(Fe,Ni)_9S_8$] and the effect this variation may have on the electrochemical behaviour of pentlandite is poorly understood. Pentlandite is the primary source of nickel and an important base metal sulfide (BMS) in the platinum industry. It hosts significant amounts of PGEs especially palladium and rhodium when compared to chalcopyrite and pyrrhotite. The aim of the project was to investigate the possible compositional variations of natural pentlandite and the effect of these variations on the electrochemical behavior thereof.

To study possible compositional variations, single pentlandite particles - in the order of 100μm in size from flotation concentrates (PGM deposits) and massive samples (massive ore bodies) - from various sources were employed. Electron microprobe analysis indicated a compositional variation of the pentlandite particles hand-picked from the flotation concentrate samples. Variation was observed in the cobalt, iron and nickel content and this was independent of the deposit. A slight compositional variation was observed from the massive pentlandite samples. The effect the compositional variation may have on the electrochemical reactivity of pentlandite was investigated using electrochemical techniques, i.e. measurement of the polarisation resistance and mixed potential as well as performing linear anodic voltammetry, current density–transients and electrochemical impedance spectroscopy (i.e. capacitance).

Poor electrochemical response of the pentlandite microelectrodes was observed. Pre–existing pores, deep pores, cracks and the brittle nature of pentlandite microelectrodes may have contributed to the poor electrochemical response of natural pentlandite particles hand-picked from the flotation concentrate. Slight compositional variations of the massive pentlandite sample influenced the electrochemical behaviour. In aerated solutions, iron enriched pentlandites were less reactive after progressive oxidation. The lower reactivity of the electrodes was a result of thick oxide films formed. This was illustrated by polarisation resistance and capacitance measurements. The lower reactivity of the electrodes was also related to the mechanism of the reduction of oxygen at oxidised passive electrode surfaces. It is however difficult to distinguish if the differences in the reactivity was a result of the Fe/Ni ratio or the influence of cobalt. Current density transients confirmed that the reactivity of a pentlandite electrode to be time dependent. The reactivity of the electrode decreased during oxidation. A variation in the electronic properties of the formed oxide film was observed. Slight compositional variation of pentlandite did not have a significant effect on the rest potential values as do changes in the type of sulfides (e.g. pyrite vs. pentlandite). This was confirmed by similar rest potential values of various pentlandite electrodes. The oxidation of synthetic pentlandite may be influenced by the chemical composition. In de-aerated solutions, anodic oxidation (as indicated by the linear anodic voltammogram) of synthetic pentlandite started at a potential lower than of the natural electrodes. In aerated solutions, the synthetic pentlandite was less reactive and formed thicker oxide films.

Keywords: Pentlandite, pyrrhotite, Cu–Ni sulfide ores, oxidation, flotation, electron microprobe, electrochemical impedance spectroscopy, electrochemistry

TABLE OF CONTENTS

1. INTRODUCTION

South Africa is one of the largest platinum producing countries in the world (Jones, 1999). The Bushveld Igneous Complex (BIC) is the major platinum-group element (PGE) reserve in South Africa. In this reserve, PGEs occur either as discrete platinum group minerals (PGMs) or in solid solution in the base metal sulfides (BMS), such as chalcopyrite, pentlandite, pyrrhotite and pyrite (Cabri, 1989; Jones, 1999). The majority of the platinum group elements in the Merensky ore are associated with pentlandite [$(Fe,Ni)_9S_8$], occurring either in pentlandite grains or at the pentlandite–gangue grain boundaries (Jones, 1999). Palladium and rhodium are the PGEs contained mostly in pentlandite (Cabri, 1992; Godel *et al*., 2007). Pentlandite is not only an important carrier of PGEs, but also the principal source of nickel.

Pentlandite [$(Fe,Ni)_9S_8$], is recovered by milling and flotation (Penberthy, 2001). Oxidation during the recovery processes depresses pentlandite, resulting in poor grade and recovery performance (Buckley & Woods, 1991; Legrand *et al*., 2005; Kelebek *et al.*, 2007). During flotation, the recovery of pentlandite is often associated with the recovery of nickel. Different nickel recoveries have been observed from various ores (Heiskanen *et al*., 1991) and, in some cases, from different areas of the deposit. Besides other factors, such as mineralogical variations in the ores and dissolution of minerals, variation in the composition of pentlandite may also be a cause of such differences. Previous research indicates compositional variation of a natural pentlandite (Brynard, *et al.*, 1976; Merkle and Von Gruenewaldt, 1986; Van Zyl, 1996; Harney and Merkel, 1991; Penberthy, 2001; and Godel *et al*., 2007). The variation seems to be independent of the reef and the deposit.

The effect these variations may have on the electrochemical oxidation of pentlandite is poorly understood. Legrand *et al*. (2005) and Buckley & Woods (1991) investigated the oxidation of a natural pentlandite. Based on their work, it appears that oxidation products are independent of pentlandite composition; both the iron-rich and nickel-rich pentlandite result in similar products. However, the effect these products may have on electrochemical behaviour of pentlandite is not clear. Chander (1984) proposed that the properties of the oxide films are responsible for the reactivity of sulfide minerals in the

flotation systems. The objective of the project was to investigate whether there is any compositional variation of pentlandite particles from the flotation concentrate samples and the massive ore bodies. The secondary aim was to determine possible effects of pentlandite composition if there are any, on the electrochemical behaviour of pentlandite using polarisation resistance, mixed potential and electrochemical impedance spectroscopy. The aim was to use these techniques to determine the electrochemical response of various pentlandite electrodes.

2. LITERATURE REVIEW

2.1 Platinum - group element (PGE) Mineralogy

The platinum–group elements (PGEs) can be recovered from the PGE dominant ores or nickel copper ores (Maier, 2005). In these ores, the PGEs are present in solid solution in sulfide minerals while the platinum-group minerals (PGMs) occur within the base metal sulfides, often at the grain boundary between sulfide and silicate (Cabri, 1989). The PGE ores can be classified into PGE dominant deposits, chromite containing deposits and nickel–copper sulfide deposits (Xiao and Laplante, 2004).

2.1.1 PGE dominant deposits

The PGE dominant deposits are the major source of the production of the PGEs. Ores from these deposits are usually mined for the PGE content, while copper, nickel and cobalt are recovered as by–products (Xiao and Laplante, 2004). The PGM ores contain approximately 1% base metal sulfides (Miller *et al*., 2005). The base metal sulfides associated with the PGEs in these deposits are largely chalcopyrite, pentlandite, pyrrhotite and in some cases pyrite. Typical deposits of this nature include the Merensky reef, UG-2 and Platreef of the Bushveld Igneous Complex (BIC) in South Africa, the Great Dyke in Zimbabwe, Stillwater Complex in USA and some Canadian deposits (e.g. Lac des Iles) (Xiao and Laplante, 2004).

2.1.1.1 Merensky reef of the Bushveld Complex

The Merensky Reef is one of the PGE–rich layers of the Bushveld Igneous Complex after the UG–2 chromitite, the second largest PGE resource in the world (Cawthorn, 1999). Most of the PGEs are hosted by the PGMs (platinum-group minerals) and to a lesser extent in solid solution within the base metal sulfides (BMS). Merensky reef has a typical PGE content of 4-10 g/t (Cabri, 1989; Jones, 1999) with a nickel and copper content of 0.13% and 0.08% of the ore respectively (Jones, 1999). PGMs in this reef have an average grain size of 45 µm, which is larger than the PGM grains in the UG–2 ore, which have an average grain size of 15 µm. The reef contains up to 3% of the base metal sulfides (BMS) composed largely of pyrrhotite (45%), pentlandite (32%), chalcopyrite (16%) and pyrite (2-4%) (Cabri, 1989; Jones, 1999; Schouwstra *et al*., 2000). The

majority of the PGMs in the reef are associated with pentlandite, occurring either in pentlandite grains or at the pentlandite–gangue grain boundaries (Cabri, 1989; Jones, 1999).

Pentlandite [$(Fe,Ni)_9S_8$] is the principal BMS host of the majority of PGEs (Godel *et al*., 2007). It contains up to 600 ppm combined PGE (Godel *et al*., 2007). Compared to other base metal sulfides, it is enriched with Pd, Rh and Co (Godel *et al.*, 2007; Brynard *et al*., 1976). Pentlandite grains analysed from the Rustenburg Platinum Mine had Co, Pd and Rh concentrations in the range of 0.5–1.4 wt %, 50 to 600 ppm and 1–100 ppm respectively (Godel *et al*., 2007). Cabri (1992) reported maximum Pd concentration in pentlandite (ppmw) to be 1164.

Other sulfide minerals associated with PGEs in this reef are: braggite (Pt,Pd)S, cooperite (PtS), laurite (RuS_2), other ferro platinum alloys (Pt-Fe) (Brynard *et al*., 1976; Jones,1999) and platinum–palladium tellurides such as moncheite ($PtTe_2$) and kotulskite (PdTe) (Cabri, 1989; Schouwstra *et al*., 2000). The gangue minerals in the reef are pyroxene, plagioclase feldspar and biotite (Jones, 1999).

2.1.1.2 Platreef

The Platreef is an ore body of platinum-group elements and base metal enriched mafic and ultramafic layers situated along the base of the northern limb (Mokopane previously known as Potgietersrus) of the Bushveld Igneous Complex (Manyeruke, 2003). The reef contains a PGE grade of 7–27 g/t (Cabri, 1989). It is enriched with palladium (Cabri, 1989; Jones, 1999) with a maximum content of 20000 ppmw in pentlandite (Cabri, 1992). The sulfide assemblage of the three Platreef horizons (i.e. Lower, Middle and Upper Platreef) on the farm Townlands, investigated by Manyeruke (2003), consisted predominantly of pyrrhotite and chalcopyrite with minor amounts of pentlandite and pyrite.

In this reef, pentlandite is associated with pyrrhotite or pyrite. Pentlandite, when associated with pyrite, it has a well-developed cleavage, resulting in the formation of triangular pits when polished (Mostert, 1982). Coarse pentlandite is found as anhedral, but when it is associated with pyrrhotite, it occurs as a mosaic of grains along boundaries

of the pyrrhotite grains (Mostert, 1982). The average amount of the sulfide minerals in the three layers was approximated to be in the range 2–5 wt % in abundance.

Other PGMs found in this reef are cooperite (PtS), braggite [(Pt,Pd)S], sperrylite ($PtAs_2$), vysotskite (PdS) and kotulskite (PdTe), intermediate isomertiete [$Pd_{11}(As,Sb)_4$], merenkyite ($PdTe_2$), minor Pt–Fe alloys and moncheite ($PtTe_2$) (Postle *et al*., 1986).

2.1.2 Chromite deposits with PGEs

In the chromium deposits, PGEs occur as alloys enriched with osmium, ruthenium and iridium (Cabri, 1989; Maier, 2005). The typical deposit of this nature is the UG-2 reef of the Bushveld Igneous Complex. In this reef, the PGEs are in the form of PGMs, a portion of which is associated with chromium. Chromium is the principal problem when processing these ores since it reports to the PGE concentrate (Maier, 2005).

2.1.2.1 UG–2 reef

Mineralogically, the reef consists mainly of chromitite (60-90%), orthopyroxenes (5-25%) and plagioclase (5-15%), with minor amounts of talc, chlorite and phlogopite and smaller amounts of base metal sulfides and other platinum-group minerals (Cabri, 1989; Jones, 1999). The base metal sulfides are composed largely of pentlandite, chalcopyrite, pyrrhotite and pyrite, with pentlandite being the major base metal sulphide. The reef has a typical PGE content of 4.4-10.6 g/t and lower nickel and copper contents when compared to the Merensky reef (Cabri, 1989; Jones, 1999). The sulfides generally occur at the interstices of the chromite grains and grain boundaries of the gangue minerals, where they are partially or fully enclosed in the chromite and silicate minerals (Feng and Aldrich, 1999). The UG–2 ore has finer sulfide grains of 15 µm compared to sulfide grains in the Merensky ore of 45 µm (Jones, 1999; Schouwstra *et al*., 2000). The PGMs have an average grain size of 15 µm hence ore is milled at approximately 80% less than 45 µm in order to liberate PGM minerals (Jones, 1999). Nickel and copper content of the UG–2 reef was found to be 0.07% and 0.018% in the ore respectively; this is slightly lower than the copper and nickel content in the Merensky reef (nickel and copper contents of 0.13% and 0.08% of the ore respectively) (Jones, 1999). The gangue minerals in the reef are chromitite, orthopyroxenes and plagioclase and minor amounts of talc and phlogopite. The UG–2 ore is enriched with rhodium (Jones, 1999). The PGMs of the

UG–2 ore comprise laurite (RuS_2), cooperate (PtS), braggite [(Pt,Pd)S], Pt–Ru–Cu sulfide, Pt–Pb–Cu sulfide, Pt–Fe alloy and minor vysoskite (PdS) (Cabri, 1989).

2.1.3 Nickel–copper dominant deposits

The nickel-copper dominant ores are mined primarily for the value of nickel and the copper, while PGEs are recovered as by–products of the process. The flotation concentrates of these ores contain both pyrrhotite and pentlandite. Pyrrhotite is regarded as the primary source of the undesirable sulfur in the smelters. The presence of pyrrhotite in these concentrates results in the high SO_2 emissions during smelting (Senior *et al.*, 1994). Separation of pyrrhotite from pentlandite flotation concentrate has thus become a major concern in minimising SO_2 emissions. Typical deposits of this nature are Sudbury in Canada, Noril'sk in Russia and Nkomati Mine in Mpumalanga South Africa (Maier, 2005). In South Africa, the PGMs are found within the massive sulfide body of the Uitkomst Complex situated in the Mpumalanga Province.

2.1.3.1 Nkomati Mine deposit, South Africa

The Nkomati Mine is a Ni-Cu-Co-PGE deposit located within the Uitkomst Complex. It is a layered igneous intrusion situated between Badplaas and WatervalBoven in the Mpumalanga Province of South Africa (Van Zyl, 1996; Bradford *et al.*, 1998). Currently, it exploits a magmatic Ni–Cu–Co–PGE massive sulfide deposit associated with the Uitkomst Complex. The Uitkomst Complex contains both the massive and disseminated sulfide ores. The massive sulfide ore body has a typical PGE content of 7 ppm (Maier *et al.*, 2004). In the massive sulfide ore body, pyrrhotite, pentlandite and chalcopyrite are the dominant sulfide minerals (Van Zyl, 1996; Theart and de Nooy, 2001). The ore consists of the following: pyrrhotite 70 (wt %), pentlandite 9 (wt %), chalcopyrite 6.3 (wt %), pyrite 3.8 (wt %) and 10.5 (wt %) magnetite (Theart and de Nooy, 2001; Maier *et al.*, 2004). Within the massive sulfide ore body, PGMs occur mostly as irregular to sub–rounded particles enclosed in the sulfide minerals, or less commonly, in the silicate minerals (Theart and de Nooy, 2001).

Polished sections from the massive sulfide body prepared by Theart and De Nooy (2001) indicated 20% (by mass) of the total PGMs occurring within pentlandite particles. Pentlandite is mostly intergrown with other minerals, especially pyrrhotite.

Pentlandite occurs throughout the Uitkomst Complex and was observed as two distinct textural varieties, i.e. as granular, polycrystalline aggregates associated with pyrrhotite or as flame–like exsolutions in pyrrhotite (Van Zyl, 1996; Theart and De Nooy, 2001). The granular pentlandite occurs along cracks on the grain boundaries of pyrrhotite or as veinlets in the pyrrhotite. Within coarse-grained pentlandite, pyrrhotite forms islands. Granular pentlandite may also be present as discrete grains in the gangue. Flame–like pentlandite is found along pyrrhotite grain boundaries on the boundaries between granular pentlandite and pyrrhotite or on the contact between pyrrhotite and chromite (where pyrrhotite is interstitial to the chromite) as well as on contacts between pyrrhotite and secondary magnetite (Van Zyl, 1996). Secondary magnetite forms irregular rims around pentlandite or occurs as veins in the cracks existing in the granular pentlandite (Van Zyl, 1996). Typical grain size of pentlandite is in the range 50 to 100 μm in diameter (Theart and de Nooy, 2001). The occurrence of pentlandite within the pyrrhotite matrix indicate that pentlandite is generally associated with pyrrhotite.

2.2 Pentlandite

2.2.1 Chemical composition of pentlandite

The composition of pentlandite varies with the sulfide assemblage (Harris & Nickel, 1972; Misra and Fleet, 1973; Riley, 1977). Sulfide assemblage refers to sulfide minerals co-existing with pentlandite in a polished section made from the collected representative sample. The electron microprobe has been widely used to determine the composition of pentlandite from New Zealand, Canada Australia and South Africa (Bushveld Igneous Complex and Uitkomst Complex deposits) (Harris and Nickel, 1972; Misra and Fleet, 1973; Brynard *et al*., 1976; Riley, 1977; Van Zyl, 1996; Penberthy, 2001).

2.2.1.1 Composition of pentlandite from New Zealand and Australian sulfide assemblages

Riley (1977) summarised the composition of Australian and New Zealand pentlandites from literature; and the author found the composition of pentlandite to vary from $Fe_6Ni_{2.5}Co_{0.5}S_8$ to $Fe_{0.7}Ni_{2.5}Co_{5.8}S_{7.8}$ depending on the co-existing sulfide minerals. The iron to nickel ratio (Fe:Ni) of the pentlandite mineral varied with the sulfide assemblage (see Table 2.1). The cobalt content of pentlandite increased with a decrease of Fe:Ni ratio, indicating iron or nickel substitution by cobalt. Misra and Fleet (1973) also supported the possible substitution of iron or nickel in pentlandite by cobalt. Pentlandite co-existing with chalcopyrite, native copper, cuprite and troilite has a higher iron content (43.10 wt %) with an iron to nickel ratio of 2.23 when compared to pentlandite co-existing with other sulfides (see Table 2.1). Pentlandite co-existing with heazlewoodite had a higher cobalt content (43.8 wt %) than that co-existing with other sulfide minerals (see Table 2.1). Harris and Nickel (1972) regarded cobalt-pentlandite to contain cobalt of up to 52.8 wt %. The results summarised in Table 2.1 indicate the effect of sulfide assemblage on pentlandite composition.

Table 2.1: Electron microprobe analysis of pentlandite from different sulfide assemblages from Australia and New Zealand (Riley, 1977).

Element (wt %)	Chalcopyrite, Native Copper, Cuprite,Troilite	Pyrrhotite, chalcopyrite	Pyrrhotite, pyrite, smythite	Heazlewoodite
Co	4.10	9.80	11.00	43.80
Ni	19.30	30.50	30.80	18.70
Fe	43.10	27.10	25.60	5.00
S	33.60	32.70	32.40	31.80
Fe:Ni	2.23	0.89	0.83	0.27
Pentlandite	$Fe_6Ni_{2.5}Co_{0.5}S_8$	$Fe_{3.7}Ni_4Co_{1.3}S_{7.8}$	$Fe_{3.5}Ni_{4.1}Co_{1.4}S_{7.7}$	$Fe_{0.7}Ni_{2.5}Co_{5.8}S_{7.8}$

Cobalt-free pentlandite has a cobalt content of less than 0.1 wt % while an iron-free pentlandite and nickel-free pentlandite have cobalt contents of 42.47 wt % and 52.60 wt % respectively (Misra and Fleet 1973). Rajamani and Prewitt (1973) reported that an increase of cobalt content increases the microhardness and thermal stability of pentlandite. The properties of pentlandite provided by Vaughan and Craig (1978),

showed cobalt pentlandite (Co_9S_8) to have a higher Vickers microhardness (330-350 $kg.mm^{-2}$) when compared to pentlandite ($Fe_{4.5}Ni_{4.5}S_8$) with microhardness in the range of 202-231 $kg.mm^{-2}$ at a load of 100-200g. The increase in the microhardness of pentlandite may impact on the milling behaviour of pentlandite.

2.2.1.2 Pentlandite composition from Canadian sulfide assemblages

The composition of the Canadian pentlandite also varies with that of the co-existing sulfides (Harris and Nickel 1972; Misra and Fleet, 1973). Misra and Fleet (1973) reported the nickel content of pentlandite increases with that of the bulk composition of the sulfide assemblage. Misra and Fleet (1973) further reported that the solid solution limit of nickel in natural pentlandite ranges from 18.0 to 34.0 (at %) nickel. The nickel content of the pentlandite grains analysed, varied between 24.91 (at %) and 29.83 (at %) depending on the sulfide assemblage (see Table 2.2). There was a slight variation of sulfur content. The iron to nickel ratio ranged between 0.77 and 1.13 when compared to the data provided by Riley (1977).

The iron to nickel ratio of Australian pentlandite particles analysed by Riley (1977) varied between 0.27 and 0.87 (see Table 2.1). The iron to nickel ratio of an Australian pentlandite co-existing with heazlewoodite was found to be 0.27 (Riley, 1977), while that from the Canadian deposit was found to be 0.77 (see Table 2.2). There is a significant variation of iron to nickel ratio for Australian pentlandite (0.27 to 0.89) when compared to Canadian pentlandite with iron to nickel ratios of 0.77 to 1.13.

Table 2.2: Electron microprobe analyses of Canadian pentlandites from different sulfide assemblages (Misra and Fleet, 1973).

Element (at %)	Tr, HPo	HPo & MPo	HPo & MPo, Py	MPo	MPo, Py	Hz
Co	0.66	1.21	0.83	1.26	0.41	0.45
Ni	24.91	27.60	28.44	27.05	28.41	29.83
Fe	28.06	24.13	24.50	24.32	24.47	23.07
S	46.37	47.06	46.23	47.36	46.71	46.63
Cu	0.00	0.00	0.00	0.01	0.00	0.02
Fe:Ni ratio	1.13	0.87	0.86	0.90	0.86	0.77

Tr = Troilite; HPo = Hexagonal Pyrrhotite; MPo = Monoclininc Pyrrhotite; Py = Pyrite; Hz = Heazlewoodite

2.2.1.3 Composition of Pentlandite from the Merensky Reef (Bushveld Igneous Complex, South Africa)

Brynard *et al*. (1976) determined the composition of pentlandite grains from Western Platinum Mine near Marikana. The iron content of the grains ranged between 32.75 wt % and 35.75 wt%; the nickel content ranged between 32.31wt % and 35.16 wt %. The average cobalt content of the grains was 0.8 wt %. Only one grain was found to be iron-rich with an iron content slightly higher than that of the nickel (see Table 2.3). The iron to nickel ratio of the three pentlandite grains analyzed, varied from 0.93 to 1.11 (see Table 2.3). The metal to sulfur ratio (i.e. M:S normally assumed to be 9:8) varied from 9.54 to 9.77 when sulfur was normalized to 8. From these analyses, it is evident that there is a slight compositional variation of pentlandite and variation from the assumed theoretical metal to a sulfur ratio of 9:8.

Table 2.3: Pentlandite composition from the Western Platinum Mine, near Marikana (Brynard *et al*., 1976). (Sulfur was normalized to 8).

Pentlandite Composition (wt %)								
Sample	**Fe**	**Ni**	**Co**	**S**	**Total**	**Fe:Ni**	**Formula**	**M:S_8**
1	33.3	34.3	0.85	32.06	100.5	0.97	$Fe_{4.76}Ni_{4.67}Co_{0.11}$	9.54
2	35.75	32.31	0.75	31.6	100.41	1.11	$Fe_{5.20}Ni_{4.47}Co_{0.11}$	9.77
3	32.75	35.16	0.81	31.76	100.49	0.93	$Fe_{4.74}Ni_{4.84}Co_{0.11}$	9.69

In comparison, pentlandite grains from the Merensky Reef, analysed by Vermaak and Hendriks (1976), had average cobalt content of 0.9 wt % with an iron to nickel ratio of 0.98 (Table 2.4). These analyses are similar to those found by Brynard *et al*. (1976).

Table 2.4: The composition of pentlandite from the Merensky reef (Vermaak and Hendriks, 1976). (Sulfur was normalized to 8).

Pentlandite Composition						
Element	**Fe**	**Ni**	**Co**	**S**	**Fe:Ni ratio**	**M:S_8 ratio**
wt %	32.95	33.55	0.9	33.2	0.98	9.09

Godel *et al*. (2007) determined the composition of pentlandite grains from the Rustenburg Platinum Mine (also from the Merensky reef) from different layers of the reef [Upper Chromitite, Anorsthosite, Melanorite, Lower chromitite (LC) and coarse–grained

melanorite (CGM)]. The cobalt content of the grains analysed varied from 0.33 to 0.67 wt %. The cobalt content of these grains is lower than those analysed by Brynard *et al*. (1976) and Vermaak and Hendriks (1976) analysed, indicating a possible cobalt variation. The iron to nickel ratio is still within similar ranges of 0.8 to 1 (see Table 2.5). Iron-rich pentlandite was found in the upper chromitite layer.

These analyses indicate compositional variation of pentlandite mostly in cobalt content ranging from 0.33 wt % to 0.9 wt %. The iron to nickel ratio is within similar ranges of 0.9 to 1. Both iron and nickel rich pentlandites occur within the Merensky reef.

Table 2.5: Average composition of pentlandite from the Rustenburg Platinum Mine (Godel *et al*., 2007). (Sulfur was normalized to 8).

Pentlandite Composition (wt %)								
Element	**Fe**	**Ni**	**Co**	**Cu**	**S**	**Total**	**Fe:Ni ratio**	**M:S_8 ratio**
Upper chromitite	34.41	31.52	0.67	<0.01	32.54	99.14	1.09	9.18
Anorthosite	31.18	34.87	0.36	<0.01	32.58	98.98	0.89	9.12
Melanorite	31.23	33.65	0.33	<0.01	32.08	97.29	0.93	9.1
LC & CGM	32.59	32.98	0.57	<0.01	32.62	98.76	0.99	9.08

Merkle and Von Gruenewaldt (1986) investigated the presence and compositional variation of cobalt rich pentlandites with stratigraphic height. The analysis showed that in the upper zone of the Western Bushveld Complex at Bierkraal, pentlandite is consistently cobalt rich (see Table 2.6), with cobalt content ranging up to 57.94 wt %. The composition varied significantly with depth. Cobalt rich pentlandite grains showed a low iron and nickel content (see Table 2.6), indicating iron and nickel substitution for cobalt.

Table 2.6: Composition of pentlandite from Western Bushveld Complex at Bierkraal Mine (Merkle and Von Gruenewaldt, 1986). (Sulfur was normalized to 8).

Element (wt %)						
Depth (m)	**S**	**Fe**	**Ni**	**Co**	**Total**	**M:S_8 ratio**
551.5	33.86	7.82	1.31	57.94	100.93	8.67
1040.2	33.03	14.06	9.02	44.93	101.04	9.07
1082	32.86	16.64	4.88	45.49	99.87	9
1112.7	32.35	26.22	25.18	15.54	99.29	9.21

2.2.1.4 UG-2 ore

There is a slight compositional variation on pentlandite grains from UG–2 with variation in the cobalt content (see Table 2.7). Penberthy (2001) determined the composition of the pentlandite grains from the UG-2 ore. The iron to nickel ratio varied from 0.89 to 1.07 and the cobalt content was in the range 0.45 to 0.73 wt % (see Table 2.7). Sample C1 had a higher nickel content (34.34 wt %) compared to iron with a content of 30.62 wt % (Table 2.7). Penberthy (2001) suggested this to be a feature from millerite bearing assemblage. Samples A1 and B4 showed a high iron content of 32.92 wt % and 33.88 wt % respectively. The variation of the iron to nickel ratio of pentlandite from the UG–2 ore is within the range of pentlandite from the Merensky reef.

Table 2.7: Electron microprobe analysis of pentlandite grains from the UG-2 reef (Penberthy, 2001). (Sulfur was normalized to 8).

Pentlandite Composition (wt %)								
Sample	**Fe**	**Ni**	**Co**	**Cu**	**S**	**Total**	**Fe:Ni ratio**	**M:S_8 ratio**
A1	32.92	32.63	0.45	0.04	32.99	99.03	1.01	8.96
B4	33.88	31.8	0.73	0.05	33.39	99.85	1.07	8.93
C1	30.62	34.34	0.46	0.05	32.79	98.26	0.89	8.94

Cobalt content of UG–2 pentlandite grains varied from 0.45 to 0.73 wt %. The cobalt content is within the range of grains analysed from the Rustenburg Platinum mine (see Table 2.5). Pentlandites from the Merensky reef and UG–2 have a similar Fe to Ni ratio with a slight variation in the cobalt content.

2.2.1.5 Composition of pentlandite from the Uitkomst Complex, Ni–Cu deposit

The composition of pentlandite from the Uitkomst Complex also depends on the co-existing sulfide assemblage. Nkomati Mine is situated within the Uitkomst Complex. An electron microprobe analyses performed by Van Zyl (1996) on pentlandite grains from the Uitkomst Complex indicated a variation of iron, nickel and cobalt content of pentlandite throughout the Uitkomst Complex. The iron content ranged between 23.40 and 28.85 at % and the nickel content varied between 23.08 and 27.43 at %. The average nickel content was 25.67 at %. The cobalt content ranged between 0.3 at % and 1.75 at %

with an average of 0.97 at %. Compared to pentlandite grains from the Merensky and UG–2 reefs, the grains had a higher cobalt content (greater than 1 wt %) except for cobalt pentlandites analysed from Bierkraal Mine that were analysed. The iron to nickel ratio is still within the range of pentlandites from the Merensky reef (0.9 to 1). Van Zyl (1996) found that the composition of pentlandite varies with the sulphide assemblage (see Table 2.8). Pentlandite co-existing with violarite has a cobalt content greater than 2 wt % and, when co-existing with chalcopyrite, pyrrhotite and pyrite has a cobalt content lower than 2 wt % (see Table 2.8). Violarite ($FeNi_2S_4$) is a mineral that forms as a result of pentlandite transformation after oxidation of iron within pentlandite. The iron to nickel ratio varied from 0.85 to 0.91. This is in the same range as pentlandite grains from the Bushveld Igneous Complex that were analysed.

There is a compositional variation of pentlandite from the Uitkomst Complex and the variation depends on the sulfide assemblage in which pentlandite occurs. This is similar to pentlandite from the PGM deposits.

Table 2.8: Electron microprobe analysis of pentlandite grains from the Uitkomst Complex (Van Zyl, 1996).

Pentlandite composition from Uitkomst Complex (wt %)								
Assemblage	**Fe**	**Ni**	**Co**	**Cu**	**S**	**Total**	**Fe:Ni ratio**	**M:S_8 ratio**
Po+Pn+Cp+Py	30.63	34.2	1.25	-	33.25	99.33	0.896	8.89
Po+Pn+Cp+Py	30.92	35.78	1.21	-	33.3	101.21	0.864	9.11
Po+Pn+Cp	30.26	35.79	1.49	-	33.54	101.08	0.845	9
Po+Pn+Cp	29.83	34.13	1.48	-	33.62	99.06	0.874	8.7
Po+Pn+Cp+Py	31.19	34.31	1	-	33.16	99.66	0.909	8.97
Po+Pn+vl+Cp	30.03	33.26	2.26	0.07	33.44	99.06	0.903	8.77

Po = pyrrhotite; Pn = pentlandite; Cp = chalcopyrite; py = pyrite; vl = violarite

2.2.2 Oxidation of pentlandite

Oxidation induces undesirable effects during pentlandite flotation. It leads to the formation of hydrophilic hydroxide layers that depress the mineral during flotation (Buckley and Woods 1991; Legrand *et al.*, 2005) by inhibiting collector interaction. During pentlandite oxidation, iron migrates from the bulk to the surface where is it oxidised, forming an iron oxide or oxyhydroxide overlayer on the mineral surface, with

nickel oxide forming within the iron oxide layer (Richardson and Vaughan, 1989; Buckley and Woods, 1991; Legrand *et al.*, 2005). An Auger electron spectroscopy (AES) depth profile performed by Legrand *et al.* (2005) showed migration of iron from the pentlandite sub-surface to the surface (see Figure 2.1). This profile confirmed preferential oxidation of iron.

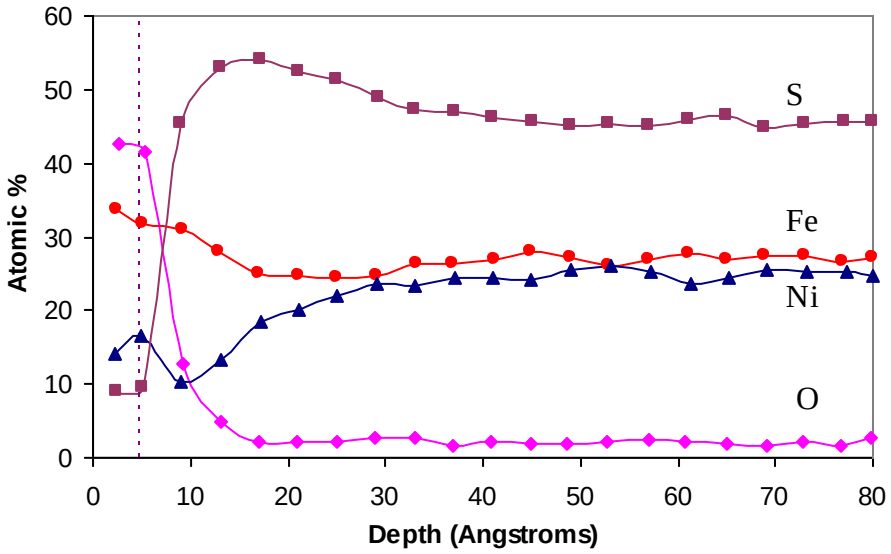

Figure 2.1: The AES depth profile of Voisey's Bay pentlandite, after reaction in pH 9.3 solution for 90 minutes (re-drawn from data published by Legrand *et al.*, 2005).

During oxidation of pentlandite, products forming are independent of the composition. The oxidation of both iron-rich and nickel-rich pentlandites result in similar oxidation products (see Table 2.9). Legrand *et al.* (2005) and Buckley and Woods (1991) determined the oxidation products of natural iron-rich and nickel-rich pentlandites, using X–ray photoelectron spectroscopy. Buckley and Woods (1991) employed nickel-rich pentlandite with the composition ranging between $Fe_4Ni_{4.5}Co_{0.04}S_8$ to $Fe_{4.5}Ni_5Co_{0.03}S_8$. Legrand *et al.* (2005) employed pentlandite with a composition as indicated in Table 2.10. The cobalt content of 0.9 at % (1.17 wt %) is similar to the cobalt content of pentlandite from the South African Uitkomst Complex. Iron-rich pentlandite oxidised to FeOOH (Fe^{3+}) and $Ni(OH)_2$ (Legrand *et al.*, 2005), while a nickel-rich pentlandite oxidised to $Fe_2O_3.H_2O$ and nickel oxide, leaving a metal deficient pentlandite as indicated by equation 1 (Buckley and Woods, 1991). In both cases, the preferential oxidation of iron was observed. Violarite formation was detected in nickel-rich pentlandite (Buckley

and Woods, 1991). A restructured nickel–iron sulfide thiospinel [$Fe_{0.5}Ni_{2.5}S_4$] formed, in addition to nickel and iron oxide (equation2). Cobalt content did not show any effect on the oxidation.

$$Fe_4Ni_5S_8 + (3x/4)\ O_2 + (x/2)\ H_2O = 2Fe_{4-x}\ Ni_5\ S_8 + (x/2)\ Fe_2O_3 \cdot H_2O \quad (1)$$

$$Fe_4Ni_5S_8 + (9/4)\ O_2 + (3/2)\ H_2O = 2Fe_{0.5}\ Ni_{2.5}\ S_4 + (3/2)\ Fe_2O_3 \cdot H_2O \quad (2)$$

Table 2.9: Oxidation products of both iron and nickel-rich natural pentlandite.

Fe–rich (Legrand *et al*., 2005)	Ni–rich (Buckley and Woods, 1991)
23.8 at % Ni; 28.1 at % Fe; 0.9 at % Co; 47.1 at % S	$Fe_4Ni_{4.5}Co_{0.04}S_8$ to $Fe_{4.5}Ni_5Co_{0.03}S_8$
Preferential oxidation of iron (Fe)	Preferential oxidation of iron (Fe)
FeOOH, $Ni(OH)_2$	$Fe_2O_3.H_2O$, Ni oxide species
pH 9.3 using CaO	pH 9.2 in sodium tetraborate

Table 2.10: Electron microprobe analysis of pentlandite from Voisey's Bay ore deposit (Legrand *et al*., 2005).

Pentlandite composition								
Element	Fe	Ni	Co	Cu	As	S	Fe:Ni ratio	$M:S_8$ ratio
at %	28.1	23.8	0.9	0.1	0.1	47.1	1.18	8.98
wt %	34.54	30.75	1.17	<0.14	<0.16	33.24	-	-

2.2.3 Oxidation of a synthetic pentlandite

In comparison to a natural pentlandite, synthetic pentlandite oxidises to a small extent in air but rapidly in water, resulting in the outermost layers becoming predominantly iron–oxygen species with small quantities of nickel–oxygen species (Richardson and Vaughan, 1989). The surface alteration of a synthetic pentlandite with composition $Fe_{4.5}Ni_{4.5}S_8$ (i.e. with equal amounts of iron and nickel), was studied by Richardson and Vaughan (1989). Richardson and Vaughan (1989) employed XPS, AES and Mossbauer spectroscopy techniques to investigate the surface alteration of the oxidised synthetic pentlandite. It was proposed that the subsurface of pentlandite had been transformed to violarite ($FeNi_2S_4$). The oxidation products of a synthetic pentlandite were found to be

similar to that of a natural pentlandite determined by Legrand *et al.* (2005) [FeOOH and $Ni(OH)_2$] and Buckley and Woods (1991) ($Fe_2O_3.H_2O$ and nickel oxide) - indicating that products are independent of the composition.

Chamberlain (1996) studied the oxidation of nickel-rich and iron-rich synthetic pentlandites at temperatures 385°C to 600°C. An iron-rich synthetic pentlandite with a composition $Fe_{5.80}Ni_{3.15}S_8$ was employed. This pentlandite was oxidised in a temperature of 385–570°C. At 500°C both iron-rich and nickel-rich pentlandite dissociated to form a metal-rich pentlandite phase and monosulphide solid solution (mss). The pentlandite and monosulphide solid solution phases with compositions of $Fe_{4.68}Ni_{4.60}S_8$ and $Fe_{0.72}Ni_{0.25}S_1$ respectively, formed after the oxidation of iron-rich pentlandite. Nickel-rich pentlandite produced a pentlandite and monosulphide solid solution phase with compositions $Fe_{3.60}Ni_{5.82}S_8$ and $Fe_{0.35}Ni_{0.66}S_1$ respectively. In both cases, hematite (FeOOH), nickel oxide and $FeSO_4$ were observed as the oxidation products of iron-rich and nickel-rich pentlandites. The composition of iron-rich and nickel-rich pentlandite employed influenced the composition of the pentlandite phase formed after the oxidation of pentlandite and percentage mass gain. The percentage mass gain of oxidised iron-rich pentlandite was found to be 3.85% and 3.50% for oxidised nickel-rich pentlandite (Chamberlain, 1996). The mass gain of oxidised pentlandite was attributed to the formation of hematite.

From these results, it is clear that oxidation of a synthetic and natural pentlandite produce similar products and that compositional variation of a synthetic pentlandite may result in differences in the thickness and composition of oxide layers forming on the surface. This may similarly be a case with a natural pentlandite.

2.2.4 Flotation of pentlandite

Froth flotation is a technique commonly used to separate sulfide minerals from gangue. During flotation, oxidation depresses sulfide minerals, resulting in poor grade-recovery performance (Heiskanen *et al.*, 1991; Kelebek, *et al.*, 2007). Depression of sulfide minerals is a result of the hydrophilic nature of the oxidation products forming on the mineral surfaces (Woods, 1984). It is for this reason that flotation of sulfide minerals is

usually performed with thiol type collectors, such as xanthate. By controlling pulp conditions, the flotation of minerals without the use of collectors can be achieved (Heyes and Trahar, 1977; Woods, 1984). Pentlandite is one of the main sources of nickel worldwide and can be recovered from nickel–copper sulfide and PGM ores by milling and flotation. The difficulty in recovering pentlandite from these ores is mostly associated with oxidation and the brittle nature of pentlandite (Heiskanen *et al.*, 1991; Vos, 2006; Kelebek *et al.,* 2007). In the flotation operations, pentlandite has been observed to slime when compared with other sulfide minerals (Vos, 2006). However, mineralogical variations, pH, aeration and the extent of oxidation may enhance the depression effect or improve the floatability of pentlandite in these ores (Heiskanen *et al*., 1991; Kelebek *et al.*, 2007).

2.2.4.1 Effect of pH and mineralogical variations

Heiskanen *et al*. (1991) investigated the collectorless floatability of sulfides using nickel, noritic and serpentitic ores. Noritic ore contained 0.31% Ni, 0.14% Cu and 8% Fe as sulfidic compounds and the serpentitic ore contained 0.9% Ni and 0.45% Cu with a total sulfide content of 14%. In both ore types, increased nickel recoveries were observed at low pH values. The formation of elemental sulfur and polysulfide at mineral surfaces or the formation of metal deficient (sulfide-rich) surfaces may have been the mechanism responsible for the improved collectorless floatability of sulfides in acidic solutions (Trahar, 1984; Woods, 1984). In alkaline solutions, both ores depicted low nickel, iron and copper recoveries indicating poor floatability of these sulfides. In acidic and alkaline media, different nickel recoveries were observed from low grade Noritic and Serpentitic ores, indicating the possible effect of mineralogical variations (see Figure 2.2 and 2.3). However, it is not clear whether the distinction in the nickel recoveries from different ores is enhanced by the mineralogical variations of the ores or by the chemical variations of sulfide minerals.

From these results, it is clear that improved recoveries are obtained at low pH values and that mineralogical variations may influence the floatability of nickel sulfide minerals.

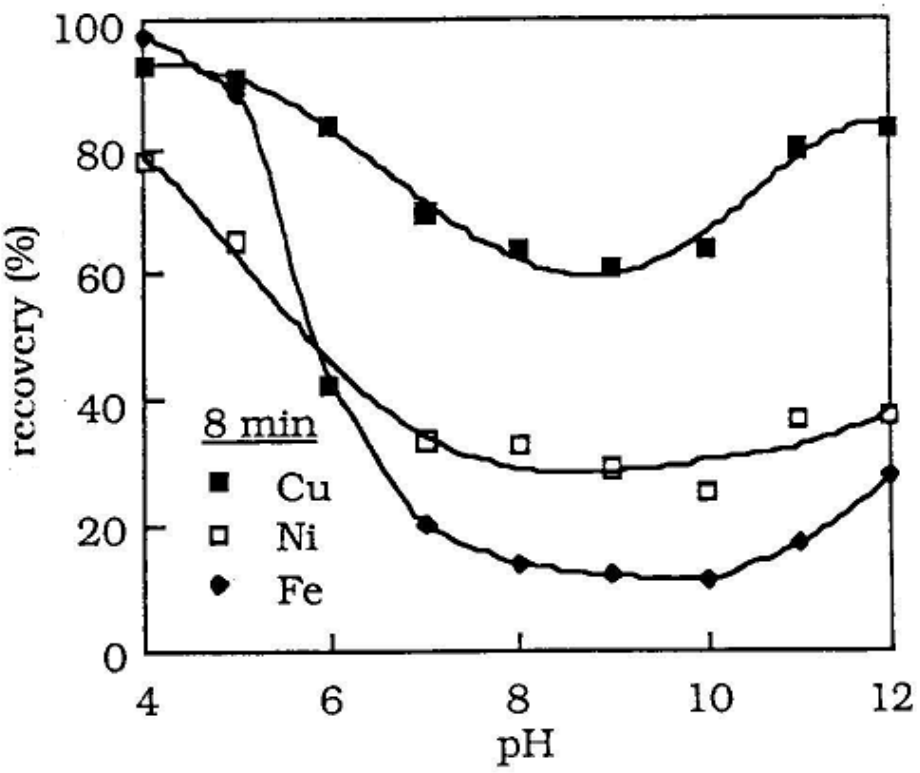

.

Figure 2.2: Effect of pH on metal recoveries with the Noritic ore (low nickel grade containing 0.31% Ni) - ground in a steel mill (Heiskanen *et al.*, 1991).

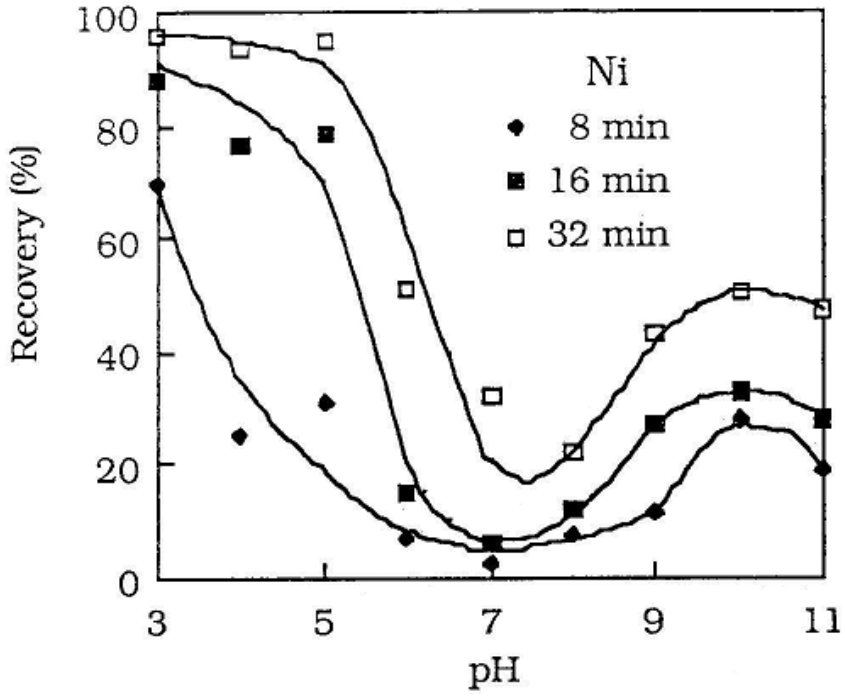

Figure 2.3: Effect of pH and time on nickel recovery with serpentine ore - ground in a steel mill (Heiskanen *et al.*, 1991).

2.2.4.2 Effect of aeration on the recovery of nickel from nickel-copper sulfide ores

Aeration has been seen to improve collectorless flotation of nickel sulfide minerals (Heiskanen *et al*., 1991; Kirjavainen *et al*., 2002; Kirjavainen & Heiskanen, 2007). Heiskanen *et al*. (1991) studied the effect of pulp aeration on natural floatability of nickel at a pH of 8, using a noritic ore type. Twenty minutes of aeration improved the flotation efficiency of nickel (see Figure 2.4). However, aeration times longer than twenty minutes resulted in a depressing effect. In a collector induced flotation, the copper activation process was found to be less effective on highly oxidised pentlandite and pyrrhotite surfaces (Gerson & Jasieniak, 2008). A poor nickel grade–recovery relationship was observed for a stockpiled nickel copper sulfide ore (Kelebek *et al*., 2007). The performance of stockpiled feed was attributed to the effect of oxidation. Kelebek *et al*. (2007) proposed that activation by ions released into the stockpiled feed may have contributed to the grade-recovery relationship.

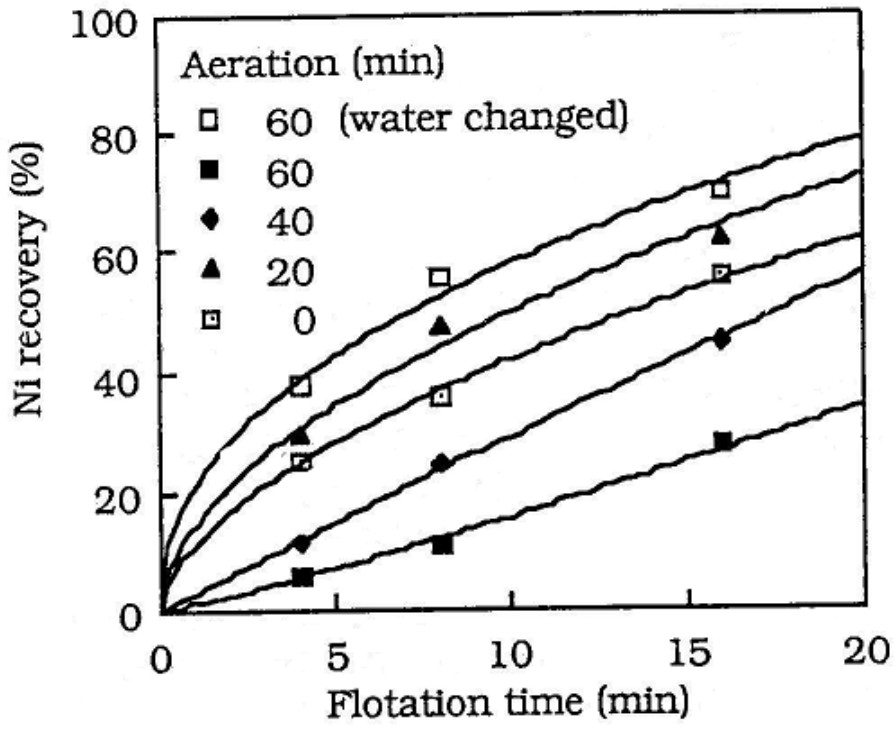

Figure 2.4: Effect of aeration on nickel recovery at pH 8; Noritic ore was ground in a steel mill. (Noritc ore is a low grade nickel ore containing 0.31% Ni) (Heiskanen *et al*., 1991).

.

2.2.4.3. The effect of compositional variation of pentlandite on flotation properties

Chanturiya *et al*. (2004) showed the flotation kinetics of pentlandite with varying chemical compositions from copper–nickel ore of the Pechenga ore field. The ore had a sulfide content of 10%. It consisted of: 53.98 wt % pyrrhotite, 29.25 wt % pentlandite and violarite, 2.81 wt % of chalcopyrite, 5.7 wt % magnetite and silicates. The ore was ground to -0.1mm. The flotation was performed at a pH of 9, in three stages: between bath time flotation, basic flotation and control flotation. Reagents used were: xanthate (170 g/t) as collector, aerofroth as frother (120 g/t), sodium bicarbonate (2000 g/t) and copper sulphate (50 g/t). In the first flotation stage (i.e. between bath flotation) 2000 g/t of sodium bicarbonate, 102 g/t xanthate and 60 g/t of aerofroth were added. The tails of the first flotation test were floated in basic flotation stage where 50g/t of copper sulphate, 51 g/t of xanthate and 36 g/t of aerofloat were added. The tails of basic flotation test were then floated in the control flotation stage. Aerofroth and xanthate were added at concentrations of 24 g/t and 17 g/t respectively. X-ray diffraction was employed to evaluate the chemical composition of violarite and pentlandite (Chanturiya *et al.*, 2004).

From the X-ray diffraction data, nickel-rich pentlandite was found to be the easiest to float when compared to cobalt and iron-rich pentlandite as well as to ordinary pentlandite (Figure 2.5). The distinction in the flotation kinetics of pentlandites with various compositions was attributed to the effect of chemical composition on open circuit potential.

Chanturiya *et al.* (2004) proposed that when the open circuit potential of pentlandite is lower than that of the mineral contacting with it, the anodic process (i.e. adsorption of xanthate) will be concentrated predominantly on the surface of pentlandite. In a case wherein the open circuit potential is higher than the mineral contacting with it, the anodic process will be enhanced on the other mineral, thus resulting in low flotation recoveries. However, no data was provided to illustrate this effect.

Iron-rich pentlandite is defined as a pentlandite with a greater molar quantity of iron than of nickel; nickel-rich pentlandite is defined as a greater nickel quantity than iron quantity;

cobalt-rich pentlandite is defined as a pentlandite wherein cobalt is the prevailing component, i.e. ordinary pentlandite-molar quantities of nickel and iron are equal

.

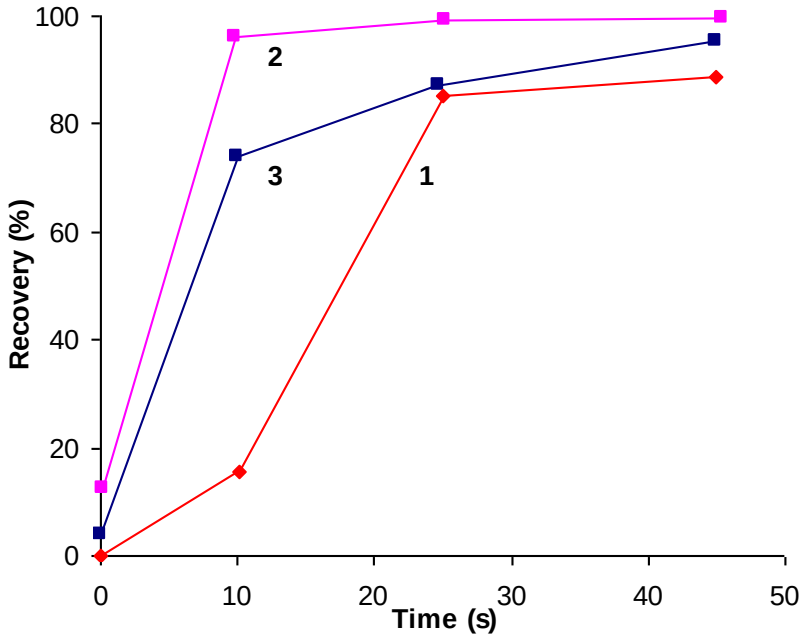

Figure 2.5: Flotation kinetics of pentlandite: (1) Fe-rich and ordinary pentlandite, (2) Ni-enriched pentlandite and (3) Co-enriched pentlandite (re-drawn from data published by Chanturiya *et al*., 2004).

2.2.4.3. Effect of galvanic interactions

Galvanic interaction can be defined as an electrochemical reaction that occurs as a result of one metal being in contact with another metal in a conducting, corrosive environment (Oldfield, 1988). Sulfide minerals are semi-conductors (Vaughan and Craig, 1978). In sulfide flotation, galvanic interactions occur when two sulfide minerals are in contact in the same solution or when a sulfide mineral is in contact with grinding media (Nakazawa and Iwasaki, 1985; Cheng and Iwasaki, 1992; Ekmekci and Demirel, 1997; Bozkurt *et al*., 1998; Greet *et al*., 2005). The galvanic interaction is stimulated by the potential difference that exists between the two sulfides. The mineral with the lowest rest potential becomes anode while the one with the highest rest potential becomes cathode (Vaughan and Craig, 1978; Jones, 2005). When two sulfide minerals are in contact, the rest potential or equilibrium potential of the system will fall somewhere between the reversible potentials of the two minerals. The system will thus be oxidising to the anode and reducing to the cathode.

Several authors investigated the effect of galvanic interactions on the flotation behaviour of various sulfides (Nakazawa and Iwasaki, 1985; Cheng and Iwasaki, 1992; Ekmekci and Demirel, 1997; Bozkurt *et al*., 1998). The floatability of pyrrhotite was improved when it was in contact with pyrite (Nakazawa and Iwasaki, 1985). This was attributed to the shift in reduction of oxygen from pyrrhotite site to pyrite and the oxidation of xanthate on pyrrhotite. A similar observation was observed for pyrrhotite in contact with chalcopyrite (Cheng and Iwasaki, 1992). Increased xanthate adsorption (i.e. oxidation of xanthate) was observed on pyrrhotite. When pyrrhotite was in contact with chalcopyrite, a reduction of oxygen was enhanced on chalcopyrite and oxidation of xanthate on pyrrhotite. Bozkurt *et al*. (1998) investigated the adsorption of xanthate on pentlandite in the presence of pyrrhotite. In contrast, when pentlandite was in contact with pyrrhotite, the oxidation of xanthate to dixanthogen (equation 3) was enhanced on the pentlandite surface and the reduction of oxygen (equation 4) on the pyrrhotite surface due to the differences in the open circuit potentials.

$$2X^- \rightarrow X_2 + 2e^- \quad (3)$$

$$\frac{1}{2}O_2 + H_2O + 2e^- \rightarrow 2OH^- \quad (4)$$

From previous studies, it is evident that in collector-induced flotation, oxidation of sulfide minerals arising from galvanic interactions changes the reagent adsorption chemistry amongst minerals. The differences in the floatability of sulfide minerals are determined by the differences in the activity of the reduction of oxygen (Rand, 1977). Rand (1977) showed that the activity for the reduction of oxygen varies considerably amongst different sulfides (see Figure 2.6). Pyrite was found to be the most active mineral and pyrrhotite the least active mineral. How the galvanic effect may be influenced by the mineralogical variations of the minerals has not been substantiated.

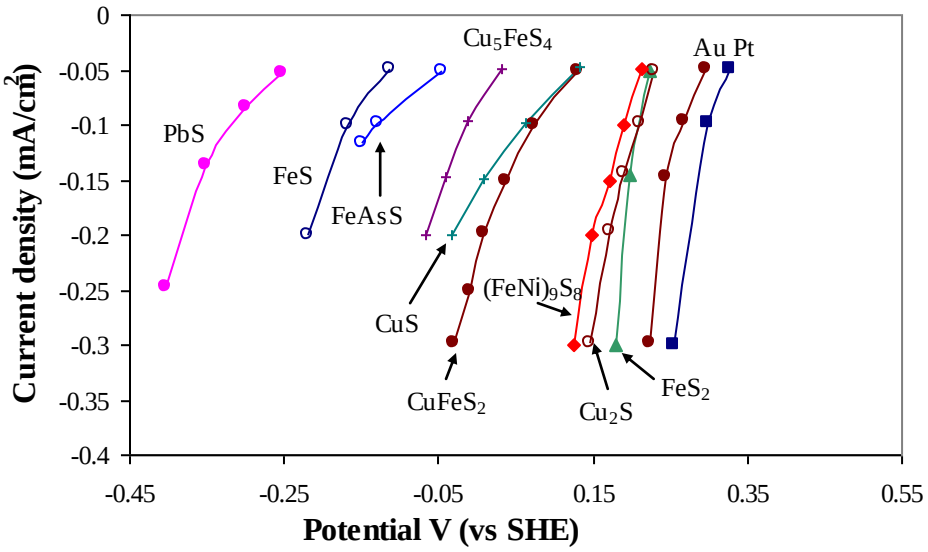

Figure 2.6: Current potential curves for oxygen reduction on a range of sulfide minerals at pH 9.2 (re-drawn from data published by Rand, 1977).

The floatability of sulfide minerals can also be affected by the galvanic interaction that occurs between the sulfide mineral and the grinding media. When sulfide minerals are brought into contact with ferrous grinding media, grinding media acts as the anode since it has the lowest rest potential compared to all other components in the system (Greet *et al*., 2005). Ferrous grinding media will be oxidized, producing iron oxide species that will cover the floating mineral and thus lower its recovery. This effect is reduced by replacing ferrous grinding media with chrome grinding media (Greet *et al.*, 2005).

2.3 Electrochemistry

Electrochemical studies have been widely used to elucidate the oxidation behaviour of sulfide minerals in aqueous media (Trahar, 1984; Woods, 1984; Buckley and Woods, 1991; Khan and Kelebek, 2004; Vermaak *et al*., 2004). Pentlandite is a metallic conductor (Craig and Vaughan, 1978). In aqueous media, reactions occurring on a pentlandite surface in the presence and absence of oxygen are electrochemical in nature. Therefore, the surface chemistry of pentlandite can be analysed using electrochemical techniques. Electrochemical techniques such as cyclic voltammetry and rest potential measurements have been used to characterize the oxidation reactions occurring on pentlandite in alkaline media (Hodgson and Agar, 1989; Buckley and Woods, 1991; Khan and Kelebek, 2004).

2.3.1 Cyclic voltammetry

Cyclic voltammetry provides useful information on the oxidation state of a mineral surface, including the potentials at which reduction or oxidation of the mineral surface occurs. Buckley and Woods (1991) investigated the electrochemical oxidation of a stationary natural pentlandite electrode, obtained from Kambalda, Australia and with a composition in the range $Fe_4Ni_{4.5}Co_{0.04}S_8$ to $Fe_{4.5}Ni_5Co_{0.03}S_{8.}$ The voltammetric investigation was carried out in a sodium tetraborate solution of pH 9.2 in the absence of oxygen. The anodic peaks formed at a potential of 0.05 V_{SHE} (A1) and 0.55 V_{SHE} (A2); these peaks were associated with the formation of iron (III) hydroxide species, and sulphates respectively (see Figure 2.7). The cathodic peak observed at a potential of -0.4 V_{SHE} (C1) was associated with the reduction of formed iron oxide (III). A reduction peak at a potential of -0.4 V_{SHE} serves as an indication that the oxidation products stay on the pentlandite surface. XPS investigations, on the same electrode, confirmed the presence of iron and nickel oxides on the pentlandite surface during oxidation after an hour.

It is evident from the cyclic voltammetric investigation that in aqueous media iron is preferentially removed from pentlandite irrespective of its composition. This is similar to the oxidation behaviour observed on a synthetic pentlandite. However, in cases where there was significant compositional variation, a different behaviour was observed for different forms of chalcopyrite (Vaughan *et al.*, 1995).

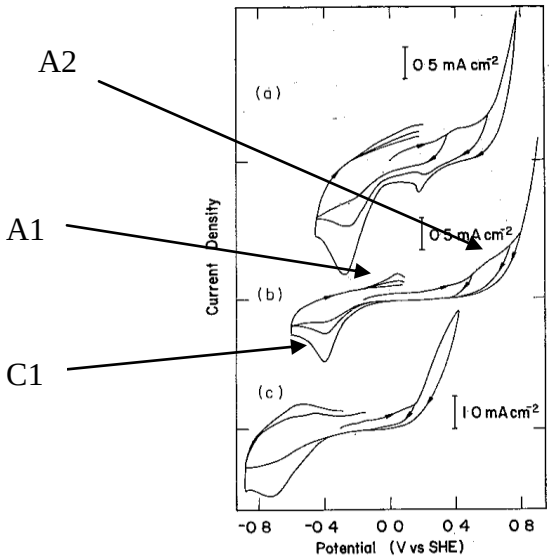

Figure 2.7: Voltammograms of natural Kambalda pentlandite electrodes in solutions of pH 4.6 (a), 9.2 (b) and 13 (c) (Buckley and Woods, 1991).

Vaughan *et al*. (1995) employed linear potential sweep voltammetry (i.e. half-cyclic voltammetry) to investigate the electrochemical oxidation of different forms of chalcopyrite with significant compositional variations. Synthetic chalcopyrite [$CuFeS_2$], haycockite [$Cu_4Fe_5S_8$], mooihoekite [$Cu_9Fe_9S_{16}$] and talnakhite [$Cu_9Fe_8S_{16}$] were used to conduct the investigation in various electrolytes at various electrode potentials. In an alkaline medium at a pH of 9.2, clear differences were observed (see Figure 2.8). At lower potentials of 0.22 V_{SCE} (SCE–saturated calomel electrode = +0.242 V_{SHE}), chalcopyrite had a lower current density indicating its low reactivity when compared to other sulfides. At potentials above 0.22 V_{SCE}, chalcopyrite resulted in high current density, showing its increased reactivity. Other sulfides (i.e. haycockite, mooihoekite, talnakhite) resulted in lower current densities, indicating that they have readily oxidised to form passivating oxidation products that retard further oxidation. Possible reasons for the differences in the reactivity of the different forms of chalcopyrite were attributed to the different oxidation products.

Proposed reactions responsible for behaviour of the electrodes at potentials below 0.22 V_{SCE} were considered:

$$Cu_xFe_yS_z + 3yOH^- \rightarrow Cu_xS_z + yFe(OH)_3 + 3ye^- \quad (5)$$

$$2Cu_xFe_yS_z + 6yOH^- \rightarrow 2Cu_xS_z + yFe_2O_3 + 3yH_2O + 6ye^- \quad (6)$$

At potentials above 0.4 V_{SCE}, the following reactions were considered to occur:

$$Cu_xS_z + 2OH^- \rightarrow xCu(OH)_2 + zS + 2xe^- \quad (7)$$

$$Cu_xS_z + 2xOH^- \rightarrow xCuO + zS + xH_2O + 2xe^- \quad (8)$$

$$Cu_xS_z + (2x + 8z)OH^- \rightarrow xCuO + zSO_4^{2-} + (x + 4z)H_2O + (2x + 6z)e^- \quad (9)$$

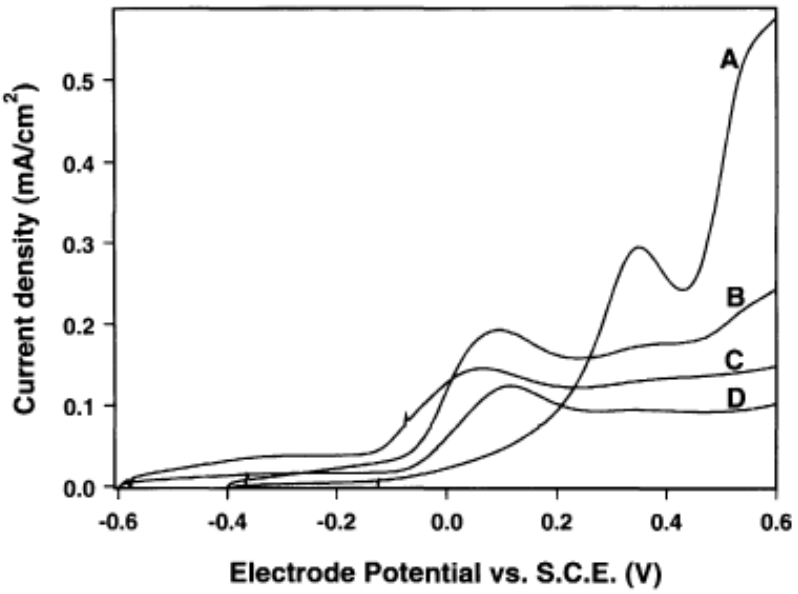

Figure 2.8: Linear potential sweep voltammograms of Cu-Fe-S compounds in 0.1 M $Na_2B_4O_7$ at 298 K; scan rate 20 mV/s: Chalcopyrite (A), haycockite (B), mooihoekite (C), talnakhite (D) (Vaughan *et al.*, 1995).

Oxidation of chalcopyrite was enhanced at potentials above 0.2 V_{SCE}. Possible reactions responsible for the oxidation are as follows:

$$Cu_xFe_yS_z + (4x + 6y)OH^- \rightarrow 2xCuO + yFe_2O_3 + (2x + 3y)H_2O + 2zS + (4x + 6y)e^- \quad (10)$$

$$2Cu_xFe_yS_z + (4x + 6y + 16z)OH^- \rightarrow 2xCuO + yFe_2O_3 + (2x + 3y + 8z)H_2O + 2zSO_4^{2-} + (4x + 6y + 12z)e^- \quad (11)$$

Vaughan *et al*. (1995) proposed that at higher potentials, sulfur within chalcopyrite might be oxidising to sulfate, making oxidation film porous and giving high currents. Current density measured with time at electrode potentials from rest potential to 0.4 V_{SCE} confirmed that the oxidation rates of the chalcopyrite, haycockite and mooihoekite are time dependent (see Figure 2.9). Figure 2.9 shows changes in current density with time for the electrodes at pH 9.2.

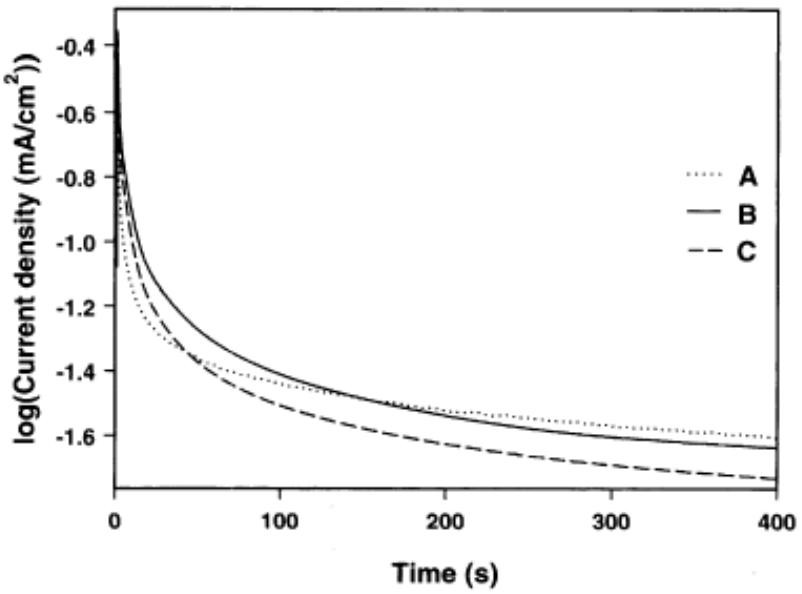

Figure 2.9: Current density–time transients in response to a step in electrode potential from rest potential to 0.4 V_{SCE} in 0.1 M $Na_2B_4O_7$ at 298 K: Chalcopyrite (A), haycockite (B), mooihoekite (C) (Vaughan *et al*, 1995).

The work performed on different forms of chalcopyrite indicates that linear anodic voltammetry may be used to determine the effect of compositional variation on the electrochemical oxidation. From the results, it is evident that anodic oxidation of electrodes with significant compositional variation are time dependent and depend strongly on the oxidation products.

2.3.2 Rest potential

The rest potential (i.e. mixed potential) of a mineral electrode is the potential difference across the mineral–solution interface when the mineral electrode surface is at equilibrium with the electrochemical reactions occurring at the surface (Woods, 1984). Its measure provides information on the identity of reactions occurring at the electrode/solution interface and can be related to the reactivity of the mineral surface. Figure 2.10 indicates the rest potential measured for pentlandite electrode in an air saturated tetraborate solution of pH 9.2 (graph 1). After 50 minutes, the rest potential of a pentlandite electrode was 0.246 V_{SHE} (Khan and Kelebek, 2004). This is similar to the findings of Buckley and Woods (1991). The rest potential (i.e. mixed potential) obtained at this

potential is the equilibrium potential attained on the electrode surface due to the reduction of oxygen on the surface and oxidation of pentlandite.

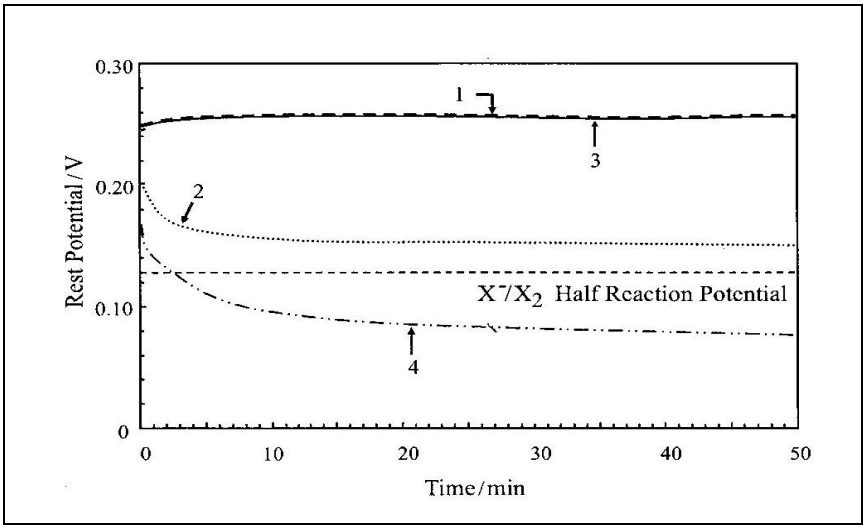

Figure 2.10: Rest potential of a pentlandite electrode under various xanthate and dissolved oxygen concentrations at pH 9.2. (1) DO (dissolved oxygen) = 8.15 mg/l, X (xanthate) = 0 mol/m^3, (2) DO = 0.1 mg/l, X = 0 mol/m^3, (3) X = 8.15 mg/l, X (xanthate) = 0.1 mol/m^3, (4) X = 0.1 mg/l, X (xanthate) = 0.1 mol/m^3 (Khan and Kelebek, 2004).

In comparison to pentlandite, the rest potential of pyrrhotite in an air saturated borate solution of pH 9.2 was found to be 0.18 V_{SHE} (see Figure 2.11) after 50 minutes (Khan and Kelebek, 2004); this is lower than of pentlandite indicating an increased reactivity of pyrrhotite and a poor catalyst for the reduction of oxygen (Rand, 1977). The effect mineralogical variations may have on the rest potential measurements of pentlandite is currently unknown. The variation of rest potential of pyrites from a wide variety of geological environments with different minor and trace element content was found to be considerably less than the difference in rest potentials between pyrite and other mineral sulfides of different chemistry (Abraitis *et al*., 2004). Mineralogical variations of sulfide minerals may not have a significant effect on the rest potential measurements.

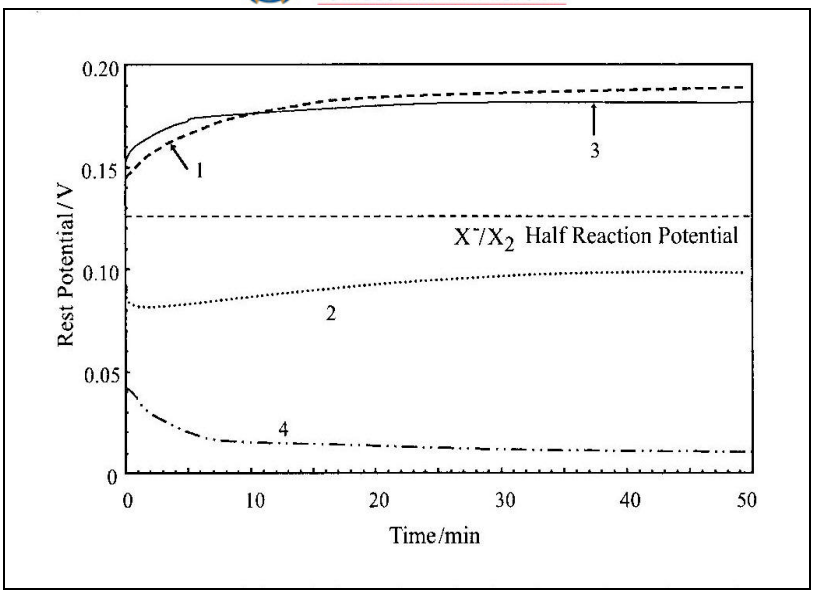

Figure 2.11: Rest potential variation of pyrrhotite electrode under various dissolved and xanthate conditions as indicated by the numbers (1-4) at a pH 9.2. (1) DO (dissolved oxygen) = 8.15 mg/l, X (xanthate) = 0 mol/m^3, (2) DO = 0.1 mg/l, X = 0 mol/m^3, (3) X = 8.15 mg/l, X (xanthate) = 0.1 mol/m^3, (4) X = 0.1 mg/l, X (xanthate) = 0.1 mol/m^3 (Khan and Kelebek, 2004).

2.3.3 Electrochemical Impedance Spectroscopy

Electrochemical Impedance Spectroscopy (EIS) has been widely used in electrochemical systems to ascertain the mechanism of reduction or oxidation reactions occurring on various electrodes (Macdonald & McKubre, 1982; Silverman, 1986; Mendiratta, 2000). When an electrode is placed in an electrolyte, it undergoes Faradaic process, involving the transfer of charge across the electrode–electrolyte interphase (Mendiratta, 2000; Jones, 2005). It is the electrode–electrolyte phenomena that may be modeled using the impedance AC circuit theory to facilitate the understanding of the mechanism and the rate of the reactions in an electrochemical aqueous system. The electrochemical impedance technique models the electrochemical reactions in terms of circuit elements, such as resistors, capacitors and inductors. The oxidation characteristics of sulfide minerals may be studied using this technique. Changes in the surface layer of oxidised sulfide mineral can also be drawn from these measurements.

The electrochemical oxidation of sulfide minerals is electrochemical in nature and involves transfer of electron (Biegler *et al*., 1975; Trahar, 1984; Woods, 1984). The rate

of oxidation is governed by electron transfer at the electrode and the mass transfer rate of the reactants toward the interface.

2.3.3.1 Characterisation of an electrochemical process

An activation or diffusion controlled electrochemical reaction may be characterized by electrochemical impedance spectroscopy using Bode and Nyquist plots. When an AC voltage is applied across a circuit composed of resistors only, the resultant current is also a sine or cosine wave of the same frequency with no phase shift. However if the circuit consists of capacitors and inductors, the resulting current will be shifted in time - known as a phase angle shift. The resulting response is measured as the impedance Z. The impedance may be expressed in terms of real (Z') and imaginary (Z") components. When the components are plotted against each other, the plot is known as a Nyquist plot. It is the shape of this plot that characterises an electrochemical reaction.

A simple electrochemical process under activation control is characterised by a semi-circle on a Nyquist plot (see Figure 2.12) with increasing frequency in a counter-clockwise direction. At very high frequency, the imaginary part (Z") disappears leaving only the solution resistance R_Ω. At very low frequency, the imaginary part (Z") disappears again, leaving a sum of solution resistance (R_Ω) and polarization resistance (Rp). The circuit to model this simple charge process is indicated in Figure 2.13.

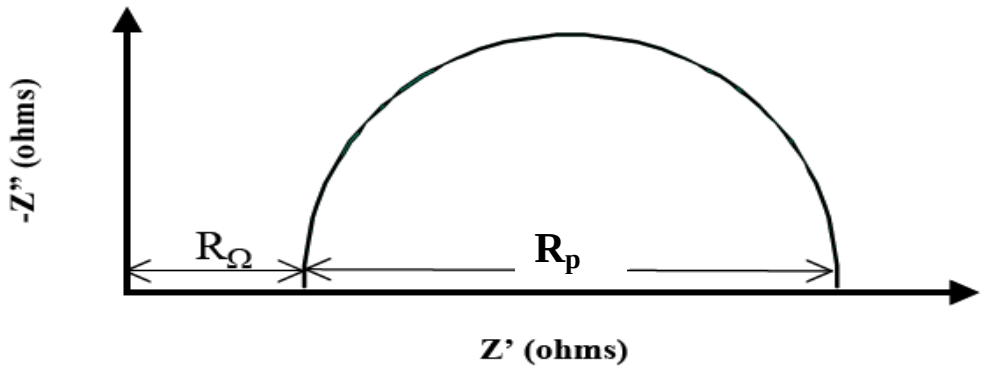

Figure 2.12 Nyquist plot of a simple charge transfer process (Mendiratta, 2000).

The model circuit for a simple charge process consists of a resistor (Rp) in parallel with a capacitor (C): the two that are in series with a solution resistance (see Figure 2.13).

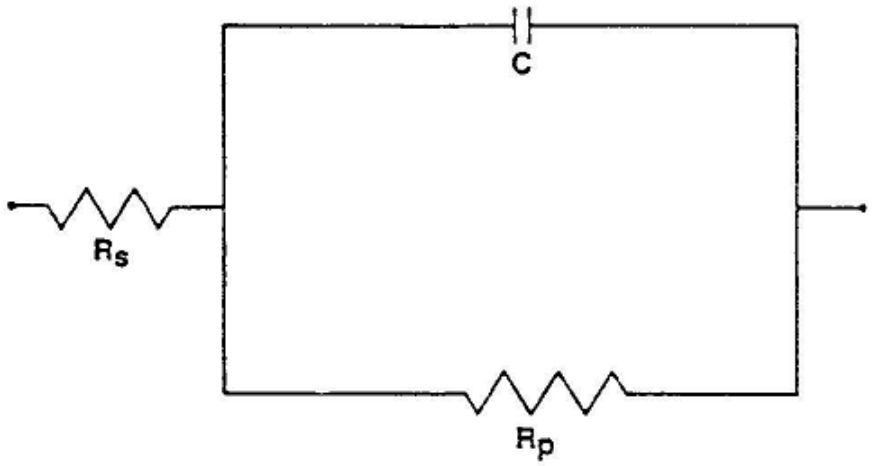

Figure 2.13: Circuit that models simple charge transfer process indicated in Figure 2.9 (Silverman, 1986).

Electrochemical impedance behaviour of an electrode in the case of a diffusion-controlled process has a unique characteristic, known as Warburg impedance. Figure 2.14 shows a Nyquist plot for a diffusion-controlled process. In the low frequency limit, the current is a constant 45 degrees out of phase with potential excitation. This situation is influenced by the diffusion through some type of surface becoming the dominating process. A circuit used to model this type of a process in indicated in Figure 2.15.

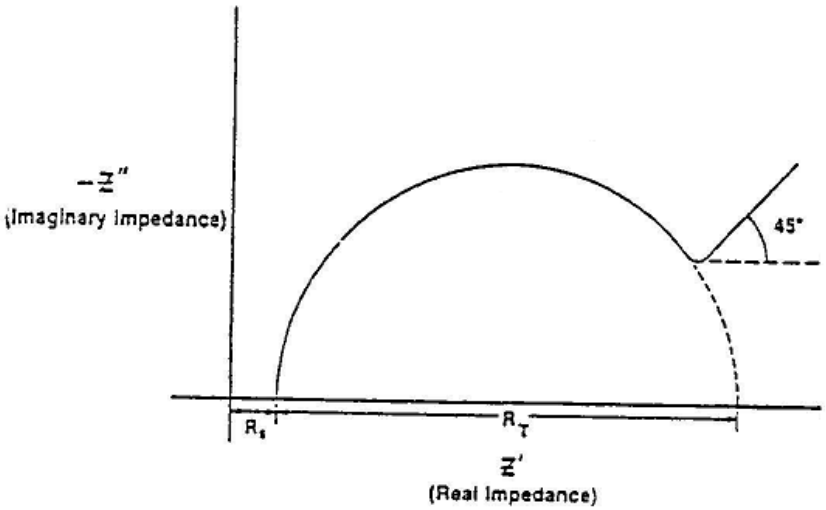

Figure 2.14: Nyquist plot for a simple charge transfer process in the presence of diffusion (Silverman, 1986).

A circuit used to model a diffusion-controlled process consists of a Warburg impedance component in addition to a simple charge transfer process circuit (see Figure 2.13).

In the presence of oxygen, the electrochemical oxidation of pentlandite may follow diffusion controlled behaviour.

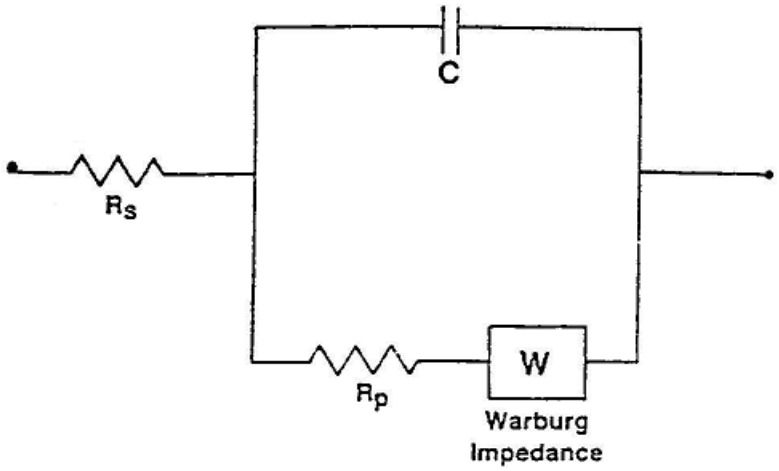

Figure 2.15: Circuit that models impedance in a diffusion controlled reaction (Silverman, 1986).

An alternative method to plot a simple charge transfer process is by Bode plot (Silverman, 1986). A Bode plot is a plot of impedance (Z) against frequency and the inverse of a phase shift (Θ) against frequency (see Figure 2.16). The advantage of this plot is that the frequency is explicit and may be used to produce semi-circles when plotted as Nyquist plots. Similar with the Nyquist plot, circuit elements such as Rp (polarization resistance), R_Ω (solution resistance) and C (capacitance) can be determined from the plot. Rp is obtained at very low frequency as the difference between the low frequency limit and the high frequency limit, while Rs (i.e. R_Ω) is obtained at high frequency.

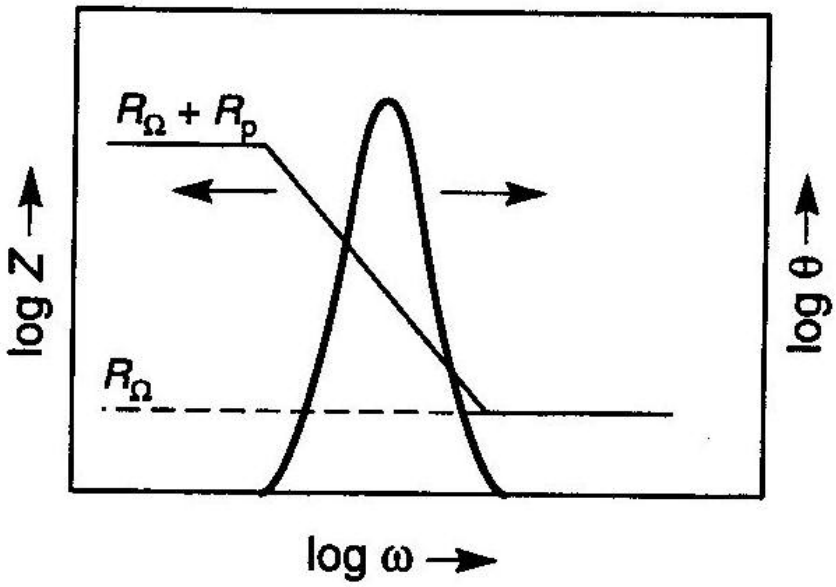

Figure 2.16: Bode plot for simple charge transfer process circuit (Jones, 2005).

2.3.3.2 Polarisation resistance

Polarisation resistance is one of the circuit elements the electrochemical impedance technique employs to model the electrode-electrolyte interphase. The electrode-electrolyte that is also acting as a capacitor offers a resistance to the transfer of electrons occurring due to polarisation. Such a resistance is known as charge transfer resistance or polarisation resistance (Rp). The significance of this resistance is that it is inversely proportional to the rate of the reactions (Silverman, 1986; Mendiratta, 2000). As a result, it may be used as a measure to probe the reactivity of an electrode. The advantage of the technique is that it is non-destructive and may be repeated numerous times on the same electrode (Jones, 2005).

The polarisation resistance method has been previously used to study the oxidation kinetics of various sulfide minerals (Tolley *et al*., 1996; Mendiratta, 2000). For freshly cleaved chalcocite, chalcopyrite and pyrite, oxidation increased the polarisation resistance in aerated borate solution (Tolley *et al*., 1996). The increase was attributed to the formation of increasing iron hydroxide amounts at the surface. Extended oxidation periods, resulted in a further increase in the polarisation resistance values, indicating reduced reactivity of the electrode. In deaerated borate solution of pH 9.2, Mendiratta

(2000) observed large polarisation resistance values for a freshly fractured pyrite electrode after progressive oxidation between potentials of -0.28 V_{SHE} and 0.75 V_{SHE} indicating the decreased reactivity of pyrite. However, in all the studies conducted, the polarisation resistance was determined from the electrochemical impedance data (i.e. from the Bode and or the Nyquist plot) as a single value. In the Bode plot, Rp was obtained at very low frequency as the difference between the low frequency limit and the high frequency limit as already discussed in section 2.3.3.1. In the Nyquist plot, polarisation resistance was estimated as the radius of the semi-circle in the kinetically controlled region (see Figure 2.12 for an example of the Nyquist plot). The disadvantage of using the Bode plot and the Nyquist plot is that in some instances the polarisation resistance (i.e. Rp) is estimated by extrapolation.

The previous work indicates that oxidation increases polarisation resistance. The measure of polarisation resistance with time will provide insight into the oxidation behaviour of pentlandite in an oxygen-rich environment.

2.3.3.3 Capacitance

Capacitance measurement is a measure of the storage of charge during half an AC cycle with the charge returned during the other half of the cycle (Morrison, 1984). The capacitance effect is a result of the double layer charging effect (C_D) and possible surface layers (C_s) forming at the electrode (Vermaak *et al.*, 2004). Formation of surface layers cause total electrode capacitance to decrease, as indicated by equation 5.

$$\frac{1}{C} = \frac{1}{C_D} + \frac{1}{C_S} \qquad [12]$$

A decrease in the circuit capacitance value is used as a measure to indicate the formation and growth rate of films. However, the capacitance that develops does not only indicate the formation of the surface layers but may also indicate the conductivity characteristics of the oxide film. The conductivity characteristics of the formed film may result in the variation of the dielectric constant of the oxide film and cause the capacitance value to increase instead (Craig, 1991; Rahim, 1995). The higher the dielectric constant, the more

a film behaves like an insulator. A conducting oxide film will have a lower dielectric constant than a non-conducting (i.e. more insulating) oxide film. A lower dielectric constant results in a higher capacitance value: see equations 13 to 15, where C is the capacitance of the oxide, Rp = polarisation resistance, f = frequency, t = thickness of the oxide film, A = true surface area of the electrode, ε is the electric permittivity of the film, ε_o- is the permittivity of the free space and K = dielectric constant (Craig, 1991).

$$C = \frac{1}{2\pi R_p f} \quad [13]$$

$$t = \frac{A\varepsilon}{C} \quad [14]$$

$$\varepsilon = K\varepsilon_0 \quad [15]$$

The properties of oxide films forming on sulfide minerals when oxidised are important in understanding the oxidation or reduction reactions (Chander, 1984). Ionic conductivity, electronic conductivity, composition, structure, thickness and reactivity are characteristics of oxide film considered important in understanding the oxidation or reduction reactions on sulfide minerals (Chander, 1984). Capacitance measurements may be used to indicate the formation of the oxide layer and to elucidate the conductivity characteristics of formed films.

3. CONCLUSIONS

It has been found that nickel sulfides from different sources (ores) display different behaviour during froth flotation. Different nickel recoveries have been observed from different ores, and in some cases, from different areas of the same deposit. Beside other factors, such as mineralogical variations in the ores and dissolution of minerals, variation in the composition of pentlandite may also be a cause of such differences. Previous research confirms the compositional variation of pentlandite with significant variations of the chemical composition of pentlandite from different levels of the deposit or the reef. It is therefore expected that there is a compositional variation of pentlandite. The possible

effect these variations may have on the electrochemical behaviour of pentlandite is not clear. Currently, it is known that oxidation of pentlandite results in similar products irrespective of composition. The possible effect of composition on the characteristics of these oxidation products forming on the pentlandite surface has not been investigated. Properties of the oxide films such as composition, electronic conductivity, thickness and resistance may be influenced the compositional variation of the sulfide mineral and responsible for the reactivity of sulfide minerals in the flotation systems.

4. RESEARCH OBJECTIVE

The preceding literature overview indicated that there is a compositional variation of natural pentlandite from representative samples collected from various ore bodies. Pentlandite is recovered by milling and flotation and the previous mineralogical studies have not been performed from the flotation concentrate samples. The objective of the project was to determine if there is any compositional variation of pentlandite from the specific flotation concentrate samples collected and compositional variation of massive samples. The secondary aim was to determine the possible effect of pentlandite composition on the electrochemical behaviour of pentlandite with time using electrochemical techniques. The electrochemical studies performed on pentlandite, describe the behaviour thereof as a function of potential (as the electrochemical oxidation behaviour of sulfide minerals is also time dependent).

5. EXPERIMENTAL PROCEDURE

The following section describes the experimental methods employed in this study. The section identifies the deposits used to source pentlandite particles from PGE concentrates and massive pentlandite samples. The following aspects are discussed: methods employed to hand-pick pentlandite particles from the flotation concentrate; the procedure followed to construct and prepare pentlandite microelectrodes as well as the massive electrodes; the mineralogical analysis performed on pentlandite; and the techniques employed to perform the electrochemical measurements.

5.1 Samples employed

Pentlandite particles in the range ±100 μm in size from industrial processes and massive natural pentlandite samples were employed.

Pentlandite particles in the range of ±100 μm in size were employed as a result of the interest in the electrochemical behaviour of sulfide minerals from the actual flotation operations. Most fundamental electrochemistry studies of flotation processes are undertaken on synthetic or natural mineral samples of high purity. The natural sulfide samples are usually sourced from mineral dealers or locations where specimens are in the massive form. However, the chemical composition and behaviour of these samples do not always correspond with that of the sulfide mineral particles found in the actual plant operations (Vermaak *et al.*, 2006). The ±100 μm pentlandite particles were hand-picked from the concentrates of the flotation operations of Lebowa Merensky, Lebowa UG-2, Platreef and Nkomati Mine.

In the flotation operations, sulfide minerals are recovered in the flotation concentrate. It was for this reason that pentlandite particles had to be hand-picked from flotation concentrate samples in order to investigate the possible compositional variation of the particles recovered. It would be better to pick particles from the feed only as variations in chemical composition may result in particles ending up in the tails instead of the concentrate. Particles were picked from the concentrate purely because of the higher concentration of these particles. The PGE (i.e. Lebowa Merensky, Lebowa UG–2 and Platreef) and Ni-Cu sulfide (Nkomati Mine) deposits were used (see Figure A1 to A5 in

Appendix A for the geological maps indicating the location of the deposits). Pentlandite is recovered from the PGE and nickel-copper ores (Cabri, 1989; Xao and Laplante, 2004; Maier, 2005; Godel *et al*., 2007). The PGE and nickel-copper sulfide deposits were chosen to probe any differences between the pentlandite particles sourced from the PGE and nickel-copper sulfide flotation concentrates.

Pentlandite is predominantly associated with pyrrhotite and occurs as stringers or blebs in pyrrhotite or flame-like exsolutions in pyrrhotite (Francis *et al.*, 1976; Van Zyl, 1996; Theart and De Nooy, 2001). The typical grain size of pentlandite is in the range of 50 to 100 µm in diameter (Theart and De Nooy, 2001). Pentlandite particles in the range of ±100 µm size were hand-picked in order to make microelectrodes from the largest possible particles.

Massive natural pentlandite samples were sourced from the Pechenga deposit (Kola Peninsula in Russia), Nkomati Mine (Uitkomst Complex in South Africa) and Phoenix Mine (Botswana) (see Figures A6 to A9, in Appendix A for the geological maps indicating the location of the deposits). The received massive pentlandite from Kola Peninsula is shown in Figure 5.1. Pentlandite may occur in a massive (blocky) form. The massive (blocky) pentlandite often contains islands of pyrrhotite (Francis *et al.*, 1976). Massive pentlandite samples with minimal phases of other sulfide minerals were employed (see Figures C6 to C10 in Appendix C).

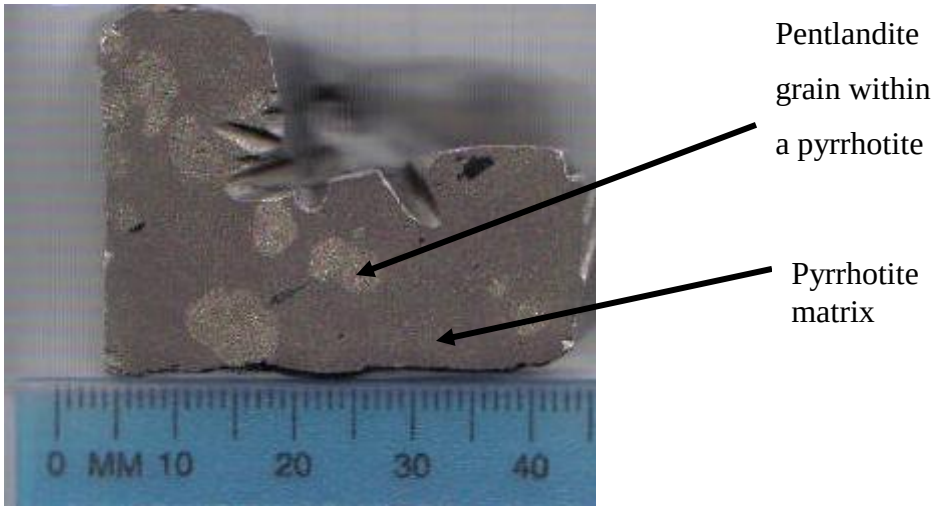

Figure 5.1: Massive sulfide received from Kola Peninsula (Russia) showing pentlandite grains (yellowish) within a pyrrhotite matrix massive sample.

5.2 Analysis of the flotation concentrate samples

5.2.1 X-ray diffraction (XRD) analysis, X-ray fluorescence spectroscopy (XRF) and scanning electron microscopy (SEM)

A PANalytical X'Pert Pro powder diffractometer instrument (XRD) with X'Celerator detector and variable divergence and receiving slits was used to identify crystalline minerals in the flotation concentrate samples. Each phase has a unique powder diffraction pattern and it is therefore possible to distinguish between compounds as the diffraction method is sensitive to crystal structure and not just composition (Loubser and Verryn, 2008). Each sample was milled in a McCrone micronizing mill and prepared for XRD using a back loading preparation method. The phases were identified by using PANalytical X'Pert Highscore plus software. The specifications on the XRD instrument and settings are shown in Table 5.1. X–ray diffraction was employed to determine and quantify the mineral composition of the received flotation concentrate samples (see Table B2, Figure B2 in Appendix B). The relative amount of pentlandite (wt %) was estimated by the Rietveld method using the Autoquan program. The amount of pentlandite was quantified to identify concentrate flotation samples with a higher concentration of pentlandite. Samples with as high a pentlandite concentration as possible were employed to ease the hand-picking of particles. Only the quantity of the pentlandite in the flotation samples is reported. X-ray diffraction (XRD) analyses were performed at the Geology Department at the University of Pretoria.

Table 5.1: Instrument and data collection parameters.

Instrument	PANalytical X'Pert Powder
Radiation	Co-Kα
Temperature	25°C
Specimen	Flat - plate rotating
Power setting	35 kV, 50 nA
Detector	X'Celerator detector
Range of 2Θ	5-90° 2Θ

X–ray fluorescence spectroscopy (XRF) was used to determine the bulk chemical composition of the flotation concentrate samples. The samples were prepared as pressed powder briquettes and introduced into the ARL 9400XP+ XRF spectrometer. Analyses were executed using the UniQuant software. The software analysed for all elements in the periodic table between Na and U, but only elements found above the detection limits were reported. XRF was employed to determine the content of major elements (i.e. copper and nickel) in the received flotation concentrate samples. All elements were expressed as oxides, except for Zn, Fe, Pb, Mn, Cu and Cd, which are usually associated with sulfur as sulfides. The nickel and copper contents of the flotation concentrate samples are reported in Table B1, Appendix B. The nickel oxide concentration was used as an indication of the pentlandite content within the samples.

A scanning electron microscope (SEM) (JSM-6300) was employed to identify the presence of liberated pentlandite particles in the polished sections of flotation concentrate samples. The samples were coated with gold prior to the analysis. Single liberated particles were identified by examining the polished sample with back-scattered electron imaging using a Centaurus back-scattered detector. The analysis was performed by a Voyager analysis system using a Si (Li) lithium drifted silicon detector with a Norvar window: analysing X-rays produced at 15 kV acceleration voltage with a working distance of 25 mm using 100 seconds of analysis time. Scanning electron microscope analyses were performed at IMMRI at the University of Pretoria. Back-scattered electron micrographs of the polished samples, indicating liberated pentlandite particles, are shown in Figures B1 and B2 in Appendix B. The micrographs show the presence of liberated pentlandite particles. It was thus not necessary to mill the flotation concentrate to further liberate pentlandite particles. Single liberated pentlandite particles in the range of ±100 µm were required to make microelectrodes.

5.3 Identification and separation of pentlandite particles from the flotation concentrate

5.3.1 Pre–concentration of pentlandite particles

Pentlandite is predominantly associated with pyrrhotite and occurs as stringers or blebs in pyrrhotite or flame like exsolutions in pyrrhotite (Francis *et al.,* 1976; Van Zyl, 1996;

Theart and De Nooy, 2001). Typical grain size of pentlandite (i.e. pentlandite from the massive sulfide body of the Uitkomst Complex, Mpumalanga, South Africa-nickel copper sulfide deposit) is in the range of 50 to 100 μm in diameter (Theart and De Nooy, 2001). Scanning electron microscope micrographs indicated the presence of liberated pentlandite particles larger than 100 μm in size. To concentrate these pentlandite particles, the slime content of the flotation concentrate samples was reduced by dry screening at 106 μm and 90 μm.

5.3.2 Hand-picking of pentlandite particles

Under an optical microscope, it was difficult to identify pure pentlandite particles from pyrrhotite, chalcopyrite and pyrite particles. As a result, the scanning electron microscope was employed to identify pentlandite particles from other base metal sulfides.

All shiny, bronze and yellow particles (approximately thirty particles per slide) were attached to a carbon tape (i.e. a black conductive tape) and adhered on 26 x 30 mm tinplate (see Figure 5.2 for the back-scattered micrograph showing particles on the tape). Energy dispersive X-ray analysis of the scanning electron microscope was used to identify pentlandite particles from base metal sulfides attached to the tape.

Since pentlandite is an Fe–Ni–S mineral, it was identified by Fe, Ni and S peaks on an EDX spectrum (see Figure 5.3). The 26 x 30 mm tinplate was properly marked to identify the position of pentlandite particles on the plate. Liberated pentlandite particles without the presence of other sulfide mineral phases were hand-picked. Particles with varying shapes were hand-picked. The investigation was not performed on pentlandite particles with a specific shape.

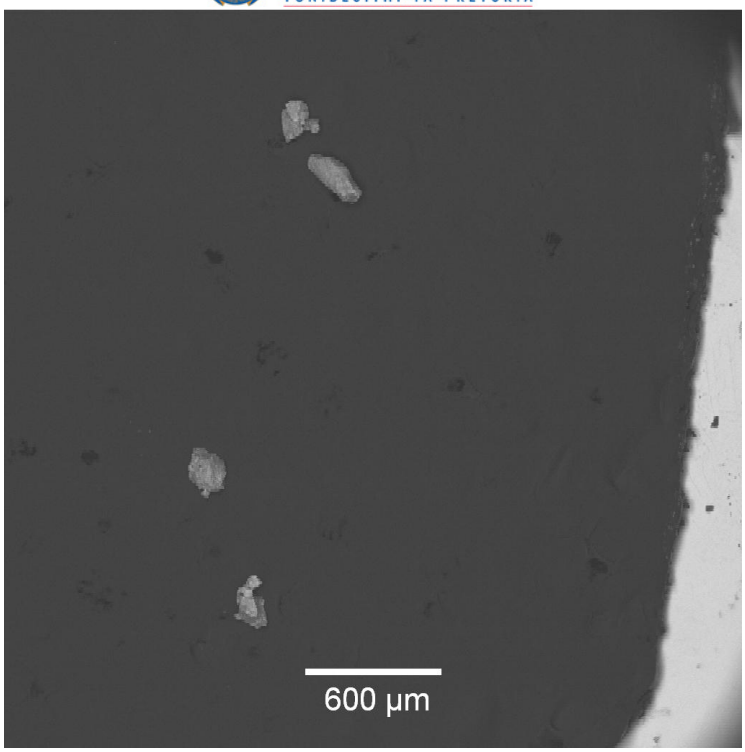

Figure 5.2: Back-scattered electron micrograph showing sulfide particles on a carbon tape. Acceleration voltage of 15 kV.

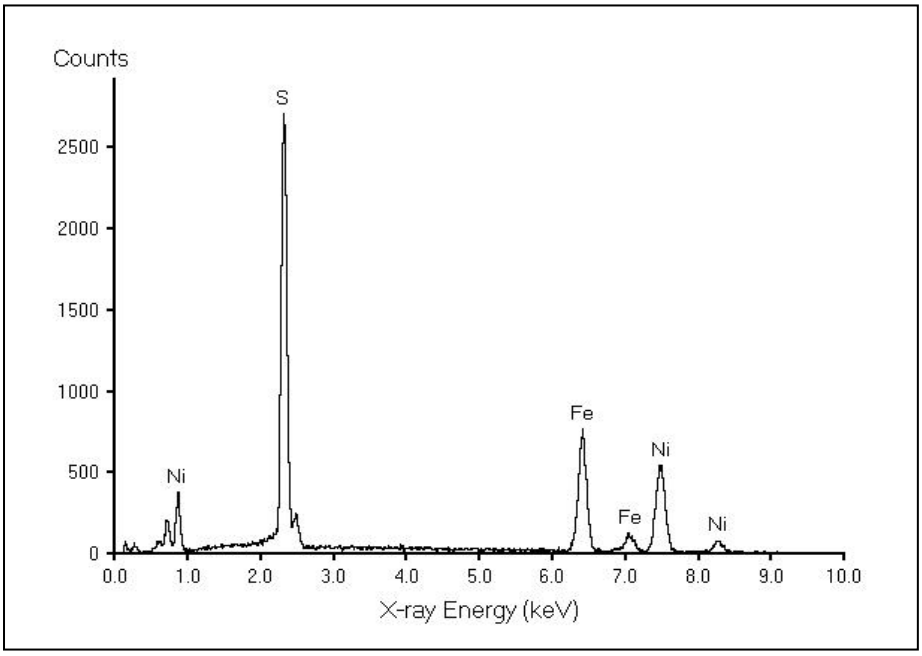

Figure 5.3: The energy dispersive X-ray spectrum (EDX) of a pentlandite particle.

5.4 Electrode preparation

Pentlandite electrodes were prepared from hand-picked pentlandite particles and massive pentlandite samples. Electrodes were prepared to achieve the necessary electrical contact required for the subsequent electrochemical measurements.

5.4.1 Massive electrode preparation

Massive pentlandite electrodes were prepared from massive samples sourced from the Nkomati Mine (Uitkomst Complex, South Africa), Pechenga deposit in Kola Peninsula (i.e. Russia) and Phoenix Mine (Botswana). Sourced massive samples indicated the presence of other mineral phases - mostly pyrrhotite. Pentlandite grains (in the range of ±2 mm to ±4 mm in diameter) with minimal sulfide mineral phases were removed from the massive samples with a dentist drill and dremill tool (a cutting tool). A 180 grade SiC paper was used to grind away any pyrrhotite phase on the edges of the pentlandite grain. A 0.5 mm copper wire and conductive epoxy [Part A (CW 2400) and Part B (CW 2400)] were used to achieve an electrical contact with the massive pentlandite grain. The resistance between the wire and the massive pentlandite grain was measured to ensure a low resistance (± 0.5 Ω).

The massive pentlandite grain-wire assembly was cold mounted (embedded) in a non-conducting epoxy resin (i.e. Struers epofix kit) supplied by IMP Scientific and Precision Company. The epoxy resin and hardener were mixed at a ratio of 15 parts resin to 2 parts hardener (by volume). Bubbles formed when stirring a mixture of the resin and hardener, were evacuated. The massive pentlandite-wire assembly was cold mounted in a 30 mm diameter perspex tubes. The perpex tube had an inner and outer diameter of 20 mm and 30 mm respectively. The resin was allowed to cure for 10 hours at room temperature.

To expose and prepare the surface of the electrode for subsequent electron microprobe analysis and electrochemical measurements, the epoxy was polished away. A Nikon SMZ-10A optical microscope was employed to investigate the surface for exposure during coarse polishing. A P-180 grade SiC paper was employed to polish away the epoxy resin. When the mineral was very close to being exposed, finer polishing stage was employed. A P-1200 grade SiC paper was employed to slowly expose the massive

pentlandite sample. Slow polishing was required to ensure that the epoxy does not break away from the edges of the sample (Vermaak *et al.*, 2006). After a small area of the surface was exposed (couple of microns), a 2400 grade SiC paper was employed to slowly expose the mineral surface further. A Jeol JSM-6300 scanning electron microscope (i.e. SEM) was employed to investigate the exposed surface for presence of other sulfide mineral phases.

A flat smooth surface required for the electron microprobe analysis was obtained using daran cloth and Struers MDNap polishing cloths, supplied by Advanced Laboratory Solutions and IMP Scientific and Precision Company respectively. Aka-daran cloth is a polishing cloth used for fine grinding with a 6-micron diamond suspension. The final smooth surface required for the electron microprobe analysis was obtained using a MDNap polishing cloth. MDNap polishing cloth is a cloth used for final polishing using 1-micron diamond suspension. The scanning electron microscope was again used to ensure that a flat smooth pentlandite surface was produced. Images of the massive samples are shown in Figures C6 to C10 in Appendix C. The massive pentlandite sample from Phoenix Mine contained a large pyrrhotite phase. The phase was covered with epoxy resin leaving a relatively pure pentlandite grain (see Figure C9, Appendix C).

5.4.2 Microelectrode preparation

Microelectrodes were prepared using approximately ±100 μm pentlandite particles (see section 5.4.1). An electrical contact with a single pentlandite particle was achieved using a wire assembly consisting of a 50 μm tungsten wire and 0.5 mm copper wire. Tungsten wire was cemented to a copper wire using silver paint (acheson silver dag 11415M, supplied by Agar Scientific). The wire assembly was mounted in an upright position and allowed to cure at room temperature. The tip of the 50 μm tungsten wire was dipped in a conductive epoxy (i.e. conductive glue) and slowly brought into contact with a single pentlandite particle placed on a glass slide using a 152 Micromanipulator (see Figure 5.4). Copper-tungsten wire assembly was injected in a pipette holder of a micromanipulator (see Figure 5.4) fitted on an optical microscope. The needle–like component travels a maximum distance of 25mm, 20mm and 25mm in the x, y and z directions respectively. Conductive epoxy was used instead of silver dag since silver dag cures too quickly (Vermaak *et al.*, 2006).

Figure 5.4: 152 Micromanipulator - a three dimensional coarse manual manipulator (The Narishe–Group).

Each pentlandite particle was carefully cemented at the bottom-end along the longest axis of the particle; this ensured good exposure and minimised the exposure of the wire or conductive epoxy after polishing. The particle–wire assembly was allowed to cure overnight at room temperature. After curing, the particle wire assembly was cold mounted in non-conducting epoxy resin (i.e. Struers epofix kit) comprising epoxy resin and hardener. Epoxy resin and hardener were mixed in a ratio of fifteen parts resin to two parts hardener (by volume). Bubbles formed in the mixture were evacuated to prevent them from being trapped around the particle, since they would interfere with the polishing of the particle. The pentlandite–wire assembly was cold mounted in a 30 mm diameter perspex tube. The epoxy resin was allowed to cure for 10 hours at room temperature - see Figure 5.5 for a schematic illustration of pentlandite microelectrode. The pentlandite surface was prepared similarly to the massive pentlandite electrode.

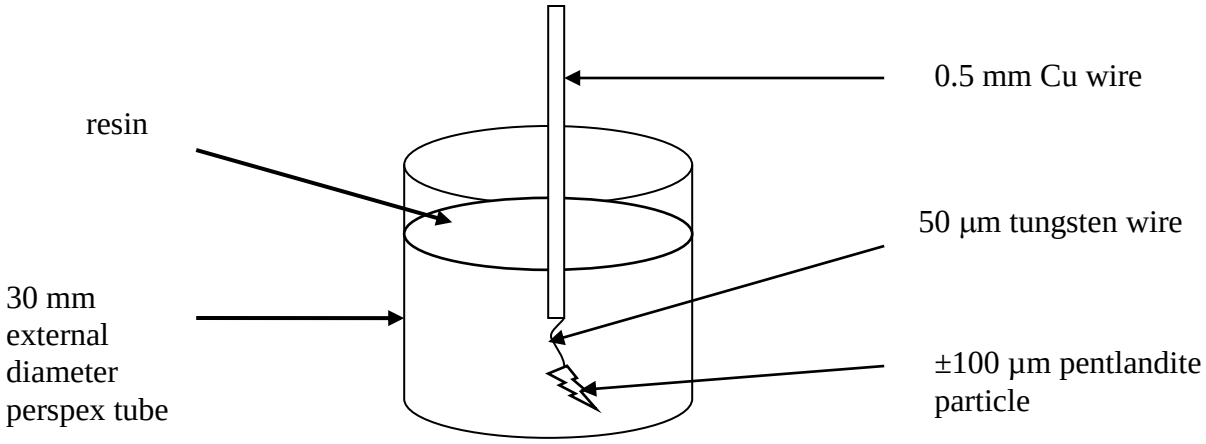

Figure 5.5: Schematic illustration of pentlandite microelectrode made from copper wire, tungsten wire and a pentlandite particle cold mounted in a Struers epofix kit resin.

5.5 Electron microprobe analysis

The composition of all hand-picked pentlandite grains was determined by electron microprobe analyses. For quantitative analysis, the surface of each pentlandite microelectrode was polished to a flat smooth surface, since any irregularities in the surface topography would alter the electron backscattering and X–ray absorption characteristics - and hence introduces errors into the analysis. For example, the surface roughness of a piece of sulfur resulted in variation in the sulfur X-ray emission across the surface (Cox, 1983) - and hence introduced errors in the analysis.

A flat, smooth surface required for the electron microprobe analysis was obtained using Aka-daran and MDNap polishing cloths. A daran cloth is a polishing cloth used for fine polishing with a 6-micron diamond suspension. The final smooth surface was obtained with a MDNap polishing cloth. MDNap polishing cloth is a cloth used for final polishing using a 1-micron diamond suspension. Polishing cloths were supplied by IMP Scientific Precision Company.

A Jeol JSM–6300 scanning electron microscope (i.e. SEM) was employed to investigate the surface for exposure of other sulfide mineral phases (see Figures C1 to C5, in Appendix C for back-scattered electron images of the microelectrodes).

Electron microprobe analysis was carried out with a Cameca SX-100 electron microprobe at the University of Pretoria. Pentlandite grains were analysed for Fe, Ni, Co, Cu and S. The following standards were used: troilite for S and Fe, nickel oxide for Ni, cobalt metal for Co and chalcopyrite for Cu. The electron microprobe was operated at an acceleration potential of 20 kV with a beam current of 20 μA. Counting time for Fe, Ni, Co and Cu was 20 seconds and 10 seconds for S. The number of spots analysed on each pentlandite particle was limited by particle size. Three to four spot analyses were performed on each pentlandite particle. The size of the pentlandite particle analysed was in the order of a ±100 μm. To minimize any analytical error, all pentlandite particles were analysed under the same electron microprobe calibration. Typical analytical errors were in the range indicated in Table 5.2.

Table 5.2: Analytical reproducility of S, Fe, Ni and Co in pentlandite calculated at the 95% confidence level.

Element	wt %	±
S	32.92	0.73
Fe	31.82	0.90
Ni	33.04	0.45
Co	0.8	0.06

5.6 Electrochemical measurements

Since pentlandite is a metallic conductor (Vaughan and Craig, 1978), electrochemical measurements were employed to investigate the electrochemical behaviour of massive and microelectrode pentlandite. All the electrochemical experiments were carried out in a conventional three-electrode cell using: mounted massive and microelectrode pentlandite as stationary working electrodes, inert platinum wires fitted in glass tubes with fritted glass ends as counter electrodes, and silver / silver chloride electrode as the reference electrode. Potentials were recorded against Ag/AgCl electrode filled with saturated KCl, giving a potential of +0.2 V against a standard hydrogen electrode (SHE). Inert platinum wires were placed at equal distances from the working electrode. In all the experiments, the working electrode was kept stationary. All the measurements were conducted in a 0.05 M sodium borate ($Na_2B_4O_7$) buffer solution (pH 9.3) at a temperature of 25°C

(±1°C). The solution was prepared using analytical grade sodium borate with distilled water of a final resistivity of 18 MΩ.cm. Potential was controlled with Schlumberger 1287 potentiostat. A Faraday Cage was employed to shield the experimental cell and the electrical connections from the external source of AC voltage (Suter *et al*., 1995) using insulated cables (i.e. BNC-BNC fully-insulated plugs with shrouded BNC plugs and impedance of 50 Ω, supplied by RS Components).

The following measurements were performed:

a) Polarisation resistance of the electrodes was measured over time at equilibrium potential. Measurements were performed in a borate solution in equilibrium with air [dissolved oxygen concentration (DO) of ~ 5 ppm]. A new pentlandite electrode was created between the experimental runs by polishing in 0.05 μm Alumina–B slurry, followed by rinsing with de-aerated de-ionised water to remove any adhering alumina particles from the surface of the electrode. After rinsing, the electrode was immediately transferred into the cell for the measurements. The massive (blocky) pentlandite often contains islands of pyrrhotite (Francis *et al.,* 1976). The polishing method was employed to maintain a pentlandite electrode with minimal pyrrhotite phase or other mineral sulfide, in order to prevent increased exposure of other mineral phases. Repeatable measurements were obtained from the polishing employed. The polarisation resistance technique scanned around the equilibrium potential (i.e. 10 mV above and below rest potential), giving cathodic currents (i.e. negative currents) below rest potential and anodic currents (i.e. positive currents) above rest potential. The technique simultaneously measured rest potential values (i.e. mixed potential). Polarisation resistance was measured as the slope of polarisation curve at equilibrium potential using Ohm's law (see Figure 5.6). Equilibrium potential (i.e. rest potential) was determined as the potential where anodic current was equal to the cathodic current. Polarisation resistance measurements were recorded at a scan rate of 10 mV/s.

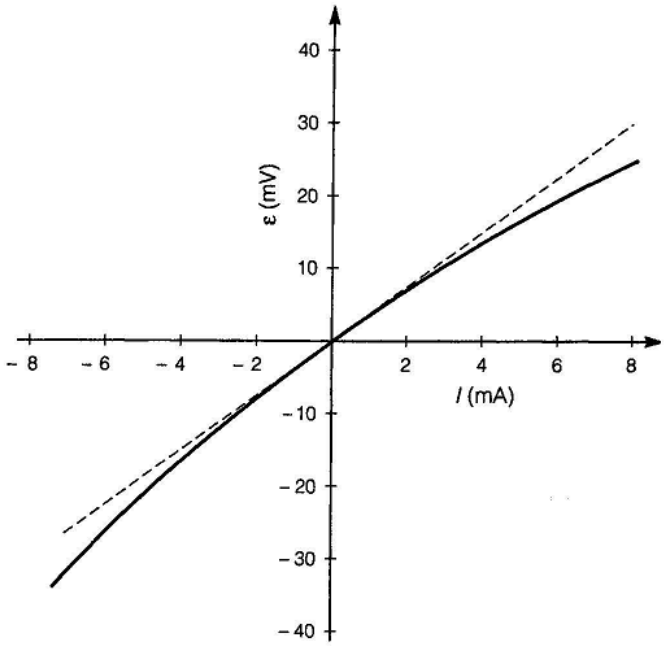

Figure 5.6: Tangent across a polarization curve to measure polarization resistance (Jones, 2005).

b) Capacitance measurements were conducted with a Schlumberger 1287 potentiostat in conjunction with Schlumberger 1260 frequency response analyser in equilibrium with air. Capacitance was measured during polarisation at a potential of 0.2 V_{SHE}. The measurements were performed whilst applying potential to follow the change in an electrode over time as the electrochemical reactions take place similarly to the polarisation resistance measurements. Capacitance measurements were also performed over time. A new electrode was created between the experimental runs by polishing in 0.05 μm Alumina–B slurry. De-aerated de-ionised water was employed to rinse and remove the alumina particles from the electrode.

c) Electrochemical impedance spectroscopy measurements were performed at the corrosion potential to characterise the reactions occurring at the surface of the electrode. The measurements were performed to determine whether the oxidation of pentlandite follows a simple charge transfer process or a diffusion controlled process. Section 2.3.3 sheds more light on the diffusion and simple charge

transfer controlled reactions. A new electrode was created by polishing in alumina slurry under a stream of de-aerated distilled water.

d) Linear potential sweep voltammetry measurements were conducted in a de-aerated borate solution (DO < 0.07 ppm). The solution was de-aerated for two hours using high purity (99.998%) nitrogen (N_2) gas. A new electrode was created by wet grinding on a 2400 grade SiC paper followed by polishing using 0.05 μm Alumina–B slurry. Wet grinding and polishing were performed using de-aerated de-ionised water. The anodic oxidation of the electrode was performed over a potential range of -0.4 to 0.6 $V_{SHE.}$ Variation of current against potential was measured at a scan rate of 10 mV/s. Linear potential sweep voltammetry was employed to investigate the anodic oxidation of the mineral in the absence of oxygen (in order to measure the oxidation of pentlandite without interference by the simultaneous reduction of dissolved oxygen). The polarisation resistance measured the reactivity of pentlandite in the presence of oxygen. In the presence of oxygen, the reactivity of pentlandite is driven by the two reactions-oxidation of the mineral and the reduction of oxygen at the surface of the electrode. Current–time transients were performed in a de-aerated borate solution at selected potentials. The current transients were performed to show the passivation characteristics of pentlandite electrodes.

The exposed areas of massive and microelectrode pentlandite electrodes were determined after each experimental run by taking digital images and using imaging software (i.e. Image Tool). The software program was calibrated using the spatial calibration measurement from the analysis menu (UTHSCSA Image tool, 1997).

The spatial calibration command defines a unit of measurement and correct for magnification within an image for all dimensional analyses. An optical microscope image of the massive pentlandite was loaded into the image tool program. A scale and its unit of measure in the loaded image were used as a line of known dimension and, therefore, used to calibrate the program. Exposed areas of microelectrodes were in the range 3000 μm^2 to 8000 μm^2. Exposed areas of the massive electrodes are indicated in Table 5.3. The electrochemical measurements of the microelectrodes were challenging. (A further

discussion of the microelectrodes is provided in section 6.3.1). After final polishing, the massive electrodes were quickly transferred into the electrochemical cell. All the sample preparation operations were performed in air.

Table 5.3: Composition and average surface area of massive pentlandite electrodes employed.

Electrode	Source	Composition	Area (cm^2)
A	Russia	$Fe_{4.27}Ni_{4.75}Co_{0.14}S_8$	0.057
B	Russia	$Fe_{4.27}Ni_{4.76}Co_{0.13}S_8$	0.103
C	Russia	$Fe_{4.28}Ni_{4.79}Co_{0.14}S_8$	0.01
D	Phoenix	$Fe_{4.07}Ni_{4.78}Co_{0.13}S_8$	0.058
E	Synthetic	$Fe_{4.44}Ni_{4.48}S_8$	0.29

5.7. TOF-SIMS

After the electrochemical measurements, TOF-SIMS (time-of-flight secondary ion mass spectroscopy) analyses were performed on the natural massive pentlandite electrodes. The measurements were performed to evaluate the surface of massive pentlandite after polishing using a 2400 grade SiC paper. The measurements were employed to investigate the possible reasons for the experimental challenges encountered with the microelectrodes, which are discussed in detail in section 6.3.1. The massive electrode was removed from the epoxy resin, ground on a 2400 grade SiC paper and oxidised in an air-saturated buffered $Na_2B_4O_7$ solution for thirty minutes. A massive pentlandite sample (in the range ±2 mm to ± 5 mm in diameter) from Kola Peninsula (Russia) was employed. At the end of the oxidation time, the electrode was removed from the solution and carefully transferred into the TOF-SIMS chamber arrangement.

6. RESULTS AND DISCUSSION

6.1. Composition of pentlandite particles from flotation concentrate

An electron microprobe analysis was performed on selected single natural pentlandite particles hand-picked from Lebowa Merensky (LMP), Lebowa UG–2 (LUP), Platreef and Nkomati Mine flotation concentrate samples in South Africa. No systematic picking of pentlandite particles was followed-pentlandite particles were hand-picked at random. All pentlandite particles were analysed for the following major elements: Fe, Ni, Co, Cu and S. Three to five spot analyses were performed on a pentlandite particle. For a ±100 µm particle in diameter, the number of spots analysed was limited by the size of the particle.

6.1.1 Composition of pentlandite particles from Platreef

Table 6.1 shows the composition of pentlandite particles hand-picked from the Platreef sample. The iron content of these particles varies between 31.58 and 42.87 wt %; nickel varies from 21.82 to 34.78 wt %. The Fe:Ni ratio ranges from 0.9 to 1.96. Samples 12, 15, 16 and 13 are enriched with iron; the iron content is slightly higher than the nickel content. The cobalt content varies between 0.65 wt % and 0.95 wt %. Pentlandite particles analysed from the Western Platinum Mine (i.e. a Merensky deposit) had an average cobalt content of 0.8 wt % which is in the range of analysed pentlandite particles (Brynard *et al*., 1976).

Samples B1-1 and B1-2 are enriched with iron content. The iron content varies between 38.29 and 42.87 wt % - a feature of pentlandite co-existing with troilite (Harris and Nickel, 1972). These particles were hand-picked from the Sheba's Ridge-a Platreef deposit.

Table 6.1: Electron microprobe analysis of pentlandite from the Platreef deposit.

Sample no.	(wt %)						Fe:Ni ratio	n
	S	Fe	Co	Ni	Cu	Total		
10	32.93	32.27	0.87	33.5	0.13	99.69	0.96	5
12	33.47	33.16	0.67	32.76	0.01	100.07	1.01	3
15	33.19	33.36	0.86	32.29	0.01	99.71	1.03	3
14	33.17	31.16	0.68	34.78	0.03	99.82	0.9	3
11	33.13	31.6	0.65	34.27	0	99.66	0.92	4
1	32.86	31.67	0.69	34.33	0.05	99.6	0.92	3
16	33.28	34.34	0.73	31.49	0.24	100.09	1.09	4
13	33.02	33.74	0.74	31.9	0	99.41	1.06	4
B1-1	33.13	38.29	0.95	26.75	0.22	99.33	1.43	3
B1-2	34.06	42.87	0.86	21.82	0.22	99.82	1.96	3
2	33.13	31.58	0.7	34.86	0.06	100.32	0.91	4

n: Number of spots analysed

The average pentlandite composition of pentlandite particles from the Platreef flotation concentrate varies from $Fe_{4.31}Ni_{4.58}Co_{0.09}S_8$ to $Fe_{5.78}Ni_{2.8}Co_{0.11}S_8$ with respect to the atomic iron content; the metal to sulfur ratio ranges from 8.72 to 9.11 (see Table 6.2). It is evident that individual pentlandite grains deviate from the assumed stoichiometric formula of M_9S_8. Deviation of the composition of pentlandite from the assumed M_9S_8 formula was also observed by Merkle and Von Gruenewaldt (1986).

Table 6.2: Variation of pentlandite composition, stoichiometric formula M_9S_8 and theoretical sulfur content (47.06 at %) for particles hand-picked from Platreef.

Sample	Average composition	M:S_8 ratio	Sulfur (atomic %)
10	$Fe_{4.52}Ni_{4.46}Co_{0.12}S_8$	9.11	46.84
12	$Fe_{4.55}Ni_{4.28}Co_{0.09}S_8$	8.92	47.29
15	$Fe_{4.62}Ni_{4.25}Co_{0.11}S_8$	8.98	47.11
14	$Fe_{4.31}Ni_{4.58}Co_{0.09}S_8$	8.99	47.09
11	$Fe_{4.38}Ni_{4.52}Co_{0.09}S_8$	8.99	47.09
1	$Fe_{4.43}Ni_{4.57}Co_{0.09}S_8$	9.09	46.81
16	$Fe_{4.74}Ni_{4.14}Co_{0.1}S_8$	9.00	47.05
13	$Fe_{4.69}Ni_{4.22}Co_{0.1}S_8$	9.01	47.02
B-1	$Fe_{5.31}Ni_{3.53}Co_{0.12}Cu_{0.03}S_8$	8.99	47.10
B-2	$Fe_{5.78}Ni_{2.8}Co_{0.11}Cu_{0.03}S_8$	8.72	47.86
2	$Fe_{4.35}Ni_{4.62}Co_{0.09}S_8$	9.06	46.85

6.1.2 Composition of pentlandite particles from Lebowa Merensky flotation concentrate

Table 6.3 summarises the microprobe analysis of pentlandite particles hand-picked from the Lebowa Merensky flotation concentrate. Iron content varies from 29.01 to 32.05 wt % with Fe:Ni ratio in the range 0.79 to 0.95. Cobalt content varies between 0.2 wt % and 0.66 wt %. Compared to pentlandite particles from the Platreef concentrate, the particles depict a lower cobalt content. All pentlandite particles hand-picked from the concentrate were enriched with nickel, with a nickel content varying between 33.59 and 36.86 wt %. The composition of the analysed pentlandite particles is similar to that of pentlandite particles analysed from the Rustenburg Platinum Mine (i.e. a Merensky deposit) obtained from different layers of the reef [Upper Chromitite, Anorsthosite, Melanorite, Lower chromitite (LC) and coarse-grained melanorite (CGM)] (Godel *et al.*, 2007). Godel *et al.* (2007) analysed pentlandite grains with a cobalt content ranging between 0.33 and 0.67 wt % and the iron to nickel ratio of the grains varied between 0.8 and 1.

Table 6.3: Average electron microprobe analysis of pentlandite particles hand-picked from Lebowa Merensky flotation concentrate.

Sample no.	(wt %)						Fe:Ni ratio	n
	S	Fe	Co	Ni	Cu	Total		
7	33.02	29.01	0.4	36.7	0	99.13	0.79	3
16	33.4	30.52	0.37	35.21	0	99.5	0.87	3
19	33.24	31.76	0.3	35.09	0.06	100.45	0.91	3
17	33.39	29.37	0.66	36.86	0.02	100.3	0.8	3
1	33.32	30.89	0.42	34.94	0.01	99.58	0.88	4
14	32.87	31.19	0.2	35.06	0	99.32	0.89	3
20	32.69	29.71	0.48	36.34	0.1	99.32	0.82	3
10	33.32	32.05	0.65	33.59	0.03	99.64	0.95	3

n : number of spots analysed on each pentlandite particle

The average composition of pentlandite particles from Lebowa Merensky ranges from $Fe_{4.04}Ni_{4.86}Co_{0.05}S_8$ to $Fe_{4.42}Ni_{4.41}Co_{0.09}S_8$ with respect to the atomic iron content, with a $M:S_8$ ratio of 8.85 to 9.11 (see Table 6.4). The average composition of the particles deviates from the assumed theoretical formula. The atomic sulfur content varies between 46.76 and 47.47 at % - this is similar to the theoretical sulfur content of 47.06 at %.

Table 6.4: Variation of pentlandite particles from Lebowa Merensky from theoretical M:S_8 formula and theoretical sulphur (atomic %).

Sample no.	Average composition	M:S_8	Sulfur (atomic %)
7	$Fe_{4.04}Ni_{4.86}Co_{0.05}S_8$	8.95	47.21
16	$Fe_{4.20}Ni_{4.61}Co_{0.05}S_8$	8.85	47.47
19	$Fe_{4.39}Ni_{4.61}Co_{0.04}S_8$	9.05	46.93
17	$Fe_{4.04}Ni_{4.82}Co_{0.09}S_8$	8.95	47.18
1	$Fe_{4.26}Ni_{4.58}Co_{0.06}S_8$	8.9	47.35
14	$Fe_{4.36}Ni_{4.66}Co_{0.03}S_8$	9.05	46.92
10	$Fe_{4.42}Ni_{4.41}Co_{0.09}S_8$	8.91	47.3
20	$Fe_{4.17}Ni_{4.86}Co_{0.06}S_8$	9.11	46.76

6.1.3 Composition of pentlandite particles from the Lebowa UG-2 flotation concentrate

Table 6.5 summarises the composition of the pentlandite particles from the Lebowa UG-2 flotation concentrate. The composition of the particles is similar to that of pentlandite grains from the Platreef and Lebowa Merensky samples. The iron content varies between 30.91 wt % and 32.57 wt % while nickel ranges from 33.57 wt % to 36.07 wt %. All four pentlandite particles analysed, were enriched with nickel. The Fe:Ni ratio varies between 0.84 and 0.97. In all cases, the Fe:Ni ratio is close to 1. The cobalt content ranges from 0.6 wt % to 0.71 wt %. There is a similar compositional variation for pentlandite particles from Lebowa UG-2, Lebowa Merensky and Platreef.

Table 6.5: Average pentlandite composition hand-picked from the Lebowa UG-2 flotation concentrate.

Sample no.	wt %						Fe:Ni ratio
	S	Fe	Co	Ni	Cu	Total	
3	33.07	32.57	0.74	33.57	0.1	100.05	0.97
1	33.26	31.99	0.6	34.08	0.02	99.95	0.94
5	33.39	30.91	0.6	35.43	0.05	100.37	0.87
9	33.44	30.17	0.71	36.07	0.04	100.41	0.84

The composition of pentlandite particles analysed is similar to the grains Penberthy (2001) analysed from the UG-2 ore. Pentlandite particles 3 and 9 (see Table 6.5) have a cobalt content similar to sample B4 (see Table 6.6).

Table 6.6: Average pentlandite composition from UG-2 deposits (Penberthy, 2001).

Sample no.	UG- 2 (wt %)						Fe:Ni ratio
	Fe	Ni	Co	Cu	S	Total	
A1	32.92	32.63	0.45	0.04	32.99	99.03	1.01
B4	33.88	31.8	0.73	0.05	33.39	99.85	1.07
C1	30.62	34.34	0.46	0.05	32.79	98.26	0.89

Pentlandite particles hand-picked from Lebowa UG-2 also show considerable deviation from the assumed stoichiometric formula of M_9S_8. The composition varies between $Fe_{4.14}Ni_{4.71}Co_{0.09}S_8$ and $Fe_{4.52}Ni_{4.42}Co_{0.08}S_8$ with respect to the atomic iron content (see Table 6.7); with metal to sulfur variation in the range of 8.96 to 9.04. The sulfur content of all the compositions was found to vary between 46.87 at % and 47.18 at %. The variation was found to be similar to the theoretical value of 47.06 at % (Harris and Nickel, 1972; Merkle and Von Gruenewaldt, 1986).

Table 6.7: Stoichiometric variation of pentlandite particles from Lebowa UG-2 from assumed formula of M_9S_8.

Sample	Average composition	M:S_8	Sulfur (atomic %)
3	$Fe_{4.52}Ni_{4.42}Co_{0.08}S_8$	9.04	46.87
1	$Fe_{4.42}Ni_{4.48}Co_{0.06}S_8$	8.96	47.12
5	$Fe_{4.25}Ni_{4.64}Co_{0.08}S_8$	8.97	47.13
9	$Fe_{4.14}Ni_{4.71}Co_{0.09}S_8$	8.96	47.18

6.1.4 Composition of pentlandite particles from Nkomati Mine flotation concentrate

Microprobe analysis indicates compositional variation of pentlandite in the cobalt content (see Table 6.8). Cobalt ranges from 1.058 wt % to 2.39 wt %. Iron ranges between 29.89 wt % to 30.95 wt %; nickel ranges from 33.98 wt % to 34.95 wt %. The composition of pentlandite varies with the sulfide assemblage - sulfide minerals co-existing with pentlandite in a polished section (Van Zyl, 1996). The composition of analysed pentlandite particles from the Nkomati Mine concentrate is similar to grains analysed from the Uikomst Complex from specific assemblages (Van Zyl, 1996). Using the cobalt content, the composition corresponds to pentlandite grains analysed from the following assemblages: pyrrhotite + pentlandite + chalcopyrite, pyrrhotite + pentlandite +

chalcopyrite + pyrite and pyrrhotite + pentlandite + chalcopyrite + violarite (see Tables 6.8 and 6.9).

Table 6.8: Microprobe analysis of pentlandite particles hand-picked from Nkomati flotation concentrate.

Sample no.	(wt %)						Fe:Ni ratio	n	Assemblage*
	S	Fe	Co	Ni	Cu	Total			
12	33	30.9	1.43	34.78	0.07	100.17	0.89	3	Po+Pn+Cp
11	33.36	30.88	1.42	34.43	0	100.09	0.9	3	Po+Pn+Cp
8	33.07	30.8	1.4	34.59	0.04	99.9	0.89	3	Po+Pn+Cp
7	33.18	30.59	1.33	34.73	0	99.84	0.88	3	Po+Pn+Cp+Py
10	33.77	30.83	1.29	34.54	0	100.43	0.89	4	Po+Pn+Cp+Py
4	33.22	30.15	2.39	33.98	0	99.74	0.89	4	Po+Pn+vl+Cp
3	33.21	30.51	1.11	34.92	0.02	99.78	0.87	3	Po+Pn+Cp+Py
2	33.12	30.95	1.2	34.5	0	99.77	0.9	3	Po+Pn+Cp+Py
Massive	32.84	29.89	1.08	34.95	0	98.75	0.86	3	Po+Pn+Cp+Py

Abbreviations: Po = Pyrrhotite; Pn = pentlandite; Cp = chalcopyrite; Py = pyrite
*Assemblage adopted from the analysis obtained from the Uitkomst Complex (Van Zyl, 1996).

Van Zyl (1996) found pentlandite in sulfide assemblage containing violarite to have a cobalt content of 2.26 wt % (see Table 6.9). This is similar to the cobalt content of sample 4.

Table 6.9: Composition of pentlandite particles from the Uitkomst Complex (Van Zyl, 1996).

Assemblage	Pentlandite composition from Uitkomst Complex (wt %)					Fe:Ni ratio
	Fe	Ni	Co	Cu	S	
Po+Pn+Cp+Py	30.63	34.2	1.25	-	33.25	0.896
Po+Pn+Cp+Py	30.92	35.78	1.21	-	33.3	0.864
Po+Pn+Cp	30.26	35.79	1.49	-	33.54	0.845
Po+Pn+Cp	29.83	34.13	1.48	-	33.62	0.874
Po+Pn+Cp+Py	31.19	34.31	1	-	33.16	0.909
Po+Pn+vl+Cp	30.03	33.26	2.26	0.07	33.44	0.903

Pentlandite particles from Nkomati Mine that were analysed showed deviation from the assumed stoichiometric formula of $(Fe,Ni,Co)_9S_8$. The average composition varied between $Fe_{4.17}Ni_{4.47}Co_{0.31}S_8$ and $Fe_{4.30}Ni_{4.61}Co_{0.19}S_8$ with respect to the atomic iron

content, with the M:S_8 ratio ranging from 8.7 to 9.04 (see Table 6.10). The sulfur content varied from 46.96 at % to 47.77 at %.

Table 6.10: Stoichiometric variation of pentlandite particles from the Nkomati Mine from the assumed formula of M_9S_8 and a theoretical sulfur content of 47.06 atomic %.

Sample no.	Average composition	M:S_8 ratio	Sulfur (atomic %)
12	$Fe_{4.30}Ni_{4.61}Co_{0.19}S_8$	9.1	46.77
11	$Fe_{4.25}Ni_{4.51}Co_{0.19}S_8$	8.95	47.2
8	$Fe_{4.28}Ni_{4.57}Co_{0.18}S_8$	9.04	46.96
7	$Fe_{4.24}Ni_{4.58}Co_{0.17}S_8$	8.98	47.1
10	$Fe_{4.19}Ni_{4.47}Co_{0.17}S_8$	8.83	47.54
4	$Fe_{4.17}Ni_{4.47}Co_{0.31}S_8$	8.95	47.19
3	$Fe_{4.22}Ni_{4.60}Co_{0.15}S_8$	8.7	47.16
2	$Fe_{4.29}Ni_{4.55}Co_{0.16}S_8$	9	47.05
Massive	$Fe_{4.18}Ni_{4.65}Co_{0.143}S_8$	8.97	47.13

6.1.5 Compositional variation of pentlandite particle within flotation concentrate

Comparing the composition of all pentlandite particles analysed (in atomic percent), it is evident that there is a slight compositional variation of pentlandite in cobalt content, as significant variation in iron and nickel as was observed by several authors (Merkle and Von Gruenewaldt, 1986; Van Zyl, 1996; Penberthy, 2001; Godel *et al.*, 2007). The variation is independent of the deposit. Cobalt content varies between 0.16 and 1.85 atomic %. The iron and nickel contents vary between 23.81 and 34.58 atomic % and between 16.75 and 28.66 atomic % respectively (see Figure 6.1 & 6.2 and Appendix D, Tables D1 to D32). Two pentlandite particles hand-picked from the Platreef (i.e. Sheba's ridge flotation concentrate) were enriched with iron, having an iron content higher than 30 atomic %.

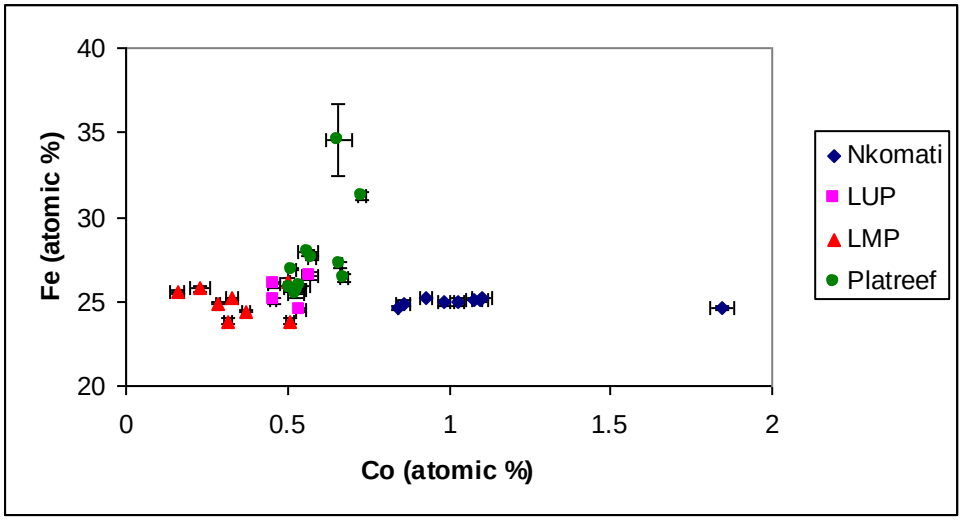

Figure 6.1: Variation of iron content with cobalt in natural pentlandite particles hand-picked from the Lebowa Merensky (LMP), Lebowa UG-2, Platreef and Nkomati Mine flotation concentrates. Also represented are the 95% confidence intervals of iron and cobalt.

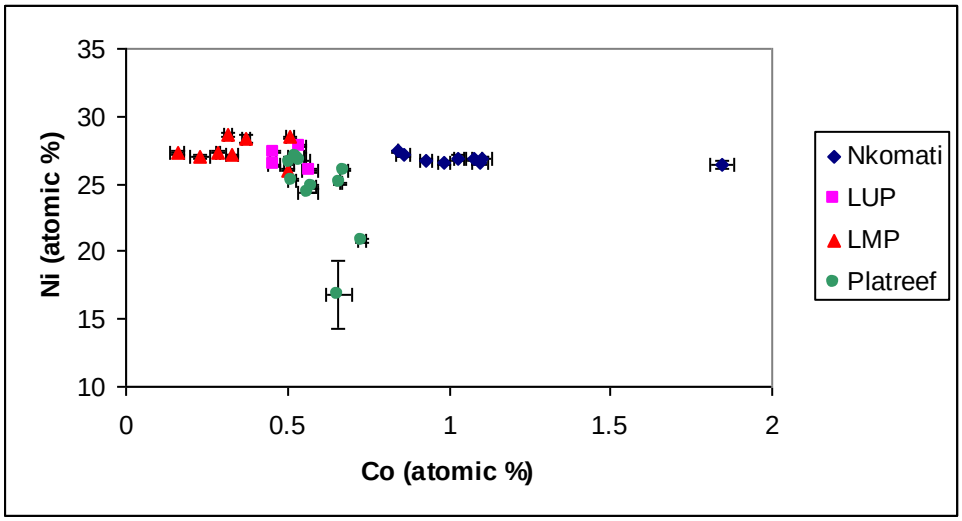

Figure 6.2: Variation of nickel content with cobalt in natural pentlandite particles hand-picked from the Lebowa Merensky (LMP), Lebowa UG-2 (LUP), Platreef and Nkomati Mine flotation concentrates. Also represented are the 95% confidence intervals of nickel and cobalt.

Compositional variation of pentlandite is related to the variation of the bulk rock chemistry (i.e. compositional variation of bulk rock) which is mined as a consequence of magmatic differentiation i.e. crystallisation of silicates from molten magma (Merkle and Von Gruenewaldt, 1986). Crystallisation of silicates has a significant influence on sulfide bulk composition, which in turn is reflected in the compositional change of individual sulfide minerals (Merkle and Von Gruenewaldt, 1986).

Numerous research data has shown that the composition of natural pentlandite varies over a wide range (Harris and Nickel, 1972; Riley, 1977; Merkle and Von Gruenewaldt, 1986; Van Zyl, 1996). The more typical isomorphism is Ni ↔ Fe; less typical is Ni ↔ Co and Fe ↔ Co though cobalt variation occurs occasionally (Chanturiya *et al*., 2004). Figures 6.1 and 6.2 show no correlation between Fe & Co and Ni & Co, indicating no cobalt substitution for nickel and iron. In contrast, Figure 6.3 shows a direct correlation between Fe & Ni, indicating typical Ni ↔ Fe isomorphism. It is evident that in cobalt poor pentlandite, cobalt substitution is unlikely.

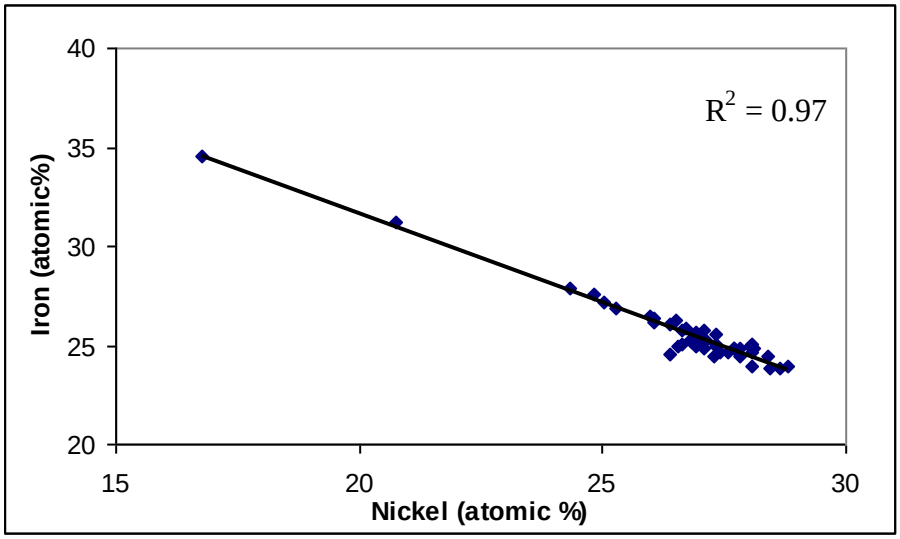

Figure 6.3: Variation of iron with nickel in natural pentlandite particles hand-picked from the Lebowa Merensky (LMP), Lebowa UG-2 (LUP), Platreef and Nkomati Mine flotation concentrates.

Figures 6.1 and 6.2 also show ranges of the true values of the mean at 95% confidence limits. From these values, it is clear that the composition of most of the pentlandite particles analysed is uniform throughout each particle - this could be related to the relatively small size (± 100 μm). One grain showed large confidence limits. This could have been due to the homogeneity of the grain.

6.1.6 Variation in sulfur content

A theoretical pentlandite formula $(Ni, Fe, Co)_9S_8$ contains 47.06 at % sulfur (Harris and Nickel, 1972). Figure 6.4 shows sulfur content of pentlandite particles analysed to vary from the theoretical sulfur value of 47.06 at %. The average sulfur content of all

pentlandite particles ranges between 46.76 and 47.86 at %, which is similar to the theoretical sulfur content. The 95% confidence limit of sulfur for some pentlandite particles deviates from the theoretical sulfur content (see Figure 6.4).

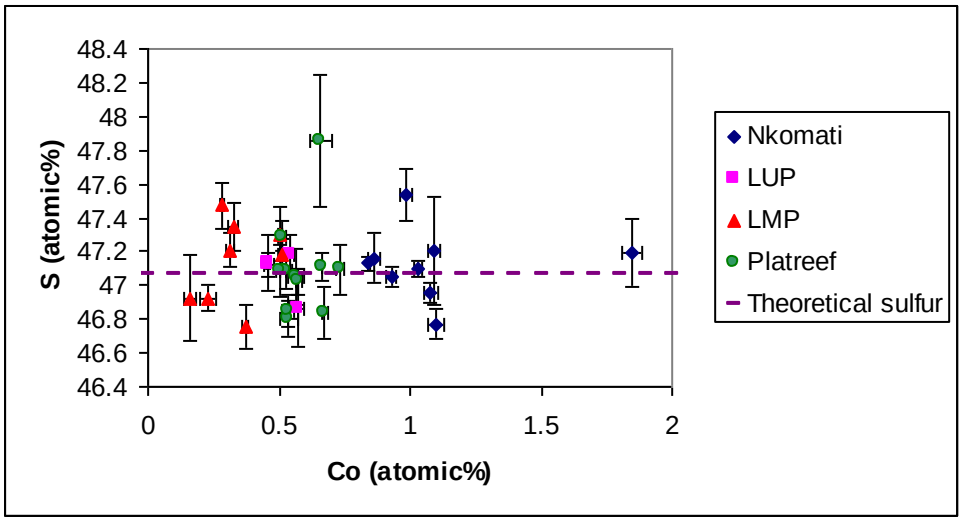

Figure 6.4: Atomic sulfur content of all natural pentlandite particles hand-picked from Nkomati, LUP-Lebowa UG-2, LMP-Lebowa Merensky and Platreef flotation concentrate samples. Also represented are the 95% confidence intervals of sulfur and cobalt.

6.1.7 Metal-sulfur ratio

Pentlandite is assumed to have the general formula of $(Fe,Ni,Co)_9S_8$ where metals can substitute for each other extensively within the limits estimated by Knob and Ibrahim (1961), resulting in a metal to sulfur ratio of Me_9S_8. The formula for pentlandite particles analysed in this study deviates from the assumed stoichiometric formula of $(Fe,Ni,Co)_9S_8$. Figure 6.5 shows metal to sulfur ratios (for sulfur normalised to an atomic portion of 8) of pentlandite particles analysed to deviate from the assumed formula for sulfur with an atomic proportion of eight. Confidence limits were computed at the 95% level. Deviation of natural pentlandite from the assumed formula is similar to the observations of Merkle and Von Gruenewaldt (1986). Deviation of the formula from the assumed theoretical pentlandite formula is an indication of non–stoichiometry. To validate the non–stoichiometry of pentlandite, the reproducibility of the analytical data should fall within the limits of analytical uncertainty. The reproducibility of the analytical data did not all

fall within the limits of the analytical uncertainty (see Table 5.2 and Appendix D, Tables D1 to D32). Not all pentlandite particles were non-stoichiometric.

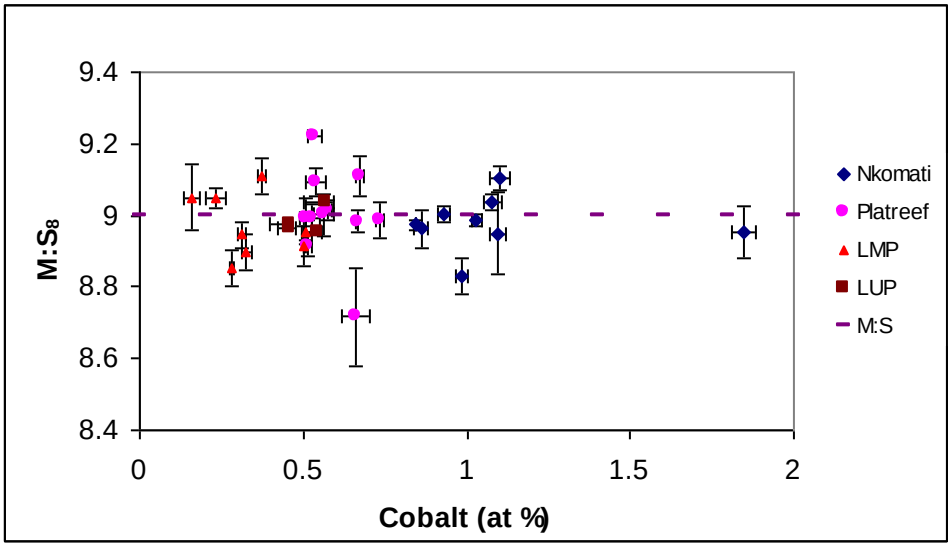

Figure 6.5: Deviation of metal to sulfur ratio of pentlandite particles from the assumed theoretical ratio of $M_9:S_8$. The particles were hand-picked from the flotation concentrate samples from the Nkomati Mine, Platreef, LMP-Lebowa Merensky and LUP-Lebowa UG-2.

6.2 Massive pentlandite

Massive pentlandite samples were sourced from Pechenga in the Kola Peninsula (Russia) and Phoenix Mine (Botswana). Only pentlandite samples from the Kola Peninsula and Phoenix Mine were employed. Other massive samples received contained either large phases of other mineral sulfides or the pentlandite grains were too small. Pentlandite samples from Pechenga deposit in Kola Peninsula (Russia) and Phoenix deposit (Botswana) with a low volumetric quantity of other mineral sulfide phases were analysed (see Figures C6 to C9 in Appendix C). The composition of these samples was determined by an electron microprobe. Samples were analysed for Fe, Co, Ni and S under the same conditions as that for the microelectrodes. Seven to ten spot analyses were performed per sample. Nine Russian and two Phoenix pentlandites were analysed.

6.2.1 Composition of massive pentlandite

The samples did not show significant compositional variations. Figures 6.6 and 6.7 show the iron and nickel content of natural massive pentlandite samples to varying between 23.93 and 25.02 at % and 27.27 and 28.81 at % respectively. Cobalt composition ranges

between 0.76 and 1 at %. A similar composition was observed from an electron microprobe analysis of pentlandite from Sudbury (Hall and Stewart, 1973). Table 6.11 shows the composition of pentlandite from Sudbury (Ontario) with a cobalt content of 0.85 at %.

All the massive pentlandite samples analysed were enriched with nickel content (see Table D33 to D43, Appendix D). In addition to the natural massive samples, a synthetic pentlandite was employed. The synthetic pentlandite sample had an iron and nickel content of 26.23 at % and 26.49 at % respectively. The synthetic sample did not contain cobalt. In comparison to the pentlandite particles hand-picked from the flotation concentrate, massive samples did not show significant compositional variations. However, the metal to sulfur ratios indicated larger variations than did the microelectrodes (compare Figures 6.5 and 6.9).

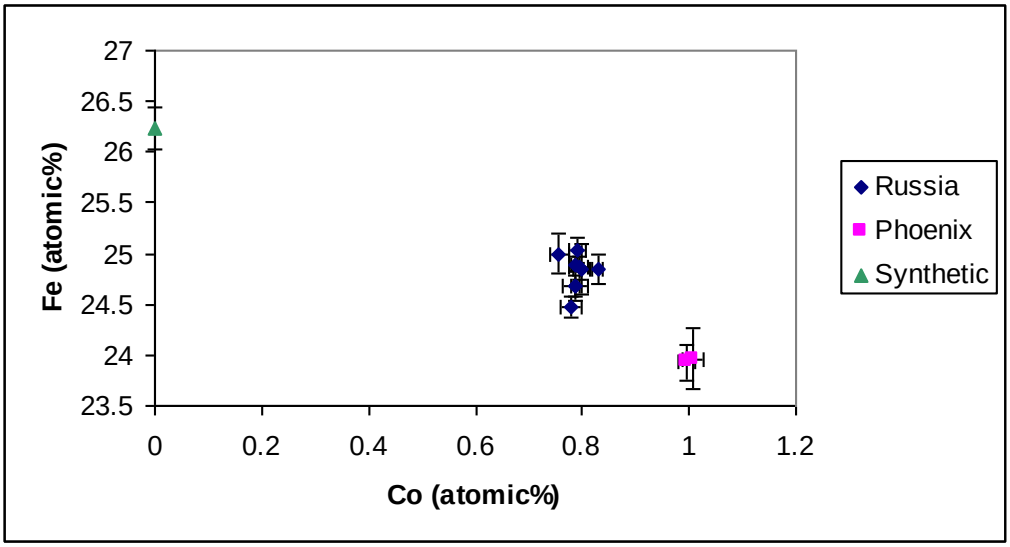

Figure 6.6: Variation of iron content with cobalt for massive pentlandite samples from the Kola Peninsula (Russia), Phoenix deposits (Botswana) and synthetic pentlandite.

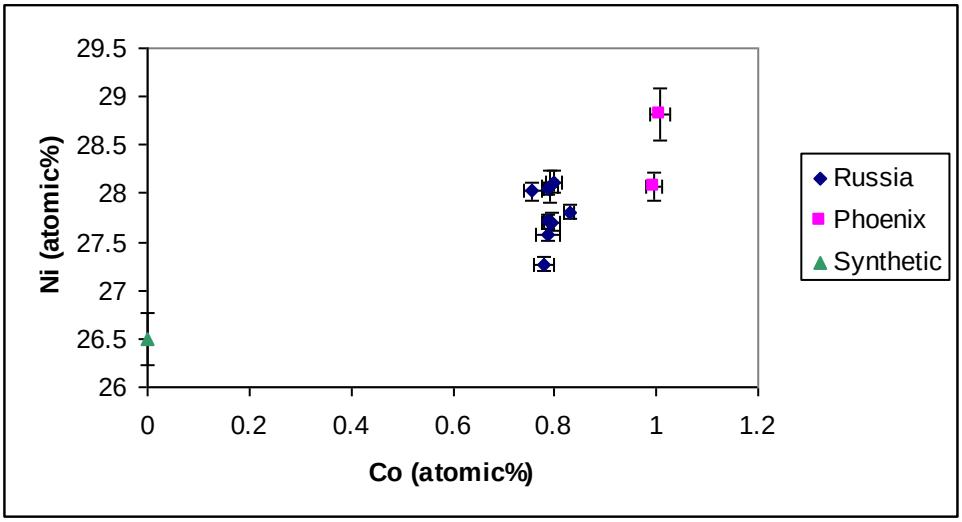

Figure 6.7: Variation of nickel content with cobalt for massive pentlandite samples from the Kola Peninsula (Russia), Phoenix deposit (Botswana) and a synthetic pentlandite.

Table 6.11: Composition of massive pentlandite from Sudbury, Ontario (Hall & Stewart, 1973).

	Element				
	Fe	Ni	Co	S	Total
wt %	30	36.1	1.1	33	100.2
at %	24.42	27.96	0.85	46.78	100.0

6.2.2 Variation of the sulfur content

Massive samples analysed depicted a sulfur content ranging between 46.1 and 47.48 at % (see Figure 6.8); this is close to the theoretical sulfur content of 47.02 at % (Harris and Nickel, 1972; Merkle and Von Gruenewaldt, 1986). All the pentlandite samples analysed, indicated relatively constant sulfur content.

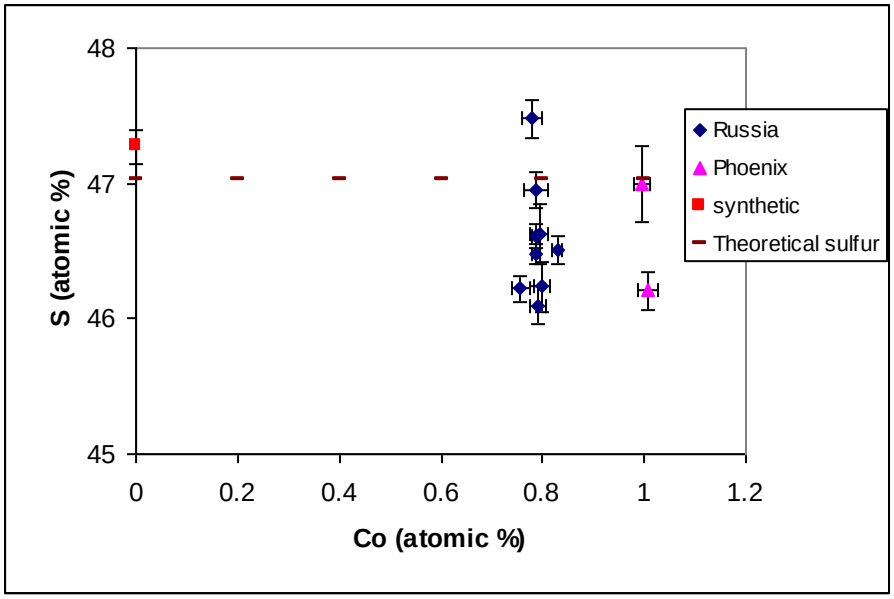

Figure.6.8: Sulfur content of massive pentlandite samples sourced from the Kola Peninsula (Russia), Phoenix deposit (Botswana) and a synthetic pentlandite.

6.2.3 Variation of pentlandite formula from assumed theoretical formula

The average composition of massive natural pentlandite ranges from $Fe_{4.07}Ni_{4.78}Co_{0.17}S_8$ to $Fe_{4.34}Ni_{4.87}Co_{0.137}S_8$ with respect to the atomic iron content (Tables 6.12 and 6.13). The synthetic pentlandite sample had an average composition of $Fe_{4.44}Ni_{4.48}S_8$ with approximately equal quantities of iron and nickel.

Table 6.12: Average composition of massive pentlandite samples from the Kola Peninsula (Russia) (sulfur normalized to 8).

Sample no.	**Average composition**
10	$Fe_{4.27}Ni_{4.76}Co_{0.14}S_8$
3	$Fe_{4.27}Ni_{4.75}Co_{0.14}S_8$
1	$Fe_{4.21}Ni_{4.70}Co_{0.13}S_8$
11	$Fe_{4.24}Ni_{4.82}Co_{0.14}S_8$
5	$Fe_{4.28}Ni_{4.79}Co_{0.14}S_8$
9	$Fe_{4.30}Ni_{4.87}Co_{0.14}S_8$
13	$Fe_{4.12}Ni_{4.60}Co_{0.13}S_8$
12	$Fe_{4.34}Ni_{4.87}Co_{0.14}S_8$
14	$Fe_{4.32}Ni_{4.85}Co_{0.13}S_8$

Table 6.13: Average composition of massive pentlandite samples from the Phoenix deposit (Botswana) and synthetic pentlandite (sulfur normalized to 8).

Sample	**Average composition**
Phoenix 2	$Fe_{4.15}Ni_{4.99}Co_{0.17}S_8$
Phoenix 1	$Fe_{4.07}Ni_{4.78}Co_{0.17}S_8$
Synthetic	$Fe_{4.44}Ni_{4.48}S_8$

Deviation of the pentlandite composition from the assumed theoretical formula indicates non-stoichiometry in pentlandite. The metal to sulfur ratio of analysed massive pentlandite samples ranged between 8.92 and 9.31 (see Figure 6.9). Analytical error of analysed data should fall within the expected limits of analytical uncertainty for non-stoichiometry to hold. Merkle and Von Gruenewaldt (1986) observed a variation of non–stoichiometry and the analytical data were within the analytical uncertainty.

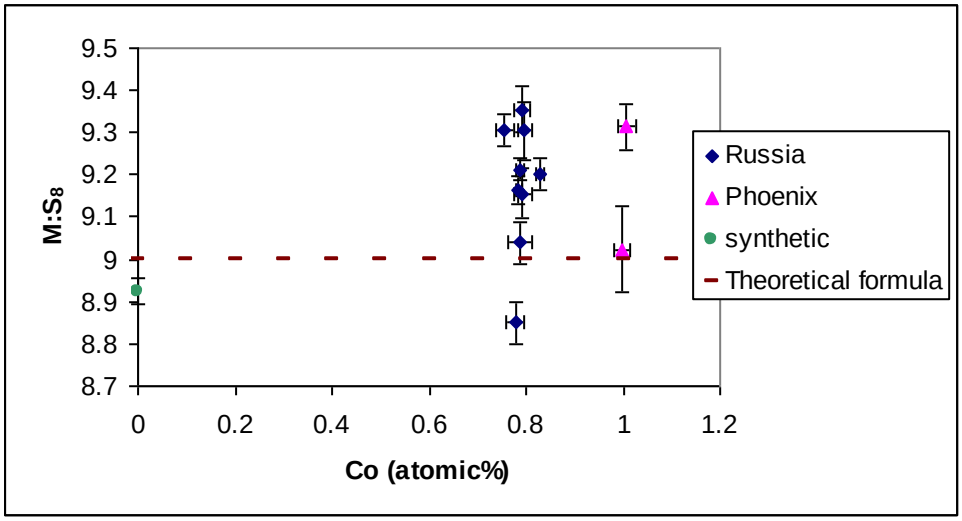

Figure 6.9: Deviation of metal to sulfur ratio of massive pentlandite samples from the assumed theoretical ratio of $M_9:S_8$.

6.3 Electrochemical measurements

Since pentlandite is a metallic conductor (Vaughan and Craig, 1978), electrochemical techniques such as polarisation resistance, voltammetry, electrochemical impedance spectroscopy and current density-time transients were employed to investigate the electrochemical behaviour of natural massive and microelectrode pentlandite samples.

6.3.1 Natural microelectrode pentlandite

A microelectrode technique was employed to investigate the electrochemical behaviour of natural pentlandite particles (±100μm) hand-picked from the flotation concentrate samples. The technique involves cementation of a single particle to a wire using conductive epoxy and a micromanipulator, as already discussed in section 5.4.2. During voltammetry, the potential of the electrode was scanned over a wide potential range (i.e. -0.2 V_{SHE} to 0.8 V_{SHE}). Before each measurement, a fresh electrode surface was created by wet abrading on a 2400 grade SiC grinding paper, followed by polishing using 0.05 μm alumina slurry.

Figure 6.10 shows a back-scattered electron image of a polished pentlandite microelectrode, after electron microprobe analysis and prior to electrochemical measurements. Subsequent re-grinding (2400 grade SiC) after electrochemical measurements exposed increasingly deep cracks and pores (see Figures 6.11 and 6.12), which probably contributed to poor repeatable electrochemical response of the microelectrodes (see example of poor reproducibility in Figure E1, Appendix E).

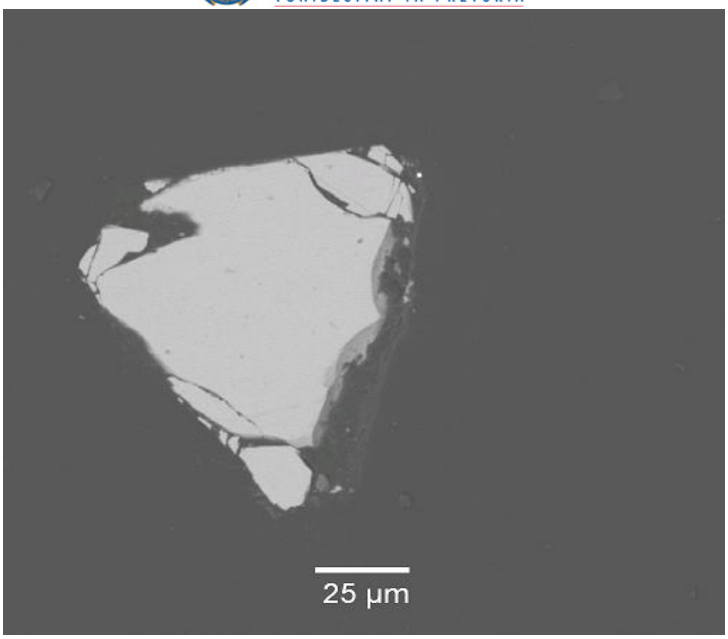

Figure 6.10: Back-scattered electron image of a pentlandite microelectrode after polishing for microprobe analysis and prior to electrochemical measurements, showing a flat smooth surface (LMP19-Lebowa Merensky pentlandite particle). Acceleration voltage of 15 kV.

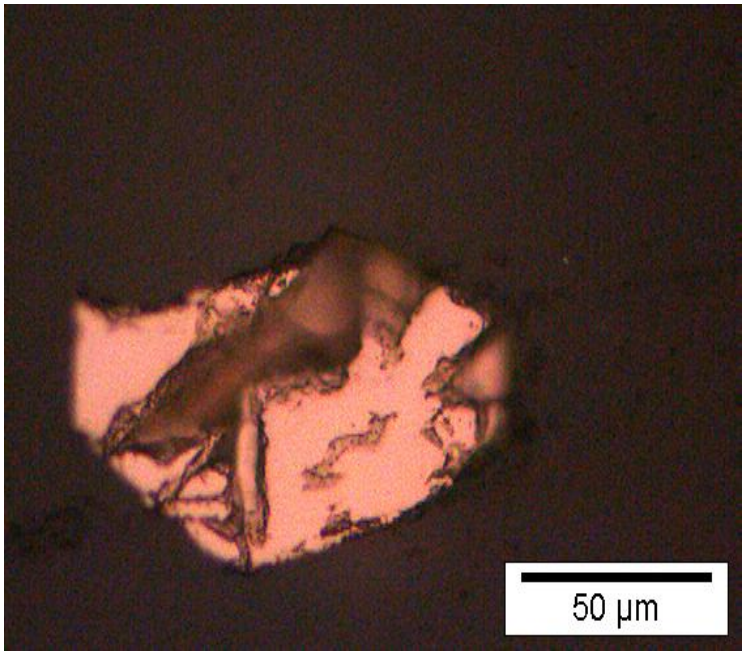

Figure 6.11: Optical microscope image of pentlandite microelectrode (LMP19-Lebowa Merensky particle) after grinding with 2400 grade SiC paper in preparing the surface for subsequent electrochemical measurements.

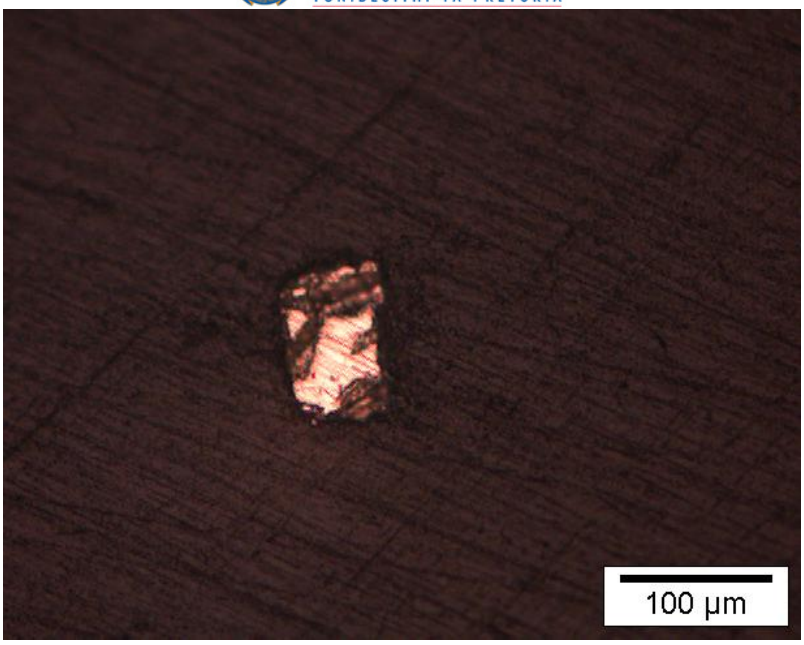

Figure 6.12: Optical microscope image of pentlandite microelectrode hand-picked from Nkomati flotation concentrate, after grinding with 2400 grade SiC paper in preparing the surface for subsequent electrochemical measurements.

A polarisation resistance technique was employed to investigate the electrochemical behaviour of natural pentlandite particles in equilibrium with air (DO = 5 ppm) inside a Faraday cage. When an electrode is placed in an electrolyte, the electrode–electrolyte interface offers a resistance to the transfer of charge at the surface-electrons, produced as a result of the oxidation of the mineral. It is this resistance that is measured by the polarisation resistance technique. The significance of this resistance is that it is inversely proportional to the rate of the reactions occurring at the surface of the electrode (Silverman, 1986; Mendiratta, 2000). Its measurement can be used to investigate the reactivity of sulfide minerals. The advantage of the technique is that it is non–destructive and numerous measurements may be performed on the same electrode (Jones, 2005).

To reduce the incidence of deep cracks and pores at the surface, a new electrode surface was created by polishing the electrode with a 0.05 µm alumina suspension on an MDNap polishing cloth before each test. Repeatable measurements were expected since the polarisation resistance technique does not change the surface of the electrode significantly during oxidation. The technique scans around the rest potential of the electrode. The polishing procedure employed was not expected to increase deep pores and cracks at the electrode surface. However, it was found that after polishing more pores

were exposed, resulting in poorly repeatable electrochemical responses of the microelectrodes.

A Faraday cage is an enclosure formed by a conducting material (see Figure 6.13) to shield the experimental cell and its electrical connections from electromagnetic interferences. Because the measured current is small when using the pentlandite microelectrodes, any electromagnetic interference would mask the electrochemical response of the electrodes; and it was thought that such interference might account for the poor reproducibility (Suter *et al*., 1995).

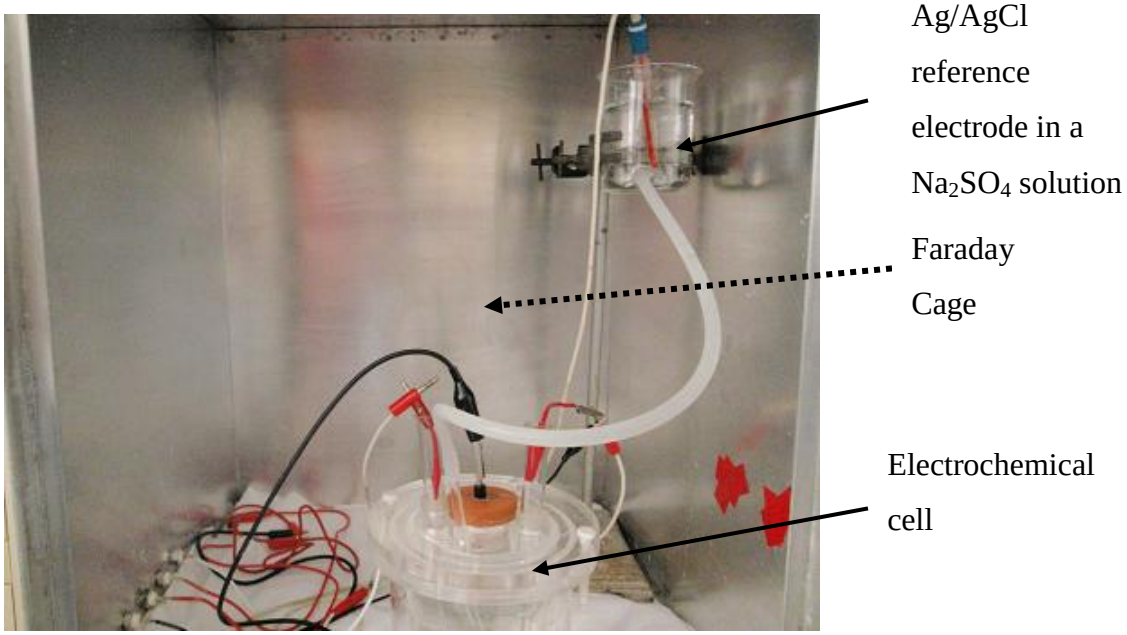

Figure 6.13: Faraday Cage employed to shield the experimental set-up from any magnetic interference in order to increase the detection limit of measured currents.

However, it was found that the use of a Faraday Cage did not improve the reproducibility of the electrochemical response of the pentlandite micro-electrodes; and it was concluded that the poor reproducibility was probably due to the presence of deep pores within a natural pentlandite. Defects change the mineral surface and the bulk electronic structure (Rosso and Vaughan, 2006) and can therefore change the electrochemical behaviour. In line with the proposed effect of electrode preparation on electrochemical response, the conductivity of natural minerals varies with the presence of impurities, variation in size of mineral crystals or destruction of the crystal lattice by heating, grinding, fracturing or oxidation (Harvard, 1928).

To investigate the effect of using a Faraday Cage, the electrochemical response of a natural pentlandite electrode (with exposed area of 0.00234 cm^2) was measured when the experimental set-up was placed inside and outside the cage. No major differences in current density (see Figure 6.14) were observed. Three linear anodic measurements were performed in each case and they were repeatable (see Figure E2 in appendix E).

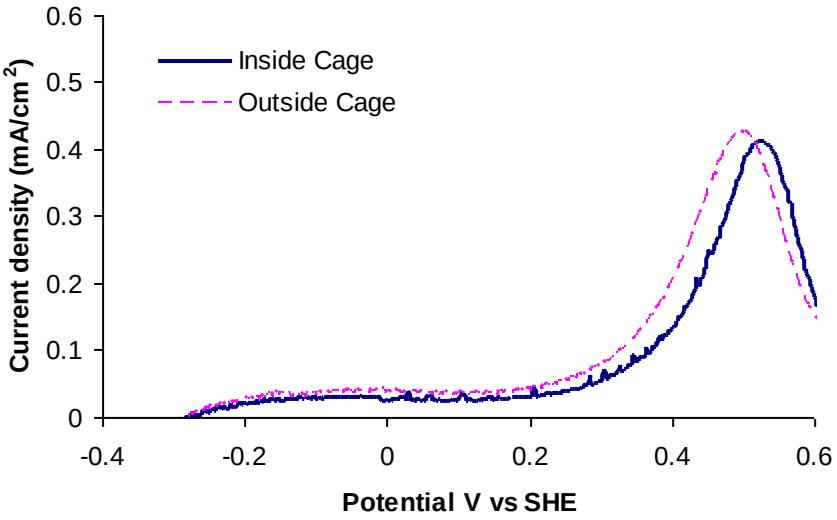

Figure 6.14: Linear potential sweep voltammogram of a natural pentlandite electrode with exposed area of 0.00234 cm^2, measured in a 0.05 M $Na_2B_4O_7$ (pH 9.3) at 25 °C, at a scan rate of 10 mV/s inside and outside the Faraday Cage.

During electrochemical oxidation of a synthetic pentlandite in water, at a potential of 0.8V, Richardson and Vaughan (1989) observed shrinkage cracks at the surface. These authors reported the cracks to have formed due to the removal of excess metal atoms, largely iron and the formation of violarite. Violarite is believed to have transformed from pentlandite at the sub-surface and is responsible for the formation of shrinkage cracks (Richardson and Vaughan, 1989). The effect of iron vacancies and shrinkage cracks on the electronic structure of pentlandite has not been substantiated experimentally. Legrand *et al*. (1997) also confirmed that pentlandite has a high level of micro–fracturing.

The microelectrode technique was previously successfully applied to natural pyrite particles hand–picked from the flotation concentrate of an auriferous pyrite ore from Carlin, Nevada (Vermaak *et al*., 2006). Repeatable measurements were made and no deep cracks and pores were observed at the pyrite surface after abrading the surface using a P-4000 grade silicon carbide paper (see Figure 6.15). This could have been due to the

differences in the grade of silicon carbide paper employed. The surface of pentlandite electrode was abraded with a 2400 grade silicon carbide paper instead. However, the differences in the hardness and toughness of the two minerals may have also contributed to this effect.

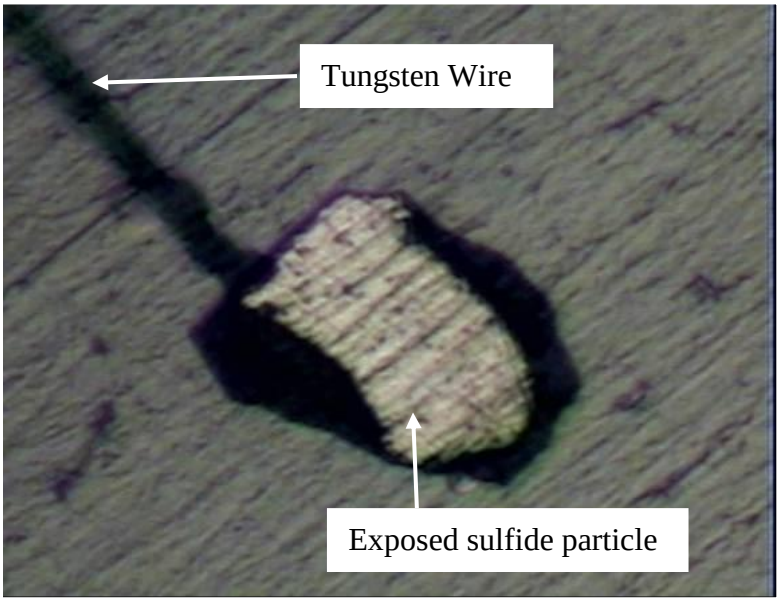

Figure 6.15: Optical microscope image of pyrite electrode handpicked from the flotation concentrate after abrading on a P-4000 grade silicon carbide paper (Vermaak *et al.*, 2006).

In sulfide flotation, pentlandite is known to break faster than other sulfides and hence slimes easily (Vos, 2006). This supports the suggestion that a difference in the mechanical behaviour is responsible for the difficulty of making reproducible measurements with pentlandite micro-electrodes. To investigate mechanical differences between pyrite and pentlandite, microhardness measurements were performed on natural massive pentlandite and pyrite samples. Table 6.14 shows hardness measurements performed on massive pentlandite from the Kola Peninsula (Russia) and a massive pyrite sample. Pentlandite is much softer than pyrite, with hardness of 212 kg/mm^2 compared to 962 kg/mm^2 for pyrite; these are within the expected range (Vaughan and Craig, 1978).

Microhardness measurements were also performed on a single microelectrode. An even lower micro Vickers hardness of 95.8 kg/mm^2 was measured using a load of 100g and dwell time of 15s. Figures 6.16 to 6.18 show images of the pentlandite microelectrode, massive pentlandite and massive pyrite after microhardness tests showing the indentation made from the diamond indenter with cracks around the indentation. In contrast, no

indentation cracks were observed on a massive pyrite sample after the application of a load of 100g. It was for this reason that the applied load was increased to 200g, resulting in a hardness of 962 kg/mm^2.

Table 6.14: Vickers microhardness values for massive pyrite and pentlandite (load time of 15s).

Sample	Composition	VHN (kg/mm^2)	Vaughan and Craig (1978)	Applied load (g)
Pentlandite	$Fe_{4.3}Ni_{4.87}Co_{0.14}S_8$	212	202-231 kg/mm^2	100
Pyrite	$FeS_{1.94}$	962	913-2056 kg/mm^2	200

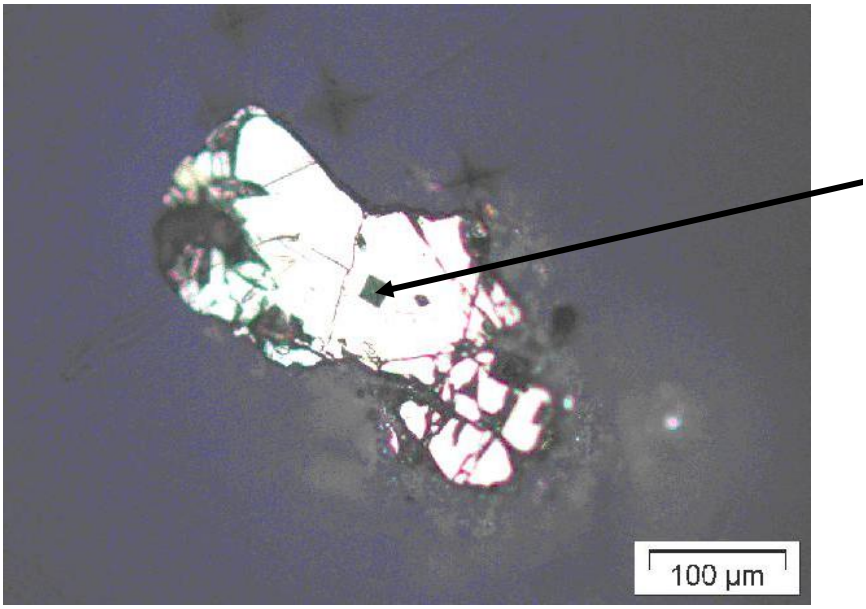

Figure 6.16: Optical microscope image of a natural pentlandite microelectrode showing the Vickers indentation after the application of a load of 100g.

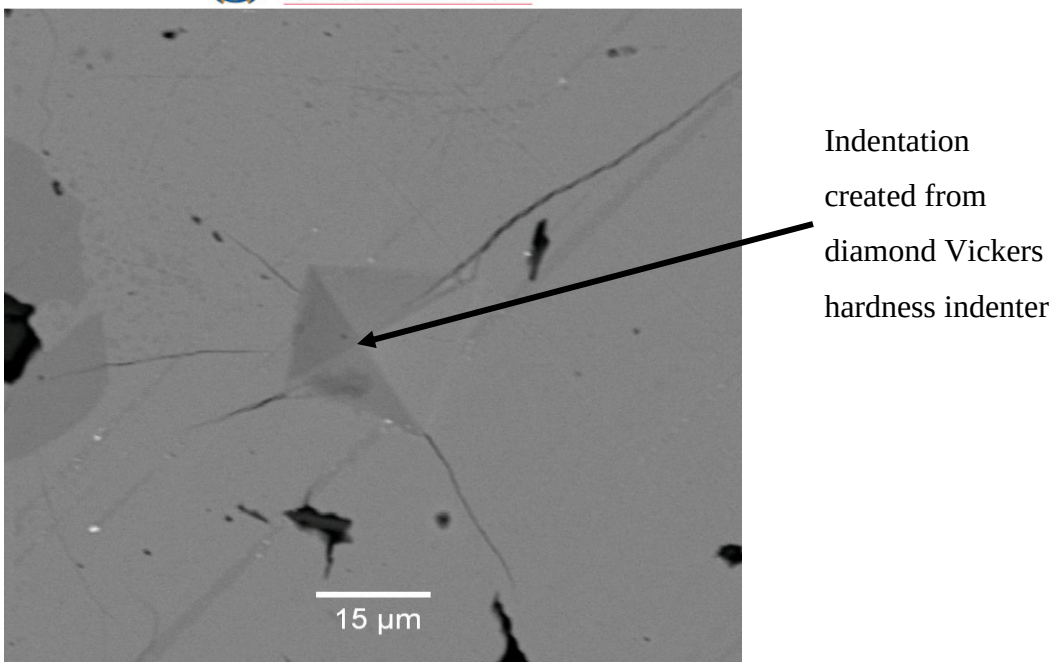

Figure 6.17: Secondary electron image (acceleration voltage 15 kV) of the massive pyrite sample, showing the Vickers indentation on a massive natural pentlandite sample after the application of a load of 100g, with evidence of indentation cracks.

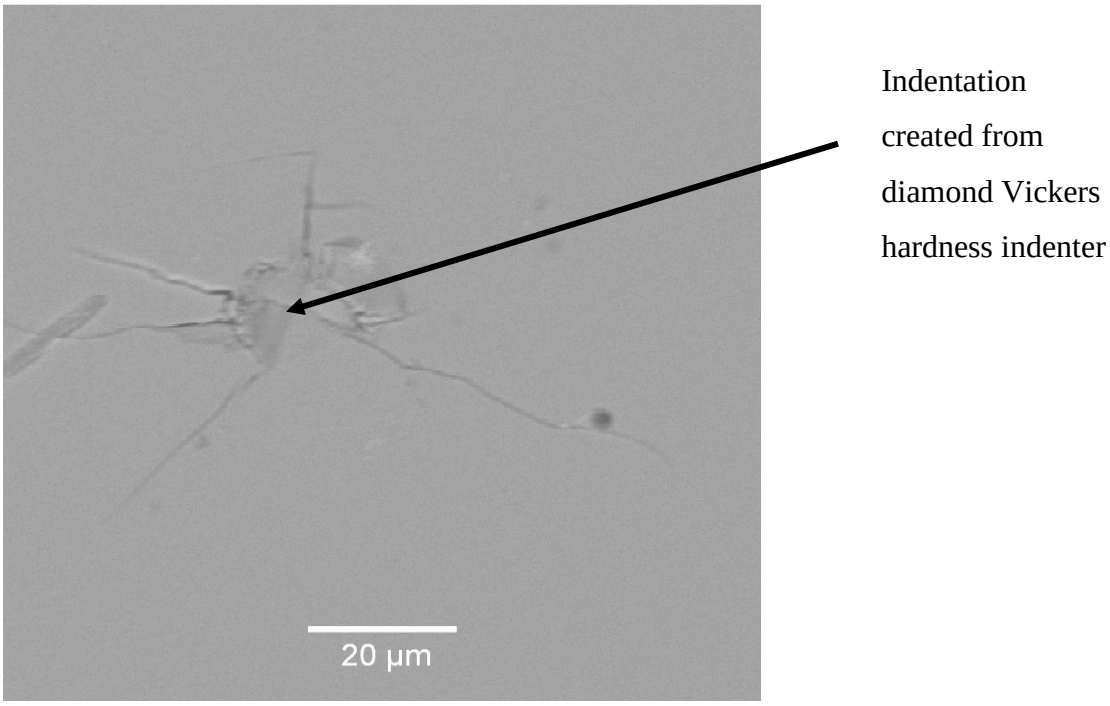

Figure 6.18: Secondary electron image (acceleration voltage 15 kV) of the massive pyrite sample, showing the Vickers indentation on a massive natural pyrite sample after the application of a load of 200g, with evidence of indentation cracks.

It is likely that the poor electrochemical response of pentlandite microelectrodes is a result of the exposure of pre-existing pores and cracks by polishing. At first, the

electrochemical measurements were performed after electron microprobe analysis of the microelectrodes. However, the extent of polishing that was required to achieve the flat, smooth surface, which is essential for accurate microprobe measurements meant that too little of the electrode remained to allow for re-polishing of the electrode in preparation for electrochemical measurements. Instead, electrochemical measurements were performed on newly prepared pentlandite microelectrodes, prior to electron microprobe analysis. During the electrochemical measurements, a poorly repeatable electrochemical response of the microelectrodes was observed. Deep pores were again observed (see Figure 6.19), indicating undesired gaps between the sulfide and the resin (Scharifker, 1992; Vermaak *et al.*, 2006).

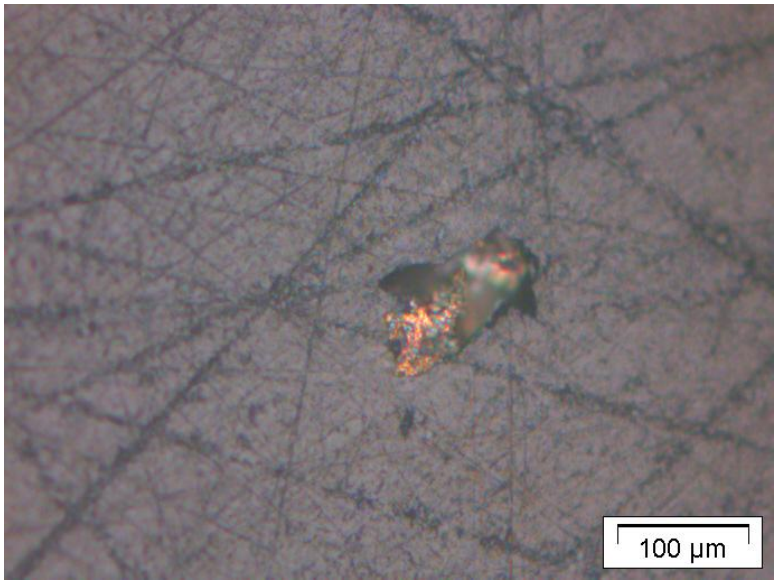

Figure 6.19: Optical image of pentlandite microelectrode after electrochemical measurement, prior to electron microprobe analysis, indicating the presence of pores and undesired gaps between the sulfide and resin.

Optical images obtained when analyzing the electrodes in a time of flight secondary ion mass spectroscopy (TOF-SIMS) confirmed an increase in pores at a natural massive pentlandite sample after electrochemical oxidation and polishing (see Figures 6.20 and 6.21). A massive pentlandite sample was oxidized in a $Na_2B_4O_7$ solution (pH 9.3) at various time intervals. Prior to oxidation, the mineral surface was polished with a 2400 grade silicon carbide paper. Polishing with a 2400 grade silicon carbide paper and electrochemical oxidation after thirty minutes resulted in deep pores in the massive pentlandite (see Figures 6.20 and 6.21).

From visual observations, the undesired gap between the epoxy and synthetic pentlandite electrode, disturbed the current during polarisation resistance measurements. Removing the gap, by further abrading the surface on a 2400 grade SiC paper, the desired electrochemical response of the synthetic electrode was observed. These observations, confirmed the effect of undesired gaps on the electrochemical response of the electrode during electrochemical measurements.

Pre-existing pores and cracks and electrochemical oxidation of pentlandite may have contributed to the poor electrical conductivity of pentlandite microelectrodes.

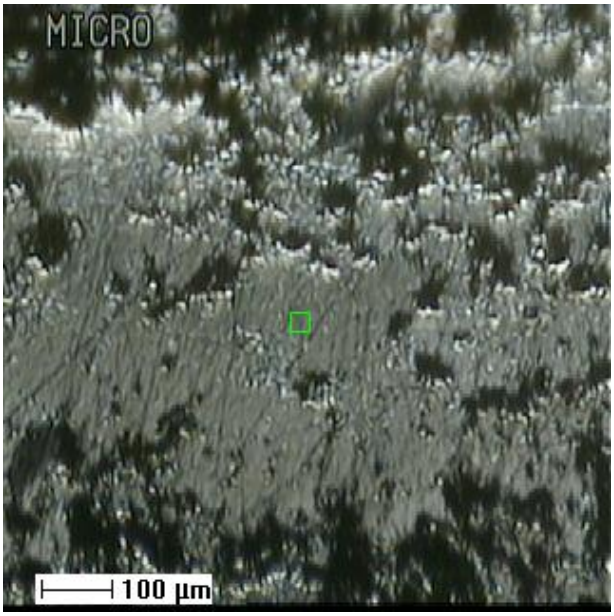

Figure 6.20: Optical image (from a TOF-SIMS instrument) of a natural massive pentlandite sample with evidence of pores after mechanical polishing and electrochemical oxidation.

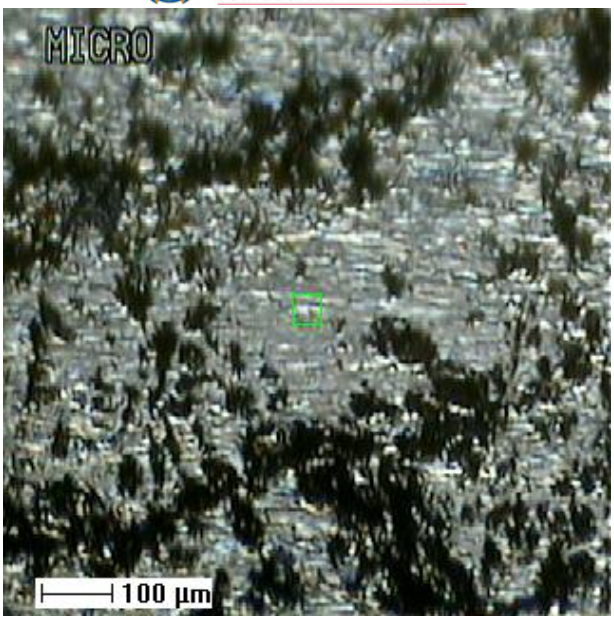

Figure 6.21: Optical image (from a TOF-SIMS instrument) showing electrochemically oxidised pentlandite, with evidence of increased pores after polishing and electrochemical oxidation.

6.3.2 Electrochemical measurements using massive natural pentlandite samples

Due to the poor performance of the pentlandite microelectrodes (±100 µm particles), massive pentlandite samples were used to test the effect of pentlandite composition on electrochemical behaviour. These samples were sourced from the Kola Peninsula deposit (Russia) and the Phoenix deposit (Botswana). It was difficult to source pure massive pentlandite samples from various deposits. Pentlandite and pyrrhotite are intimately associated together (Francis *et al.*, 1976; Van Zyl, 1996; Theart and De Nooy, 2001). Pentlandite occurs as stringers, blebs, flame-like exsolutions in pyrrhotite or as granular pentlandite in pyrrhotite (Francis *et al.*, 1976; Van Zyl, 1996; Theart and De Nooy, 2001). Pentlandite may occur in a massive (blocky) form (Francis *et al.*, 1976). The massive (blocky) pentlandite often contains islands of pyrrhotite (Francis *et al.*, 1976). It was for this reason that it was difficult to source pure massive pentlandite samples from various deposits; this limited the investigation (i.e. variations in chemical composition-samples employed did not display significant compositional variation as discussed in section 6.2.1).

Using massive pentlandite electrodes, electrochemical measurements were performed in a 0.05 M $Na_2B_4O_7$ buffer solution of pH 9.3 in equilibrium with air. The variation of

current as a function of potential was obtained by changing potential with time at a scan rate of 10 mV/s. Polarisation resistance was computed as the slope of the polarisation curve (i.e. potential vs current density) at the equilibrium potential (i.e. rest potential) at two minutes intervals, using Ohm's law. To understand the behaviour of pentlandite, relatively pure natural massive electrodes with minimal amounts of other mineral sulfides were employed (Figures C6 to C9, Appendix C).

Figure 6.22 depicts changes in the polarisation resistance of pentlandite as a function of time. Polarisation resistance measurements were repeatable, see Figures E3 and E4 in Appendix E. In the figure (i.e. Figure 6.22), curve A, B, C and D represents polarisation resistance for pentlandite electrodes with composition $Fe_{4.27}Ni_{4.75}Co_{0.14}S_8$, $Fe_{4.27}Ni_{4.76}Co_{0.14}S_8$, $Fe_{4.28}Ni_{4.79}Co_{0.14}S_8$ and $Fe_{4.07}Ni_{4.78}Co_{0.17}S_8$, respectively. The figure clearly indicates a rapid increase in the polarisation resistance during the first 300 seconds. This is probably due to the preferential oxidation of iron (i.e. migration of iron to pentlandite surface) forming iron hydroxide layer (Buckley and Woods, 1991; Legrand *et al*., 2005). It appears that as the mineral oxidises and oxide film grows at the surface increasing the resistance to the reaction between the pentlandite electrode and reduction of oxygen (the oxidation of pentlandite and the reduction of oxygen are the expected simultaneous complementary electrochemical reactions at the surface). Such oxidation products have been previously identified on the natural and synthetic pentlandite (Richardson and Vaughan, 1989; Buckley and Woods, 1991; Legrand *et al*., 2005). Legrand *et al.* (1997) confirmed the growth of iron hydroxide at a pentlandite surface using X-ray photoelectron spectroscopy (XPS).

Nickel oxide was identified on the pentlandite surface in addition to iron hydroxide (Buckley and Woods, 1991; Legrand *et al*., 2005). After 2500s, the polarisation resistance of electrodes A, B, C and D increased to final Rp values of 15.8 $k\Omega.cm^2$, 14 $k\Omega.cm^2$, 15.2 $k\Omega.cm^2$ and 11 $k\Omega.cm^2$, respectively. The differences in the final Rp value may be a result of the differences in the properties of the formed oxide film - and not necessarily of the composition of the oxidation products. The overall variation in the polarisation resistance was similar for all the electrodes investigated except for electrode D, with a lower final Rp value indicating increased reactivity.

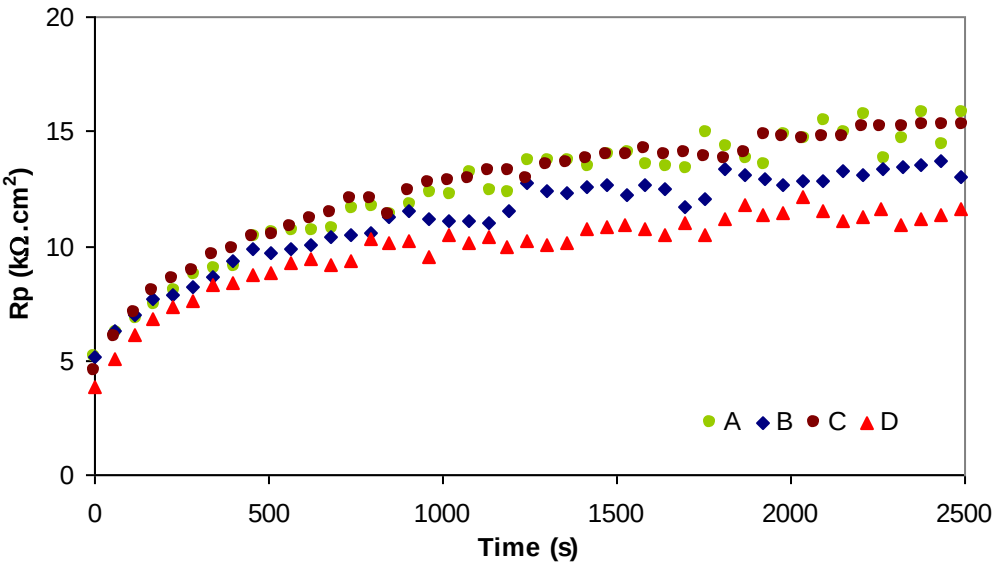

Figure 6.22: Polarisation resistance of natural massive pentlandite electrodes in an air saturated 0.05 M $Na_2B_4O_7$ solution of pH 9.3 at 25°C and a scan rate of 10 mV/s: (A)$Fe_{4.27}Ni_{4.75}Co_{0.14}S_8$ (Russia); (B) $Fe_{4.27}Ni_{4.76}Co_{0.14}S_8$ (Russia); (C)$Fe_{4.28}Ni_{4.79}Co_{0.14}S_8$ (Russia); (D) $Fe_{4.07}Ni_{4.78}Co_{0.17}S_8$ (Phoenix).

Figure 6.23 shows the rest potential values of pentlandite electrodes as a function of time in an aqueous 0.05 M $Na_2B_4O_7$ solution at 25°C in equilibrium with air. Rest potential (i.e. mixed potential) was simultaneously recorded with the polarisation resistance. It was estimated where the applied current is zero. The measurements were repeatable (see Figure E5 and E6 in appendix E). In this figure, the initial rest potential for electrodes A, B, C and D was 0.165 V_{SHE}, 0.168 V_{SHE}, 0.163 V_{SHE} and 0.116 V_{SHE}, respectively. Electrode D shows a lower initial rest potential of 0.12 V_{SHE} indicating increased reactivity (Abraitis *et al*., 2004; Khan and Kelebek, 2004). After 2500s, electrodes A, B, C and D reached a final rest potential value of 0.22 V_{SHE}, 0.215 V_{SHE}, 0.221 V_{SHE} and 0.217 V_{SHE}, respectively. The final rest potential values are close to the values reported for a pentlandite electrode at pH 9.2 in equilibrium with air (Buckley and Woods, 1991; Khan and Kelebek, 2004). Pentlandite electrodes employed showed similar final rest potential values. The similarity is in agreement with previous rest potential measurements of pyrites from various geological environments (Abraitis *et al*., 2004). Abraitis *et al*. (2004) suggested that slight mineralogical variations (between sulfides of the same type) may not have as significant effects on rest potential values as do changes in the type of sulfides (e.g. pyrite vs pentlandite).

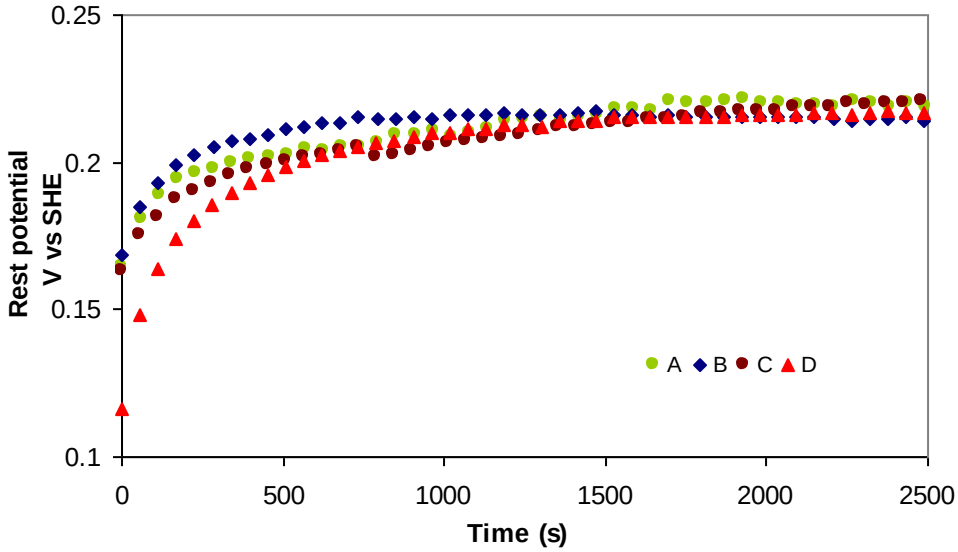

Figure 6.23: Rest potential variation of massive pentlandite electrodes in air saturated 0.05 M sodium tetraborate solution of pH 9.3 at 25°C: (A) $Fe_{4.27}Ni_{4.75}Co_{0.14}S_8$ (Russia);(B)$Fe_{4.27}Ni_{4.76}Co_{0.14}S_8$;(Russia) (C) $Fe_{4.28}Ni_{4.79}Co_{0.14}S_8$ (Russia); (D) $Fe_{4.07}Ni_{4.78}Co_{0.17}S_8$ (Phoenix).

Mineral rest potentials have been used to identify the reactions and follow the changes in the surface composition of sulfide minerals occurring at the electrode/solution interface (Heyes and Trahar, 1977; Gardner and Woods, 1979). Similar final rest potential values obtained suggest that massive pentlandite samples, with similar compositions undergo similar changes in the surface composition and therefore may produce similar oxidation products.

In order to identify possible reactions responsible for the increase in polarisation resistance and determine any differences between the anodic oxidation of the pentlandite electrodes, voltammetry measurements were performed. The voltammograms were obtained in a 0.05 M $Na_2B_4O_7$ solution in the absence of oxygen (in order to measure the oxidation of pentlandite without interference by simultaneous reduction of dissolved oxygen). In Figure 6.24, curves B, C and D represent linear voltammograms of natural massive pentlandite electrodes with a composition of $Fe_{4.27}Ni_{4.76}Co_{0.14}S_8$, $Fe_{4.28}Ni_{4.79}Co_{0.14}S_8$ and $Fe_{4.07}Ni_{4.78}Co_{0.17}S_8$ respectively. Anodic voltammograms measurements were repeatable (see Figure E7, Appendix E). The anodic oxidation of the electrodes commences at approximately -0.34 $V_{SHE,}$ indicating similar rest potential values. The potential at which the anodic oxidation of pentlandite electrode commenced, indicates the rest potential. At -0.1 V_{SHE} a small anodic peak was observed. This may be a

result of pyrrhotite. Figure 6.25 shows a voltammogram of a pyrrhotite electrode, sourced from the same deposit (i.e. Kola Peninsula, Russia). The measurements were repeatable (see Figure E8, Appendix E). The voltammogram indicates a small anodic peak at potentials below -0.1 $V_{SHE,}$ similar to that observed on the pentlandite voltammogram. On the pentlandite voltammograms, the peak was not significant.

At the pentlandite voltammograms, an anodic peak was observed at 0.1 V_{SHE}. The anodic peak at 0.1 V_{SHE} has been associated with the oxidation of Fe^{2+} to Fe^{3+} (FeOOH / $Fe(OH)_3$) (Hamilton and Woods, 1981; Buckley and Woods, 1991). At this anodic peak (0.1 V_{SHE}), increased current densities were observed with electrode C and D suggesting the increased reactivity of the electrodes.

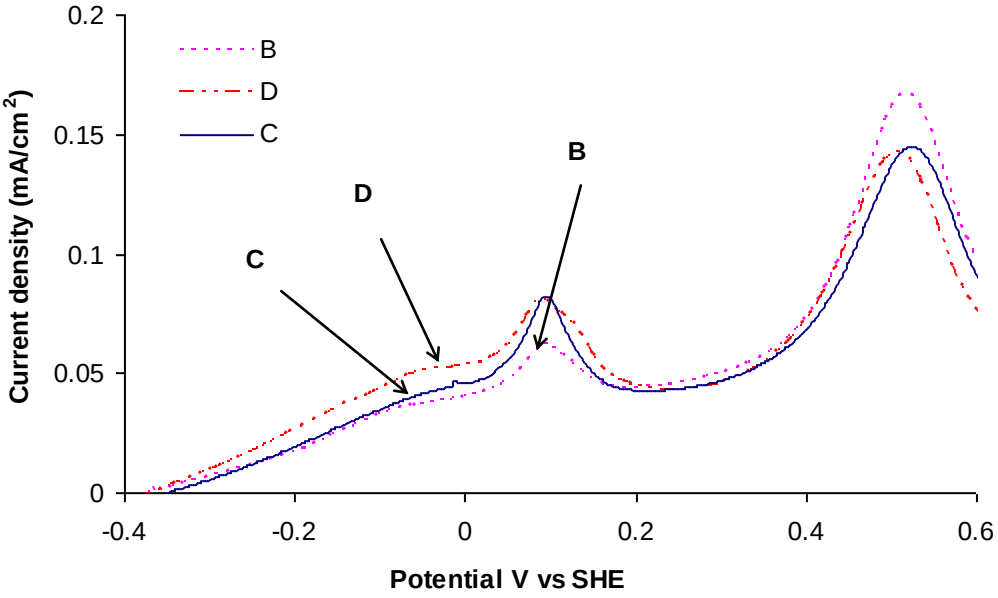

Figure 6.24: Linear potential sweep voltammograms of natural massive pentlandite electrodes in 0.05 M $Na_2B_4O_7$ at 25°C, at a scan rate of 10 mV/s: (B)$Fe_{4.27}Ni_{4.76}Co_{0.14}S_8$(Russia);(C) $Fe_{4.28}Ni_{4.79}Co_{0.14}S_8$ (Russia); (D) $Fe_{4.07}Ni_{4.78}Co_{0.17}S_8$ (Phoenix).

It is possible that at a potential of 0.1 V_{SHE} pentlandite oxidises by the following reaction (equation 16), leaving a metal deficient and sulfur rich sub-lattice:

$$Fe_xNi_yS_8 + 3\ OH^- \rightarrow Fe_{x-1}Ni_yS_8 + Fe(OH)_3 + 3e^- \qquad [16]$$

As the potential increased, the current density decreased, depicting passivating characteristics of the formed oxide on the electrode. At higher potentials (approximately

0.5 V_{SHE}), sulfur oxidises to sulphate (Hamilton and Woods, 1981; Buckley and Woods, 1991; Vaughan *et al*., 1995; Khan and Kelebek, 2004). At these potentials the oxidation of pentlandite may proceed through reaction 17 provided by Khan and Kelebek (2004):

$$Pn\ [(Fe_{4.5}Ni_{4.5})S_8] + 54.5\ OH^- \rightarrow Pn\ [4.5\ Fe(OH)_3 + (4.5\text{-}x)\ Ni(OH)_2] + x\ Ni(OH)_2 + 8\ SO_4^{2-} + 38.5e^- \quad [17]$$

The formation of polysulfides (S^{2-}) were detected on millerite (NiS) oxidised in air and de-ionised water. However, the polysulfides have not been detected at the oxidised pentlandite surface (Buckley and Woods, 1991; Legrand *et al*., 1997; Legrand *et al*., 2005). The commencement of the anodic oxidation of nickel has not been clearly identified. The anodic investigations of metallic nickel, synthetic heazlewoodite (Ni_3S_2), Fe53Ni alloy and NiS demonstrated that there are no distinctive features of the reactions of possible nickel compounds within the potential region of interest that do not overlap with the reactions of iron and sulfur (Shamsul *et al*., 1964; Buckley and Woods, 1991; Rossi *et al*., 1992; Boinet *et al*., 2003). Previous X–ray photoelectron spectroscopy (XPS) investigations confirmed the formation of nickel oxide in addition to iron oxide (Buckley and Woods, 1991; Legrand *et al*., 2005).

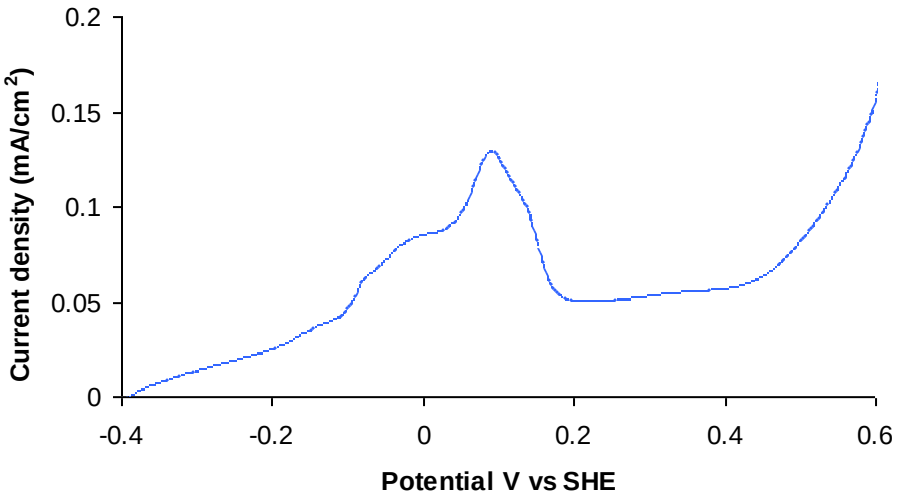

Figure 6.25: Linear potential sweep voltammogram of a natural massive pyrrhotite electrode (from the Kola Peninsula, Russia) in 0.05 M $Na_2B_4O_7$ at 25°C, at a scan rate of 10 mV/s.

The analogous formation of the anodic peaks at the same potentials depicted by the linear voltammograms, shows that the anodic oxidation of pentlandite electrodes employed

result in the same oxidation products. The polarisation resistance measurements performed in an oxygen-rich solution, were performed at the rest potential of approximately +0.2 V_{SHE} (see Figure 6.23). The value corresponds to the potential on the linear voltammogram at which substantial oxidation of natural pentlandite has occurred. This is similar to Buckley and Woods (1991) observations.

When a pentlandite electrode is immersed in a tetraborate solution in equilibrium with air, the anodic process on pentlandite is driven by the reduction of oxygen at the mineral surface. When the electrode oxidises, metal ions pass from the electrode surface into the solution (electrolyte), leaving a surplus of electrons at the surface (Craig, 1991). In the electrolyte, metal ions react with water, forming hydroxide species at the surface. The electrons flow across the surface of the electrode to the cathodic site. Dissolved oxygen in the electrolyte consumes the electrons at the surface where it is reduced to hydroxide ions. The movement of electrons released by the anodic reaction and consumed by the reduction of oxygen on the surface constitutes the current associated with the electrochemical reaction (Craig, 1991). It is the current measured during polarisation resistance measurements (Rp) where polarisation resistance is inversely proportional to the rate of the electrochemical reactions. Figure 6.26 shows a schematic illustration of a simple example of a steel oxidising in tap water (electrolyte) in the presence of dissolved oxygen. If metal ions pass into the solution easily, a small applied potential will produce high current density and therefore a low polarisation resistance. When the oxide starts to develop and grow at the surface, transport of ionic species through the oxide may be reduced (Craig, 1991). The reduction of oxygen becomes the rate determining step (Bockris and Reddy, 1970). The rate at which electrons are consumed by oxygen to be reduced to hydroxide ions will be decreased by the formation and growth of the oxide film. It is for this reason that Rp increases with time, indicating a decrease in the rate of the reactions. The total current flowing out of the anodic reaction must equal the total current flowing into the cathodic reaction (Craig, 1991). Since these two reactions depend on each other, a decrease in the rate of one will decrease the rate of the other (Craig, 1991).

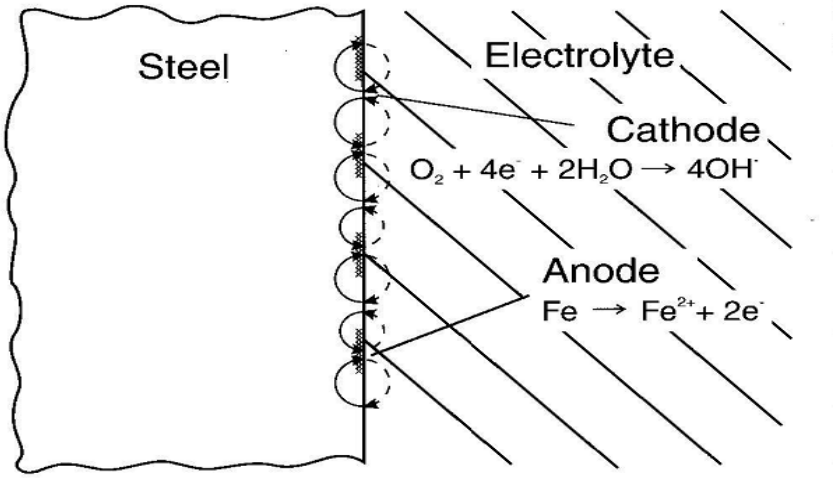

Figure 6.26: A simple schematic illustration of a steel oxidising in tap water (electrolyte) in the presence of dissolved oxygen (CISA, 1994).

The anodic oxidation observed at a potential of 0 V_{SHE} in the voltammograms (see Figure 6.24) was further investigated using current density-time transients. The measurements were repeatable (see Figure E9, Appendix E). Figure 6.27 show current density-time transients in response to an applied potential of 0 V_{SHE} in 0.05 M $Na_2B_4O_7$ solution at a pH 9.3 in the absence of oxygen. The current density of electrode D decreases rapidly during the first 10 seconds, then approaches a value above that of electrode B and C (see Figure 6.27), indicating the increased reactivity of the electrode. These results suggest, therefore, that electrode D oxidises at a faster rate and the oxide film forming is not as passivating as oxide film forming at electrode B and C.

This does show therefore that the behaviour of pentlandite electrode also depends on the type of oxide film.

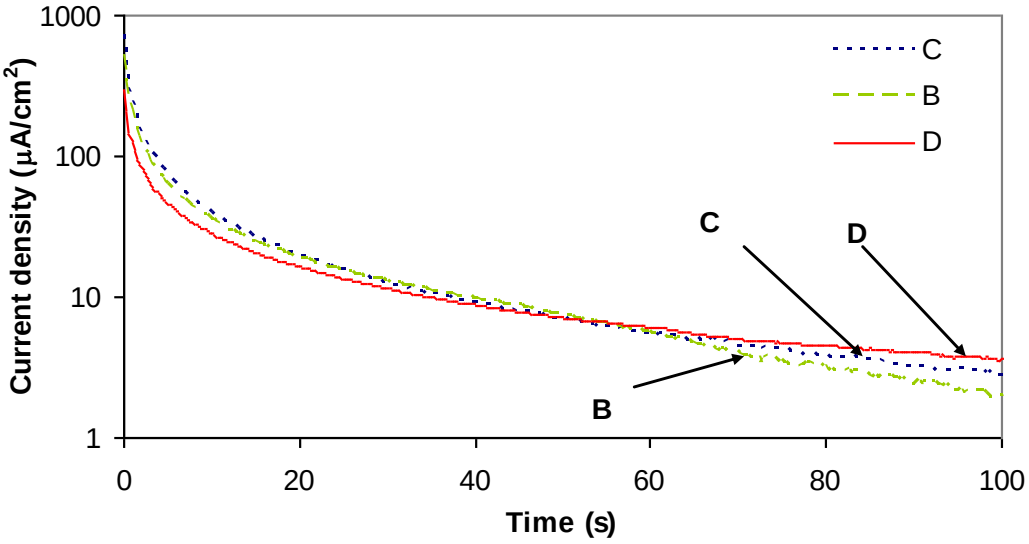

Figure 6.27: Current density-time transients of natural massive pentlandite electrodes in response to applied potential of 0 V_{SHE} in 0.05 M $Na_2B_4O_7$ at 25°C: (B)$Fe_{4.27}Ni_{4.76}Co_{0.14}S_8$(Russia);(C)$Fe_{4.28}Ni_{4.79}Co_{0.14}S_8$(Russia);(D)$Fe_{4.07}Ni_{4.78}Co_{0.17}S_8$ (Phoenix).

The polarisation resistance and rest potential measurements indicated analogous behaviour of pentlandite electrodes with a slight different behaviour from electrode D. The behaviour of electrode D is related to the formed oxide film, as depicted by the current density-time transients. In order to characterise formed products further, the electrochemical impedance spectroscopy measurements were performed. These measurements were performed to determine frequency at which the capacitance of the massive pentlandite samples can be measured.

Electrochemical impedance spectroscopy measurements were performed at the rest potential (i.e. corrosion potential) with Schlumberger 1287 Potentiostat, in conjunction with a Schlumberger 1260 frequency response analyser. The behaviour of the electrodes was measured in the form of impedance. A sulfide mineral electrode in an electrolyte can be represented by an array of resistors and capacitors (Mendiratta, 2000). Impedance is the resulting response when an AC voltage is applied across a circuit composed of capacitors and inductors, giving the resultant current of a sine or cosine wave shifted in time known as a phase angle shift (Silverman, 1986). The impedance can be expressed as follows:

$$Z = Z' - jZ'' \qquad [18]$$

where $Z' = R_s + \frac{R_p}{1+\omega^2 C^2 R_p^{\ 2}}$ [19]

and $Z'' = \frac{\omega C R_p^{\ 2}}{1+\omega^2 C^2 R_p^{\ 2}}$ [20]

Z' and Z" are the real and imaginary components of the impedance where Rp and Rs are the polarisation resistance and solution resistance respectively, C is the double layer capacitance and $\omega = 2\pi f$ where f is the frequency of the applied AC potential.

At larger frequencies where $\omega^2 C^2 R_p^{\ 2} >> 1$, the imaginary part of the impedance can be approximated by:

$$Z'' = \frac{1}{\omega C} \quad [21]$$

At these frequencies, an appropriate frequency can be determined to study the double layer capacitance. To determine the frequency at which capacitance measurements can be performed, the impedance was represented in a Bode plot. Figures 6.28 and 6.29 show the Bode plot of impedance modulus (|Z|) and phase angle (Θ) against frequency for pentlandite electrodes with similar compositions. The Figures show variation of impedance and phase angle with frequency. From the measurements, it is evident that the capacitance measurements may be performed at frequencies higher than 1000Hz. In this frequency range, the impedance is dominated by the ohmic (solution) resistance and the capacitive impedance of the electrode-electrolyte interface, allowing simple analysis of the impedance data to obtain the electrode capacitance.

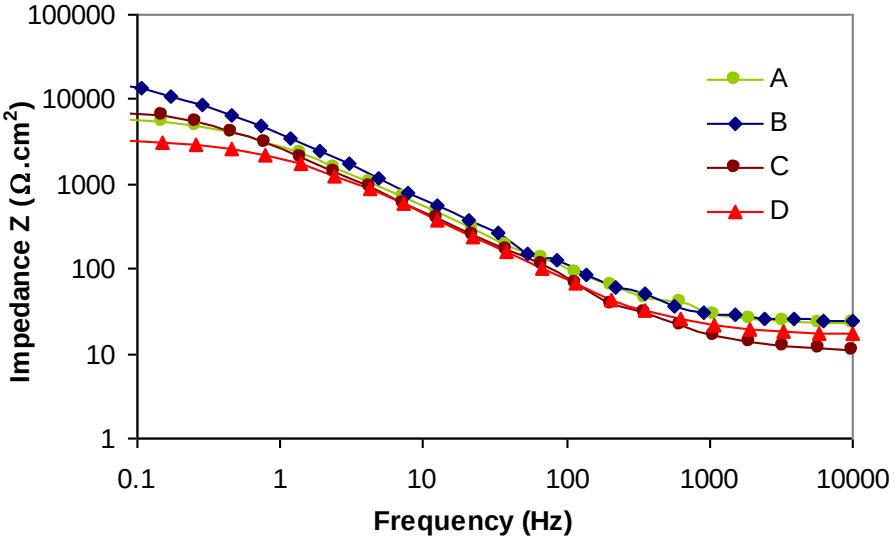

Figure 6.28: Bode plots for pentlandite electrodes at pH 9.3 in air saturated 0.05 M $Na_2B_4O_7$ solution measured at corrosion potential (i.e. equilibrium potential) indicating impedance against frequency: (A) $Fe_{4.27}Ni_{4.75}Co_{0.14}S_8$ (Russia); (B) $Fe_{4.27}Ni_{4.76}Co_{0.14}S_8$ (Russia); (C) $Fe_{4.28}Ni_{4.79}Co_{0.14}S_8$ (Russia); (D) $Fe_{4.07}Ni_{4.78}Co_{0.17}S_8$ (Phoenix).

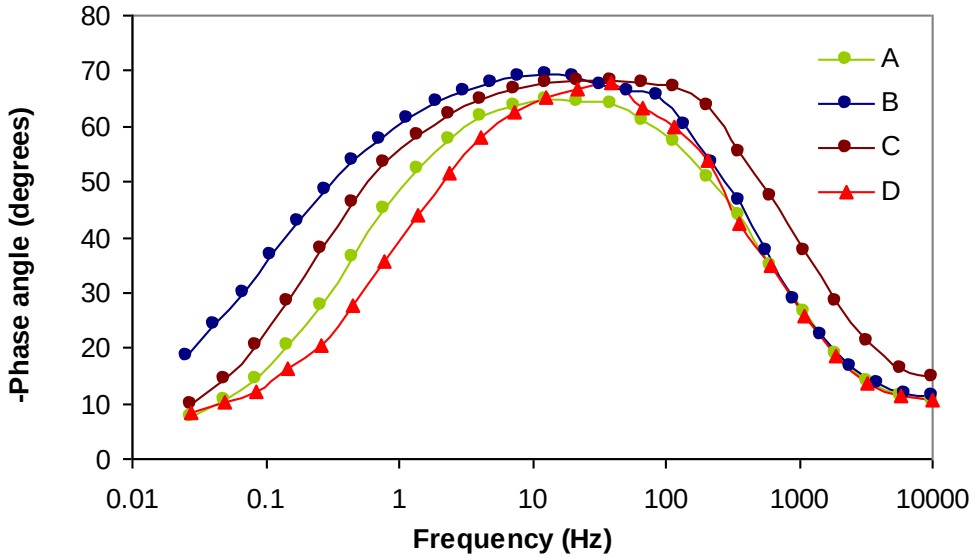

Figure 6.29: Bode plots for pentlandite electrodes at pH 9.3 in air saturated 0.05 M $Na_2B_4O_7$ solution measured at corrosion potential (i.e. equilibrium potential) indicating phase angle against frequency:(A)$Fe_{4.27}Ni_{4.75}Co_{0.14}S_8$(Russia);(B) $Fe_{4.27}Ni_{4.76}Co_{0.14}S_8$(Russia);(C)$Fe_{4.28}Ni_{4.79}Co_{0.14}S_8$(Russia);(D)$Fe_{4.07}Ni_{4.78}Co_{0.17}S_8$ (Phoenix).

To characterise the products forming at the pentlandite electrode, *in situ* capacitance measurements were conducted. Measurements were conducted in an air saturated

tetraborate solution of pH 9.3 at a frequency of 3000 Hz. The capacitance effect is a result of the double layer charging effect (C_D) and possible surface layers (Cs) forming at the electrode (Vermaak *et al*., 2004). Capacitance gives an indication of layer growth and possible differences in the electronic properties of the product layers (Craig, 1991; Rahim, 1995). The change in capacitance with time can thus be used to follow the oxidation process of a sulfide mineral. The capacitance was calculated from the imaginary part of the impedance using equation 22 where Rp is greater than R_Ω and f is the frequency and Z_{im} is the imaginary part of the impedance.

$$C = \frac{-1}{2\pi Z_{im} f} \qquad [22]$$

Figure 6.30 shows the capacitance for pentlandite electrodes over time measured at an applied potential of 0.2 V_{SHE} (which is close to the typical rest potential - see Figure 6.22). This was performed to follow changes in the pentlandite electrode surface as the electrochemical reactions take place. Capacitance measurements were repeatable (see Figure E10, Appendix E). The electrochemical impedance spectroscopy measurements performed after polarisation at the open circuit potential are not representative of the reactions occurring (Venter, 2007). During the first few seconds, the electrodes exhibited a slight decrease and relatively constant capacitance, probably as a result of the oxidation of iron to a hydrated oxide film (Buckley and Woods, 1991; Legrand *et al*., 2005). This corresponds with the increase in polarisation resistance measurements within the first 300s. After 500s, a continuous increase in capacitance was observed. In this time range, polarisation resistance measured under similar conditions increased gradually for all pentlandite electrodes (see Figure 6.22). A slight increase in capacitance was observed after 500s. The slight increase in capacitance may be a result of formation of thinner layer or variation in the electronic properties of formed film. Variation in capacitance indicates changes in the electronic properties of the product layer (Kelsall and Page, 1984; Boinet *et al*., 2003). These observations are similar to Kelsall and Page (1984) findings for a chalcopyrite electrode ($CuFeS_2$). With the pentlandite electrodes, this may have resulted from oxidation of iron to a hydrated oxide followed by formation of nickel oxide changing the dielectric constant of the oxide film (Buckley and Woods, 1991; Legrand *et*

al., 2005). Increase in capacitance may also be associated with pseudo capacitance because of product adsorption (Kelsall and Page, 1984).

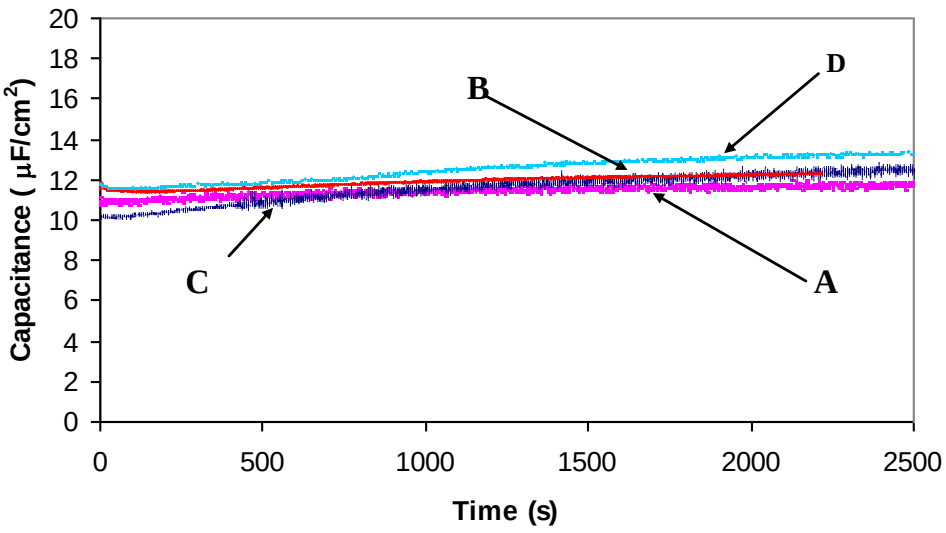

Figure 6.30: Capacitance measurements of pentlandite electrodes as a function of time measured during polarization at 0.2 V_{SHE} in a buffered 0.05 M tetraborate solution of pH 9.3: (A)$Fe_{4.27}Ni_{4.75}Co_{0.14}S_8$ (Russia); (B) $Fe_{4.27}Ni_{4.76}Co_{0.14}S_8$ (Russia); (C) $Fe_{4.28}Ni_{4.79}Co_{0.14}S_8$ (Russia); (D) $Fe_{4.07}Ni_{4.78}Co_{0.17}S_8$ (Phoenix).

The electrodes A to C show similar final capacitance values. Electrode D depicted a slight increased final capacitance value, indicating a thinner oxide layer. This is in agreement with the polarisation resistance measurements in which electrode D showed a lower final polarization resistance value, indicating the electrode to be more reactive. The similarities in the final capacitance values of electrode A to C indicate similar thickness of the oxide layers.

6.3.3 Electrochemical measurements using a synthetic pentlandite sample

Given the similar electrochemical behaviour of most of the natural massive pentlandite samples, a synthetic massive pentlandite sample was employed. The sample was employed to investigate the possible effect of chemical composition on the electrochemical response of a synthetic pentlandite with composition $Fe_{4.44}Ni_{4.48}S_8$.

Figure 6.31 shows the Rp measurements of a synthetic pentlandite in air saturated buffered $Na_2B_4O_7$ solution of pH 9.3. The polarisation resistance measurements were repeatable (see Figure E11, Appendix E). A new electrode was created by polishing between the experimental runs. At time zero, the synthetic sample indicated an initial polarisation resistance value of 6.9 kΩ.cm^2. A rapid increase in Rp within the first 300s was observed similar to the rapid polarisation resistance response of the natural massive pentlandite. The rapid increase in the polarisation resistance within the first 300s is probably a result of the preferential oxidation of iron as was previously observed by Richardson and Vaughan (1989). Richardson and Vaughan (1989) observed the formation of an iron-rich oxide layer after an initial rapid oxidation of a synthetic pentlandite with composition $Fe_{4.5}Ni_{4.5}S_8$. After 2500s, a final Rp value of 19 kΩ.cm^2 was measured. The final Rp value may be a result of formed oxide layer limiting the reduction of oxygen, preventing further rapid oxidation of the surface, measuring low currents (Richardson and Vaughan, 1989).

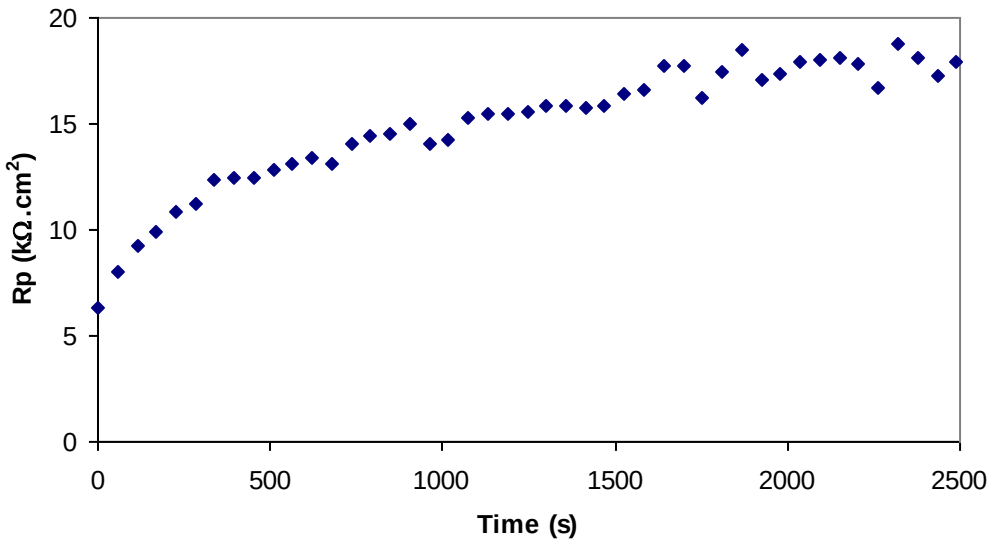

Figure 6.31: Polarisation resistance of a synthetic pentlandite with composition $Fe_{4.44}Ni_{4.48}S_8$ and exposed area of 0.29 cm^2 in an air saturated buffered 0.05 M $Na_2B_4O_7$ solution of pH 9.3.

In comparison with the natural massive pentlandite samples employed, synthetic pentlandite shows significant higher initial and final Rp values, indicating the sample to be less reactive (see Figure 6.32). The lower reactivity of the synthetic electrode may reflect a lower anodic reactivity of the electrode, lower rate of oxygen reduction at the

electrode surface or both. The results presented here, indicate a lower anodic reactivity of the synthetic sample.

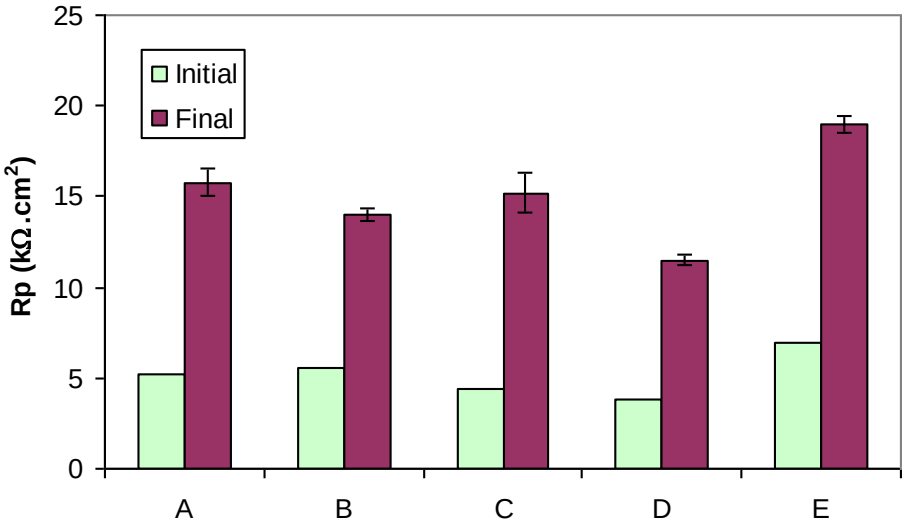

Figure 6.32: Initial and final Polarisation resistance (Rp) measurements of a synthetic and natural pentlandite in a buffered 0.05 M $Na_2B_4O_7$ solution of pH 9.3: (A)$Fe_{4.27}Ni_{4.75}Co_{0.14}S_8$(Russia);(B)$Fe_{4.27}Ni_{4.76}Co_{0.14}S_8$(Russia);(C)$Fe_{4.28}Ni_{4.79}Co_{0.14}S_8$ (Russia);(D)$Fe_{4.07}Ni_{4.78}Co_{0.17}S_8$(Phoenix);(E)$Fe_{4.44}Ni_{4.48}S_8$(synthetic).

The anodic reactivity of a synthetic pentlandite with composition $Fe_{4.44}Ni_{4.48}S_8$ was investigated using the linear anodic voltammogram. The voltammogram was measured in a 0.05 M $Na_2B_4O_7$ solution (pH 9.3) in the absence of oxygen. The measurements were repeatable (see Figure E12, Appendix E). The anodic oxidation of the synthetic sample (curve E) commenced at -0.4 V_{SHE}, slightly below the rest potential of the natural electrodes (curves B to D). This may have been influenced by the effect of iron content. The first anodic peak was observed at $0.1V_{SHE}$ (see Figure 6.33).

The anodic peak may be an indication of the oxidation of Fe^{2+} to Fe^{3+} by the following reaction:

$$Fe_{4.5}Ni_{4.5}S_8 + 3OH^- \rightarrow Fe(OH)_3 + Fe_{4.5-1}Ni_{4.5}S_8 + 3e^- \quad [23]$$

Synthetic pentlandite displays similar anodic behaviour to that of the natural pentlandite samples, with the second anodic peak forming at the same potential as with natural pentlandite samples, but at lower current density. The second anodic peak may be a result of the oxidation of sulfur to sulfate. Lower current densities were observed over the

whole potential range studied, indicating the reduced reactivity of a synthetic pentlandite sample. The reduced reactivity of the synthetic pentlandite is similar to that observed with a synthetic galena (Kim *et al*., 1994). The anodic peaks of the synthetic sample suggest that synthetic pentlandite produces similar oxidation products as does natural pentlandite.

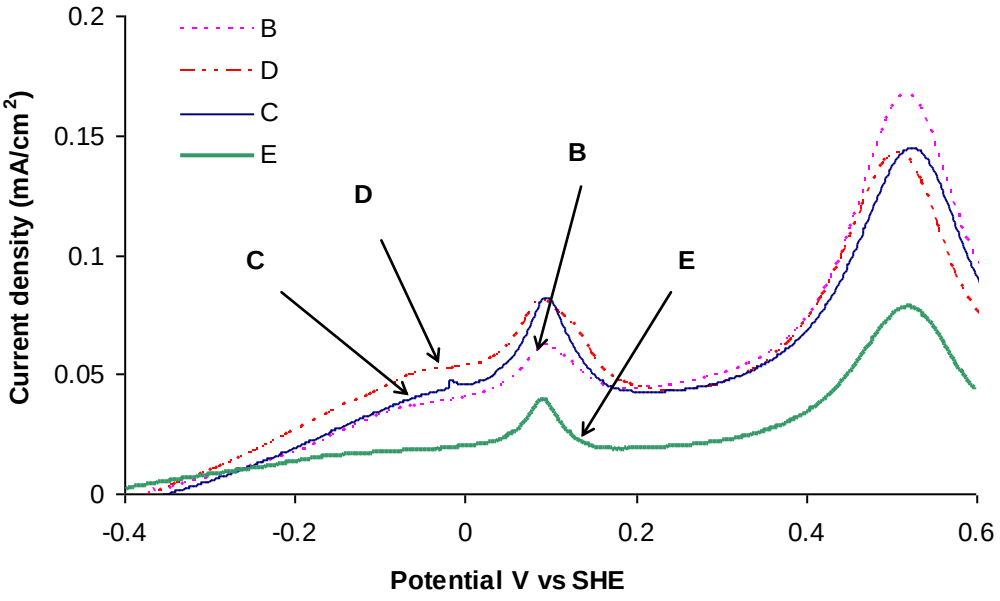

Figure 6.33: Linear potential sweep voltammograms of natural and synthetic massive pentlandite electrodes in 0.05 M $Na_2B_4O_7$ at 25°C, at a scan rate of 10m V/s: (B) $Fe_{4.27}Ni_{4.76}Co_{0.14}S_8$ (Russia); (C) $Fe_{4.28}Ni_{4.79}Co_{0.14}S_8$ (Russia); (D) $Fe_{4.07}Ni_{4.78}Co_{0.17}S_8$ (Phoenix); (E) $Fe_{4.44}Ni_{4.48}S_8$ (synthetic).

Previous X–ray photoelectron spectroscopy (XPS) investigations of a synthetic pentlandite electrochemically oxidised in water at a potential of 0.7 V, indicated iron hydroxide, nickel oxide and violarite as the oxidation products, with the possible formation of iron sulfate (Richardson and Vaughan, 1989).

The current decay during potentiostatic polarisation of synthetic pentlandite at 0 V_{SHE} and 0.2V_{SHE} (similar to the rest potential in oxygenated solutions) is shown in Figure 6.34 and 6.35 respectively. Figure 6.34 shows current density-time transients in response to an applied potential of 0 V_{SHE} in a 0.05 M $Na_2B_4O_7$ solution at a pH 9.3 in the absence of oxygen. There is a significant difference between the initial current density of a synthetic sample and the natural electrodes. During the first 10 s, the current density of the

synthetic electrode was low and then approaches a current density value, which is lower than that of the natural electrodes. This suggests that the formed oxide film may be more passivating than the film forming on natural electrodes.

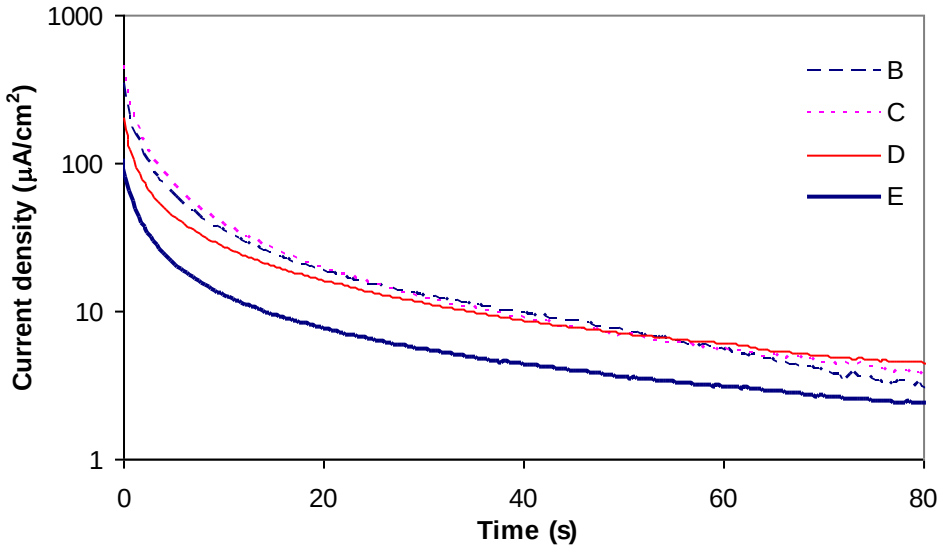

Figure 6.34: Current density-time transients of massive pentlandite electrodes in response to applied potential of 0 V_{SHE} in 0.05 M $Na_2B_4O_7$ at 25°C: (B) $Fe_{4.27}Ni_{4.76}Co_{0.14}S_8$(Russia);(C) $Fe_{4.28}Ni_{4.79}Co_{0.14}S_8$ (Russia); (D) $Fe_{4.07}Ni_{4.78}Co_{0.17}S_8$ (Phoenix); (E) $Fe_{4.44}Ni_{4.48}S_8$ (synthetic).

At an applied anodic potential of 0.2 V_{SHE}, the current density to which the anodic reaction on electrode C decreased was higher than the other electrodes indicating increased reactivity of electrode C. This is in contrast with the previous observations from the final Rp values and current density-time transients performed at 0 $V_{SHE.}$ The current density of the synthetic sample (i.e. electrode E) remained below that of the natural electrodes.

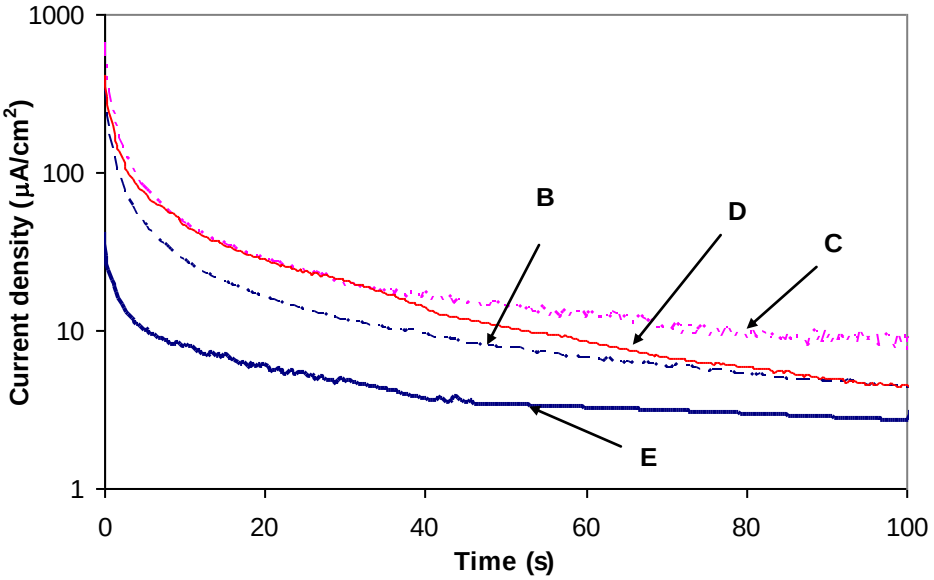

Figure 6.35: Current density-time transients of natural massive pentlandite electrodes in response to applied potential of 0.2 V_{SHE} in 0.05 M $Na_2B_4O_7$ at 25 °C: (B)$Fe_{4.27}Ni_{4.76}Co_{0.14}S_8$(Russia);(C)$Fe_{4.28}Ni_{4.79}Co_{0.14}S_8$(Russia);(D)$Fe_{4.07}Ni_{4.78}Co_{0.17}S_8$ (Phoenix); (E) $Fe_{4.44}Ni_{4.48}S_8$ (synthetic).

Microscope images of electrode C and D are shown in Figures 6.36 and 6.37. Electrode C is more porous than electrode D. The increased porosity of electrode C perhaps enhanced the apparent reactivity of the electrode; the exchange current density of an electrode is a strong function of the electrode composition and surface roughness (Craig, 1991). However, the minor difference in the capacitance between electrodes C and D (Figure 6.30) does not support the suggestion of a significant role of increased porosity.

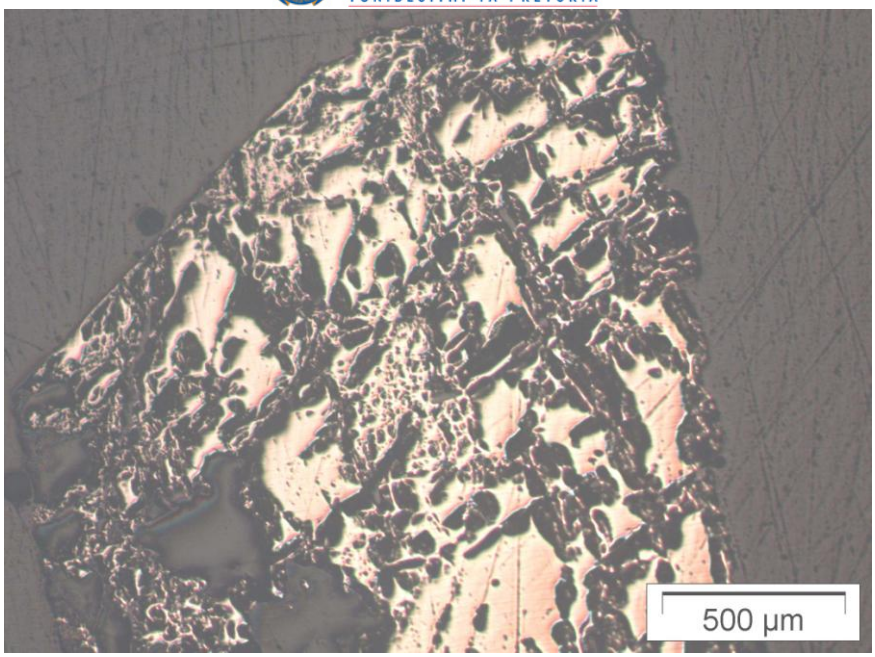

Figure 6.36: Microscope image of natural massive pentlandite with composition $Fe_{4.28}Ni_{4.79}Co_{0.14}S_8$ from Russia (electrode C).

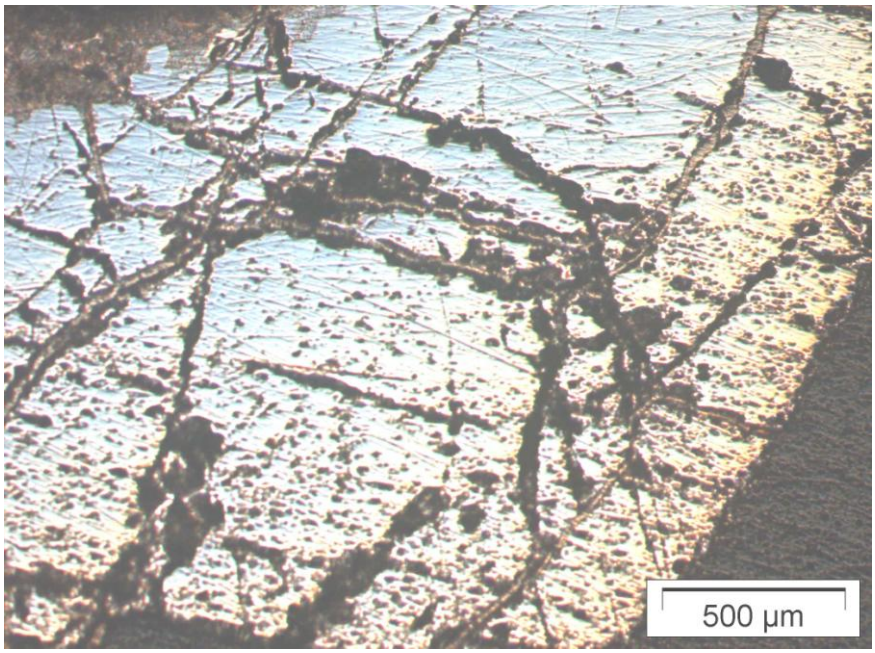

Figure 6.37: Microscope image of natural massive pentlandite with composition $Fe_{4.07}Ni_{4.78}Co_{0.17}S_8$ from the Phoenix deposit (electrode D).

The behaviour of the synthetic sample was further investigated using rest potential measurements in a 0.05 M $Na_2B_4O_7$ solution in equilibrium with air. The rest potential values were recorded simultaneously with the polarisation resistance values. Rest potential values were computed where the net current was zero. The rest potential of a

synthetic pentlandite is slightly lower than that of the natural electrodes (see Figure 6.38). This is in contrast with the lower anodic current density of the synthetic electrode (see Figure 6.33); if the cathodic polarisation behaviour (oxygen reduction) on all the electrodes were the same, the synthetic electrode should have had a more positive rest potential (because of its lower anodic current density). However, the less positive rest potential indicates that both the anodic oxidation rate and the rate of reduction of dissolved oxygen were slower on the synthetic electrode.

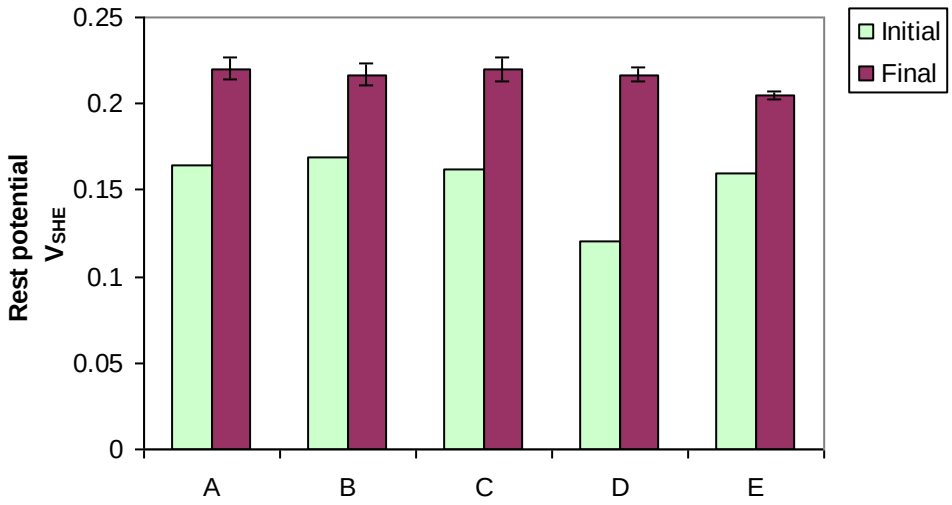

Figure 6.38: Initial and final rest potential measurements of a synthetic and natural pentlandite in a buffered 0.05 M $Na_2B_4O_7$ solution of pH 9.3: (A) $Fe_{4.27}Ni_{4.75}Co_{0.14}S_8$ (Russia); (B) $Fe_{4.27}Ni_{4.76}Co_{0.14}S_8$ (Russia); (C) $Fe_{4.28}Ni_{4.79}Co_{0.14}S_8$ (Russia); (D) $Fe_{4.07}Ni_{4.78}Co_{0.17}S_8$ (Phoenix); (E) $Fe_{4.44}Ni_{4.48}S_8$ (synthetic).

Differences in rest potential, which are also related to differences in oxygen reduction kinetics have been reported for other minerals (Rand, 1977). For example, pyrite has a rest potential much higher than other sulfide minerals; pyrite is a relatively good substrate for the reduction of oxygen (Majima, 1969; Ahlberg and Broo, 1996; Rand, 1997). In contrast, pyrrhotite is a poor substrate for the reduction of oxygen and has a rest potential much lower than that of other sulfides (Rand, 1977; Khan and Kelebek, 2004). An effect of mineral type on oxygen reduction kinetics appears surprising at first, since the rate of reduction of oxygen is expected to be limited by oxygen mass transfer at these potentials. However, the substrate can change the current density from a given oxygen diffusion flux, by changing the number of electrons involved in reduction reaction of each oxygen molecule. At a passivated iron electrode in a buffer solution, reduction of oxygen is by a two electron ($2e^-$) transfer reaction (instead of four electrons) (Jovancicevic and Bockris,

1986). The lower reactivity of high–iron pentlandites (e.g. synthetic pentlandite) may have resulted from this effect. Figures 6.39 to 6.41 show a direct correlation between pentlandite Fe:Ni ratio, iron and cobalt content and final Rp values for all the pentlandite electrodes employed, showing the effect of composition. It is however, difficult to distinguish if the differences in the reactivity are a result of Fe/Ni ratio or the influence of cobalt. The lack of sufficient pentlandite samples may have also contributed to these ambiguous conclusions.

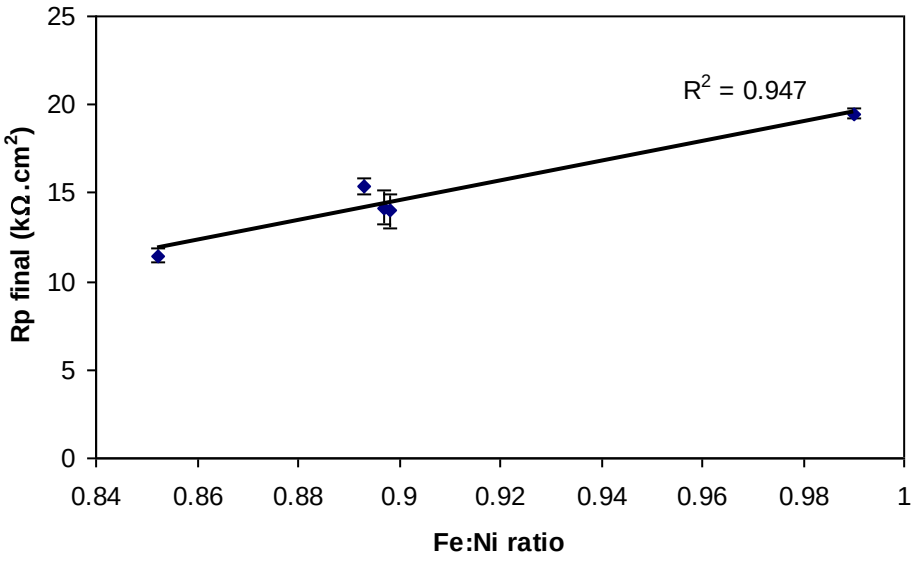

Figure 6.39 Final polarisation resistance (Rp) as a function of pentlandite Fe:Ni ratio for all the pentlandite electrodes employed including the synthetic sample.

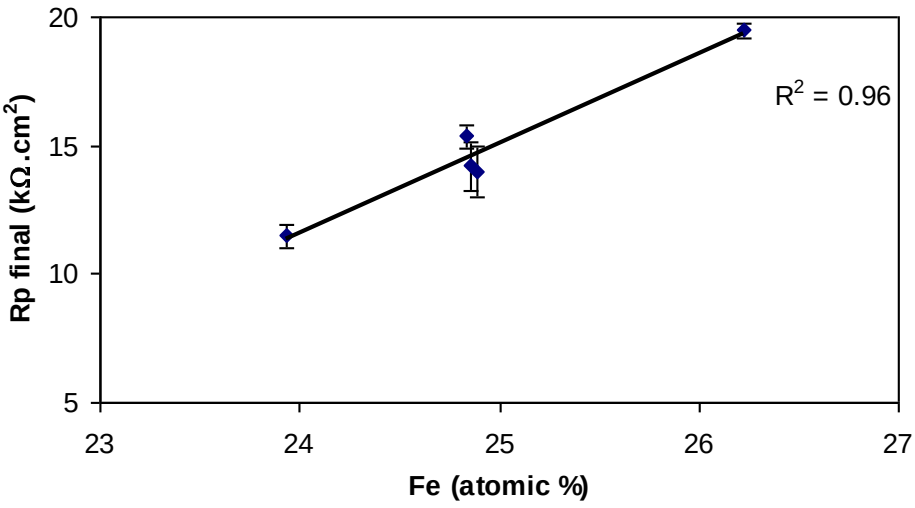

Figure 6.40: Final polarisation resistance (Rp) as a function of Fe (atomic %) for all the pentlandite electrodes employed including the synthetic sample.

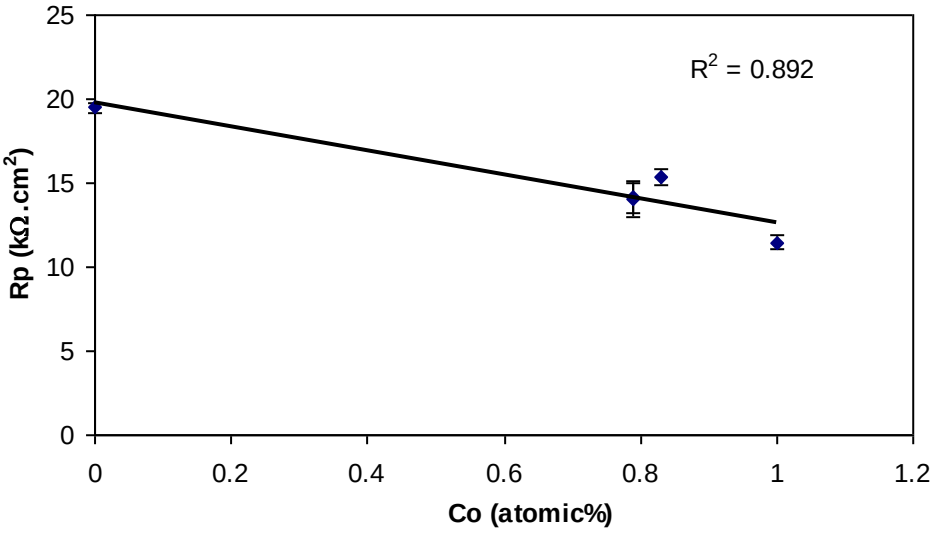

Figure 6.41: Final polarisation resistance (Rp) as a function of cobalt content for all the pentlandite electrodes employed including the synthetic sample.

In addition, the kinetics of the reduction of oxygen depends on the roughness of the surface (Craig, 1991; Ahlberg and Broo, 1996); a rough electrode enhances the reduction of oxygen (Biergler *et al*., 1975). A natural electrode was more porous than a synthetic electrode (see Figures 6.42 and 6.43). Other natural electrodes were less porous than the synthetic electrode (see Figure 6.37 and 6.43). However, the lack of a large difference in capacitance indicates that the differences in surface roughness did not have a major effect in these measurements.

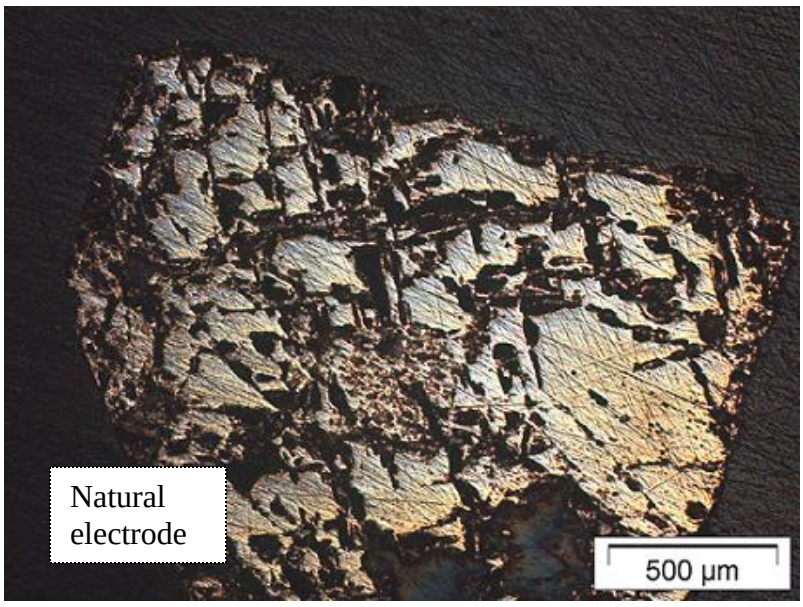

Figure 6.42: Microscope image of a rough natural pentlandite electrode.

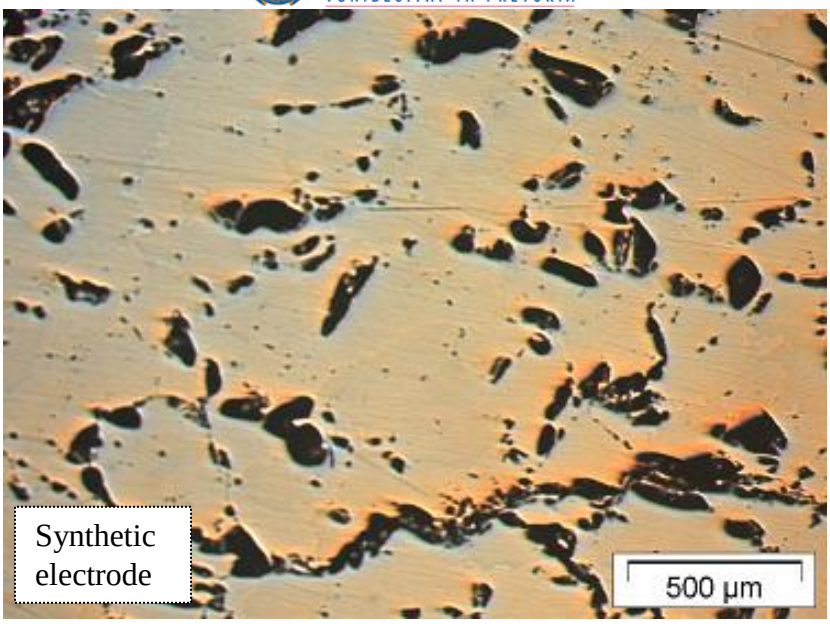

Figure 6.43: Microscope image of a synthetic pentlandite sample employed.

The formed oxide films on a synthetic pentlandite, were characterised by *in situ* capacitance measurements, in an air saturated tetraborate solution of pH 9.3, at a frequency of 3000 Hz. Measurements were performed while polarising at a potential of 0.2 $V_{SHE,}$ to follow any changes in the electrode surface. A final capacitance value of 8.65µF/cm^2 was measured (see Figure 6.44). A slight increase in capacitance was observed. This may be an indication of the changes in the electronic properties of the formed oxide films (Boinet *et al*., 2003). The capacitance measurements were repeatable (see Figure E13, Appendix E). In comparison with the natural electrodes, the capacitance value is significantly lower (see Figure 6.45). The low capacitance value may be a result of either a thicker oxide layer or a layer with a smaller dielectric constant. However, the lower capacitance is also associated with a lower anodic current density (see Figure 6.33) confirming that the electrode is less reactive anodically.

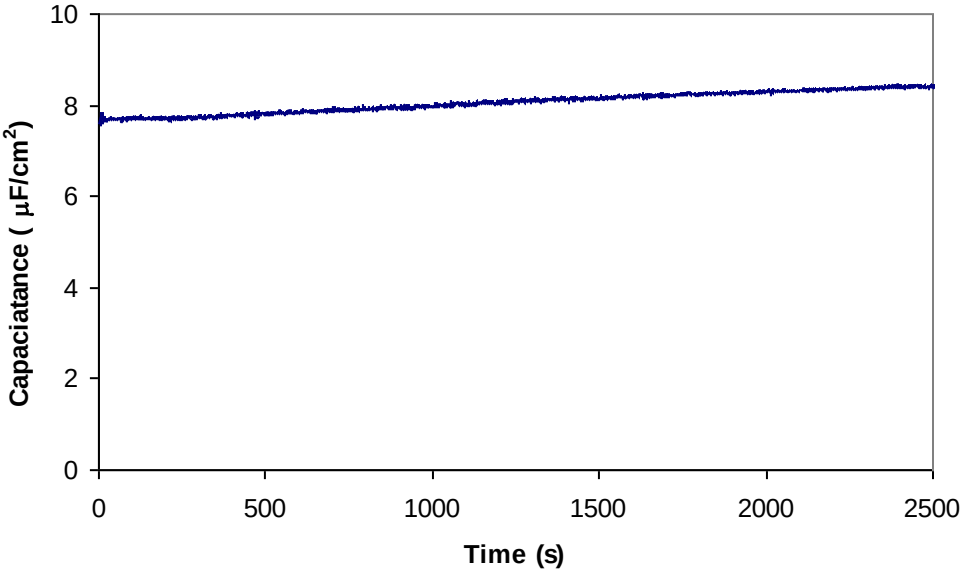

Figure 6.44: Capacitance measurements of a synthetic pentlandite electrode ($Fe_{4.44}Ni_{4.48}S_8$) as a function of time, measured during polarisation at 0.2 V_{SHE}, in a buffered 0.05 M $Na_2B_4O_7$ solution of pH 9.3 at 25°C.

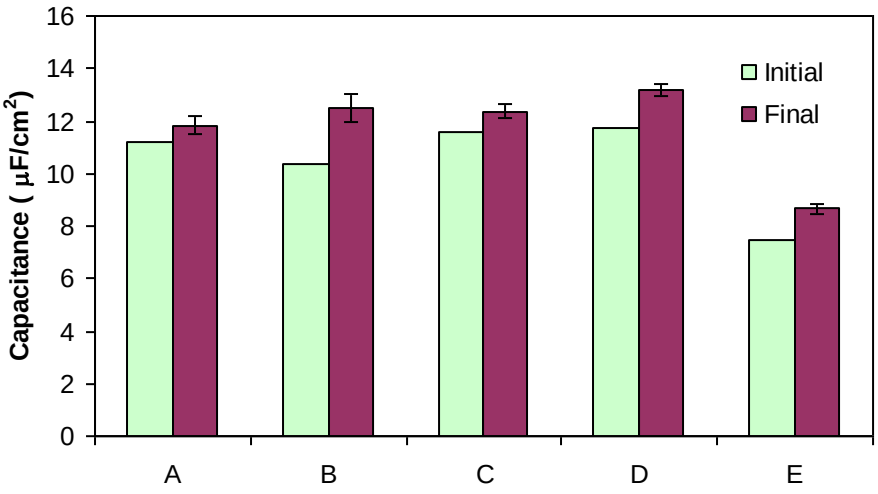

Figure 6.45: Initial and final capacitance measurements of a synthetic and natural massive pentlandite, measured in a buffered 0.05 M $Na_2B_4O_7$ solution of pH 9.3, in equilibrium with air, at 25°C, measured during polarisation at 0.2 V_{SHE}: (A) $Fe_{4.27}Ni_{4.75}Co_{0.14}S_8$ (Russia); (B) $Fe_{4.27}Ni_{4.76}Co_{0.14}S_8$ (Russia); (C) $Fe_{4.28}Ni_{4.79}Co_{0.14}S_8$ (Russia); (D) $Fe_{4.07}$ $Ni_{4.78}Co_{0.17}S_8$ (Phoenix); (E) $Fe_{4.44}Ni_{4.48}S_8$ (synthetic).

Figures 6.46 and 6.47, show a direct correlation between pentlandite Fe/Ni ratio, cobalt content and final capacitance values. It is also difficult to distinguish between the effect of Fe/Ni ratio and cobalt content on the final capacitance values. If the final capacitance values measured indicate the thickness of the formed film, it would therefore mean that high iron-pentlandite electrodes produce thicker oxide films. Thick oxide films strongly inhibit the reduction of oxygen, and the thickness is inversely proportional to the oxygen reduction current (Schultze *et al*., 1983; Chang and Wen, 2006). The thickness of deposited FeOOH on gold influenced the rate of the oxygen reduction (Schultze *et al*., 1983). On thicker oxide films, the reduction of oxygen follow a two electron ($2e^-$) transfer reaction (instead of four electrons) (Chang and Wen, 2006) similar to that observed on passivated iron electrode (Jovancicevic and Bockris, 1986).

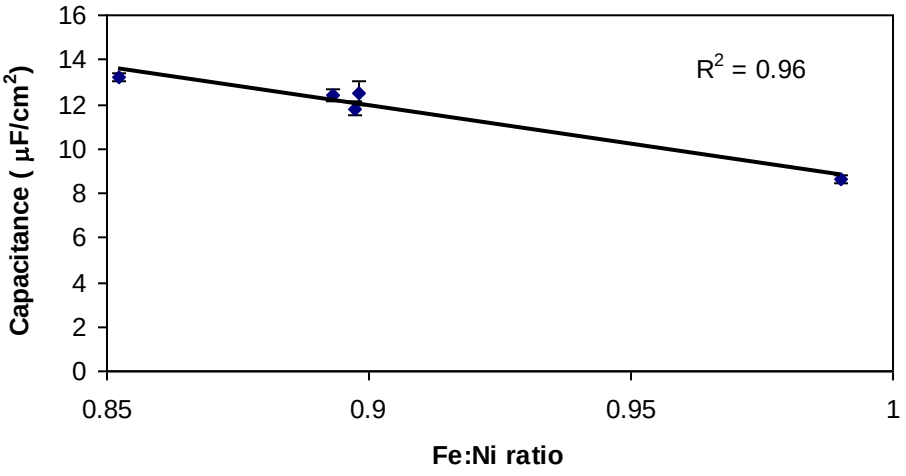

Figure 6.46: Final capacitance values of all pentlandite electrodes employed (including the synthetic electrode) as a function of the pentlandite Fe/Ni. The values are the same as those indicated in Figure 6.45.

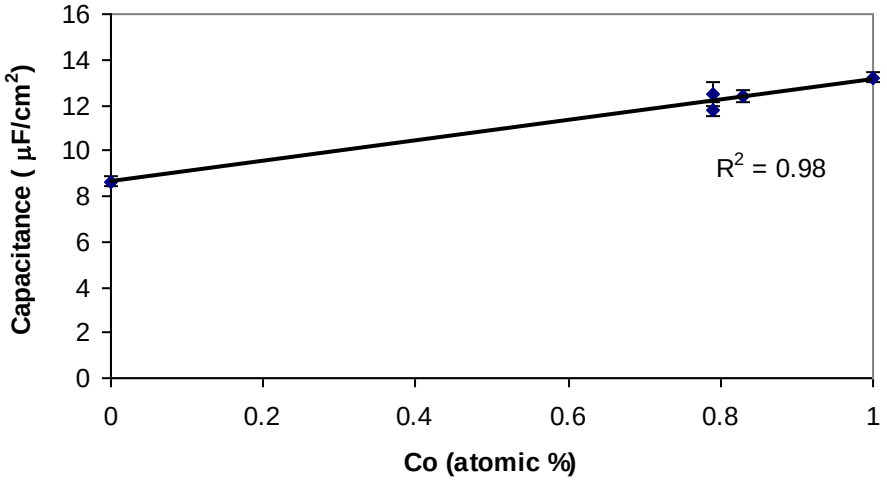

Figure 6.47 Final capacitance values of all pentlandite electrodes (including the synthetic electrode) as a function of pentlandite cobalt content (atomic %).

7. CONCLUSIONS

Based on this study, the following conclusions are made:

- There is a compositional variation of natural pentlandite particles hand-picked from the flotation concentrate. The electron microprobe analysis performed, indicated the variation in the cobalt, iron and nickel content and the variation was independent of the deposit. Massive pentlandite samples did not show significant compositional variation. A slight variation was observed in the cobalt and iron content. The sulfur content was relatively constant in all the samples analysed.

- Pre-existing pores, cracks and the brittle nature of pentlandite may contribute to the poor electrochemical response of natural pentlandite particles (hand-picked from the flotation concentrate) during the electrochemical measurements.

- In aerated solutions, iron enriched pentlandites are less reactive after progressive oxidation. This was illustrated by the polarisation resistance and the capacitance measurements. It is however difficult to distinguish if the differences in the reactivity are a result of the Fe/Ni ratio or the influence of cobalt. Current density transients confirmed that the reactivity of pentlandite electrode is time dependent. As the electrode oxidises, the reactivity of the electrode decreases which is indicated by the decrease in current density.

- A variation in the electronic properties of the formed oxide film at the pentlandite surface was observed. This was indicated by the capacitance measurements.

- Slight compositional variation of pentlandite does not have a significant effect on the rest potential values as do changes in the type of sulfides (e.g. pyrite vs. pentlandite). This was confirmed by similar rest potential values of various pentlandite electrodes.

- The oxidation of synthetic pentlandite may be influenced by the chemical composition. In de-aerated solutions, the anodic oxidation (as shown by the linear anodic voltammogram) of the synthetic pentlandite started at a potential lower

than of the natural electrodes. In aerated solutions, the synthetic pentlandite was less reactive and formed thicker oxide films.

8. RECOMMENDATIONS

The nature, poor electrochemical response of small natural pentlandite particles (±100μm) and the scarcity of clean massive natural pentlandite with significant compositional variation, requires the use of synthetic minerals. The behaviour of synthetic minerals do not always correspond to that of the sulfide minerals found in the actual plant operations. For a complete study on the effect of composition on the electrochemical behaviour of pentlandite, it is recommended that synthetic samples with significant varying compositions be used.

The brittle nature of pentlandite requires a special polishing method for extensive electrochemistry study of natural pentlandite, to minimise the exposure of increased cracks and pores.

9. REFERENCES

Abraitis, P.K., Pattrick, R.A.D., and Vaughan, D.J., 2004, *Variations in the compositional, textural and electrical properties of natural pyrite: a review*, International Journal of Minerals Processing, vol. 74, pp. 41-59.

Ahlberg, E., and Broo, A.E., 1996, *Oxygen reduction at sulphide minerals. 3 The effect of surface pre-treatment on the oxygen reduction at pyrite*, International Journal of Mineral Processing, vol. 47, pp. 49-60.

Basile, F., Bergner, J., Bombart, C., Rondot, B., Le Guevel, P., and Lorang, G., 2000, *Electrochemical and analytical (XPS and AES) study of passive layers formed on Fe-Ni alloys in borate solutions*, Surface and Interface Analysis, vol. 30, pp. 154-157.

Biegler, T., Rand, D.A.J., and Woods, R., 1975, *Oxygen reduction on sulphide minerals. I Kinetics and mechanism at rotated pyrite electrodes*, Electroanalytical Chemistry and Interfacial Electrochemistry, vol. 60, pp. 151-162.

Bockris, J.O'M., and Reddy, A.K.N., 1970, *The electronation of oxygen*, Modern Electrochemistry, vol. 2, pp. 1251-1263.

Boinet, M., Maximovitch, S., and Dalard, F., 2003, *Study of nickel passivation in a borate medium*, Journal of Materials Science, vol. 38, pp. 4041-4046.

Bozkurt, V., Xu, Z., and Finch, J.A., 1998, *Pentlandite / pyrrhotite interaction and xanthate adsorption*, International Journal of Mineral Processing, vol. 52, pp. 203-214.

Bradford, L., McInnes, C., Stange, W., De Beer, C., David, D., and Jardin, A., 1998, *The development of the proposed milling circuit for the Nkomati main concentrate plant*, Minerals Engineering, vol. 11., pp. 1103-1117.

Brynard, H.J., De Villiers, J.P.R., and Viljoen, E.A., 1976, *A Mineralogical investigation of the Merensky reef at the Western Platinum Mine, near Marikana, South Africa*, Economic Geology, vol. 71, pp. 1299-1307.

Buckley, A.N., and Woods, R., 1991, *Surface composition of pentlandite under flotation related conditions*, Surface and Interface Analysis, vol.17, pp. 675-680.

Buckley, A.N., and Woods, R., 1991b, *Electrochemical and XPS studies of the surface oxidation of synthetic heazlewoodite (Ni_3S_2)*, Journal of Applied Electrochemistry, vol. 21, pp. 575-582.

Cabri, L.J., 1989, *Platinum-group elements: Mineralogy, Geology and Recovery*, Canadian Institute on Mining and Metallurgy, CIM special volume 23, pp. 199-217.

Cabri, L.J., 1992, *The distribution of trace precious metals in minerals and mineral products: The 23rd Hallimond lecture*, Mineralogical Magazine, vol. 56, pp. 289-308.

Cawthorn, R.G., 1999, *The platinum and palladium resources of the Bushveld Complex*, South African Journal of Science, vol. 95, pp. 481-489.

Cawthorn, R.G., Lee, C.A., Schouwstra, R.P., and Mellow, P., 2002, *Relationship between PGE and PGM in the Bushveld Complex*, The Canadian Mineralogist, vol. 40, pp. 311-328.

Chamberlain, A.C., 1996, *The effect of stoichiometry on oxidation, pyrolitic decomposition and ignition behaviour of pentlandite*, PhD Thesis, Curtin University of Technology, Western Australia.
[Online available]: http://0-adt.curtin.edu.au.innopac.up.ac.za/theses/available/adt-WCU20020828.134228/

Chander, S., 1984, *Metastable equilibria and kinetic effects in sulfide mineral flotation*, In Proceedings of the International Symposium on Electrochemistry in

Mineral and Metal Processing, Edited by, P.E., Richardson, S., Srinivasan and R. Woods, Electrochemical Society, USA, pp.21-23.

Chang, C., and Wen, T., 2006, *Kinetics and mechanism of oxygen reduction at hydrous oxide film covered platinum electrode in alkaline solution*, Electrochimica Acta, vol. 52, pp. 623-629.

Chanturiya,V., Makarov, V., Forsling, W., Makarov, D., Vasil'eva, T., Trofimenko, T., and Kuznetsov, V., 2004, *The effect of crystallochemical peculiarities of nickel sulphide minerals on flotation of copper-nickel ore*, International Journal of Mineral Processing, vol. 74, pp. 289-301.

Cheng, X., and Iwasaki, I., 1992, *Effect of chalcopyrite and pyrrhotite interaction on flotation separation*, Mineral and Metallurgical Processing, vol. 9, pp. 73-79.

CISA: Corrosion Institute of Southern Africa, 1994, *Corrosion Control in Southern Africa*, Mintek, Randburg, pp. 1-5.

Cox, M.G.C., 1983, *Experimental determination of X-ray intensities*, In Quantitative electron-probe microanalysis, Edited by V.D., Scott, G., Love, Ellis Horwood Limited, England, pp.125-134.

Craig, B.D., 1991, *Kinetics of Corrosion*, Fundamental aspects of corrosion films in Corrosion Science, Plenum press, New York, pp. 29-37.

De Waal., S.A., Maier, W.D., Armstrong, R.A., and Gauert, C.D.K., 2001, *Parental magma and emplacement of the Stratiform Uitkomst Complex, South Africa*, The Canadian Mineralogist, vol. 39, pp. 557-571.

Ekmekci, Z., and Demirel, H., 1997, *Effects of galvanic interaction on collectorless flotation behaviour of chalcopyrite and pyrite*, International Journal of Mineral Processing, vol. 52, pp. 31-48.

Feng, D., and Aldrich, C., 1999, *Effect of particle size on flotation performance of complex sulphide ores*, Minerals Engineering, vol. 12, pp. 721-731.

Francis, C.A., Fleet, M.E., Misra,K., and Craig, J.R., 1976, *Orientation of exsolved pentlandite in natural and synthetic nickeliferous pyrrhotite*, American Mineralogist, vol., 61, pp. 913-920.

Gain, S.B., and Mostert, A.B., 1982, The Geological setting of the platinoid and base metal sulfide mineralization in the Platreef of the Bushveld Complex on Drenthe, South of Potgietersrus, Research report (University of Pretoria. Institute for Geological Research on the Bushveld Complex), nr. 28, ISBN: 086979468X.

Gardner, J.R., and Woods, R., 1979, *An electrochemical investigation of natural floatability of chalcopyrite*, International Journal of Mineral Processing, vol. 6, pp. 1-16.

Gerson, A.R., and Jasieniak, M., 2008, *The effect of surface oxidation on the cu activation of pentlandite and pyrrhotite*, Proceedings of the XXIV International Minerals Processing Congress, Beijing, China, pp. 1054-1063.

Godel, B., Barnes, S., and Maier, W.D., 2007, *Platinum group elements in sulphide minerals and whole rocks of the Merensky reef (Bushveld Complex, South Africa): Implications for the formation of the reef*, Journal of Petrology, vol.48, pp. 1569-1604.

Graterol, M., and Naldrett, A.J., 1971, *Mineralogy of the Malbridge No.3 and No. 4 nickel–iron sulphide deposits with some comments on Low Temperature equilibrations in the Fe-Ni-S system*, Economic Geology, vol. 66, pp. 886-900.

Greet, C.J., Kinal, J., Steinier, P., 2005, *Grinding media its effect on pulp chemistry and flotation behaviour-fact or fiction*, Centenary of flotation Symposium, AusIMM, Brisbane, pp. 967-972.

Hall, S.R., and Stewart, J.M., 1973, *Crystal structure of argentian pentlandite $(Fe,Ni)_8AgS_8$ compared with the refined structure of pentlandite $(Fe,Ni)_9S_8$*, Canadian Mineralogist, vol. 12, pp. 169-177.

Hamilton, I.C., and Woods, R., 1981, *An investigation of surface oxidation of pyrite and pyrrhotite by linear potential sweep voltammetry*, Journal of Electroanalytical Chemistry, vol. 118, pp. 327-343.

Harney, D.M.W., and Merkle, R.K.W., 1991, *Sulfide mineralogy at the main magnetite layer, upper zone, eastern Bushveld Complex and the effect of hydrothermal process on pentlandite composition*, Research report (University of Pretoria. Institute for Geological Research on the Bushveld Complex), nr. 89, pp. 1-25, ISBN: 0869798227.

Harris, D.C., and Nickel, E.H., 1972, *Pentlandite compositions and associations in some natural minerals*, Canadian Mineralogist, vol. 11, pp. 861-878.

Harvey, R.D., 1928, *Electrical conductivity and polished mineral surface*, Economic Geology, vol. 23, pp. 778-803.

Heiskanen, K., Kirjavainen, V., and Laapas, H., 1991, *Possibilities of collectorless flotation in the treatment of pentlandite ores*, International Journal of Mineral Processing, vol. 33, pp. 263-274.

Heyes, G.W., and Trahar, W.J., 1977, *The natural floatability of chalcopyrite*, International Journal of Mineral Processing, vol.4, pp. 317-344.

Hodgson, M., and Agar, G.E., 1989, *Electrochemical investigations into the flotation chemistry of pentlandite and pyrrhotite: process water and xanthate interactions*, Canadian Metallurgical Quartely, vol. 28, pp. 189-198.

Jones, R.T., 1999, *Platinum smelting in South Africa*, South African Journal of Science, vol. 95, pp. 525-534.

Jones, D.A., 2005, *Principles and Prevention of Corrosion*, 2nd edition. Prentice-Hall, USA, pp. 143-167.

Kelebek, S., and Nanthakumar, B., 2007, *Characterization of stockpile oxidation of pentlandite and pyrrhotite through kinetic analysis of their flotation*, International Journal of Minerals Processing, vol.84, pp. 69-80.

Kelebek, S., Nanthakumar, B., and Katsabanis, P.D., 2007, *Oxidation of complex Ni-Cu sulphide ores and its implication for flotation practice*, Canadian Metallurgical Quartely, vol. 46, pp. 279-284.

Kelsall, G.H., and Page, P.W. 1984. *Aspects of chalcopyrite ($CuFeS_2$) electrochemistry*, In Proceedings of the International Symposium on Electrochemistry in Mineral and Metal Processing, Edited by, P.E., Richardson, S., Srinivasan and R. Woods, Electrochemical Society, USA, pp.303-320.

Khan, A., and Kelebek, S., 2004, *Electrochemical aspects of pyrrhotite and pentlandite in relation to their flotation with xanthate, Part 1: Cyclic voltammetry and rest potentials measurements*, Journal of Applied Electrochemistry, vol. 34, pp. 849-856.

Kim, B.S., Hayes, R.A., Prestige, C.A., Ralston, J., and Smart, R.St.C., 1994, *Scanning tunneling microscopy studies of galena: the mechanism of oxidation in air*, Applied Surface Science, vol. 78, pp. 385-397.

Kinnaird, J.A., Hutchinson, L., Schurmann, L., Nex, P.A.M., and De Lange, R., 2005, *Petrology and mineralisation of the southern Platreef: northern limb of the Bushveld Complex, South Africa*, Mineralium Deposita, vol. 40, pp. 576-597.

Kirjavainen, V., Schreithofer, N., and Heiskanen, K., 2002, *Effect of some process variables on floatability of sulfide nickel ores*, International Journal of Minerals Processing, vol. 65, pp. 59-72.

Kirjavainen, V., and Heiskanen, K., 2007, *Some factors that affect beneficiation of sulphide nickel-copper ores*, Minerals Engineering, vol.20, pp. 629-633.

Korsakova, O.P., 2008, *Pleinstocene marine deposits in the Coastal areas of Kola Peninsula (Russia)*, Quaternary International, pp. 1-13.

Legrand, D.L., Bancroft, G.M., and Nesbitt, H.W., 1997, *Surface characterization of pentlandite (Fe,Ni)$_9$S$_8$ by X–ray photoelectron spectroscopy*, International Journal of Mineral Processing, vol. 51, pp. 217-228.

Legrand, D.L., Bancroft, G.M., and Nesbitt, H.W., 2005, *Oxidation of pentlandite and pyrrhotite surfaces at pH 9.3. I Assignment of XPS spectra and chemical trends*, American Mineralogist, vol.90, pp. 1042-1054.

Loubser, M., and Verryn, S., 2008, *Combining XRF and XRD analyses and sample preparation to solve mineralogical problems*, South African Journal of Geology, vol. 111, pp. 229-238.

Macdonald, D.D., and McKubre, M.C., 1982, *Impedance measurements in electrochemical systems*, Modern Aspects of Electrochemistry, vol. 14, pp. 61-67.

Majima, H., 1969, *How oxidation affects selective flotation of complex sulphide ores*, Canadian Metallurgical Quartely, vol. 8, pp. 269-282.

Maier, W.D., Gomwe, T., Barnes, S.J., Li, C., and Theart, H., 2004, *The Platinum group elements in the Uitkomst Complex, South Africa*, Economic Geology, vol. 99, pp. 499–516.

Maier, W.D., 2005, *Platinum-group element (PGE) deposits and occurrences: Mineralization styles, genetic concepts and exploration criteria*, Journal of African Earth Sciences, vol. 41, pp. 165-191.

Maier, W.D., Barnes, S.J., Chinyepi, G., Barton, J.M., Eglington, Jr.B., and Setshedi, L., 2008, *The composition of magmatic Ni-Cu-(PGE) sulfide deposits in the Tati and Selebi-Phikwe belts of eastern Botswana*, Mineralium Deposita, vol. 43, pp. 37-60.

Manyeruke, T.D., 2003, *The Petrography and geochemistry of the Platreef on the farm Townlands, near Potgietersrus, northern Bushveld Complex*, MSc Thesis, University of Pretoria, South Africa.

Mendiratta, N.K., 2000, *Kinetic studies of sulfide mineral oxidation and xanthate adsorption*, PhD thesis, Virginia Polytech Institute and State University, Blacksburg, Virginia.

Merkle, R.K.W., and Von Gruenewaldt, G., 1986, *Compositional variation of Co-rich pentlandite: Relation to the evolution of the upper zone of the Western Bushveld Complex, South Africa*, Canadian Mineralogist, vol. 24, pp. 529-546.

Miller, J.D., Li, J., Davidtz, J.C., and Vos, F., 2005, *A review of pyrrhotite flotation chemistry in the processing of PGM ores*, Minerals Engineering, vol. 18, pp. 855-865.

Misra, K.C., and Fleet, M.E., 1973, *The chemical composition of synthetic and natural pentlandite assemblages*, Economic Geology, vol.68, pp. 518-539.

Morrison, S.R., 1984, Electrochemistry at semiconductor and oxidized metal electrodes, Plenum, New York.

Mostert, A.B., 1982, *A mineralogical and petrological investigation of the Platreef on Drenthe 778 LR, northwest of Potgietersrus*, MSc thesis, University of Pretoria, South Africa.

Nakazawa, H., and Iwasaki, J., 1985, *Effect of pyrite-pyrrhotite contact on their floatabilities*, Mineral and Metallurgical Processing, vol. 2, pp. 206-220.

Naldrett, T., Kinnaird, J., Wilson, A., Chunnett, G., 2008, *Concentration of PGE in the earth's crust with special reference to the Bushveld Complex*, Earth Science Frontiers, vol. 15, pp. 264-297.

Narishe Group Product Catalogue, http://products.narishe-group.com/group1/M-152/injection, viewed, 16 April 2009.

Nkoane, B.M., Sawula, G.M., Wibetoe, G., and Lund, W., 2005, *Identification of Cu and Ni indicator plants from mineralized locations in Botswana*, Journal of Geochemical Exporation, vol. 86, pp. 130-142.

Oldfield, J.W.,1988, *Electrochemical theory of galvanic corrosion*, *In Galvanic Corrosion*, Edited by P.H., Harvey, American Society for Testing and Materials, Philadelphia, pp. 5-22.

Penberthy, C.J., 2001, *The effect of mineralogical variation in the UG-2 chromitite on recovery of platinum-group elements*, PhD thesis, University of Pretoria, South Africa.

Postle, J.T., Rosloe, W.E., Watanabe, R.Y., and Martin, P.S., 1986, *Review of Platinum group elements Deposits in Ontario*, Canada, pp. 6-33.

Rahim, M.A., 1995, *Variation of the dielectric constant of anodic oxide films on titanium with oxygen evolution*, Journal of Applied Electrochemistry, vol. 25, pp. 881-885.

Rajamani,V., and Prewitt, C.T., 1973, *Crystal chemistry of natural pentlandites*, Canadian Mineralogist, vol.12, pp. 178-87.

Rand, D.A.J., 1977, *Oxygen reduction of sulphide minerals*, Journal of Electroanalytical Chemistry, vol. 83, pp. 19-32.

Rao, K.V., and Smakula, A., 1965, *Dieletric properties of cobalt oxide, nickel oxide and their mixed crystals*, Journal of Applied Physics, vol. 36, pp. 2031-2038.

Richardson, S., and Vaughan, D.J., 1989, *Surface alteration of pentlandite and spectroscopic evidence for secondary violarite formation*, Mineralogical Magazine, vol.53, pp. 213-222.

Riley, J.F., 1977, *The Pentlandite group $(Fe,Ni,Co)_9S_8$: New data and an appraisal of structure–composition relationships*, Mineralogical Magazine, vol.41, pp. 345-349.

Rognvald, B., Barnes, S., De Caritat, P.,Chekushin, V.A., Reimann, M.C., and Zientek, M.L., 2009, *Emissions from the copper–nickel industry on the Kola Penisula and at Noril'sk, Russia*, Atmospheric environment, vol., 43, pp. 1474-1480.

Rossi, A., Calinski, C., Hoppe, H.W., Strehblow, H.H., 1992, *A combined ISS and XPS investigation of passive film formation on Fe53Ni*, Surface and Interface analysis, vol. 18, pp. 269-276.

Rosso, K.M., and Vaughan, D.J., 2006, *Sulfide Mineral Surfaces*, Reviews in Mineralogy and Geochemistry, vol. 61, pp. 505-556.

Scharifker, B.R., 1992, *Microelectrode techniques in electrochemistry*, *In Modern Aspects of electrochemistry*, No. 22, Edited by J.O'.M., Bockris, B.E., Conway and R.E. White, Plenum Press, New York and London, pp. 467-519.

Schouwstra, R.P., Kinloch, E.D., and Lee, C.A., 2000, *A Short geological review of the Bushveld Complex*, Platinum Metals, vol. 44, pp. 33-39.

Schultze, J.W., Mohr, S., and Lohrengel, M.M., 1983, *Electrode reactions at modified surface dependent on reaction site, γ-FeOOH as an example*, Journal of Electroanalytical Chemistry, vol. 154, pp. 57-68.

Senior, G.D., Shannon, L.K., and Trahar, W.J., 1994, *The Flotation of pentlandite from pyrrhotite with particular reference to the effects of particle size*, International Journal of Mineral Processing, vol. 42, pp. 169–190.

Shamsul Hug, A.K.M., Rosenberg, A.J., and Makrides, A.C., 1964, *Electrochemical behaviour of nickel compounds. II Anodic dissolution and oxygen reduction in perchlorate solutions*, Journal of the Electrochemical Society, vol. 111, pp. 278-286.

Silvermann, D.C., 1986, *Primer on the AC Impedance technique, In: Electrochemical techniques for corrosion engineering*, Edited by R., Baboian, Houston: NACE, pp.73-79.

Smart, R.C., Skinner, W.M., and Gerson, A.R., 1999, *XPS of sulphide mineral surfaces: Metal deficient, polysulphide, defects and elemental sulphur*, Surface and Interface analysis, vol. 28, pp. 101-105.

Suter, T., Peter, T., and Böhni, H., 1995, *Microelectrochemical investigations of MnS inclusions*, Materials Science Forum, vol. 192-194, pp. 25-40.

Theart, H.F.J, and De Nooy, C.D., 2001, *The Platinum Group Minerals in two parts of the Massive Sulphide Body of the Uitkomst Complex, Mpumalanga, South Africa*, South African Journal of Geology, vol. 104, pp. 287-300.

Thomas, M.T., Petersen, D.A., Hartley, J.N., and Freeman, H.D., 1981, *Application of surface spectroscopies to interfacial problems in mineral processing*, *In*: *Proceedings of the Engineering Foundation Conference on Interfacial Phenomena in Mineral Processing*, Edited by B. Yarar and Spottiswood, D.J., pp. 33-92.

Tolley, W., Kotlyar, D., and Van Wagoner, R., 1996, *Fundamental electrochemical studies of sulfide mineral flotation*, Minerals Engineering, vol. 9, pp. 603–637.

Trahar, W.J., 1984, *The influence of pulp potential in sulphide flotation, In: Principles of Mineral Flotation, The Wark Symposium*, Edited by M.H., Jones and W.T. Woodcock, pp. 117-135.

UTHSCSA Image Tool, 1997, http://ddsdx.uthscsa.edu/dig/download.html, viewed 16April 2009.

Van Zyl, A., 1996, *The sulphides of the Uitkomst Complex, Badplaas*, South Africa, MSc thesis, University of Pretoria, South Africa.

Vaughan, D.J., and Craig, J.R., 1978, *Mineral Chemistry of Metal Sulfides*, Cambridge University Press, London, pp. 382-397.

Vaughan, D.J., England, K.E.R., Kelsall, G.H., and Yin, Q., 1995, *Electrochemical oxidation of chalcopyrite ($CuFeS_2$) and the related metal–enriched derivatives $Cu_4Fe_5S_8$, $Cu_9Fe_9S_{16}$ and $Cu_9Fe_8S_{16}$,* American Mineralogist, vol. 80, pp. 725-731.

Venter, J.A., 2007, *Dithiocarbonate and trithiocarbonate interactions with pyrite and copper*, MSc thesis, University of Pretoria, South Africa.

Vermaak, C.F., and Hendricks, L.P., 1976, *Review of the mineralogy of the Merensky reef with specific reference to new data on the precious metal mineralogy*, Economic Geology, vol. 71, pp. 1244-269.

Vermaak, M.K.G., Venter, J.A., and Pistorius, P.C., 2004, *Electrochemical studies of the interaction of ethyl xanthate with Pd-Bi-Te*, Journal of the South African Institute of Mining and Metallurgy, vol. 104, pp. 667-670.

Vermaak, M.K.G, Miller, J.D., and Moats M.S., 2006, *Single particle microelectrodes for electrochemical analysis of flotation processes,* ECS Transactions, vol. 2, pp. 21-33.

Vos, C.F., 2006, *The role of long chain trithiocarbonates in the optimization of Impala Platinum's flotation circuit*, MEng thesis, University of Pretoria, South Africa.

Woods, R., 1984, *Electrochemistry of sulphide flotation*, The Australian Institute of Mining and Metallurgy, Symposium Series No 40, Principles of Mineral Flotation, pp. 91-115.

Xiao, Z., and Laplante, A.R., 2004, *Characterising and recovering the platinum group minerals–a review*, Minerals Engineering, vol. 17, pp. 961-979.

APPENDIX A: Geological Maps

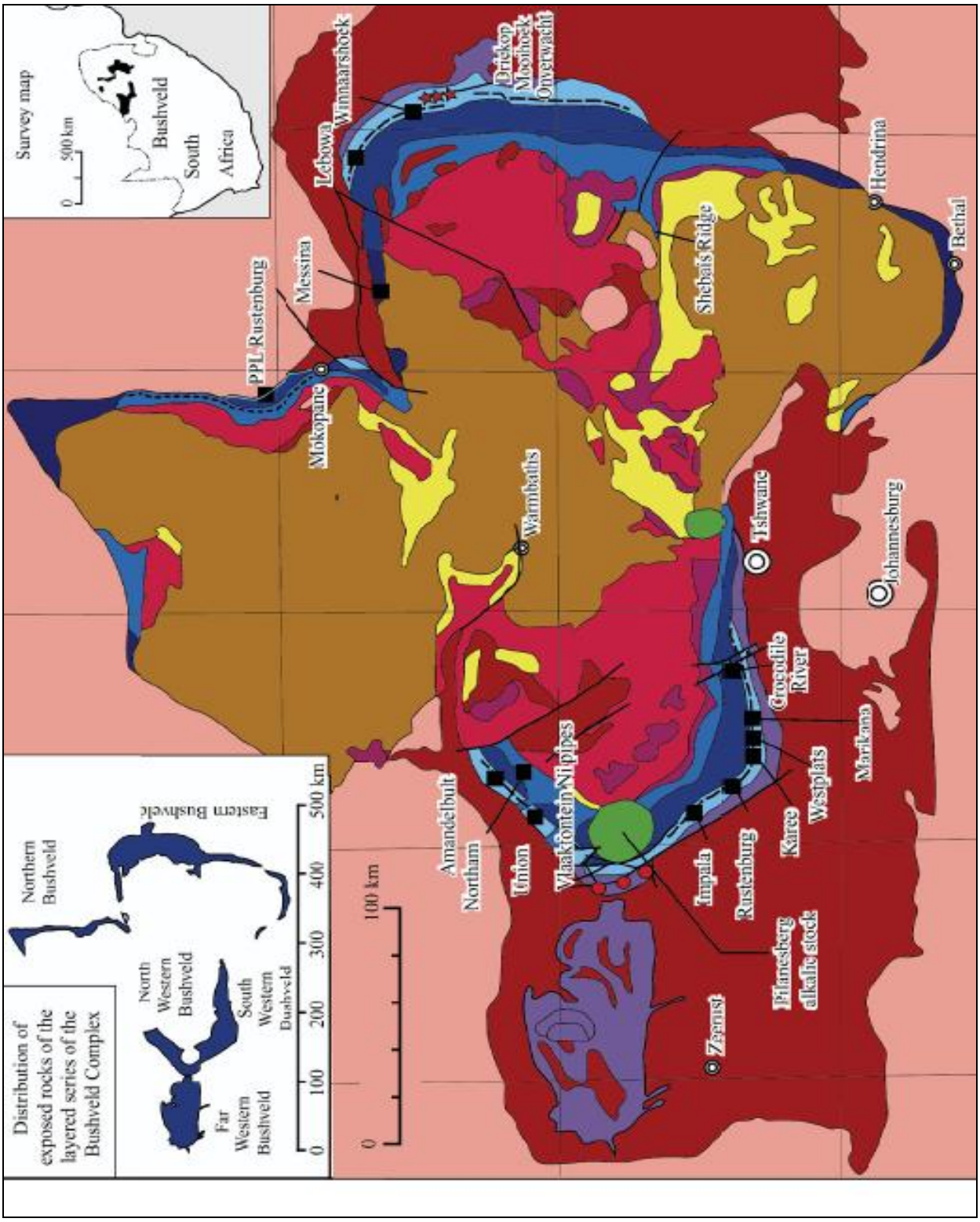

Figure A1: Geological map of the Bushveld Complex, showing the Lebowa granite suite and Sheba's ridge location within the Complex (Naldrett *et al*., 2008).

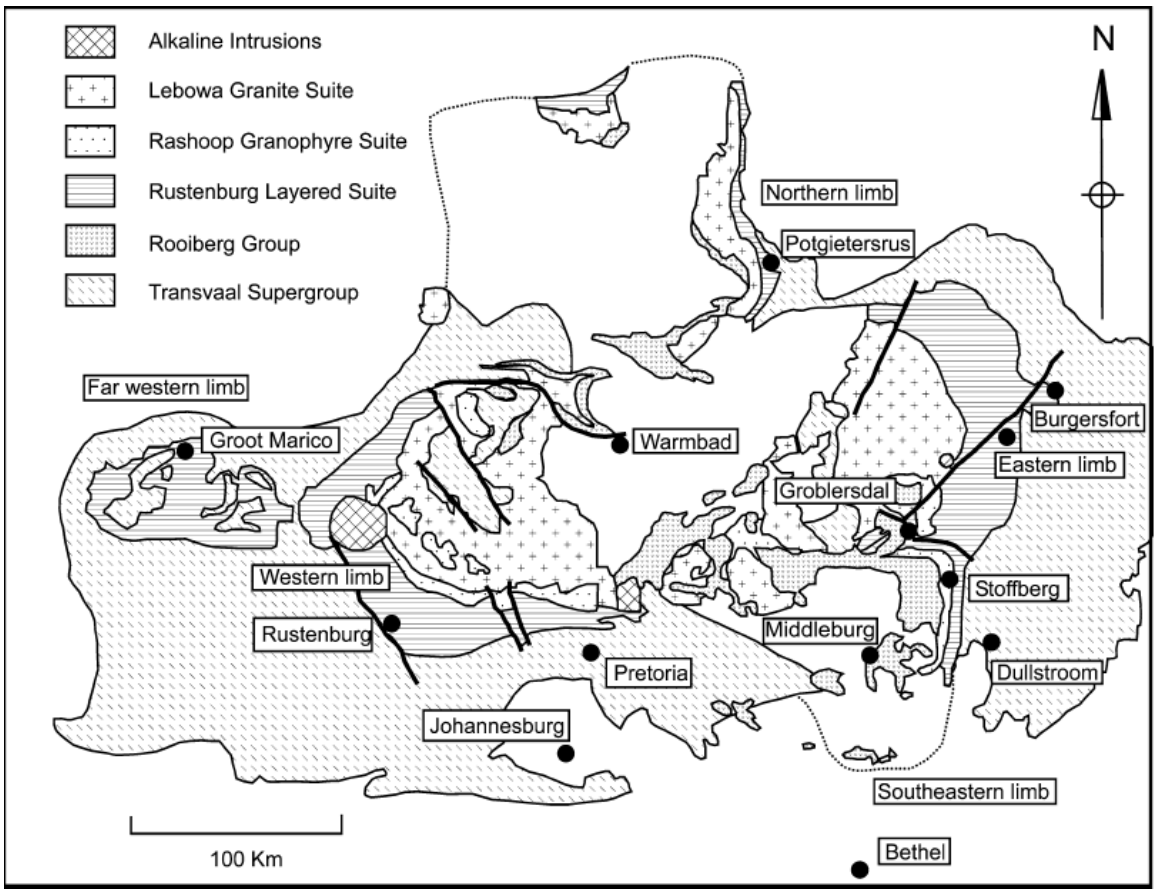

Figure A2: General Map of the Bushveld Complex, showing the location of different limbs, including the Lebowa granite suite (Kinnaird *et al*., 2005).

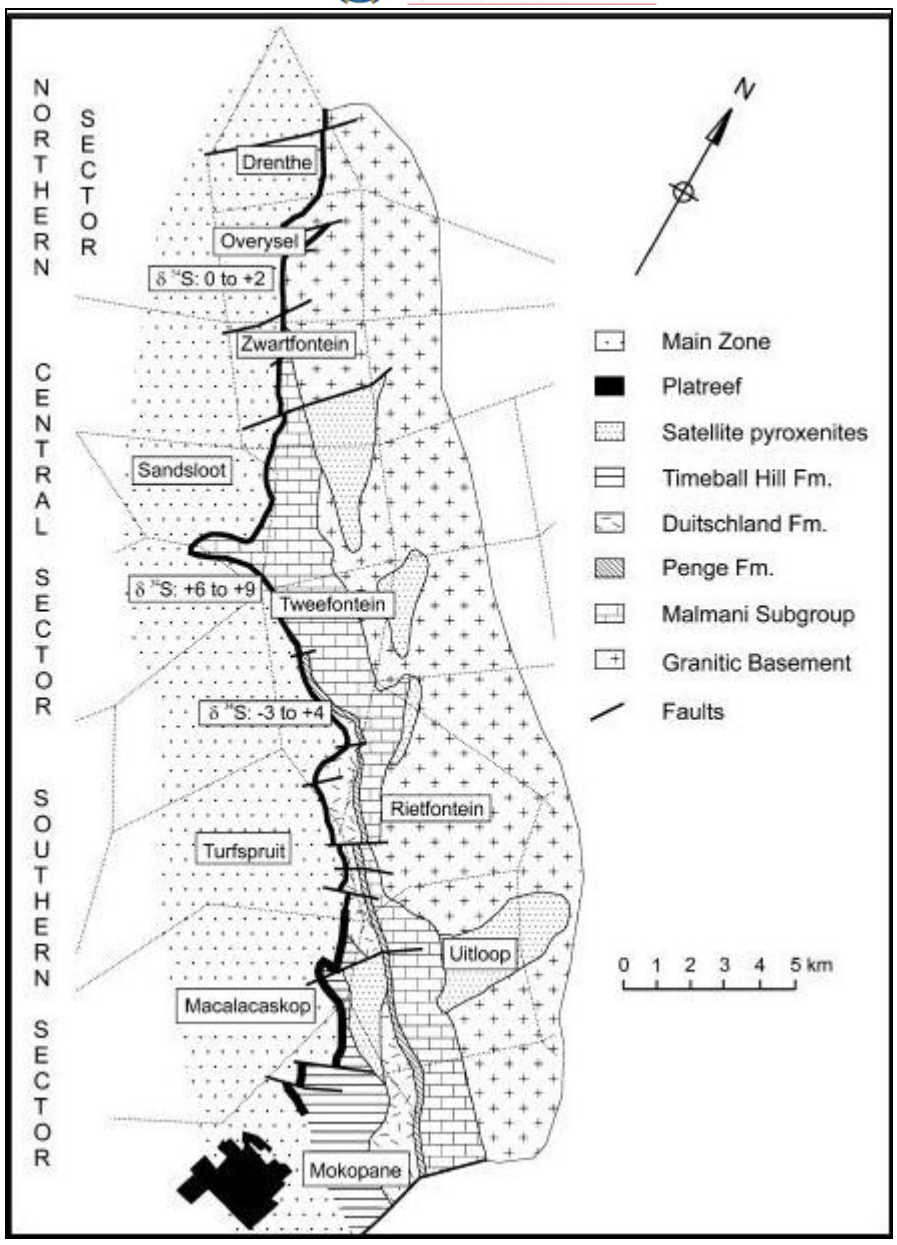

Figure A3: Geological map of the northern limb of the Bushveld Complex, showing the Platreef (Kinnaird *et al.*, 2005).

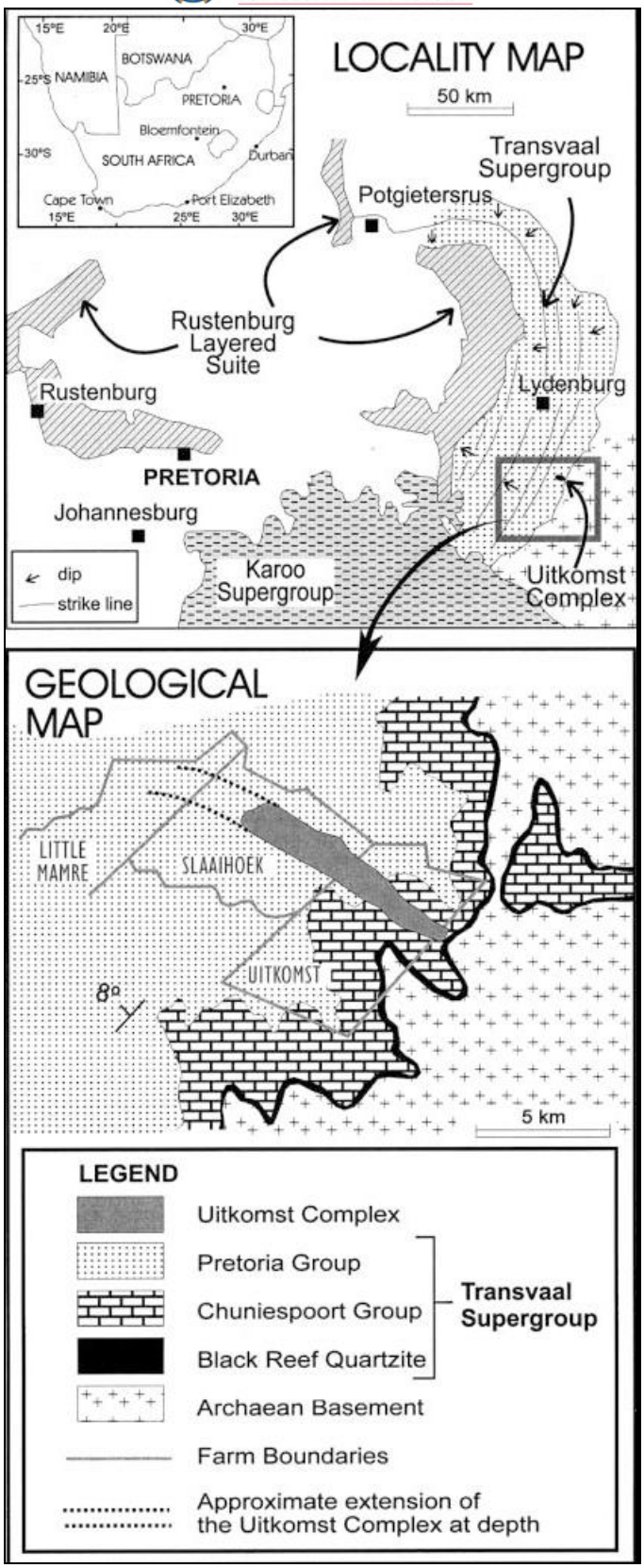

Figure A4: Locality and simplified geological map of the Uitkomst Complex (De Waal *et al.*, 2001).

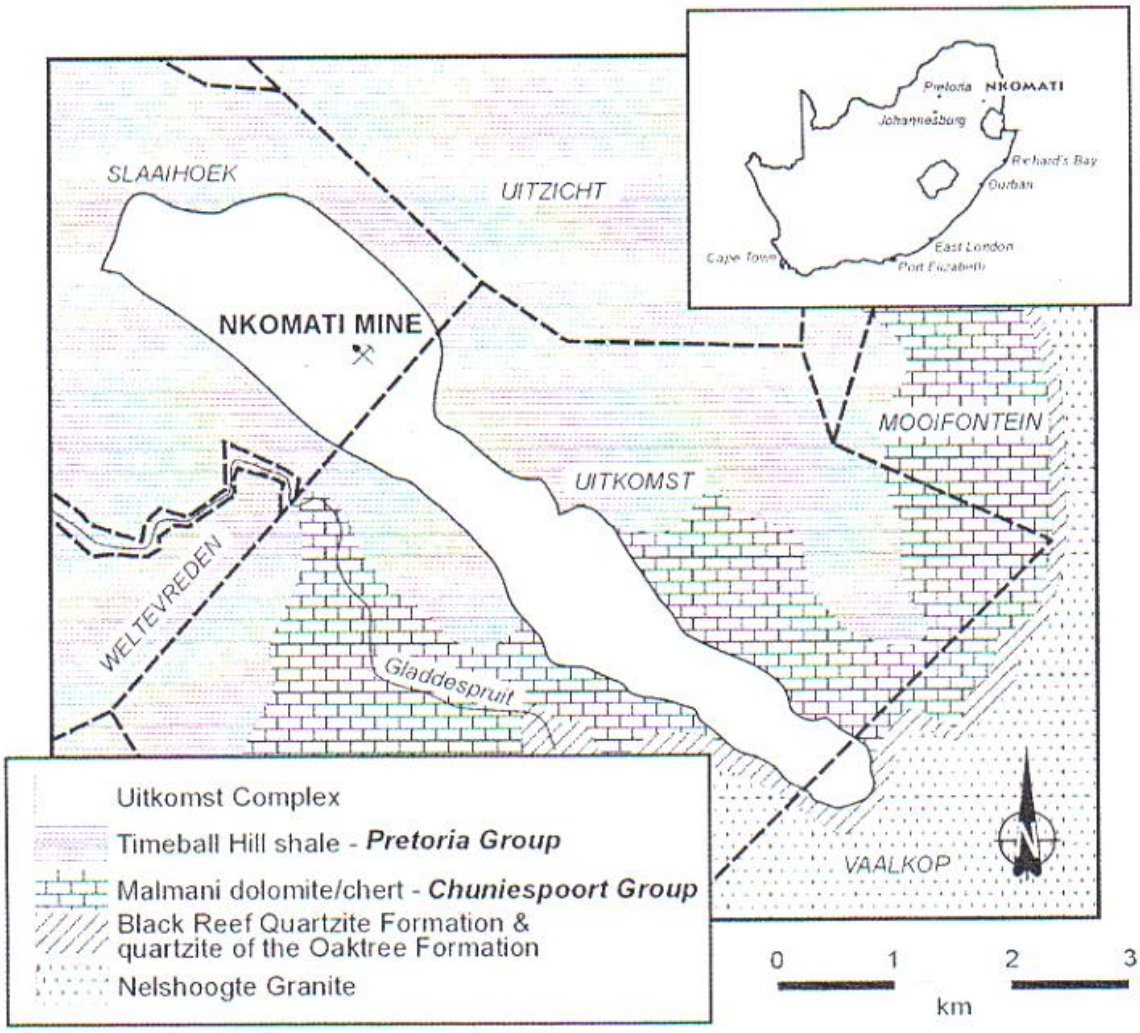

Figure A5: Location of Nkomati Mine within the Uitkomst Complex (Theart and De Nooy, 2001).

Figure A6: Geological map of Botswana (Nkoane *et al*., 2005).

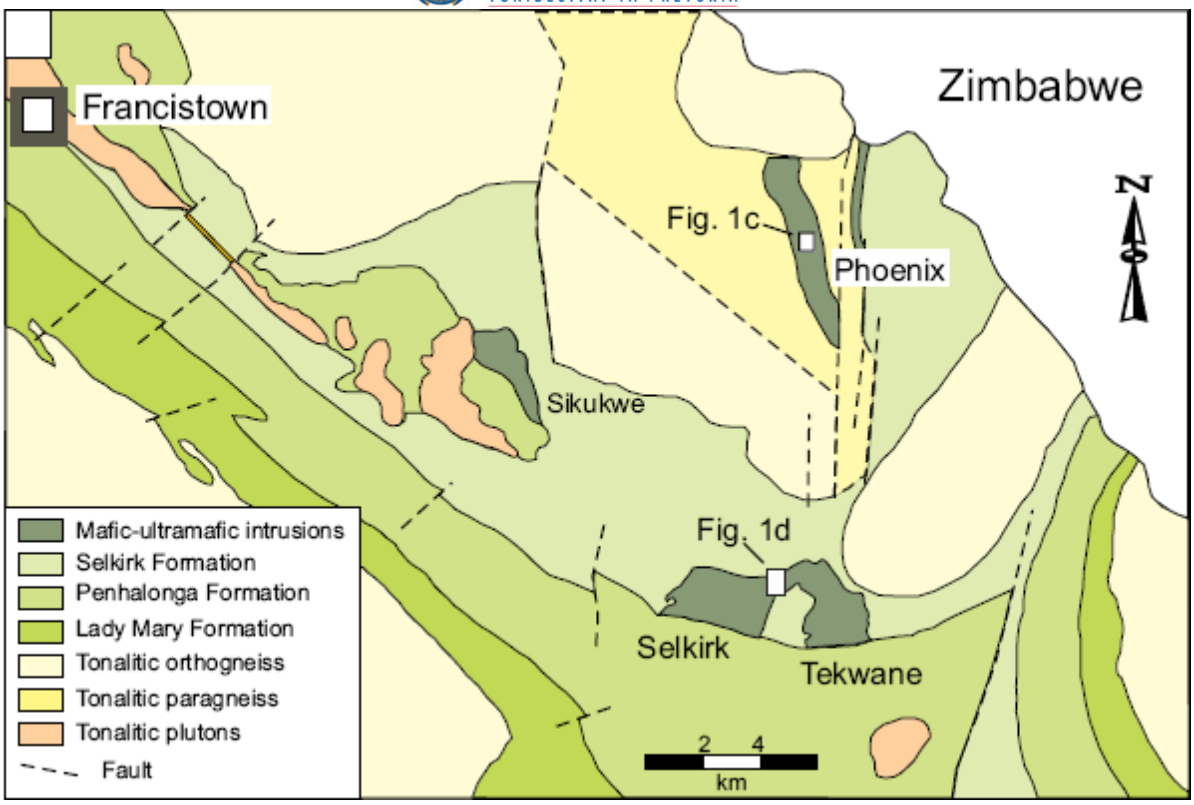

Figure A7: Geological map of the central portion of the Tati greenstone belt, indicating the locality of the Phoenix deposit (Maier *et al*., 2008).

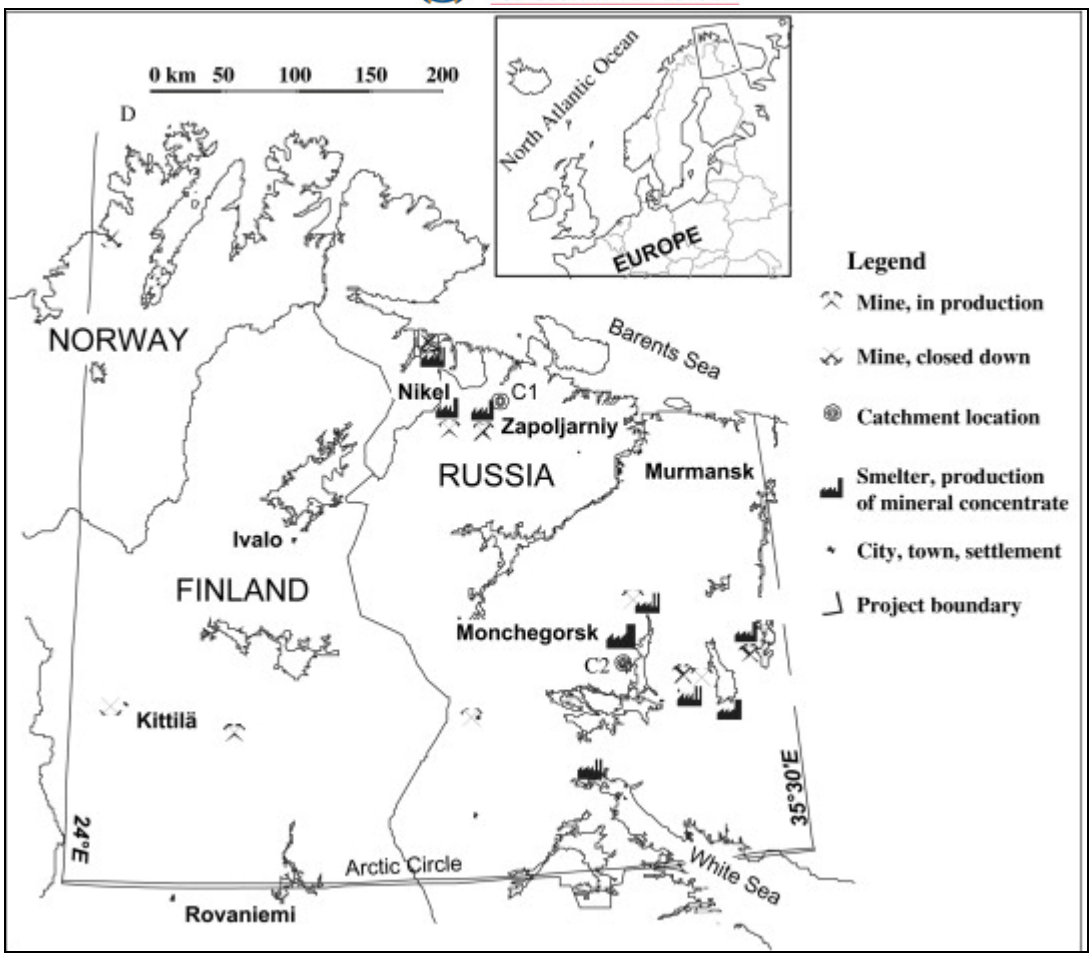

Figure A8: Geological location of Russia in Europe (Boyd *et al*., 2009).

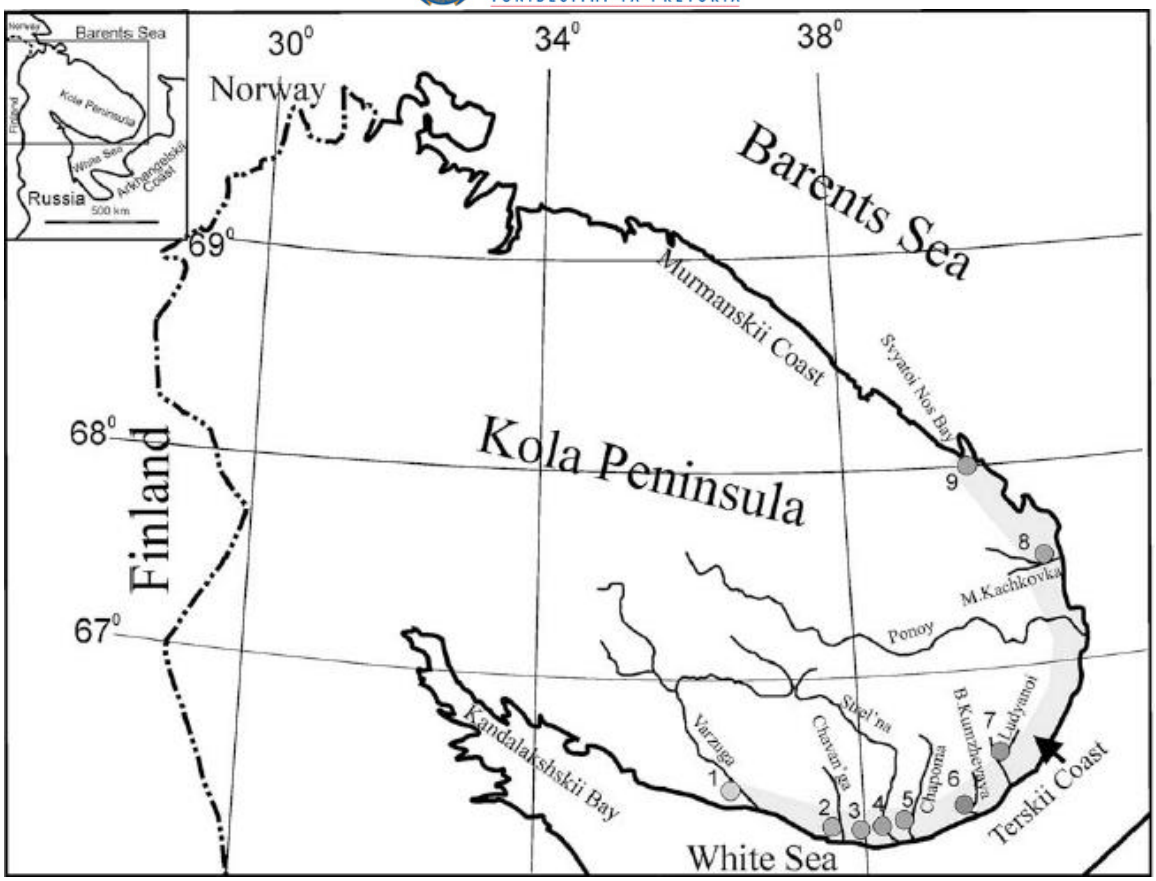

Figure A9: Geological location of the Kola Peninsula in Russia (Korsakova, 2008).

APPENDIX B: Mineralogical analysis of the flotation concentrate samples

Table B1: XRF analysis of the nickel and copper content of the flotation concentrate samples received from different platinum group minerals deposits and copper nickel deposits; LUP-Lebowa UG-2, LMP-Lebowa Merensky, UG–2, Platreef and Nkomati Mine

Deposits	%Ni	%Cu
LUP	1.33	1.06
LMP	3.86	2.52
Platreef	25.73	2.34
Nkomati	10.96	10.00

Table B2: XRD analysis of the pentlandite contents in the flotation concentrate samples received from different platinum group minerals deposits and copper nickel deposits; LUP-Lebowa UG2, LMP-Lebowa Merensky, UG–2, Platreef and Nkomati Mine (only data on the selected sulfides is presented - percent of the flotation concentrate).

%	LMP	±	LUP	±	Nkomati	±	Platreef	±
Pentlandite	9.53	0.69	3.22	0.75	25.35	0.72	63.51	0.51
Chalcopyrite	6.58	0.51	3.15	0.72	31.19	0.81	6.73	0.3
Pyrite	2.67	0.29	0.71	0.3	3.15	0.23	4.29	0.25
Pyrrhotite	3.3	0.38	0.28	0.1	35.86	0.87	24.25	0.375

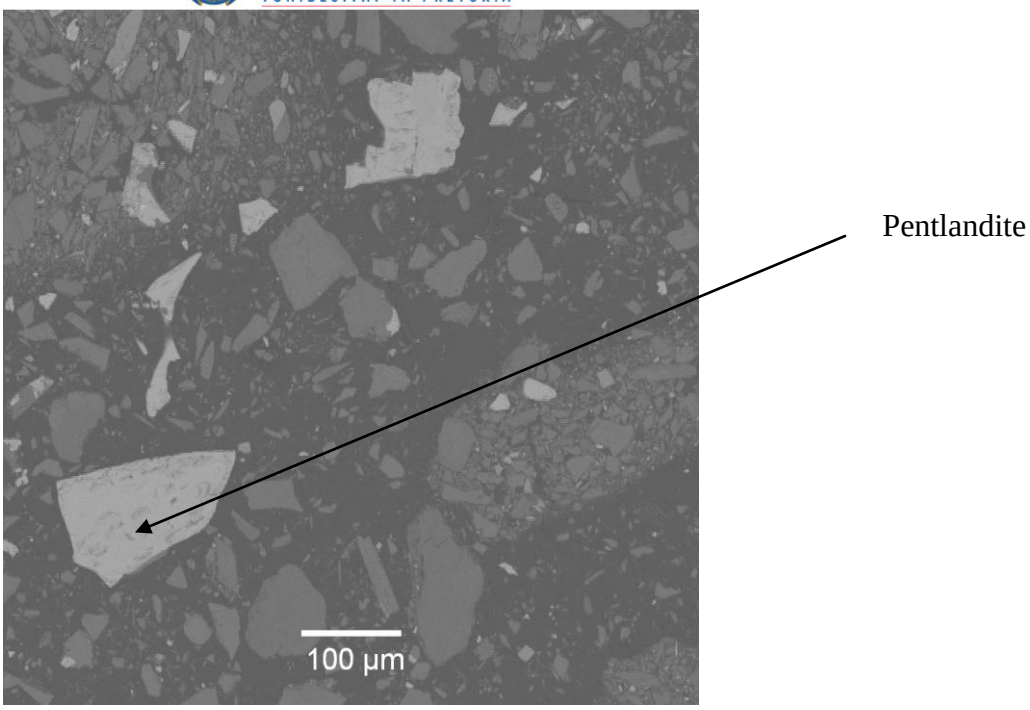

Figure B1: Back-scattered electron micrograph of a polished section of Lebowa UG–2 (LUP) flotation concentrate, showing a liberated pentlandite particle. Accelerating voltage = 15 kV.

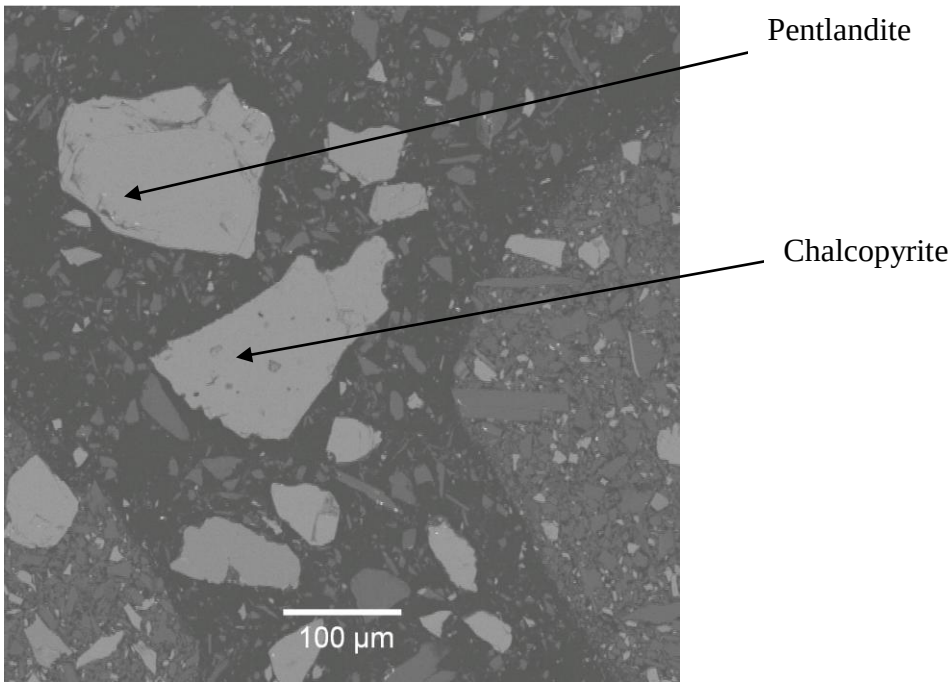

Figure B2: Back-scattered electron micrograph of a polished section of Lebowa Merensky (LMP) flotation concentrate, showing a liberated pentlandite particle. Accelerating voltage = 15 kV.

APPENDIX C: Back-scattered electron micrographs of pentlandite microelectrodes

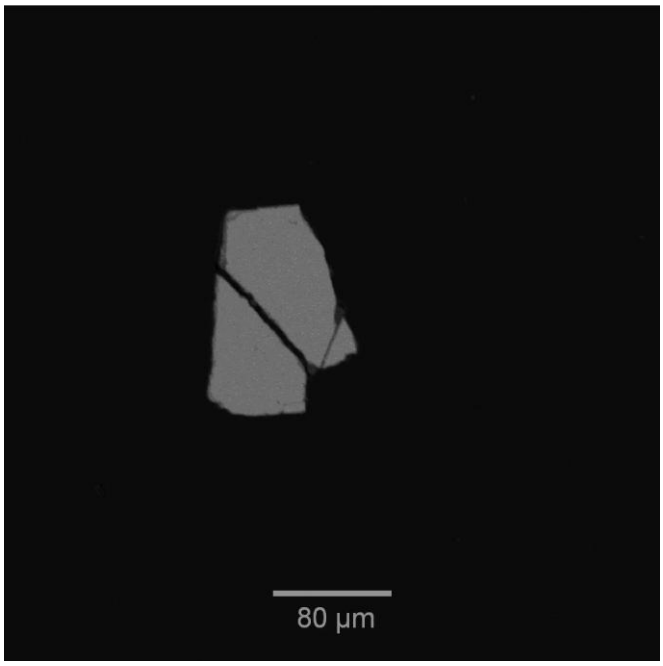

Figure C1: Back-scattered electron micrograph of pentlandite particle, hand-picked from the Lebowa Merensky flotation concentrate. Accelerating voltage = 15 kV.

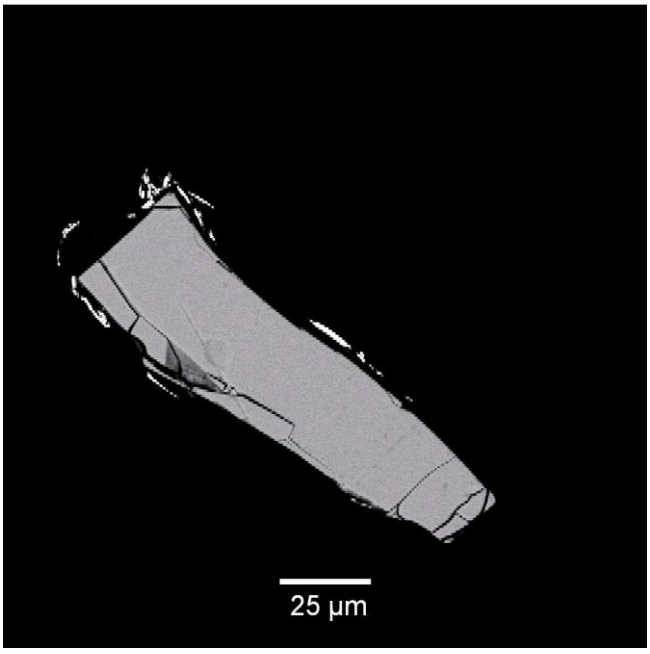

Figure C2: Back-scattered electron micrograph of a pentlandite particle, hand-picked from the Lebowa Merensky flotation concentrate. Accelerating voltage 15 kV.

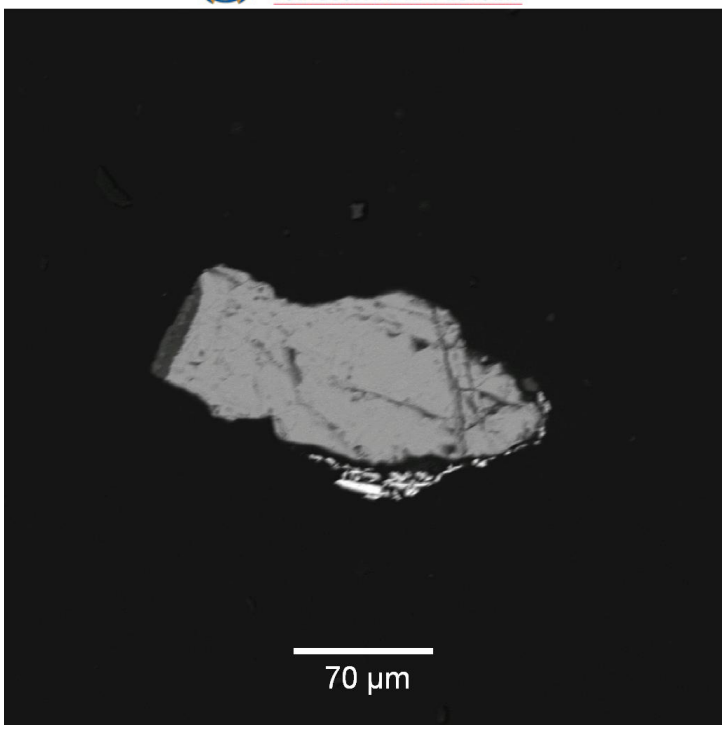

Figure C3: Back-scattered electron micrograph of a pentlandite particle, hand-picked from the Sheba's Ridge flotation concentrate (Platreef). Accelerating voltage 15 kV.

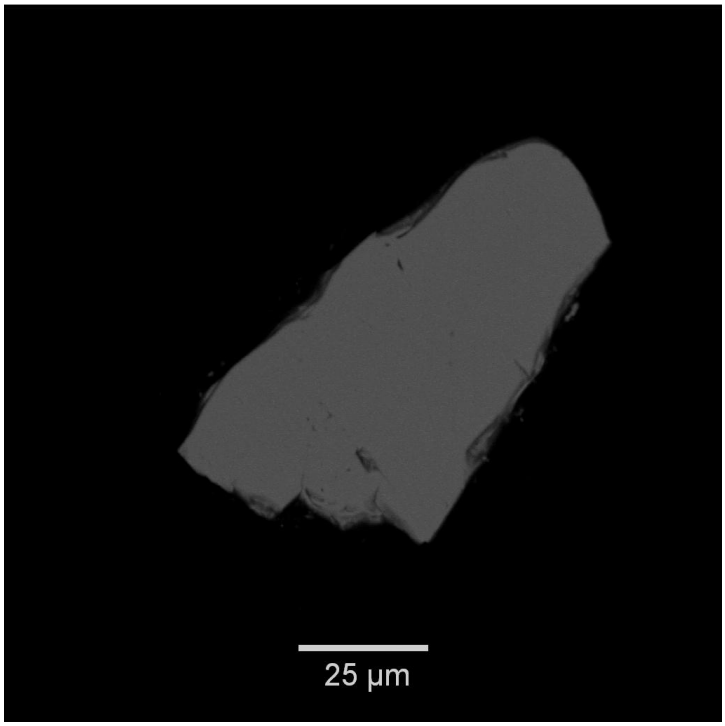

Figure C4: Back-scattered electron micrograph of a pentlandite particle hand-picked from Nkomati Mine flotation concentrate. Accelerating voltage 15 kV.

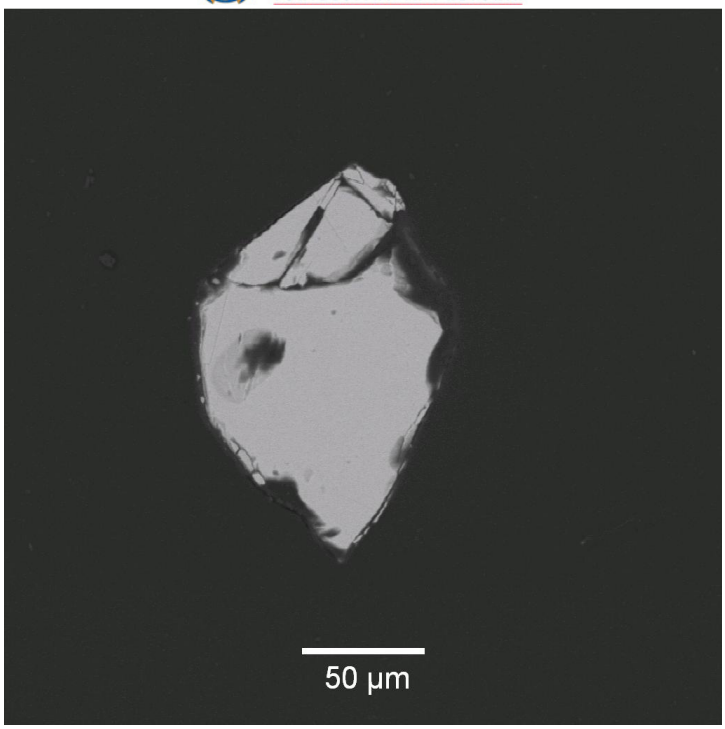

Figure C5: Back-scattered electron micrograph of pentlandite particle hand-picked from Lebowa UG-2 flotation concentrate. Accelerating voltage 15 kV.

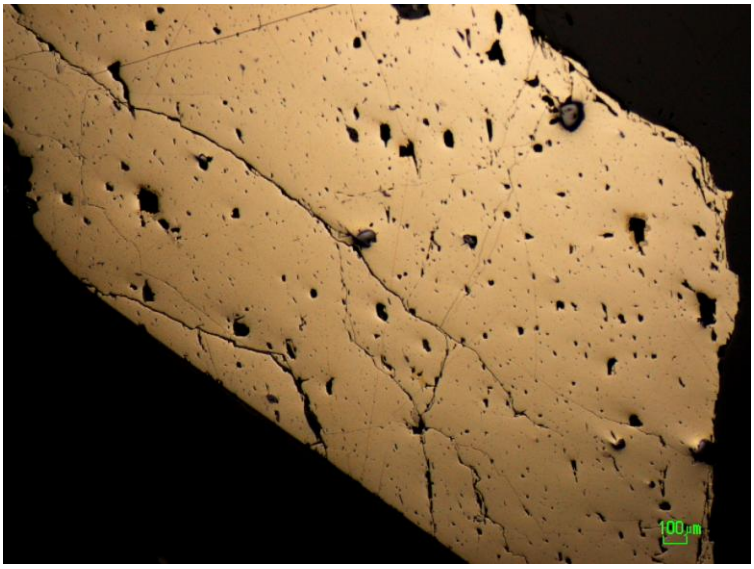

Figure C6: Optical microscope image of a massive pentlandite sample from the Kola Peninsula deposit (Russia).

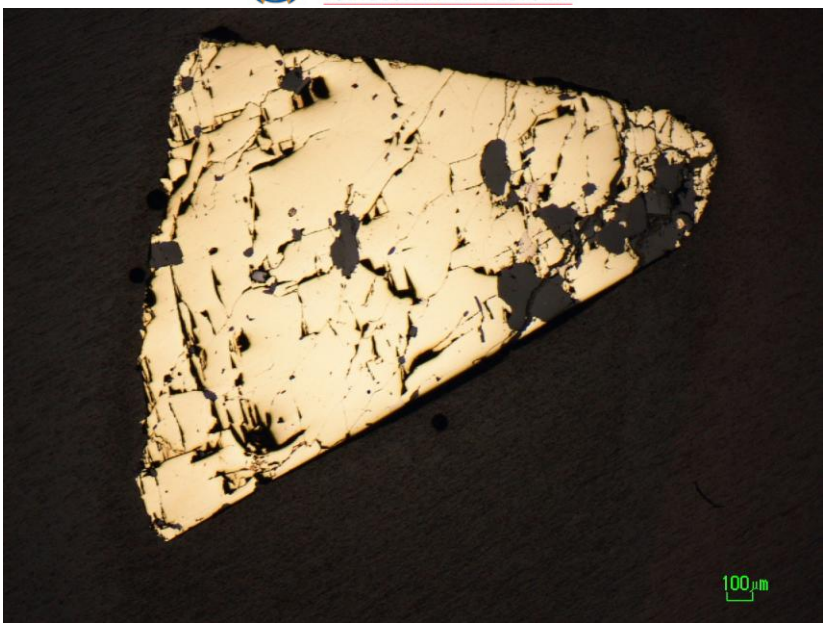

Figure C7: Optical microscope image of a massive pentlandite sample from the Kola Peninsula deposit (Russia).

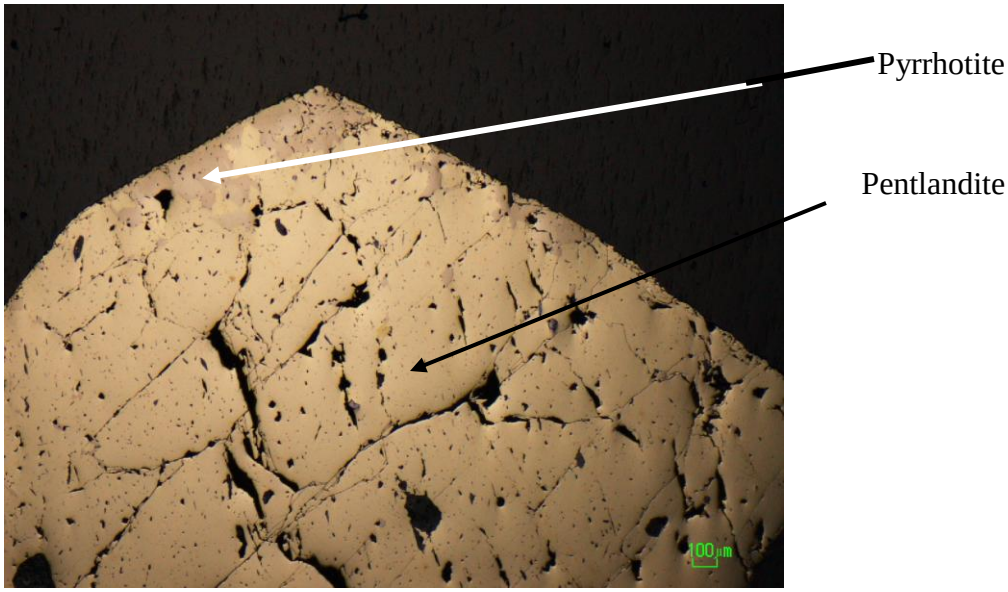

Figure C8: Optical microscope image of a massive pentlandite sample from the Kola Peninsula deposit (Russia).

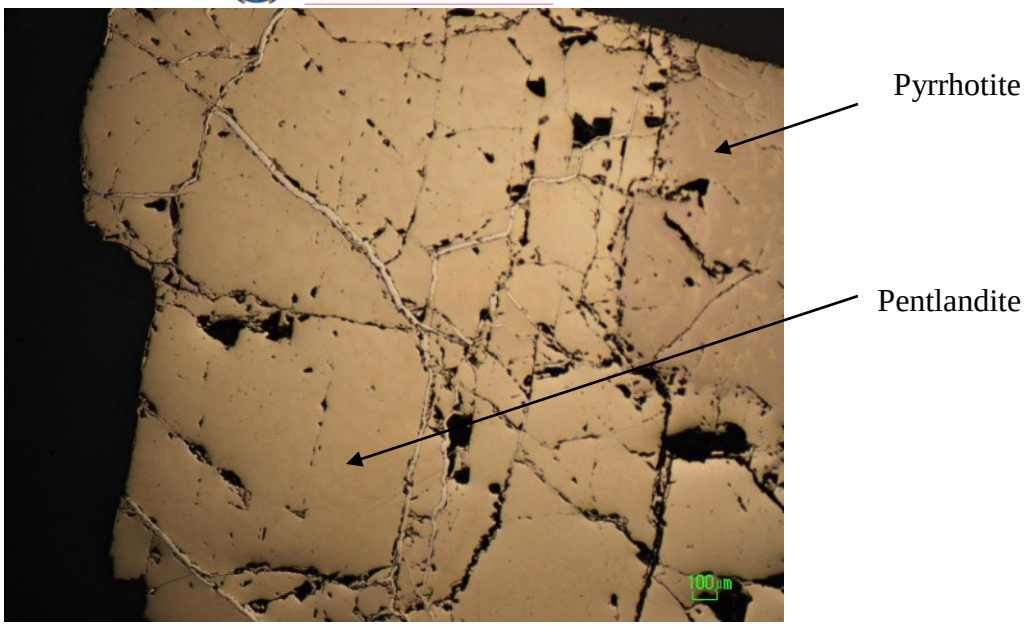

Figure C9: Optical microscope image of a massive pentlandite sample from the Phoenix deposit indicating pentlandite and pyrrhotite phase.

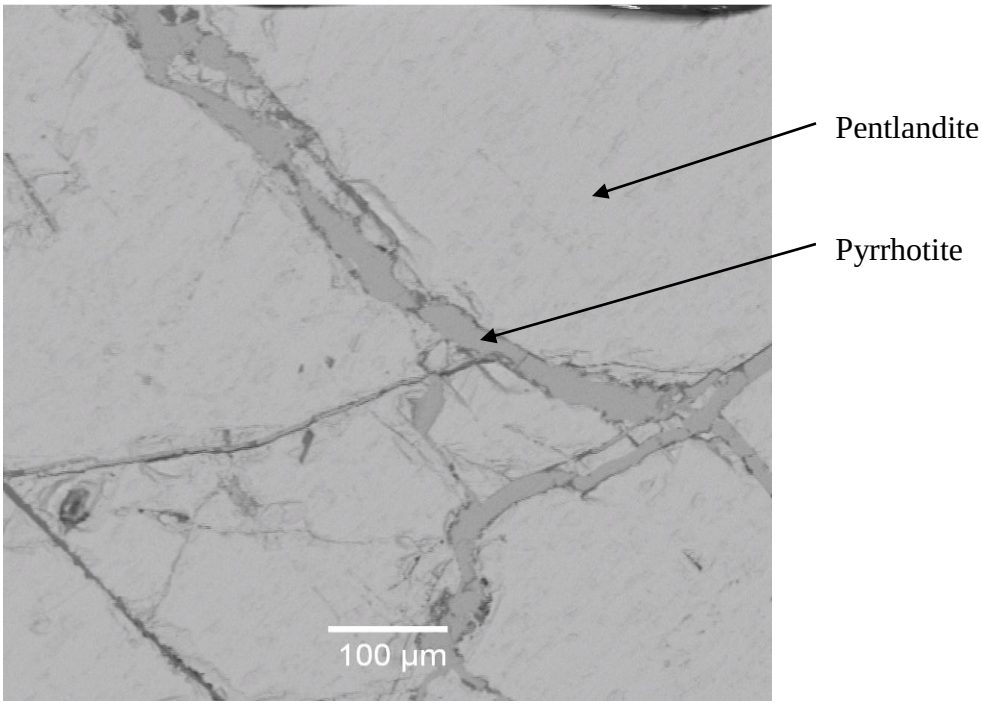

Figure C10: Back-scattered electron micrograph of a massive pentlandite sample sourced from the Phoenix deposit. Accelerating voltage 15 kV.

APPENDIX D: **Microprobe analyses of the pentlandite microelectrodes and the massive electrodes**

1. Composition of pentlandite particles handpicked from the Platreef flotation concentrate

Table D1: Composition of Platreef 10 pentlandite particle.

n	1			2			3			4			5		
Element	wt %	At %	Atomic	wt %	At %	Atomic	wt %	At %	Atomic	wt %	At %	Atomic	wt %	At %	Atomic
Fe	32.48	26.69	4.65	32.37	26.43	4.53	32.06	26.09	4.44	32.45	26.42	4.45	31.99	26.17	4.45
Ni	33.05	25.84	4.50	33.64	26.13	4.48	33.75	26.13	4.44	33.52	25.97	4.44	33.53	26.10	4.44
Co	0.86	0.67	0.12	0.90	0.70	0.12	0.86	0.66	0.11	0.86	0.66	0.11	0.87	0.67	0.11
Cu	0.18	0.13	0.02	0.08	0.06	0.01	0.12	0.09	0.01	0.20	0.14	0.01	0.06	0.04	0.01
S	32.61	46.67	8.00	32.83	46.68	8.00	33.19	47.03	8.00	33.01	46.81	8.00	32.99	47.01	8.00
Total	99.18	100.00		99.82	100.00		99.98	100.00		100.04	100.00		99.44	100.00	

Table D1.1: Average Composition of Platreef 10 pentlandite particle.

Element	wt %	±	stdev	At %	**Atomic Proportion**
Fe	32.270	0.20	0.23	26.36	4.52
Ni	33.498	0.23	0.27	26.03	4.46
Co	0.870	0.02	0.02	0.67	0.12
Cu	0.128	0.05	0.06	0.09	0.02
S	32.93	0.19	0.22	46.84	8.00
Total	99.69			100.00	

Table D2: Composition of Platreef 12 pentlandite particle.

n	1			2			3		
Element	wt %	At %	Atomic	wt %	At %	Atomic	wt %	At %	Atomic
Fe	33.19	26.90	4.55	33.16	26.88	4.54	33.14	26.93	4.56
Ni	32.85	25.33	4.29	32.69	25.21	4.26	32.73	25.30	4.28
Co	0.68	0.52	0.09	0.65	0.50	0.08	0.67	0.52	0.09
Cu	0.00	0.00	0.00	0.04	0.03	0.00	0.00	0.00	0.00
S	33.47	47.24	8.00	33.56	47.38	8.00	33.39	47.25	8.00
Total	100.19	100.00		100.10	100.00		99.93	100.00	

Table D2.1: Average Composition of Platreef 12 pentlandite particle.

Element	wt %	±	stdev	At %	**Atomic Proportion**
Fe	33.16	0.03	0.03	26.90	4.55
Ni	32.76	0.09	0.08	25.28	4.28
Co	0.67	0.02	0.02	0.51	0.09
Cu	0.013	0.03	0.02	0.01	0.00
S	33.47	0.10	0.09	47.29	8.00
Total	100.07			100.00	

Table D3: Composition of Platreef 15 pentlandite particle.

n	1			2			3		
Element	wt %	At %	Atomic	wt %	At %	Atomic	wt %	At %	Atomic
Fe	33.10	27.00	4.58	33.49	27.20	4.62	33.49	27.36	4.65
Ni	32.38	25.13	4.26	32.40	25.03	4.25	32.08	24.94	4.24
Co	0.86	0.66	0.11	0.86	0.66	0.11	0.86	0.67	0.11
Cu	0.03	0.02	0.00	0.00	0.00	0.00	0.00	0.00	0.00
S	33.21	47.18	8.00	33.31	47.11	8.00	33.05	47.03	8.00
Total	99.58	100.00		100.06	100.00		99.48	100.00	

Table D3.1: Average composition of Platreef 15 pentlandite particle.

Element	wt %	±	stdev	At %	**Atomic**
Fe	33.36	0.25	0.23	27.19	4.62
Ni	32.29	0.20	0.18	25.04	4.25
Co	0.86		0.00	0.66	0.11
Cu	0.01	0.02	0.02	0.01	0.00
S	33.19	0.15	0.13	47.11	8.00
Total	99.71			100.00	

Table D4: Composition of Platreef 14 pentlandite particle.

n	1			2			3			4		
Element	wt %	At %	Atomic	wt %	At %	Atomic	wt %	At %	Atomic	wt %	At %	Atomic
Fe	30.95	25.33	4.30	30.98	25.31	4.29	31.13	25.34	4.30	31.57	25.60	4.37
Ni	34.70	27.02	4.59	34.62	26.91	4.56	34.84	26.98	4.58	34.95	26.97	4.60
Co	0.67	0.52	0.09	0.72	0.56	0.09	0.68	0.52	0.09	0.65	0.50	0.09
Cu	0.00	0.00	0.00	0.08	0.06	0.01	0.03	0.02	0.00	0.02	0.01	0.00
S	33.07	47.13	8.00	33.15	47.17	8.00	33.25	47.13	8.00	33.22	46.92	8.00
Total	99.39	100.00		99.55	100.00		99.93	100.00		100.41	100.00	

Table D4.1: Average composition of Platreef 14 pentlandite particle.

Element	wt %	±	stdev	At %	Atomic
Fe	31.16	0.28	0.29	25.39	4.31
Ni	34.78	0.14	0.15	26.97	4.58
Co	0.68	0.03	0.03	0.53	0.09
Cu	0.03	0.03	0.03	0.02	0.00
S	33.17	0.08	0.08	47.09	8.00
Total	99.82			100.00	

Table D5: Composition of Platreef 11 pentlandite particle.

n	1			2			3		
Element	wt %	At %	Atomic	wt %	At %	Atomic	wt %	At %	Atomic
Fe	31.46	25.74	4.36	31.79	26.00	4.43	31.55	25.63	4.35
Ni	34.11	26.55	4.50	34.15	26.58	4.53	34.56	26.71	4.53
Co	0.67	0.52	0.09	0.63	0.49	0.08	0.66	0.51	0.09
Cu	0.00	0.00	0.00	0.00	0.00	0.00	0.01	0.01	0.00
S	33.12	47.19	8.00	32.94	46.93	8.00	33.32	47.14	8.00
Total	99.36	100.00		99.51	100.00		100.10	100.00	

Table D5.1: Average composition of Platreef 11 pentlandite particle.

Element	wt %	±	stdev	At %	Atomic
Fe	31.60	0.19	0.17	25.79	4.38
Ni	34.27	0.28	0.25	26.62	4.52
Co	0.65	0.02	0.02	0.51	0.09
Cu	0.00	0.01	0.01	0.00	0.00
S	33.13	0.22	0.19	47.09	8.00
Total	99.65			100.00	

Table D6: Composition of Platreef 1 pentlandite particle.

n	1			2			3			4		
Element	wt %	At %	Atomic	wt %	At %	Atomic	wt %	At %	Atomic	wt %	At %	Atomic
Fe	31.74	25.98	4.45	31.97	25.95	4.43	31.69	25.89	4.41	31.29	25.808	4.414
Ni	34.35	26.75	4.59	34.54	26.68	4.56	34.31	26.67	4.55	34.1	26.762	4.577
Co	0.72	0.56	0.10	0.67	0.52	0.09	0.65	0.50	0.09	0.73	0.5706	0.098
Cu	0.04	0.03	0.00	0.01	0.01	0.00	0.02	0.01	0.00	0.12	0.087	0.015
S	32.74	46.68	8.00	33.14	46.85	8.00	32.99	46.93	8.00	32.56	46.772	8.00
Total	99.59	100.00		100.33	100.00			100.00		98.8	100	

Table D6.1 Average composition of Platreef 1 pentlandite particle.

Element	wt %	±	stdev	At %	Atomic
Fe	31.67	0.28	0.28	25.91	4.43
Ni	34.33	0.18	0.18	26.71	4.57
Co	0.69	0.04	0.04	0.54	0.09
Cu	0.05	0.05	0.05	0.03	0.01
S	32.86	0.25	0.26	46.81	8.00
Total	99.60			100.00	

Table D7: Composition of Platreef 16 pentlandite particle.

n	1			2			3			4		
Element	wt %	At %	Atomic	wt %	At %	Atomic	wt %	At %	Atomic	wt %	At %	Atomic
Fe	34.18	27.88	4.73	34.59	28.14	4.80	34.31	27.84	4.71	34.29	27.68	4.72
Ni	31.43	24.39	4.14	31.46	24.35	4.15	31.44	24.27	4.11	31.64	24.30	4.15
Co	0.77	0.60	0.10	0.69	0.53	0.09	0.71	0.55	0.09	0.76	0.58	0.0
Cu	0.00	0.00	0.00	0.07	0.05	0.01	0.13	0.09	0.02	0.76	0.54	0.092
S	33.18	47.13	8.00	33.13	46.93	8.00	33.44	47.25	8.00	33.36	46.90	8
Total	99.56	100.00		99.94	100.00		100.03	100.00		100.81	100.00	

Table D7:1 Average composition of Platreef 16 pentlandite particle.

Element	wt %	±	stdev	At %	Atomic
Fe	34.34	0.17	0.17	27.88	4.74
Ni	31.49	0.10	0.10	24.33	4.14
Co	0.73	0.04	0.04	0.56	0.10
Cu	0.24	0.34	0.35	0.17	0.03
S	33.28	0.14	0.15	47.05	8.00
Total	100.09			100.00	

Table D8: Composition of Platreef 13 pentlandite particle.

n	1			2			3		
Element	wt %	At %	Atomic	wt %	At %	Atomic	wt %	At %	Atomic
Fe	34.00	27.71	4.71	33.49	27.46	4.67	33.72	27.57	4.70
Ni	31.83	24.68	4.20	31.87	24.87	4.22	32.01	24.91	4.24
Co	0.76	0.59	0.10	0.74	0.58	0.10	0.73	0.57	0.10
Cu	0.00	0.00	0.00	0.00	0.00	0.00	0.00	0.00	0.00
S	33.13	47.02	8.00	32.97	47.09	8.00	32.97	46.95	8.00
Total	99.72	100.00		99.07	100.00		99.43	100.00	

Table D8.1: Average composition of Platreef 13 pentlandite particle.

Element	wt %	±	stdev	At %	Atomic
Fe	33.74	0.29	0.26	27.58	4.69
Ni	31.90	0.11	0.09	24.82	4.22
Co	0.74	0.02	0.02	0.58	0.10
Cu	0.00	-	0.00	0.00	0.00
S	33.02	0.10	0.09	47.02	8.00
Total	99.41			100.00	

Table D9: Composition of Composite B sample1 pentlandite particle.

n	1			2			3		
Element	wt %	At %	Atomic	wt %	At %	Atomic	wt %	At %	Atomic
Fe	37.98	31.06	5.27	38.49	31.31	5.33	38.39	31.38	5.32
Ni	26.82	20.87	3.54	26.89	20.81	3.55	26.53	20.63	3.50
Co	0.93	0.72	0.12	0.95	0.73	0.12	0.96	0.74	0.13
Cu	0.24	0.17	0.03	0.28	0.20	0.03	0.13	0.09	0.02
S	33.13	47.18	8.00	33.14	46.95	8.00	33.13	47.16	8.00
Total	99.10	100.00		99.75	100.00		99.14	100.00	

Table D9.1: Average composition of Composite B sample1 pentlandite particle.

Element	wt %	±	stdev	At %	Atomic
Fe	38.29	0.31	0.27	31.25	5.31
Ni	26.75	0.22	0.19	20.77	3.53
Co	0.95	0.02	0.02	0.73	0.12
Cu	0.22	0.09	0.08	0.16	0.03
S	33.13	0.01	0.01	47.10	8.00
Total	99.33			100.00	

Table D10: Composition of Composite B sample2 pentlandite particle.

n	1			2			3			4		
Element	wt %	At %	Atomic	wt %	At %	Atomic	wt %	At %	Atomic	wt %	At %	Atomic
Fe	45.10	36.22	6.01	41.09	33.33	5.60	39.79	32.16	5.43	45.48	36.58	6.08
Ni	19.25	14.71	2.44	23.61	18.22	3.06	25.51	19.62	3.31	18.89	14.46	2.40
Co	0.95	0.72	0.12	0.83	0.64	0.11	0.85	0.65	0.11	0.82	0.63	0.10
Cu	0.14	0.10	0.02	0.25	0.18	0.03	0.21	0.15	0.03	0.28	0.20	0.03
S	34.49	48.24	8.00	33.71	47.63	8.00	33.68	47.42	8.00	34.36	48.14	8.00
Total	99.93	100.00		99.49	100.00		100.04	100.00		99.83	100.00	

Table D10.1: Average composition of Composite B sample2 pentlandite particle.

Element	wt %	±	stdev	At %	Atomic
Fe	42.87	2.80	2.85	34.58	5.78
Ni	21.82	3.20	3.27	16.75	2.80
Co	0.86	0.06	0.06	0.66	0.11
Cu	0.22	0.06	0.06	0.16	0.03
S	34.06	0.42	0.42	47.86	8.00
Total	99.82			100.00	

Table D11: Average composition of Platreef 2 pentlandite particle.

n	1			2			Average		
Element	wt %	At %	Atomic	wt %	At %	Atomic	wt %	At %	Atomic
Fe	31.61	25.62	4.38	31.54	25.66	4.52	31.58	25.64	4.45
Ni	34.98	26.97	4.61	34.73	26.89	4.73	34.86	26.93	4.67
Co	0.71	0.55	0.09	0.68	0.52	0.09	0.70	0.53	0.09
Cu	0.08	0.06	0.01	0.04	0.03	0.01	0.06	0.04	0.01
S	33.16	46.81	8.00	33.10	46.90	8.00	33.13	46.85	8.00
	100.54	100.00		100.09	100.00		100.32	100.00	

N - number of spots analysed

2. Composition of pentlandite particles handpicked from the Lebowa Merensky flotation concentrate

Table D12: Composition of LMP7 pentlandite particle.

n	1			**2**			3		
Element	wt %	At %	Atomic	wt %	At %	Atomic	wt %	At %	Atomic
Fe	28.71	23.62	4.00	29.11	23.88	4.05	29.21	23.94	4.06
Ni	36.78	28.79	4.87	36.59	28.56	4.84	36.72	28.63	4.86
Co	0.39	0.30	0.05	0.42	0.33	0.06	0.40	0.31	0.05
Cu	0.00	0.00	0.00	0.00	0.00	0.00	0.01	0.01	0.00
S	33.01	47.29	8.00	33.05	47.23	8.00	33.01	47.11	8.00
Total	98.89	100.00			100.00			100.00	

Table D12.1: Composition of LMP7 pentlandite particle.

Element	wt %	±	stdev	At %	Atomic ratio
Fe	29.01	0.30	0.26	23.81	4.04
Ni	36.70	0.11	0.10	28.66	4.86
Co	0.40	0.02	0.02	0.31	0.05
Cu	0.00	0.01	0.01	0.00	0.00
S	33.02	0.03	0.02	47.21	8.00
Total	99.14			100.00	16.95

Table D13: Composition of LMP16 pentlandite particle.

n	1			**2**			3		
Element	wt %	At %	Atomic	wt %	At %	Atomic	wt %	At %	Atomic
Fe	30.45	24.81	4.17	30.47	24.98	4.22	30.65	24.94	4.20
Ni	35.29	27.36	4.60	35.13	27.40	4.63	35.20	27.25	4.59
Co	0.37	0.29	0.05	0.37	0.29	0.05	0.36	0.28	0.05
Cu	0.00	0.00	0.00	0.00	0.00	0.00	0.00	0.00	0.00
S	33.51	47.55	8.00	33.15	47.33	8.00	33.55	47.54	8.00
Total	99.62	100		99.12	100		99.76	100	

Table D13.1: Average composition of LMP16 pentlandite particle.

Element	wt %	±	stdev	At %	Atomic ratio
Fe	30.52	0.12	0.11	24.91	4.20
Ni	35.21	0.09	0.08	27.34	4.61
Co	0.37	0.01	0.01	0.28	0.05
Cu	0.00	0.00	0.00	0.00	0.00
S	33.40	0.25	0.22	47.47	8.00
Total	99.50			100.00	

Table D14: Composition of LMP19 pentlandite particle.

n	1			**2**			3		
Element	wt %	At %	Atomic	wt %	At %	Atomic	wt %	At %	Atomic
Fe	32.04	25.92	4.42	31.55	25.66	4.38	31.68	25.64	4.36
Ni	35.00	26.95	4.59	35.13	27.19	4.64	35.13	27.05	4.61
Co	0.27	0.21	0.04	0.29	0.22	0.04	0.34	0.26	0.04
Cu	0.00	0.00	0.00	0.10	0.07	0.01	0.07	0.05	0.01
S	33.30	46.92	8.00	33.08	46.86	8.00	33.34	47.00	8.00
Total	100.61	100.00	100.00	100.15	100.00		100.56	100.00	

Table D14.1 Average composition of LMP19 pentlandite particle.

Element	wt %	±	stdev	At %	Atomic ratio
Fe	31.76	0.29	0.25	25.74	4.39
Ni	35.09	0.08	0.08	27.06	4.61
Co	0.30	0.04	0.04	0.23	0.04
Cu	0.06	0.06	0.05	0.04	0.01
S	33.24	0.16	0.14	46.93	8.00
Total	100.44			100.00	

Table D15: Composition of LMP17 pentlandite particle.

n	1			**2**			3		
Element	wt %	At %	Atomic	wt %	At %	Atomic	wt %	At %	Atomic
Fe	29.28	23.74	4.02	29.57	23.99	4.08	29.26	23.77	4.03
Ni	36.94	28.50	4.82	36.77	28.39	4.82	36.86	28.49	4.83
Co	0.65	0.50	0.08	0.66	0.51	0.09	0.68	0.52	0.09
Cu	0.00	0.00	0.00	0.01	0.01	0.00	0.05	0.04	0.01
S	33.47	47.26	8.00	33.33	47.10	8.00	33.36	47.19	8.00
Total	100.34	100.00		100.34	100.00		100.21	100.00	

Table D15.1 Average composition of LMP17 pentlandite particle.

Element	wt %	±	stdev	At %	Atomic ratio
Fe	29.37	0.20	0.17	23.83	4.04
Ni	36.86	0.10	0.09	28.46	4.82
Co	0.66	0.02	0.02	0.51	0.09
Cu	0.02	0.03	0.03	0.01	0.00
S	33.39	0.08	0.07	47.18	8.00
Total	100.30			100.00	

Table D16: Composition of LMP1 pentlandite particle.

n	1			**2**			3			4		
Element	wt %	At %	Atomic	wt %	At %	Atomic	wt %	At %	Atomic	wt %	At %	Atomic
Fe	31.13	25.15	4.23	30.71	25.19	4.27	30.74	25.19	4.25	30.99	25.28	4.28
Ni	35.10	26.98	4.54	34.86	27.21	4.61	34.78	27.12	4.58	35.00	27.17	4.60
Co	0.44	0.34	0.06	0.44	0.34	0.06	0.42	0.33	0.06	0.39	0.30	0.05
Cu	0.00	0.00	0.00	0.02	0.01	0.00	0.01	0.01	0.00	0.00	0.00	0.00
S	33.79	47.54	8.00	33.06	47.24	8.00	33.19	47.36	8.00	33.25	47.25	8.00
Total	100.46	100.00		99.09	100.00		99.14	100.00		99.63	100.00	

Table D16.1 Average composition of LMP1 pentlandite particle.

Element	wt %	±	stdev	At %	Atomic ratio
Fe	30.89	0.20	0.20	25.20	4.26
Ni	34.94	0.14	0.14	27.12	4.58
Co	0.42	0.02	0.02	0.33	0.06
Cu	0.01	0.01	0.01	0.01	0.00
S	33.32	0.32	0.32	47.35	8.00
Total	99.58			100.00	

Table D17: Composition of LMP14 pentlandite particle.

n	1			**2**			3		
Element	wt %	At %	Atomic	wt %	At %	Atomic	wt %	At %	Atomic
Fe	30.97	25.49	4.35	31.38	25.74	4.41	31.23	25.48	4.32
Ni	35.08	27.47	4.69	35.05	27.36	4.68	35.06	27.22	4.62
Co	0.20	0.16	0.03	0.23	0.18	0.03	0.18	0.14	0.02
Cu	0.00	0.00	0.00	0.00	0.00	0.00	0.00	0.00	0.00
S	32.71	46.89	8.00	32.70	46.72	8.00	33.19	47.16	8.00
Total	98.96	100.00		99.36	100.00		99.66	100.00	

Table D17.1 Average composition of LMP14 pentlandite particle.

Element	wt %	±	stdev	At %	Atomic Proportion
Fe	31.19	0.23	0.21	25.57	4.36
Ni	35.06	0.02	0.02	27.35	4.66
Co	0.20	0.03	0.03	0.16	0.03
Cu	0.00	0.00	0.00	0.00	0.00
S	32.87	0.32	0.28	46.92	8.00
Total	99.33			100.00	

Table D18: Composition of LMP10 pentlandite particle.

n	1			2			3		
Element	wt %	At %	Atomic	wt %	At %	Atomic	wt %	At %	Atomic
Fe	32.23	26.25	4.45	32.21	26.22	4.44	31.72	25.90	4.37
Ni	33.65	26.08	4.42	33.54	25.98	4.40	33.58	26.08	4.40
Co	0.66	0.51	0.09	0.65	0.50	0.08	0.65	0.50	0.08
Cu	0.00	0.00	0.00	0.00	0.00	0.00	0.10	0.07	0.01
S	33.25	47.16	8.00	33.35	47.29	8.00	33.37	47.45	8.00
Total	99.79	100.00		99.75	100.00		99.42	100.00	

Table D18.1: Average composition of LMP10 pentlandite particle.

Element	wt %	±	stdev	At %	Atomic Proportion
Fe	32.05	0.33	0.29	26.12	4.42
Ni	33.59	0.06	0.06	26.05	4.41
Co	0.65	0.01	0.01	0.50	0.09
Cu	0.03	0.07	0.06	0.02	0.00
S	33.32	0.07	0.06	47.30	8.00
Total	99.65			100.00	

Table D19: Composition of LMP20 pentlandite particle.

n	1			2			3		
Element	wt %	At%	Atomic	wt %	At %	Atomic	wt %	At %	Atomic
Fe	29.60	24.33	4.17	29.95	24.45	4.17	29.58	24.41	4.18
Ni	36.55	28.59	4.90	36.18	28.11	4.80	36.30	28.51	4.89
Co	0.47	0.37	0.06	0.47	0.36	0.06	0.49	0.38	0.07
Cu	0.00	0.00	0.00	0.27	0.19	0.03	0.04	0.03	0.00
S	32.63	46.71	8.00	32.97	46.88	8.00	32.47	46.67	8.00
Total	99.25	100.00		99.84	100.00		98.88	100.00	

Table D 19.1: Average composition of LMP20 pentlandite particle.

Element	wt %	±	stdev	At %	Atomic proportions
Fe	29.71	0.24	0.21	24.40	4.17
Ni	36.34	0.21	0.19	28.40	4.86
Co	0.48	0.01	0.01	0.37	0.06
Cu	0.10	0.16	0.15	0.07	0.01
S	32.69	0.29	0.26	46.76	8.00
Total	99.32			100.00	

3. Composition of pentlandite particles handpicked from the Lebowa UG–2 flotation concentrate

Table D20: Composition of LUP3 pentlandite particle.

n	**1**			**2**			**3**			**4**			**5**		
Element	wt %	At %	Atomic	wt %	At %	Atomic	wt %	At %	Atomic	wt %	At %	Atomic	wt %	At %	Atomic
Fe	32.42	26.34	4.48	32.97	26.79	4.59	32.97	26.71	4.58	32.36	26.50	4.53	32.14	26.18	4.45
Ni	33.56	25.95	4.41	33.41	25.83	4.36	33.68	25.96	4.45	33.46	26.07	4.45	33.73	26.14	4.44
Co	0.78	0.60	0.10	0.73	0.56	0.01	0.75	0.58	0.10	0.70	0.54	0.09	0.73	0.56	0.10
Cu	0.05	0.04	0.01	0.18	0.13	0.00	0.14	0.10	0.02	0.09	0.06	0.01	0.04	0.03	0.00
S	33.26	47.07	8.00	33.00	46.69	8.00	33.06	46.65	8.00	32.83	46.82	8.00	33.20	47.09	8.00
Total	100.07	100.00		100.29	100.00		100.60	100.00		99.44	100.00		99.84	100.00	

Table D20.1: Average composition of LUP3 pentlandite particle.

Element	wt %	±	At %	Atomic	Stdev
Fe	32.57	0.33	26.50	4.52	0.38
Ni	33.57	0.12	25.99	4.42	0.14
Co	0.74	0.03	0.57	0.08	0.03
Cu	0.10	0.05	0.07	0.01	0.06
S	33.07	0.15	46.87	8.00	0.17
Total	100.05		100.00		

Table D21: Composition of LUP1 pentlandite particle.

n	1			**2**			3			4		
Element	wt %	At %	Atomic	wt %	At %	Atomic	wt %	At %	Atomic	wt %	At %	Atomic
Fe	32.17	26.05	4.42	32.19	26.06	4.42	32.09	26.20	4.46	31.50	25.78	4.37
Ni	34.22	26.36	4.48	34.21	26.35	4.49	33.87	26.31	4.48	34.03	26.50	4.49
Co	0.63	0.48	0.08	0.57	0.44	0.01	0.58	0.45	0.08	0.60	0.47	0.08
Cu	0.00	0.00	0.00	0.00	0.00	0.00	0.01	0.01	0.00	0.08	0.06	0.01
S	33.41	47.11	8.00	33.44	47.15	8.00	33.08	47.04	8.00	33.11	47.20	8.00
Total	100.43	100.00		100.41	100.00		99.63	100.00		99.32	100.00	

Atomic = atomic proportion

Table D21.1: Average composition of pentlandite particle LUP1.

Element	wt %	±	At %	Atomic	Stdev
Fe	31.99	0.32	26.02	4.42	0.33
Ni	34.08	0.16	26.38	4.48	0.17
Co	0.60	0.03	0.46	0.06	0.03
Cu	0.02	0.04	0.02	0.00	0.04
S	33.26	0.19	47.12	8.00	0.19
Total	99.95		100.00		

Table D 22: Composition of pentlandite particle LUP5 from Lebowa UG–2.

n	1			**2**			3			4		
Element	wt %	At %	Atomic	wt %	At %	Atomic	wt %	At %	Atomic	wt %	At %	Atomic
Fe	30.67	24.86	4.20	30.82	24.93	4.23	31.00	25.16	4.29	31.14	25.25	4.30
Ni	35.45	27.34	4.62	35.55	27.36	4.64	35.45	27.38	4.66	35.26	27.21	4.63
Co	0.59	0.45	0.08	0.58	0.44	0.08	0.61	0.47	0.08	0.60	0.46	0.08
Cu	0.01	0.01	0.00	0.08	0.06	0.01	0.04	0.03	0.00	0.06	0.04	0.01
S	33.54	47.34	8.00	33.50	47.20	8.00	33.22	46.96	8.00	33.30	47.03	8.00
	100.26	100.00		100.53	100.00		100.32	100.00		100.36	100.00	

Table D 22.1: Average composition of pentlandite particle LUP5 from Lebowa UG-2.

Element	wt %	±	At %	Atomic	Stdev
Fe	30.91	0.20	25.05	4.25	0.21
Ni	35.43	0.12	27.32	4.64	0.12
Co	0.60	0.01	0.46	0.08	0.01
Cu	0.05	0.03	0.03	0.01	0.03
S	33.39	0.15	47.13	8.00	0.15
Total	100.37		100.00		

Table D 23: Composition of pentlandite particle LUP9.

n	1			**2**			3			4		
Element	wt %	At %	Atomic	wt %	At %	Atomic	wt %	At %	Atomic	wt %	At %	Atomic
Fe	30.16	24.40	4.13	30.12	24.44	4.14	29.98	24.33	4.11	30.42	24.62	4.19
Ni	36.12	27.80	4.71	35.99	27.79	4.71	36.07	27.85	4.71	36.09	27.79	4.73
Co	0.72	0.55	0.09	0.73	0.56	0.10	0.68	0.52	0.09	0.69	0.53	0.09
Cu	0.04	0.03	0.00	0.05	0.04	0.01	0.00	0.00	0.00	0.05	0.04	0.01
S	33.52	47.22	8.00	33.38	47.17	8.00	33.47	47.30	8.00	33.37	47.03	8.00
	100.56	100.00		100.27	100.00		100.20	100.00		100.62	100.00	

Table D 23.1: Average composition of pentlandite particle LUP9 from Lebowa UG-2.

Element	wt %	±	At %	Atomic	Stdev
Fe	30.17	0.18	24.45	4.14	0.18
Ni	36.07	0.054	27.81	4.71	0.06
Co	0.71	0.023	0.54	0.09	0.02
Cu	0.04	0.023	0.02	0.00	0.02
S	33.44	0.071	47.18	8.00	0.07
Total	100.41		100.00		

4. Composition of pentlandite particles handpicked from the Nkomati flotation concentrate

Table D 24. Composition of pentlandite particle Nkomati 12.

n	1			2			3		
Element	wt %	At %	Atomic	wt %	At %	Atomic	wt %	At %	Atomic
Fe	30.88	25.10	4.30	30.87	25.14	4.30	30.95	25.20	4.31
Ni	34.99	27.07	4.64	34.71	26.90	4.60	34.63	26.83	4.58
Co	1.47	1.13	0.19	1.40	1.08	0.18	1.41	1.09	0.19
Cu	0.02	0.01	0.00	0.10	0.07	0.01	0.08	0.06	0.01
S	32.97	46.68	8.00	33.00	46.81	8.00	33.02	46.83	8.00
Total	100.33	100.00		100.08	100.00		100.09	100.00	

Table D 24.1: Average composition of Nkomati 12 pentlandite particle.

Element	wt %	±	stdev	At %	Atomic
Fe	30.90	0.05	0.04	25.13	4.30
Ni	34.78	0.21	0.19	26.92	4.61
Co	1.43	0.04	0.04	1.10	0.19
Cu	0.07	0.05	0.04	0.05	0.01
S	33.00	0.03	0.03	46.74	8.00
Total	100.17			99.94	

Table D 25: Composition of Nkomati 11 pentlandite particle.

n	1			2			3		
Element	wt %	At %	Atomic	wt %	At %	Atomic	wt %	At %	Atomic
Fe	30.67	25.02	4.24	31.03	25.06	4.22	30.93	25.18	4.29
Ni	34.41	26.71	4.53	34.32	26.37	4.44	34.56	26.77	4.56
Co	1.40	1.08	0.18	1.41	1.08	0.18	1.45	1.12	0.19
Cu	0.00	0.00	0.00	0.00	0.00	0.00	0.01	0.01	0.00
S	33.22	47.19	8.00	33.76	47.49	8.00	33.10	46.93	8.00
Total	99.70	100.00		100.52	100.00		100.05	100.00	

Table D 25.1: Average composition of Nkomati 11 pentlandite particle.

Element	wt %	±	stdev	At %	Atomic
Fe	30.88	0.21	0.19	25.09	4.25
Ni	34.43	0.14	0.12	26.62	4.51
Co	1.42	0.03	0.03	1.09	0.19
Cu	0.00	0.01	0.01	0.00	0.00
S	33.36	0.40	0.35	47.20	8.00
Total	100.09			100.00	16.95

Table D 26: Composition of Nkomati 8 pentlandite particle.

n	1			2			3		
Element	wt %	At %	Atomic	wt %	At %	Atomic	wt %	At %	Atomic
Fe	30.80	25.14	4.29	30.68	25.06	4.27	30.92	25.13	4.28
Ni	34.62	26.89	4.59	34.50	26.81	4.56	34.64	26.79	4.56
Co	1.40	1.08	0.18	1.42	1.10	0.19	1.37	1.06	0.18
Cu	0.00	0.00	0.00	0.05	0.04	0.01	0.08	0.06	0.01
S	32.99	46.89	8.00	33.04	47.00	8.00	33.19	46.98	8.00
Total	99.81	100.00		99.69	100.00		100.20	100.00	

Table D 26.1: Average composition of Nkomati 8 pentlandite particle.

Element	wt %	±	stdev	At %	Atomic
Fe	30.80	0.14	0.12	25.11	4.28
Ni	34.59	0.09	0.08	26.83	4.57
Co	1.40	0.03	0.03	1.08	0.18
Cu	0.04	0.05	0.04	0.03	0.01
S	33.07	0.12	0.10	46.96	8.00

Table D 27: Composition of Nkomati 7 pentlandite particle.

n	1			2			3		
Element	wt %	At %	Atomic	wt %	At %	Atomic	wt %	At %	Atomic
Fe	31.09	25.17	4.27	30.53	24.86	4.22	30.16	24.77	4.21
Ni	34.64	26.69	4.53	34.82	26.98	27.14	34.74	27.14	4.62
Co	1.34	1.03	0.17	1.32	1.02	1.04	1.34	1.04	0.18
Cu	0.00	0.00	0.00	0.00	0.00	0.00	0.00	0.00	0.00
S	33.41	47.11	8.00	33.23	47.13	8.00	32.90	47.05	8.00
Total	100.48	100.00		99.90	100.00		99.14	100.00	

Table D 27.1: Average composition of Nkomati 7 pentlandite particle.

Element	wt %	±	stdev	At %	Atomic
Fe	30.59	0.53	0.47	24.93	4.24
Ni	34.73	0.10	0.09	26.94	4.58
Co	1.33	0.01	0.01	1.03	0.17
Cu	0.00		0.00	0.00	0.00
S	33.18	0.29	0.26	47.10	8.00

Table D 28: Composition of Nkomati 10 pentlandite particle.

n	1			2			3			4		
Element	wt %	At %	Atomic	wt %	At %	Atomic	wt %	At %	Atomic	wt %	At %	Atomic
Fe	30.93	25.03	4.22	30.81	24.91	4.19	31.08	25.07	4.24	30.50	24.65	4.13
Ni	34.37	26.47	4.46	34.49	26.53	4.46	34.60	26.56	4.49	34.71	26.69	4.48
Co	1.29	0.99	0.17	1.30	1.00	0.17	1.30	0.99	0.17	1.25	0.96	0.16
Cu	0.00	0.00	0.00	0.00	0.00	0.00	0.01	0.01	0.00	0.00	0.00	0.00
S	33.70	47.51	8.00	33.79	47.57	8.00	33.71	47.36	8.00	33.89	47.70	8.00
Total	100.29	100.00		100.39	100.00		100.70	100.00		100.35	100.00	

Table D 28.1: Average composition of Nkomati 10 pentlandite particle.

Element	wt %	±	stdev	At %	Atomic
Fe	30.83	0.24	0.25	24.92	4.19
Ni	34.54	0.14	0.15	26.56	4.47
Co	1.29	0.02	0.02	0.98	0.17
Cu	0.00	0.00	0.01	0.00	0.00
S	33.77	0.09	0.09	47.54	8.00

Table D 29: Composition of Nkomati 3 pentlandite particle.

n	1			2			3		
Element	wt %	At %	Atomic	wt %	At %	Atomic	wt %	At %	Atomic
Fe	30.34	24.74	4.18	30.77	25.02	4.25	30.42	24.86	4.22
Ni	34.91	27.09	4.58	34.90	27.01	4.59	34.95	27.17	4.62
Co	1.10	0.85	0.14	1.10	0.85	0.14	1.14	0.88	0.15
Cu	0.00	0.00	0.00	0.06	0.04	0.01	0.00	0.00	0.00
S	33.31	47.31	8.00	33.24	47.08	8.00	33.09	47.09	8.00
Total	99.66	100.00		100.07	100.00		99.60	100.00	

Table D 29.1: Average composition of Nkomati 3 pentlandite particle.

Element	wt %	±	stdev	At %	Atomic
Fe	30.51	0.26	0.23	24.87	4.22
Ni	34.92	0.03	0.03	27.09	4.60
Co	1.11	0.03	0.02	0.86	0.15
Cu	0.02	0.04	0.03	0.01	0.00
S	33.21	0.13	0.11	47.16	8.00

Table D 30: Composition of Nkomati 2 pentlandite particle.

n	1			2			3		
Element	wt %	At %	Atomic	wt %	At %	Atomic	wt %	At %	Atomic
Fe	31.03	25.27	4.30	31.04	25.24	4.29	30.77	25.23	4.29
Ni	34.61	26.81	4.56	34.54	26.72	4.54	34.35	26.80	4.55
Co	1.20	0.93	0.16	1.23	0.95	0.16	1.18	0.92	0.16
Cu	0.00	0.00	0.00	0.00	0.00	0.00	0.00	0.00	0.00
S	33.14	47.00	8.00	33.26	47.10	8.00	32.96	47.06	8.00
Total	99.98	100.00		100.07	100.00		99.26	100.00	

Table D 30.1: Average composition of Nkomati 2 pentlandite particle.

Element	wt %	±	stdev	At %	Atomic
Fe	30.95	0.17	0.15	25.24	4.29
Ni	34.50	0.15	0.13	26.78	4.55
Co	1.20	0.03	0.03	0.93	0.16
Cu	0.00		0.00	0.00	0.00
S	33.12	0.17	0.15	47.05	8.00

Table D 31: Composition of Nkomati 4 pentlandite particle.

	1			2			3			4		
Element	wt %	At %	Atomic	wt %	At %	Atomic	wt %	At %	Atomic	wt %	At %	Atomic
Fe	30.27	24.61	4.16	30.52	24.76	4.18	29.97	24.60	4.19	29.84	24.40	4.15
Ni	33.87	26.20	4.42	33.72	26.03	4.40	34.03	26.58	4.52	34.28	26.67	4.53
Co	2.34	1.80	0.30	2.42	1.86	0.31	2.36	1.84	0.31	2.44	1.89	0.32
Cu	0.00	0.00	0.00	0.00	0.00	0.00	0.00	0.00	0.00	0.00	0.00	0.00
S	33.46	47.38	8.00	33.52	47.36	8.00	32.87	46.99	8.00	33.04	47.05	8.00
Total	99.94	100.00		100.18	100.00		99.23	100.00		99.60	100.00	

Table D 31.1: Average composition of Nkomati 4 pentlandite particle.

Element	wt %	±	stdev	At %	Atomic
Fe	30.15	0.30	0.31	24.59	4.17
Ni	33.98	0.23	0.24	26.37	4.47
Co	2.39	0.05	0.05	1.85	0.31
Cu	0.00		0.00	0.00	0.00
S	33.22	0.31	0.32	47.19	8.00

Table D 32.1: Composition of Massive Nkomati pentlandite particle.

n	1			2			3		
Element	wt %	At %	Atomic	wt %	At %	Atomic	wt %	At %	Atomic
Fe	29.75	24.53	4.16	30.02	24.72	4.20	29.89	24.63	4.18
Ni	34.99	27.46	4.66	34.90	27.34	4.64	34.95	27.40	4.65
Co	1.08	0.84	0.14	1.08	0.84	0.14	1.08	0.84	0.14
Cu	0.00	0.00	0.00	0.00	0.00	0.00	0.00	0.00	0.00
S	32.84	47.17	8.00	32.84	47.10	8.00	32.84	47.13	8.00
Total	98.66	100.00		98.84	100.00		98.75	100.00	

Table D 32.2: Average composition of Massive Nkomati pentlandite particle.

Element	wt %	±	stdev	At %	Atomic
Fe	29.89	0.15	0.14	24.63	4.18
Ni	34.95	0.05	0.05	27.40	4.65
Co	1.08	-	0.00	0.84	0.14
Cu	0.00	-	0.00	0.00	0.00
S	32.84	-	0.00	47.13	8.00

Table D 33.1: Composition of Massive Russia 3 pentlandite sample.

n	1		2		3		4		5		6		7	
Element	wt %	At %	wt %	At %	wt %	At %	wt %	At %	wt %	At %	wt %	At %	wt %	At %
Fe	30.44	24.68	30.84	24.92	30.79	25.11	30.39	24.68	30.24	24.91	30.75	24.94	30.67	24.79
Ni	35.86	27.67	35.96	27.65	36	27.94	35.9	27.74	35.14	27.54	35.82	27.65	36.11	27.77
Co	1	0.77	1.05	0.80	1.01	0.78	1.09	0.84	1.01	0.79	1.04	0.80	1.01	0.77
Cu	0.04	0.03	0	0.00	0	0.00	0	0.00	0	0.00	0	0.00	0.01	0.01
S	33.18	46.86	33.12	46.62	32.5	46.17	33.04	46.74	32.6	46.76	32.99	46.61	33.15	46.66
Total	100.52	100.00	100.97	100.00	100.3	100.00	100.42	100.00	98.99	100.00	100.6	100.00	100.95	100.00

Table D 33.2: Atomic proportion of Russia 3 massive pentlandite.

Element	1	2	3	4	5	6	7
Fe	4.21	4.28	4.35	4.22	4.26	4.28	4.25
Ni	4.72	4.75	4.84	4.75	4.71	4.75	4.76
Co	0.13	0.14	0.14	0.14	0.13	0.14	0.13
Cu	0.00	0.00	0.00	0.00	0.00	0.00	0.00
S	8	8	8	8	8	8	8

Table D 33.3: Average composition of Russia 3 massive pentlandite.

Element	wt %	±	stdev	At %	Atomic
Fe	30.59	0.17	0.23	24.86	4.27
Ni	35.83	0.24	0.32	27.71	4.75
Co	1.03	0.02	0.03	0.79	0.14
Cu	0.01	0.01	0.01	0.01	0.00
S	32.94	0.20	0.28	46.63	8.00

Table D 34.1 Composition of Massive Russia 1 pentlandite sample.

n	1		2		3		4		5		6		7	
Element	wt %	At %	wt %	At %	wt %	At %	wt %	At %	wt %	At %	wt %	At %	wt %	At %
Fe	30.45	24.71	30.45	24.81	30.47	24.69	29.97	24.29	30.52	24.65	30.85	24.94	30.49	24.73
Ni	35.93	27.74	35.62	27.61	35.74	27.55	35.77	27.59	35.75	27.47	35.75	27.50	35.72	27.56
Co	1.02	0.78	0.95	0.73	1.03	0.79	1.09	0.84	1.06	0.81	1.02	0.78	1	0.77
Cu	0	0.00	0	0.00	0	0.00	0	0.00	0	0.00	0	0.00	0.05	0.04
S	33.1	46.77	33.01	46.84	33.29	46.97	33.5	47.29	33.47	47.07	33.23	46.78	33.21	46.91
Total	100.5	100.00	100.03	100.00	100.53	100.00	100.33	100.00	100.8	100.00	100.85	100.00	100.47	100.00

Table D 34.2: Atomic proportion of Russia 1 massive pentlandite.

Element	1	2	3	4	5	6	7
Fe	4.23	4.24	4.20	4.11	4.19	4.26	4.22
Ni	4.74	4.72	4.69	4.67	4.67	4.70	4.70
Co	0.13	0.13	0.13	0.14	0.14	0.13	0.13
Cu	0.00	0.00	0.00	0.00	0.00	0.00	0.01
S	8	8	8	8	8	8	8

Table D 34.3: Average composition of Russia 1 massive pentlandite.

Element	wt %	±	stdev	At %	Atomic
Fe	30.46	0.19	0.26	24.69	4.21
Ni	35.75	0.07	0.09	27.57	4.70
Co	1.02	0.03	0.04	0.79	0.13
Cu	0.01	0.01	0.02	0.01	0.00
S	33.26	0.13	0.18	46.95	8.00

Table D 35.1 Composition of Massive Russia 11 pentlandite sample.

n	1		2		3		4		5		6		7	
Element	wt %	At %	wt %	At %	wt %	At %	wt %	At %	wt %	At %	wt %	At %	wt %	At %
Fe	30.25	24.62	30.41	24.57	30.33	24.59	30.49	24.64	30.84	24.92	30.47	24.60	30.6	24.80
Ni	36.32	28.13	36.52	28.07	36.4	28.09	36.59	28.14	36.25	27.87	36.47	28.02	36.38	28.05
Co	1.04	0.80	1.04	0.80	1.02	0.78	1.03	0.79	1.01	0.77	1.01	0.77	1.02	0.78
Cu	0	0.00	0	0.00	0	0.00	0	0.00	0	0.00	0	0.00	0.04	0.03
S	32.76	46.44	33.1	46.57	32.95	46.54	32.98	46.43	33	46.44	33.15	46.61	32.83	46.34
Total	100.37	100.00	101.07	100.00	100.7	100.00	101.09	100.00	101.1	100.00	101.1	100.00	100.87	100.00

Table D 35.2: Atomic proportion of Russia 11 massive pentlandite.

Element	1	2	3	4	5	6	7
Fe	4.20	4.22	4.23	4.25	4.29	4.22	4.28
Ni	4.80	4.82	4.83	4.85	4.80	4.81	4.84
Co	0.14	0.14	0.13	0.14	0.13	0.13	0.14
Cu	0.00	0.00	0.00	0.00	0.00	0.00	0.00
S	8	8	8	8	8	8	8

Table D 35.3: Average composition of Russia 11 massive pentlandite.

Element	wt %	±	stdev	At %	Atomic
Fe	30.48	0.14	0.19	24.68	4.24
Ni	36.42	0.09	0.12	28.05	4.82
Co	1.02	0.01	0.01	0.79	0.14
Cu	0.01	0.01	0.02	0.00	0.00
S	32.97	0.10	0.14	46.48	8.00

Table D 36.1: Composition of Massive pentlandite 5 sample.

n	1		2		3		4		5		6		7	
Element	wt %	At %	wt %	At %	wt %	At %	wt %	At %	wt %	At %	wt %	At %	wt %	At %
Fe	30.47	24.71	31.05	25.13	30.3	24.58	30.98	25.09	30.46	24.70	30.62	24.79	30.71	24.90
Ni	36	27.78	35.94	27.67	36.22	27.96	36.07	27.80	36.18	27.92	36.14	27.84	35.91	27.71
Co	1.08	0.83	1.07	0.82	1.07	0.82	1.11	0.85	1.08	0.83	1.06	0.81	1.09	0.84
Cu	0.04	0.03	0	0.00	0	0.00	0	0.00	0	0.00	0	0.00	0	0.00
S	33.02	46.64	32.91	46.38	33.01	46.64	32.8	46.26	32.96	46.55	33.01	46.55	32.96	46.55
Total	100.61	100.00	100.97	100.00	100.6	100.00	100.96	100.00	100.68	100.00	100.83	100.00	100.67	100.00

Table D 36.2: Atomic proportions of massive pentlandite 5 sample.

Element	1	2	3	4	5	6	7
Fe	4.24	4.37	4.22	4.34	4.24	4.26	4.28
Ni	4.77	4.81	4.80	4.81	4.80	4.79	4.76
Co	0.14	0.14	0.14	0.15	0.14	0.14	0.14
Cu	0.00	0.00	0.00	0.00	0.00	0.00	0.00
S	8	8	8	8	8	8	8

Table D 36.3: Average composition of massive pentlandite 5 sample.

Element	wt %	±	stdev	At %	Atomic
Fe	30.66	0.21	0.28	24.84	4.28
Ni	36.07	0.09	0.12	27.81	4.79
Co	1.08	0.01	0.02	0.83	0.14
Cu	0.01	0.01	0.02	0.00	0.00
S	32.95	0.06	0.08	46.51	8.00

Table D 37.1: Composition of Russia 9 massive pentlandite sample.

n	1		2		3		4		5		6		7		8	
Element	wt %	At %	wt %	At %	wt %	At %	wt %	At %	wt %	At %	wt %	At %	wt %	At %	wt %	At %
Fe	30.64	24.96	30.65	24.83	30.72	24.97	30.87	25.03	30.7	24.95	30.56	24.87	31.12	25.15	29.13	24.00
Ni	36.16	28.03	36.24	27.93	36.42	28.17	36.4	28.08	36.26	28.04	36.52	28.28	36.41	28.00	36.27	28.43
Co	1.06	0.82	1.05	0.81	1.07	0.82	1.05	0.81	1.05	0.81	0.98	0.76	1.03	0.79	0.99	0.77
Cu	0	0.00	0	0.00	0	0.00	0	0.00	0	0.00	0	0.00	0	0.00	0.00	0.00
S	32.56	46.19	32.91	46.43	32.51	46.03	32.63	46.08	32.63	46.19	32.51	46.09	32.73	46.07	32.61	46.79
Total	100.4	100.00	100.9	100.00	100.72	100.00	101	100.00	100.6	100.00	100.6	100.00	101.3	100.00	99.00	100.00

Table D 37.2: Atomic proportions of Russia 9 massive pentlandite sample.

Atomic Proportion								
Element	1	2	3	4	5	6	7	8
Fe	4.32	4.28	4.34	4.35	4.32	4.32	4.37	4.10
Ni	4.85	4.81	4.90	4.88	4.86	4.91	4.86	4.86
Co	0.14	0.14	0.14	0.14	0.14	0.13	0.14	0.13
Cu	0.00	0.00	0.00	0.00	0.00	0.00	0.00	0.00
S	8	8	8	8	8	8	8	8

Table D 37.3: Average composition of Russia 9 massive pentlandite sample.

Element	wt %	±	stdev	At %	Atomic
Fe	30.55	0.42	0.60	24.85	4.30
Ni	36.34	0.08	0.12	28.12	4.87
Co	1.04	0.02	0.03	0.80	0.14
Cu	0.00		0.00	0.00	0.00
S	32.64	0.09	0.13	46.23	8.00

Table D 38.1: Composition of Russia 13 massive pentlandite sample.

n	1		2		3		4		5		6		7	
Element	wt %	At %	wt %	At %	wt %	At %	wt %	At %	wt %	At %	wt %	At %	wt %	At %
Fe	30.28	24.27	30.75	24.56	30.52	24.41	30.73	24.57	30.79	24.64	30.62	24.55	30.33	24.34
Ni	35.65	27.19	35.90	27.28	35.89	27.31	36.10	27.46	35.71	27.19	35.77	27.28	35.59	27.17
Co	1.02	0.77	0.99	0.75	1.03	0.78	1.03	0.78	1.06	0.80	0.98	0.74	1.07	0.81
Cu	0.00	0.00	0.00	0.00	0.00	0.00	0.00	0.00	0.00	0.00	0.00	0.00	0.00	0.00
S	34.21	47.76	34.09	47.41	34.10	47.50	33.90	47.20	33.98	47.36	33.97	47.43	34.11	47.67
Total	101.16	100.00	101.73	100.00	101.54	100.00	101.76	100.00	101.54	100.00	101.34	100.00	101.10	100.00

Table D 38.2: Atomic proportions of Russia 13 massive pentlandite sample.

Element	1	2	3	4	5	6	7
Fe	4.07	4.14	4.11	4.16	4.16	4.14	4.08
Ni	4.55	4.60	4.60	4.65	4.59	4.60	4.56
Co	0.13	0.13	0.13	0.13	0.14	0.13	0.14
Cu	0.00	0.00	0.00	0.00	0.00	0.00	0.00
S	8	8	8	8	8	8	8

Table D 38.3: Average composition of Russia 13 massive pentlandite sample.

Element	wt %	±	stdev	At %	Atomic
Fe	30.57	0.15	0.21	24.48	4.12
Ni	35.80	0.13	0.17	27.27	4.60
Co	1.03	0.02	0.03	0.78	0.13
Cu	0.00		0.00	0.00	0.00
S	34.05	0.08	0.11	47.48	8.00

Table D 39.1: Composition of Russia 12 massive pentlandite sample.

n	1		2		3		4		5		6		7	
Element	wt %	At %	wt %	At %	wt %	At %	wt %	At %	wt %	At %	wt %	At %	wt %	At %
Fe	30.99	25.21	30.52	24.96	30.55	24.92	30.77	25.20	30.40	24.85	30.96	25.22	30.55	24.86
Ni	36.10	27.94	36.38	28.31	36.38	28.24	36.06	28.09	36.16	28.13	36.05	27.94	36.01	27.88
Co	1.02	0.79	1.06	0.82	1.05	0.81	1.00	0.78	1.00	0.77	0.99	0.76	1.05	0.81
Cu	0.00	0.00	0.00	0.00	0.00	0.00	0.00	0.00	0.02	0.01	0.05	0.04	0.00	0.00
S	32.52	46.07	32.23	45.91	32.40	46.03	32.21	45.93	32.47	46.23	32.46	46.05	32.78	46.45
Total	100.63	100.00	100.19	100.00	100.38	100.00	100.04	100.00	100.05	100.00	100.51	100.00	100.39	100.00

Table D 39.2: Atomic proportions of Russia 12 massive pentlandite sample.

Element	1	2	3	4	5	6	7
Fe	4.38	4.35	4.33	4.39	4.30	4.38	4.28
Ni	4.85	4.93	4.91	4.89	4.87	4.85	4.80
Co	0.14	0.14	0.14	0.14	0.13	0.13	0.14
Cu	0.00	0.00	0.00	0.00	0.00	0.01	0.00
S	8	8	8	8	8	8	8

Table D 39.3: Average composition of Russia 12 massive pentlandite sample.

Element	wt %	±	stdev	At %	Atomic
Fe	30.68	0.17	0.23	25.03	4.34
Ni	36.16	0.12	0.16	28.08	4.87
Co	1.02	0.02	0.03	0.79	0.14
Cu	0.01	0.01	0.02	0.01	0.00
S	32.44	0.14	0.19	46.10	9.00

Table D 40.1: Composition of Russia 14 massive pentlandite sample.

n	1		2		3		4		5		6		7	
Element	wt %	At %	wt %	At %	wt %	At %	wt %	At %	wt %	At %	wt %	At %	wt %	At %
Fe	30.81	25.06	30.41	24.88	30.57	25.03	30.45	24.92	29.93	24.54	31.22	25.32	31.05	25.24
Ni	36.23	28.04	36.08	28.09	35.87	27.95	36.14	28.14	36.12	28.18	36.12	27.87	36.03	27.86
Co	0.94	0.72	0.99	0.77	0.96	0.74	0.96	0.74	1.03	0.80	0.98	0.75	0.98	0.75
Cu	0.00	0.00	0.00	0.00	0.00	0.00	0.00	0.00	0.00	0.00	0.00	0.00	0.00	0.00
S	32.59	46.17	32.46	46.26	32.45	46.28	32.41	46.19	32.54	46.47	32.61	46.06	32.60	46.15
Total	100.57	100.00	99.94	100.00	99.85	100.00	99.96	100.00	99.62	100.00	100.93	100.00	100.66	100.00

Table D 40.2: Atomic proportions of Russia 14 massive pentlandite sample.

Element	1	2	3	4	5	6	7
Fe	4.34	4.30	4.33	4.32	4.22	4.40	4.38
Ni	4.86	4.86	4.83	4.87	4.85	4.84	4.83
Co	0.13	0.13	0.13	0.13	0.14	0.13	0.13
Cu	0.00	0.00	0.00	0.00	0.00	0.00	0.00
S	8	8	8	8	8	8	8

Table D 40.3: Average composition of Russia 14 massive pentlandite sample.

Element	wt %	±	stdev	At %	Atomic
Fe	30.63	0.32	0.43	25.00	4.33
Ni	36.08	0.08	0.11	28.02	4.85
Co	0.98	0.02	0.03	0.76	0.13
Cu	0.00		0.00	0.00	0.00
S	32.52	0.06	0.08	46.23	8.00

Table D 41.1: Composition of Phoenix massive pentlandite 2 sample.

n	1		2		3		4		5		6		7	
Element	wt %	At %	wt %	At %	wt %	At %	wt %	At %	wt %	At %	wt %	At %	wt %	At %
Fe	29.30	23.92	28.30	23.18	29.26	23.89	29.69	24.20	30.00	24.45	29.35	24.10	29.34	24.01
Ni	36.75	28.55	37.98	29.60	37.09	28.81	36.91	28.62	36.91	28.63	36.83	28.77	36.86	28.70
Co	1.30	1.01	1.33	1.03	1.33	1.03	1.30	1.00	1.33	1.03	1.28	1.00	1.24	0.96
Cu	0.00	0.00	0.01	0.01	0.00	0.00	0.05	0.04	0.00	0.00	0.03	0.02	0.00	0.00
S	32.71	46.52	32.37	46.18	32.54	46.27	32.51	46.14	32.33	45.89	32.25	46.11	32.51	46.33
Total	100.06	100.00	99.99	100.00	100.22	100.00	100.46	100.00	100.57	100.00	99.74	100.00	99.95	100.00

Table D 41.2: Atomic proportions of Phoenix massive pentlandite 2 sample.

Element	1	2	3	4	5	6	7
Fe	4.11	4.02	4.13	4.19	4.26	4.18	4.15
Ni	4.91	5.13	4.98	4.96	4.99	4.99	4.96
Co	0.17	0.18	0.18	0.17	0.18	0.17	0.17
Cu	0.00	0.00	0.00	0.01	0.00	0.00	0.00
S	8	8	8	8	8	8	8

Table D 41.3: Average composition of Phoenix massive pentlandite 2 sample.

Element	wt %	±	stdev	At %	Atomic
Fe	29.32	0.39	0.52	23.96	4.15
Ni	37.05	0.31	0.42	28.81	4.99
Co	1.30	0.02	0.03	1.01	0.17
Cu	0.01	0.01	0.02	0.01	0.00
S	32.46	0.11	0.15	46.21	8.00

Table D 42.1: Composition of Phoenix massive pentlandite 1.

n	1		2		3		4		5		6		7	
Element	wt %	At %	wt %	At %	wt %	At %	wt %	At %	wt %	At %	wt %	At %	wt %	At %
Fe	29.79	24.23	29.68	24.01	29.22	23.73	29.66	24.08	29.81	24.12	29.42	23.76	29.20	23.58
Ni	36.48	28.23	36.78	28.31	36.32	28.07	36.27	28.01	36.62	28.20	36.07	27.72	36.42	27.99
Co	1.27	0.98	1.29	0.99	1.28	0.99	1.27	0.98	1.33	1.02	1.30	1.00	1.35	1.03
Cu	0.00	0.00	0.00	0.00	0.00	0.00	0.00	0.00	0.00	0.00	0.00	0.00	0.00	0.00
S	32.88	46.57	33.14	46.69	33.38	47.22	33.20	46.93	33.11	46.66	33.78	47.52	33.69	47.39
Total	100.42	100.00	100.89	100.00	100.20	100.00	100.40	100.00	100.87	100.00	100.57	100.00	100.66	100.00

Table D 42.2: Atomic proportions of Phoenix massive pentlandite 1 sample.

Element	1	2	3	4	5	6	7
Fe	4.16	4.11	4.02	4.10	4.14	4.00	3.98
Ni	4.85	4.85	4.76	4.77	4.83	4.67	4.72
Co	0.17	0.17	0.17	0.17	0.17	0.17	0.17
Cu	0.00	0.00	0.00	0.00	0.00	0.00	0.00
S	8	8	8	8	8	8	8

Table D 42.3: Average composition of Phoenix massive pentlandite 1 sample.

Element	wt %	±	stdev	At %	Atomic
Fe	29.54	0.19	0.26	23.93	4.07
Ni	36.42	0.17	0.23	28.08	4.78
Co	1.30	0.02	0.03	1.00	0.17
Cu	0.00		0.00	0.00	0.00
S	33.31	0.24	0.33	47.00	8.00

Table D 43.1: Composition of Russia 10 massive pentlandite.

n	1		2		3		4		5		6		7	
Element	wt %	At %	wt %	At %	wt %	At %	wt %	At %	wt %	At %	wt %	At %	wt %	At %
Fe	30.71	24.98	30.69	24.94	30.81	24.95	30.82	24.95	30.61	24.91	30.33	24.77	30.57	24.76
Ni	35.88	27.77	35.9	27.76	35.99	27.74	35.78	27.56	35.83	27.74	35.76	27.79	35.85	27.62
Co	1.02	0.79	1.02	0.79	1.01	0.78	1.02	0.78	1.01	0.78	1.01	0.78	1.05	0.81
Cu	0	0.00	0	0.00	0	0.00	0	0.00	0	0.00	0	0.00	0	0.00
S	32.8	46.47	32.86	46.51	32.99	46.54	33.14	46.72	32.87	46.58	32.81	46.66	33.19	46.81
Total	100.41	100.00	100.47	100.00	100.8	100.00	100.76	100.00	100.32	100.00	99.91	100.00	100.66	100.00

Table D 43.2: Atomic proportions of Russia 10 massive pentlandite.

Element	1	2	3	4	5	6	7
Fe	4.30	4.29	4.29	4.27	4.28	4.25	4.23
Ni	4.78	4.77	4.77	4.72	4.76	4.76	4.72
Co	0.14	0.14	0.13	0.13	0.13	0.13	0.14
Cu	0.00	0.00	0.00	0.00	0.00	0.00	0.00
S	8.00	8.00	8.00	8.00	8.00	8.00	8.00

Table D 43.3: Average composition of Russia 10 massive pentlandite.

Element	wt %	±	stdev	At %	Atomic
Fe	30.65	0.12	0.17	24.89	4.27
Ni	35.86	0.06	0.08	27.71	4.76
Co	1.02	0.01	0.01	0.79	0.13
Cu	0.00		0.00	0.00	0.00
S	32.95	0.12	0.16	46.61	8.00

Table D 44.1: Electron microprobe analysis of a synthetic pentlandite (wt %).

Element	1	2	3	4	5	6	7	8	9
Fe	32.42	32.68	32.98	32.81	31.84	32.06	32.28	32.1	33.17
Ni	34.46	34.68	34.1	34.34	34.89	34.6	34.09	34.93	34.19
S	33.57	33.59	33.68	33.85	33.53	33.54	33.59	33.56	33.54

Table D 44.2: Electron microprobe analysis of a synthetic pentlandite (Atomic %).

Element	1	2	3	4	5	6	7	8	9
Fe	26.21	26.32	26.58	26.37	25.80	25.98	26.20	25.93	26.72
Ni	26.51	26.57	26.15	26.26	26.90	26.68	26.32	26.85	26.21
S	47.27	47.11	47.27	47.38	47.31	47.34	47.48	47.22	47.06

Table D 44.3: Atomic proportion of a synthetic pentlandite (sulfur was normalized to 8).

Element	1	2	3	4	5	6	7	8	9
Fe	4.44	4.47	4.50	4.45	4.36	4.39	4.41	4.39	4.54
Ni	4.49	4.51	4.43	4.43	4.55	4.51	4.44	4.55	4.46
S	8.00	8.00	8.00	8.00	8.00	8.00	8.00	8.00	8.00

APPENDIX E: Reproducibility of the electrochemical measurements

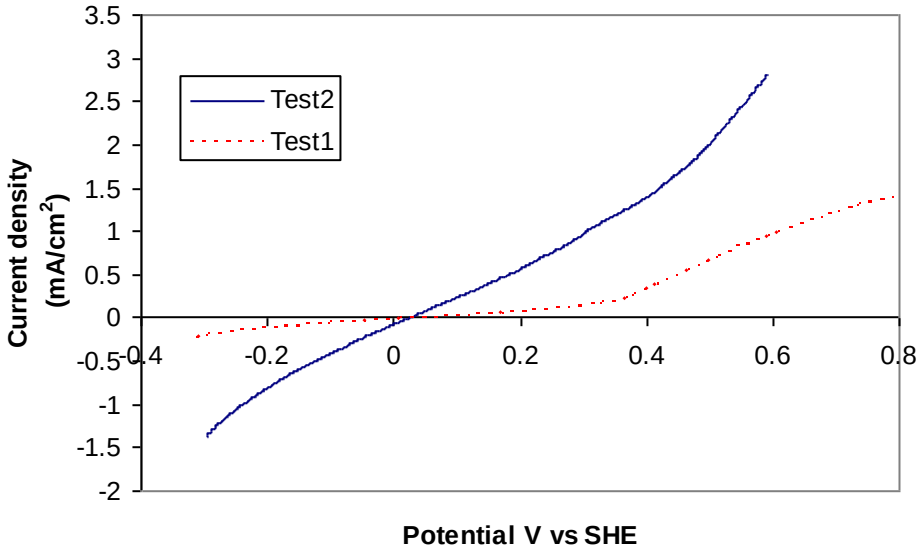

Figure E1: Linear potential sweep voltammogram of pentlandite microelectrode particle with composition $Fe_{4.04}Ni_{4.82}Co_{0.09}S_8$, hand-picked from the Lebowa Merensky flotation concentrate, showing the poor reproducibility of the voltammetry measurements, at a scan rate of 10mV/s.

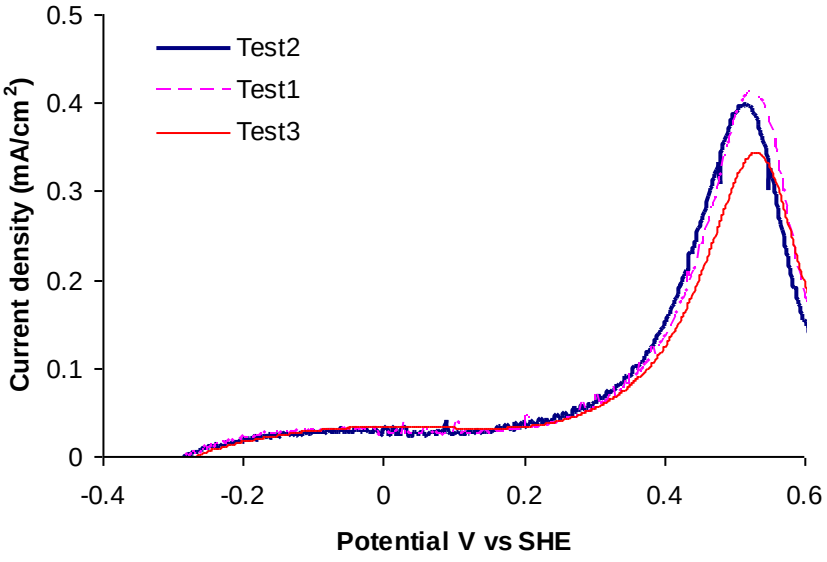

Figure E2: Linear potential sweep voltammograms of a natural pentlandite electrode (with exposed area of 0.00234 cm^2), performed inside and outside a Faraday Cage (the experimental set-up was placed inside and outside the Faraday Cage), in a $Na_2B_4O_7$ solution (pH 9.3) at 25°C. The curves show reproducibility of the voltammograms.

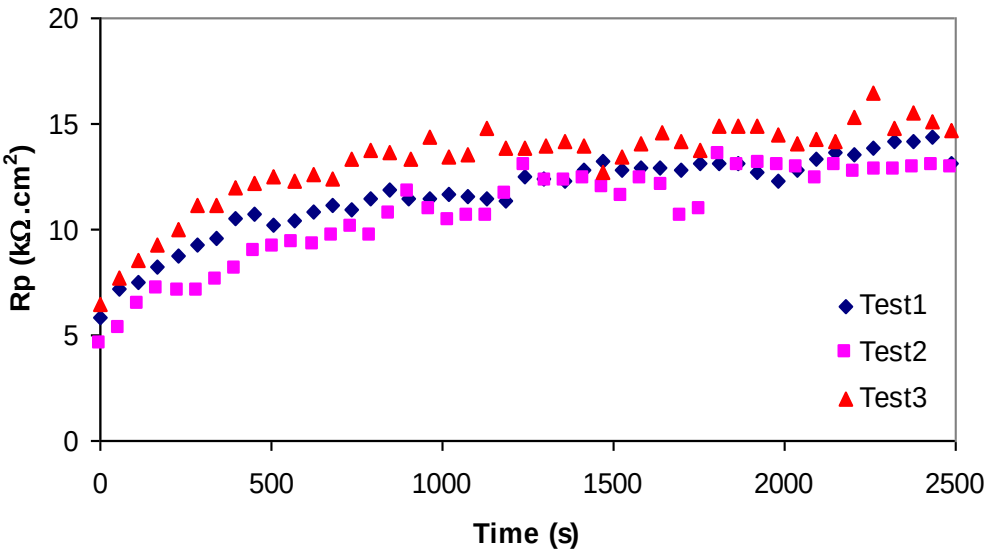

Figure E3: Repeatability of the polarisation resistance measurements of a natural pentlandite electrode, sourced from the Kola Peninsula deposit (Russia), with composition $Fe_{4.27}Ni_{4.76}Co_{0.14}S_8$ performed in 0.05 M $Na_2B_4O_7$ solution (pH 9.3) in equilibrium with air.

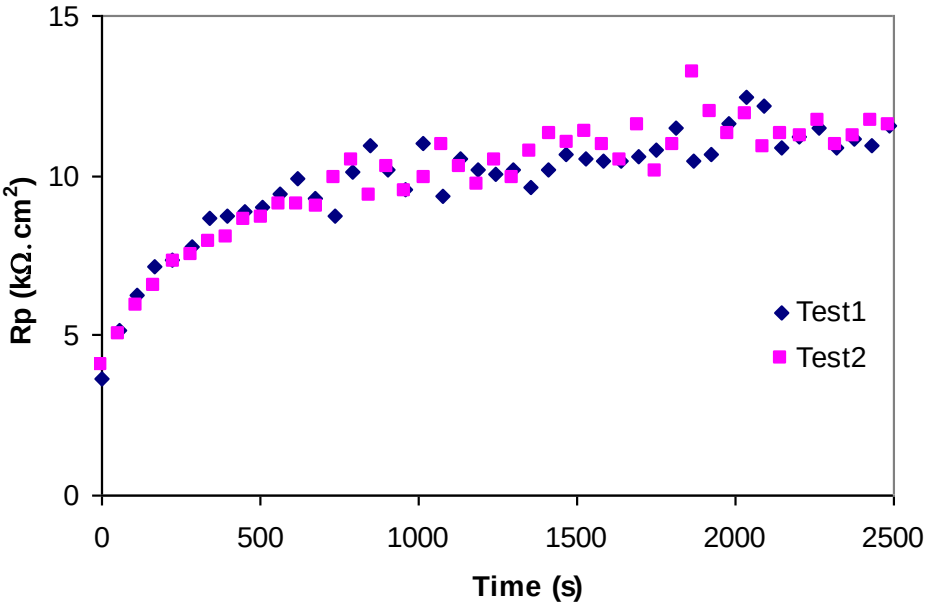

Figure E4: Repeatability of the polarisation resistance measurements of a natural massive pentlandite electrode, sourced from the Phoenix deposit with composition $Fe_{4.07}Ni_{4.78}Co_{0.17}S_8$, performed in 0.05 M $Na_2B_4O_7$ solution (pH 9.3) in equilibrium with air.

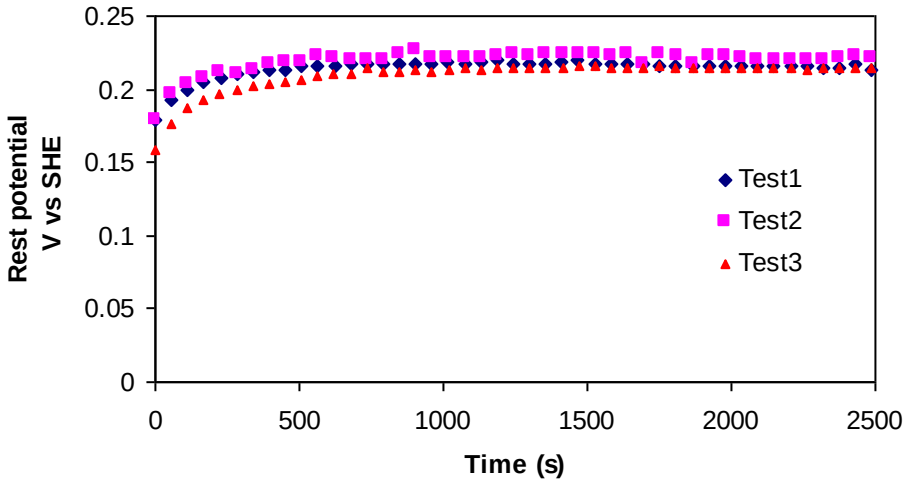

Figure E5: Repeatability of the rest potential measurements of a natural pentlandite electrode, sourced from the Kola Peninsula deposit (Russia), with composition $Fe_{4.27}Ni_{4.76}Co_{0.14}S_8$, performed in a 0.05 M $Na_2B_4O_7$ solution (pH 9.3) in equilibrium with air.

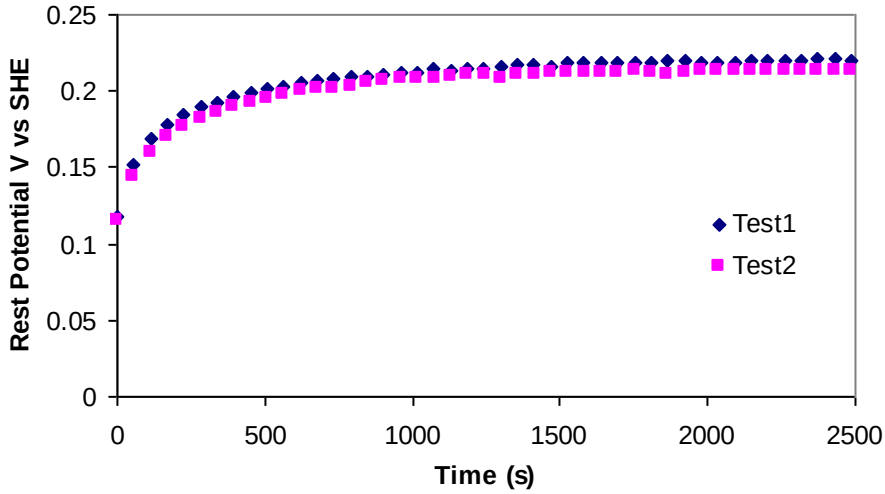

Figure E6: Repeatability of the rest potential measurements of a natural pentlandite electrode, sourced from the Phoenix deposit, with composition $Fe_{4.07}Ni_{4.78}Co_{0.17}S_8$ performed in 0.05 M $Na_2B_4O_7$ solution (pH 9.3) in equilibrium with air.

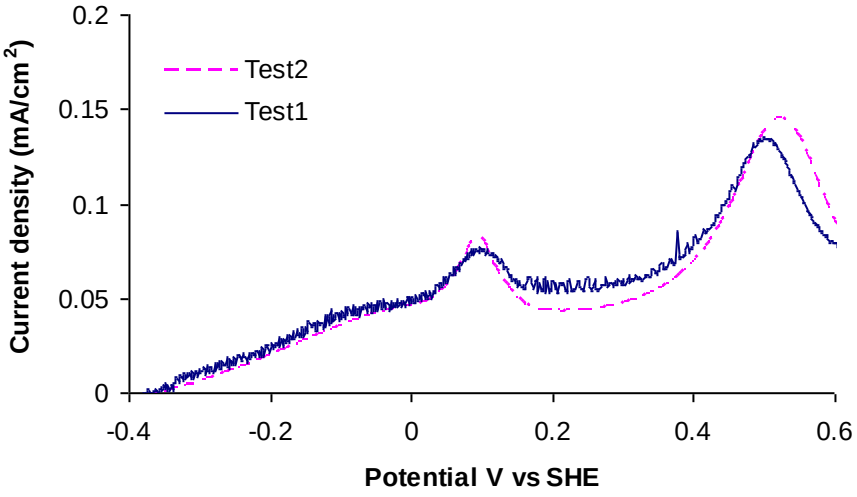

Figure E7: Reproducibility of the linear anodic voltammogram of a natural pentlandite electrode, sourced from Russia with composition $Fe_{4.28}Ni_{4.79}Co_{0.14}S_8$, performed in 0.05 M $Na_2B_4O_7$ solution (pH 9.3) in the absence of oxygen.

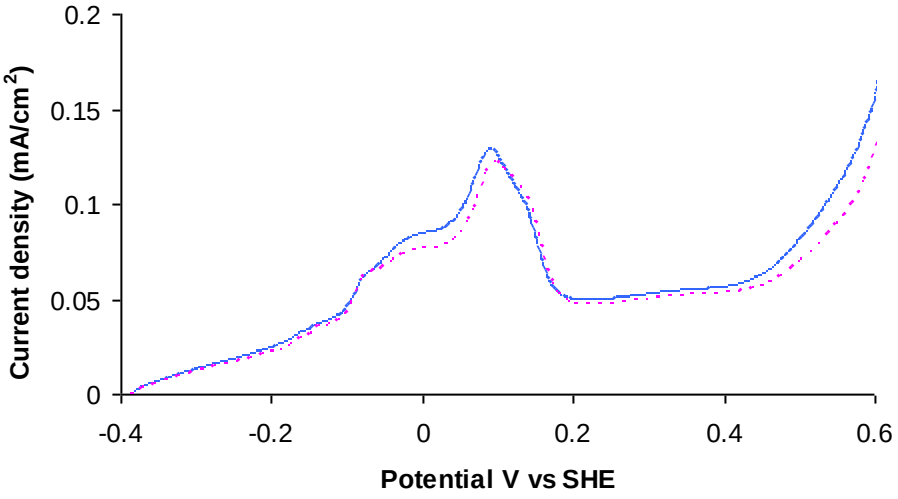

Figure E8: Reproducibility of the linear anodic voltammogram of a natural pyrrhotite electrode (sourced from Kola Peninsula, Russia), with area 0.135cm^2 performed in 0.05 M $Na_2B_4O_7$ solution (pH 9.3) in the absence of oxygen.

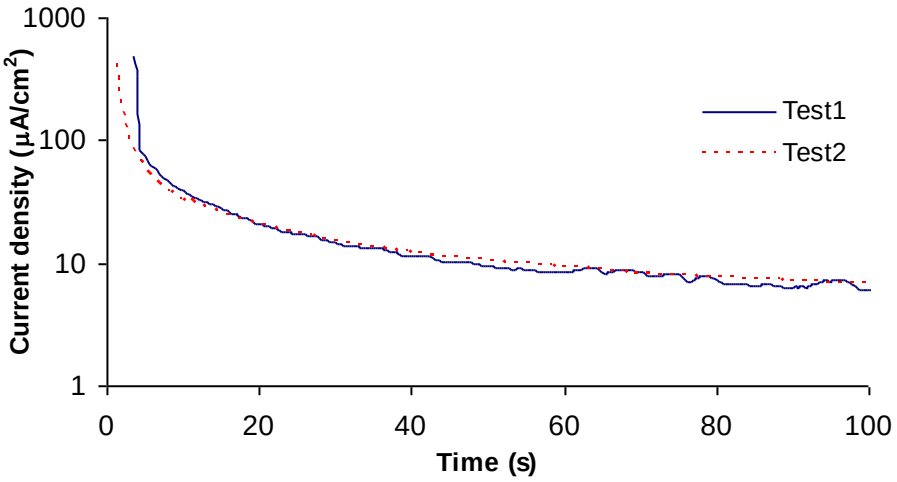

Figure E9: Reproducibility of the current density transients of a natural pentlandite electrode, sourced from Phoenix with composition $Fe_{4.07}Ni_{4.78}Co_{0.17}S_8$, performed in 0.05 M $Na_2B_4O_7$ solution (pH 9.3) in the absence of oxygen.

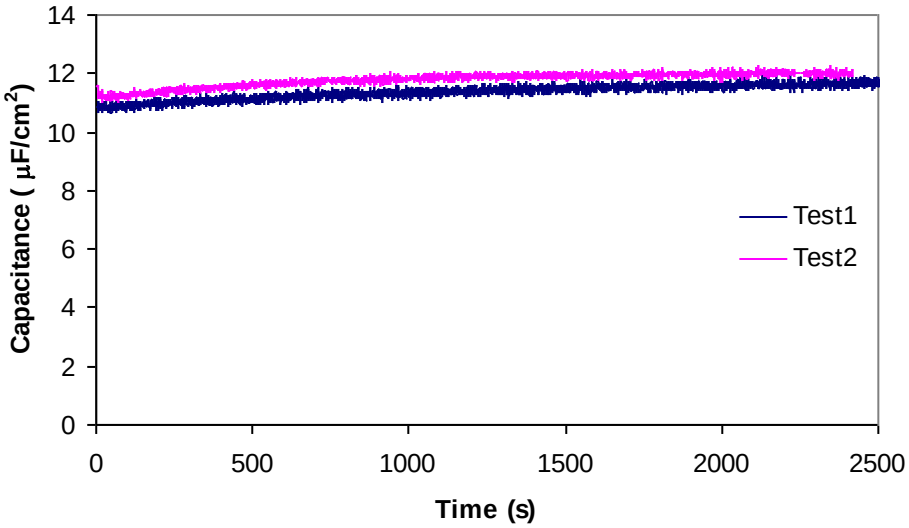

Figure E10: Reproducibility of the capacitance measurement of a natural pentlandite electrode, sourced from Russia with composition $Fe_{4.27}Ni_{4.75}Co_{0.14}S_8$, performed in 0.05 M $Na_2B_4O_7$ solution (pH 9.3) in equilibrium with air at 0.2V_{SHE}.

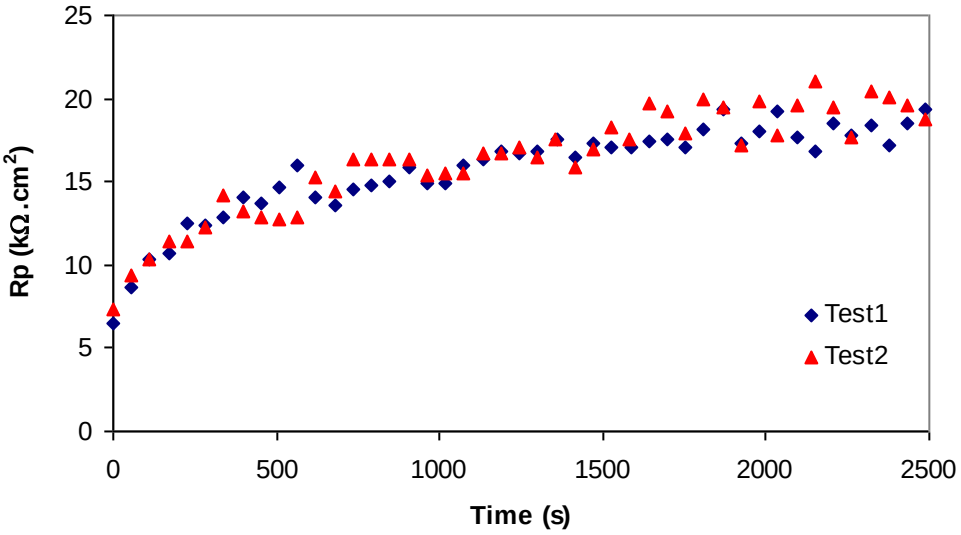

Figure E11: Repeatability of the polarisation resistance measurements of a synthetic pentlandite electrode in 0.05 M $Na_2B_4O_7$ solution (pH 9.3) at 25°C with composition $Fe_{4.44}Ni_{4.48}S_8$.

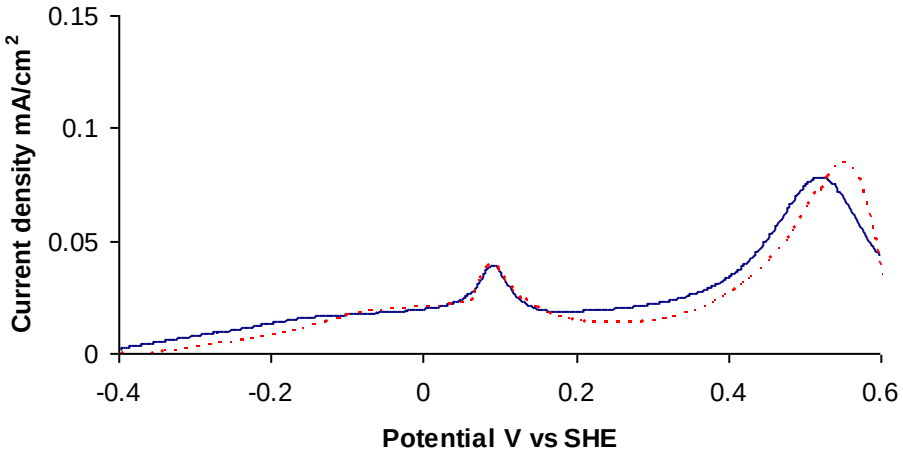

Figure E12: Repeatability of the linear anodic voltammogram of a synthetic pentlandite electrode in 0.05 M $Na_2B_4O_7$ solution (pH 9.3) at 25°C with composition $Fe_{4.44}Ni_{4.48}S_8$ in the absence of oxygen.

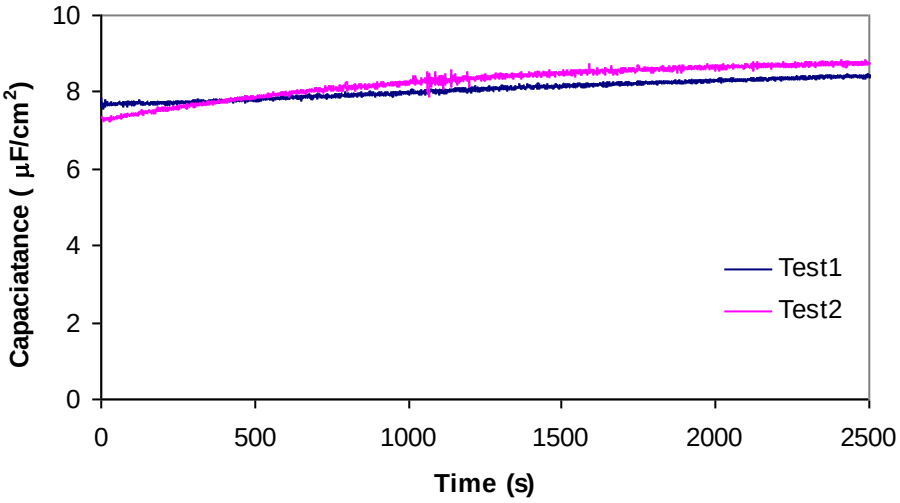

Figure E13: Reproducibility of the capacitance measurements of the synthetic pentlandite electrode in 0.05 M $Na_2B_4O_7$ solution (pH 9.3) at 25°C and at 0.2 V_{SHE} with composition $Fe_{4.44}Ni_{4.48}S_8$.